

REPORT NO.
UCB/EERC-85/15
DECEMBER 1985

EARTHQUAKE ENGINEERING RESEARCH CENTER

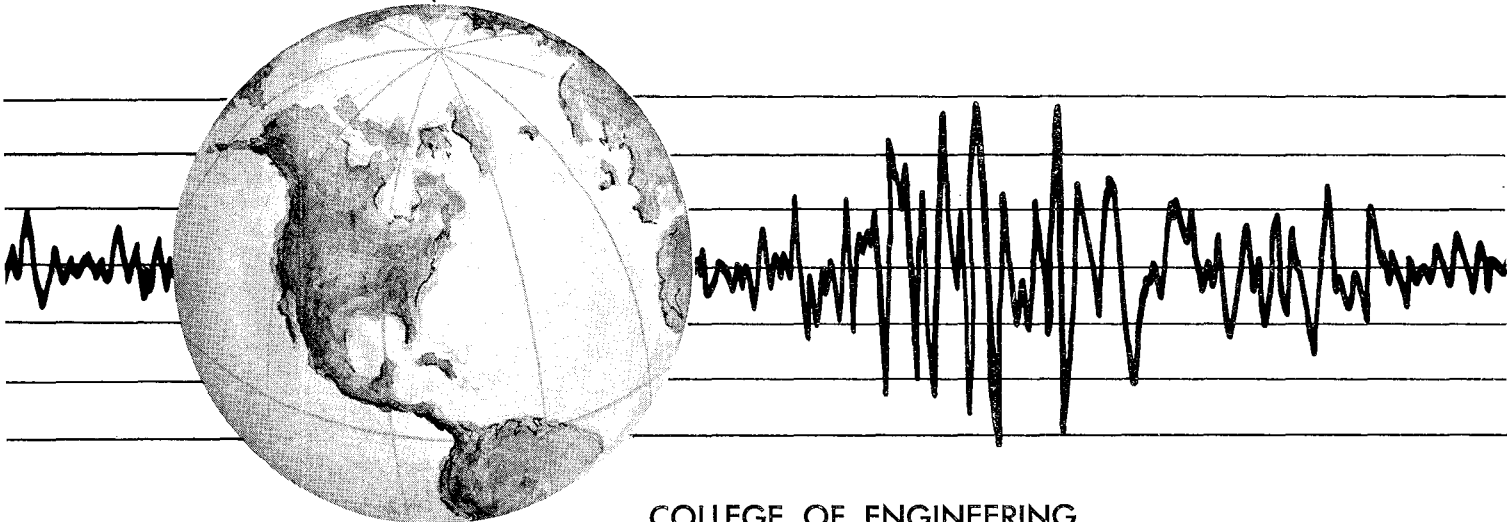
**CYCLIC LOADING TESTS OF
MASONRY SINGLE PIERS
VOLUME 4—ADDITIONAL TESTS WITH
HEIGHT TO WIDTH RATIO OF 1**

by

BJORN I. SVEINSSON
HUGH D. McNIVEN
HALUK SUCUOGLU

Report to:

National Science Foundation
Masonry Institute of America
Western States Clay Products Association
and the
Concrete Masonry Association of California and Nevada



COLLEGE OF ENGINEERING

UNIVERSITY OF CALIFORNIA • Berkeley, California

EERC

Berkeley, California

CYCLIC LOADING TESTS OF MASONRY SINGLE PIERS - VOLUME 4

ADDITIONAL TESTS WITH HEIGHT TO WIDTH RATIO OF 1

by

Bjorn I. Sveinsson

Hugh D. McNiven

and

Haluk Sucuoglu

Report to

National Science Foundation
Masonry Institute of America
Western States Clay Products Association
Concrete Masonry Association of California and Nevada

Report No. UCB/EERC-85/15

Earthquake Engineering Research Center
College of Engineering
University of California
Berkeley, California

December 1985

ABSTRACT

This report presents the results of thirty cyclic, in-plane shear tests on fixed ended masonry piers having a height to width ratio of 1.0. These thirty tests form the final part of a test program consisting of ninety-three (93) single pier tests. Previous reports have presented the test results from sixty-three (63) such tests.

The test setup was designed to simulate, insofar as possible, the boundary conditions the piers would experience in a perforated shear wall of a complete building. Each test specimen was a full scale pier 48 inches high and 40 inches wide. Three types of masonry construction were used; a hollow concrete block, hollow clay brick and a double wythe grouted core clay brick that consisted of two brick wythes and a 3 inch grouted core. All the piers were fully grouted. The parameters considered in this investigation were the level of bearing stress, the amount of horizontal reinforcement, the anchorage of horizontal reinforcement and the distribution of vertical reinforcement.

ACKNOWLEDGEMENTS

This investigation was jointly sponsored by the National Science Foundation under Grants PFR-79-08251 and CEE 8107462, the Masonry Institute of America, the Western States Clay Products Association and the Concrete Masonry Association of California and Nevada. The authors wish to thank Dr. Beverley Bolt for her review of the manuscript. The drafting was done by Mary Steele.

TABLE OF CONTENTS

ABSTRACT **i**

ACKNOWLEDGEMENTS **ii**

TABLE OF CONTENTS **iii**

SECTION 1 INTRODUCTION **1**

 1.1 Masonry in Structural Engineering 1

 1.2 The U.C. Berkeley Experimental Research Program on Masonry Piers . . . 3

 1.3 Objectives and Scope of the Tests Reported Here 5

SECTION 2 TEST SPECIMENS **9**

 2.1 Design and Construction of Test Specimens 9

 2.1.1 Types of Masonry Construction 9

 2.1.2 Reinforcement of Piers 11

 2.2 Material Properties 12

SECTION 3 TEST EQUIPMENT AND TEST PROCEDURE **25**

 3.1 Test Setup 25

 3.2 Instrumentation 26

 3.3 Control, Data Acquisition, and Data Processing Systems 27

3.4	Loading Sequence	30
SECTION 4	TEST RESULTS	39
4.1	Modes of Failure	39
4.1.1	Shear Failure	40
4.1.2	Shear-Sliding Failure	41
4.1.3	Sliding Failure	42
4.1.4	Flexural Failure	42
4.2	Load-Displacement Characteristics	43
SECTION 5	DISCUSSION OF TEST RESULTS	55
5.1	The Hysteresis Envelopes	56
5.1.1	Effect of Bearing Load	56
5.1.2	Effect of Horizontal Reinforcement	57
5.1.3	Effect of Anchorage of Horizontal Reinforcement	58
5.1.4	Effect of Distribution of Vertical Reinforcement	60
5.2	Stiffness Degradation	61
5.2.1	Effect of Vertical Load.	62
5.2.2	Effect of Horizontal Reinforcement	62
5.2.3	Effect of Type of Anchorage	62
5.2.4	Effect of Vertical Reinforcement Distribution	63
5.3	Crack Width Measurement	63
SECTION 6	SUMMARY AND CONCLUSIONS	87
SECTION 7	REFERENCES	93
APPENDIX A	PRESENTATION OF THE TEST RESULTS	95

SECTION 1 INTRODUCTION

This report presents the results of thirty two tests performed on masonry single pier specimens. These tests end a phase of an extensive program of cyclic loading tests on masonry structural elements at the University of California, Berkeley begun in 1976. The test data from earlier single-pier tests [1,2,3,4] are summarized briefly in Section 1.2, and an overview is also provided of previous research described in the literature on seismic behavior of masonry walls. In Section 1.3 the objectives and scope of the tests presented in this report are discussed.

1.1 Masonry in Structural Engineering

The wide use of masonry in building construction all over the world arises from its practical and inexpensive construction, favorable architectural characteristics, heat insulation performance and its compressive strength. Until recently, however, its properties as a structural material except for compression were not considered.

Devastating damage to masonry structures in the last twenty five years due to earthquakes has caused engineers to consider masonry as a structural material, to recognize its weaknesses and to consider ways in which these weaknesses can be overcome so that such damage can be significantly reduced. Masonry construction will continue, so it is imperative that earthquake engineers learn to devise methods to improve its ductility and its energy absorbing capabilities, that are both effective and reasonable in cost. This calls for fundamental research.

Experimental and analytical research on the seismic behavior of masonry structures during the last fifteen years has revealed that their earthquake performance can be significantly improved by properly reinforcing against tensile stresses which cause brittle failure because of the low tensile strength of masonry. The results of tests by various researchers [5,6,7] on reinforced masonry cantilever walls subjected to inplane loads indicate the existence of two basic failure modes: shear (or diagonal tension) failure and flexural failure. Shear failure is characterized by diagonal cracking of the masonry along lines of maximum principal tensile stress in the wall plane, whereas flexural failure is characterized by either yielding of tension steel followed by crushing of the masonry or by crushing of the masonry alone at the compression toe. The flexural types of failure exhibit considerable ductility, whereas the shear failures are quite sudden and brittle. Accordingly, flexure is considered to be a more favorable mode of failure than shear.

Hidalgo et al. [3] also observed combined failure modes for fixed-ended masonry piers. These were sliding-shear and sliding-flexure modes. The sliding-shear failure was displayed by squat walls and occurred as sliding of the top portion of the wall with respect to the base portion. The sliding took place along a bell-shaped crack formed by diagonal cracks which had opened during reversed loadings. The sliding-flexure mode occurred where the flexural cracks were continuous throughout a horizontal course subjected to high flexural stress reversals.

Meli [5] recognized the similarity between the flexural behavior of under-reinforced concrete beams and that of masonry walls with low flexural reinforcement and low bearing stresses. Furthermore, he demonstrated that the ultimate strength of the walls increases with increasing bearing stresses, but the failure mode changes from flexural to shear under high bearing stresses. Priestley and Bridgeman [7] showed that the flexural strength of walls can be predicted quite accurately by the ultimate strength theory developed for reinforced concrete flexural members, and that the ductility in flexure could be improved significantly by adding joint reinforcement to the crushing zone of the walls in order to confine the mortar. They also showed that a horizontal reinforcing bar contributed three times as much as a vertical reinforcing bar to the shear strength. Accordingly, they proposed the design philosophy of suppressing shear failure by using enough horizontal

reinforcement to resist without yielding the full shear load at flexural capacity, and consequently inducing flexural failure which has more desirable inelastic response characteristics. Priestley demonstrated the validity of this philosophy by testing heavily-reinforced masonry cantilever walls [8] with zero or low bearing stresses under cyclic loads. Mayes et al. [9,10] observed a similar improvement in the ductility of double-pier specimens failing in flexure with the addition of joint reinforcement as proposed by Priestley and Bridgeman [7].

Mayes et al. [9,10] and Hidalgo et al. [1,2,3] tested various fixed-ended masonry piers some of which developed high bearing stresses leading to a shear mode of failure, and observed that the structural behavior of the specimens failing in shear was much more complicated than those failing in flexure. Their tests and results, summarized by Sveinsson et al. [4], are discussed in more detail in the following section.

1.2 The U.C. Berkeley Experimental Research Program on Masonry Piers

An extended test program on the seismic behavior of masonry single piers was initiated at the Earthquake Engineering Research Center of the University of California, Berkeley in 1976. Piers were selected for investigation since observations on multistory masonry buildings damaged in earthquakes had indicated that piers were the most vulnerable elements of perforated masonry shear walls (Fig. 1.1). Fixed-end conditions and realistic bearing stresses were imposed on the piers which were then tested under cyclic lateral loads, simulating the conditions of a lower-story pier in a perforated wall subjected to earthquake excitation.

The effects of various parameters on the structural behavior of piers failing in the shear mode were investigated since this mode frequently occurs under the force and displacement boundary conditions imposed on the piers by the perforated shear walls. Furthermore, it was decided not to use the heavy reinforcement ratios present in Priestley's tests, since these were judged to be too costly for American practice. The objective was to establish which parameters are effective in improving the inelastic behavior of piers failing in the shear mode. The following parameters

were selected for investigation :

1. The type of masonry construction
2. Height to width ratio (h/w)
3. Type of grouting (partial or full)
4. Amount of horizontal and vertical reinforcement
5. The level of bearing stress.

The distribution of the number of test specimens of the single pier test program with respect to their masonry types and h/w ratios is given in the top three rows of Table 1.1.

The results of these tests, published in three research reports [1,2,3] and one summary report [4] reveal the complexity of the shear behavior of masonry piers. Within the range for which the parameters were tested, it was recognized that the ultimate shear strength was a function of the masonry compressive strength, the h/w ratio of the pier, the amount of horizontal reinforcement and the vertical compressive load acting on the pier when the ultimate strength was reached [11]. It was also observed that the ultimate shear strength was approximately the same for fully and partially grouted piers as long as the stress was based on the net area of the cross section of the wall. A positive correlation was observed between increase in horizontal reinforcement and improvement in inelastic behavior although not all the piers showed improvement nor was such improvement proportional to the increase in reinforcement. The displacement capacity of the fully grouted piers was always higher than that of the partially grouted piers. The tests were not able to develop the full yielding capacity of the horizontal reinforcing bars and therefore the anchorage between the horizontal reinforcing bars and the grout emerged as a more critical parameter than the amount of horizontal reinforcement.

Early in the single pier test program, it was recognized that the vertical steel columns, which prevented rotation of the top beam, imposed additional vertical load on the pier as the horizontal displacements increased. The top of the fixed length columns, which were pinned at both ends, moved through a circular arc when going from one displacement extreme to the other. At each arc extreme the vertical height of the columns was reduced, thus cramping and compressing the specimen. This additional vertical load, which continually changed during each load cycle, was in addition to the initial externally applied vertical load.

The test setup was subsequently modified (before the tests presented here were performed) by replacing the two vertical columns by two vertical actuators. These actuators, controlled by an electro-hydraulic servo system, could be programmed to maintain constant combined vertical load on the specimen. This modified test setup is shown in Figure 3.1.

1.3 Objectives and Scope of the Tests Reported Here

The total number of single pier specimens planned for testing were eighty at the beginning of the single pier test program. Sixty three of these eighty specimens had already been tested and the results published [1,2,3,4] prior to this final stage of the test program. The remaining seventeen piers were to be designed and tested according to the interpretation of the results obtained from the previous sixty three tests, for the final evaluation of the complete test data. The objectives of the final tests were subsequently modified, however, since the modification of the test setup used for the first sixty three tests required confirmation of some of the previous test results. The scope was widened and the tests were planned as a new series. Some changes were made in the set of parameters selected for consideration, as discussed below, in view of the findings and observations from the sixty three specimens already tested. The number of specimens tested in this last series was increased to thirty in order to investigate more thoroughly the effects of the new set of parameters on the response of the piers. Two of the specimens were tested twice for a total of thirty two tests.

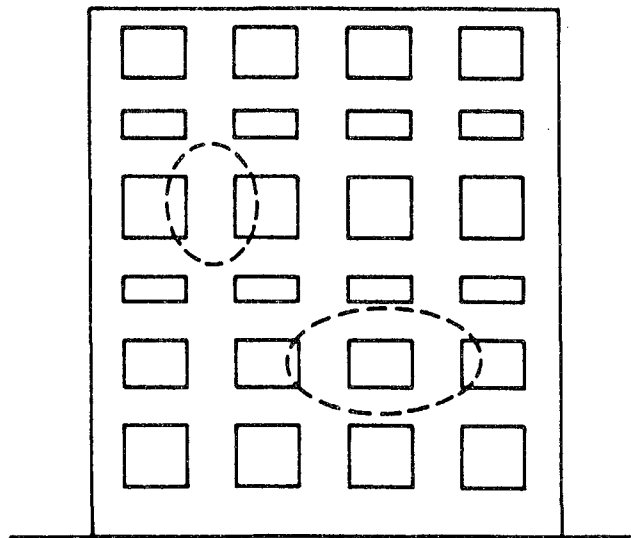
The number of specimens for each type of masonry construction is given in the last row of Table 1.1. The h/w ratio was selected to be close to one because the h/w ratio of piers in perforated shear walls, commonly met in construction practice, is usually close to one. All the piers were fully grouted, leaving the study of the inelastic behavior of partially grouted piers to a future experimental program. The following parameters were considered in this test program :

1. The level of bearing stress
2. Amount of horizontal reinforcement
3. Anchorage of horizontal reinforcing bars (four different types including joint reinforcing).
4. Distribution of vertical reinforcement

The results of the thirty two tests described here, which were performed with the improved test setup, constitute a reliable data base for the seismic behavior of masonry piers failing in the shear mode. In Sections 4 and 5 the test results are discussed and analyzed, and finally the results are summarized and conclusions drawn.

TABLE 1.1
SINGLE PIER TEST PROGRAM
 (Number of test specimens)

HEIGHT: WIDTH RATIO	TYPE OF MASONRY	HOLLOW CLAY BRICK (HCBR)	DOUBLE WYTHE GROUTED CORE CLAY BRICK (CBRC)	HOLLOW CONCRETE BLOCK (HCBL)	TOTAL NUMBER
2 : 1		9	5	0	14
1 : 1		13	7	11	31
1 : 2		6	6	6	18
1 : 1		13	5	12	30



PERFORATED SHEAR WALL

Figure 1.1 Typical Perforated Shear Wall



SECTION 2 TEST SPECIMENS

This section offers a detailed description of all the test specimens included in this test program. Construction types, reinforcing details, material properties and other pertinent information are summarized in the tables and figures contained within the section.

2.1 Design and Construction of Test Specimens

The thirty test specimens were classified into three groups according to their type of masonry construction. Twelve of the specimens were hollow concrete block (HCBL) piers, thirteen were hollow clay brick (HCBR) piers, and five were double wythe grouted core clay brick (CBRC) piers. These thirty test specimens yielded thirty two tests since two of the piers were tested twice, once with a low bearing load to induce flexural behavior and then with a high bearing load to enforce shear failure.

The overall dimensions of the specimens are given in Table 2.1. The inplane dimensions of all of the thirty test specimens were identical (Figure 2.1). The eleven (-11-) in the pier's designation (HCBL-11-15) is common to all piers in this test series and represents the H/W ratio. The thickness of the specimens varied with the type of construction.

2.1.1 Types of Masonry Construction

The three different types of masonry construction used in this test program

are described in this subsection. The construction is identified using the terminology defined in Section 2.1.

1. HCBL Piers : These were constructed from standard two-core hollow concrete blocks; the thickness of the piers was equal to the width of the concrete blocks. Two types of concrete blocks were used in the construction of the piers shown in Fig. 2.2(a). Twelve piers were constructed.

Two piers (HCBL-11-13 and HCBL-11-15) were constructed from nominal 8 inches high x 8 inches wide x 16 inches long blocks, whereas the remaining ten HCBL piers were constructed from nominal 8 inches high x 6 inches wide x 16 inches long blocks. The net cross-sectional area of the 8"x8"x16" blocks is 68 square inches and the net cross sectional area of the 8"x6"x16" blocks is 50 square inches. All of the HCBL piers were fully grouted.

2. HCBR Piers : These were constructed from standard three-core hollow clay bricks; the thickness of the piers was equal to the width of the brick units. Two types of clay bricks were used in the construction of the piers shown in Fig. 2.2(b). Thirteen piers were constructed.

Two piers (HCBR-11-15 and HCBR-11-17) were constructed from nominal 4 inches high x 8 inches wide x 12 inches long bricks, whereas the remaining eleven HCBR piers were constructed from nominal 4 inches high x 6 inches wide x 12 inches long bricks. The net cross sectional area of the 4"x8"x12" bricks is 57.4 square inches and the net cross sectional area of the 4"x6"x12" bricks is 42.7 square inches. All of the HCBR piers were fully grouted.

3. CBRC Piers : These were constructed from two wythes of 4 inches high x 4 inches wide x 12 inches long solid clay bricks shown in Fig. 2.2(c). The grout space between the wythes was 3.5 inches wide, and was completely filled after the steel reinforcement had been placed in position. This type of grouting is designated "solid grouting". The thickness of the CBRC piers was 10 inches. Five such piers were constructed.

The piers were constructed on top of 0.75 inch thick steel plates, as shown in Fig. 2.3. A similar plate was placed on top of the pier after the grout was poured. Both plates had openings to permit anchorage of the vertical steel reinforcement and keys, embedded in the grout, to provide adequate shear transfer between the masonry pier and the steel plate. The plates also had welded bolts and holes to anchor the pier to the test rig.

2.1.2 Reinforcement of Piers

Three of the four key parameters considered in the test series relate to the reinforcement of the piers. These are the quantity of horizontal reinforcement, the distribution of vertical reinforcement and the type of anchorage of the horizontal reinforcing bars. The effect of wire mesh reinforcing (Dur-O-Wal) embedded into the mortar bedjoints was also investigated. The combination of these parameters for each pier is given in Table 2.1. Details of the horizontal and vertical reinforcing bar arrangements are shown in Fig. 2.4(a) for HCBL piers, in Fig. 2.4(b) for HCBR piers and in Fig. 2.4(c) for the CBRC piers. The horizontal reinforcing bars were distributed evenly over the height of the piers. The three types of horizontal bar anchorage are shown in Fig. 2.5 and the horizontal wire mesh detail is shown in Fig. 2.6.

2.2 Material Properties

The mechanical properties of the materials used in the construction of the test specimens are shown in Table 2.2. Figures 2.2(a), 2.2(b) and 2.2(c) show the specimens used to determine the material properties.

For consistency with the previous pier tests [1,2,3] the mortar was specified as standard ASTM type M (1 cement : 1/4 lime : 2-1/4 - 3 sand, by volume), with a minimum compressive strength of 2500 psi at 28 days. The grout was specified as 1 cement : 3 sand : 2 gravel (\leq 10 mm).

ASTM A615 steel was specified for both the vertical and horizontal steel reinforcement. Yield and ultimate strengths are listed in Table 2.2. The wire mesh joint reinforcement was specified to be extra heavy Dur-O-Wal.

Three short and three tall, slender prisms for uniaxial compression tests (Fig. 2.7) and three square panels for diagonal tension tests (Fig. 2.8) were constructed from the same mortar and grout used in each set of wall piers. All the prisms and square panels were fully grouted. The height to thickness ratios were approximately 2 for the short prisms, 5 for the tall HCBL and HCBR prisms, and 4 for the tall CBRC prisms. The uniaxial compression tests were performed at a loading rate of 20,000 lb/min., and the average compressive strengths are shown in Table 2.2. The square panels were tested at a loading rate of 10,000 lb/min., and the average ultimate loads are shown in Table 2.2.

**TABLE 2.1
PIER CHARACTERISTICS**

GENERAL CHARACTERISTICS	SPECIMEN DESIGNATION	GROSS SECT. AREA (SQ.IN)	BEARING STRESS (PSI)	REINFORCEMENT		
				VERTICAL	HORIZONTAL	ANCHORAGE
MASONRY TYPE: HOLLOW CONCRETE BLOCK PIER HEIGHT = 56in. PIER WIDTH = 48in.	HCBL-11-13	366	273	2 # 5	4 # 5	90° BENT
	15	366	437	2 # 5	4 # 5	90° BENT
	17	270	400	2 # 7	4 # 5	90° BENT
	18	270	400	6 # 4	4 # 5	90° BENT
	19	270	400	2 # 7	4 # 5	180° HOOK
	20	270	400	2 # 7	2 # 5	90° BENT
	21	270	400	6 # 4	2 # 5	90° BENT
	22	270	100	2 # 7	2 # 5	180° HOOK
	23	270	400	2 # 7	DUR-O-WAL	-
	24	270	400	2 # 7	2 # 5, DUR-O-WAL	90° BENT
	25	270	250	2 # 7	2 # 5	180° HOOK
26	270	400	2 # 7	2 # 5	180° HOOK	
MASONRY TYPE: HOLLOW CLAY BRICK PIER HEIGHT = 56in. PIER WIDTH = 48in.	HCBR-11-15	354	450	2 # 5	5 # 5	90° BENT
	17	354	56	2 # 5	5 # 5	90° BENT
	17s	354	282	2 # 5	5 # 5	90° BENT
	19	270	400	2 # 7	2 # 5	90° BENT
	20	270	400	2 # 7	5 # 5	90° BENT
	21	270	400	2 # 7, 2 # 5	2 # 5	90° BENT
	22	270	400	4 # 5	5 # 5	90° BENT
	23	270	400	6 # 4	2 # 5	90° BENT
	24	270	400	6 # 4	5 # 5	90° BENT
	25	270	400	2 # 7	2 # 5	180° BENT
	26	270	400	2 # 7	5 # 5	180° HOOK
	27	270	400	2 # 7	4 # 4	END PLATE
28	270	400	2 # 5	10 # 4	END PLATE	
30	270	400	2 # 7	DUR-O-WAL	-	
MASONRY TYPE: DOUBLE WYTHE GROUTED CORE CLAY BRICK PIER HEIGHT = 56in. PIER WIDTH = 48in.	CBRC-11- 8	480	42	2 # 5	1 # 5	90° BENT
	8S	480	220	2 # 5	1 # 5	90° BENT
	9	480	330	2 # 5	5 # 5	90° BENT
	10	480	330	2 # 5	1 # 5	90° BENT
	11	480	42	2 # 5	5 # 5	90° BENT
	12	480	220	2 # 5	3 # 3	90° BENT

**TABLE 2.2
MATERIAL PROPERTIES**

SPECIMEN	COMPRESSIVE STRENGTH		ULTIMATE	VERTICAL REINFORCEMENT			HORIZONTAL REINFORCEMENT		
	PRISM 2:1 (PSI)	PRISM 2:1 (PSI)	LOAD OF SQ. PANEL (KIPS)	YIELD STRENGTH (KSI)	ULTIMATE STRENGTH (KSI)	YIELD STRAIN (IN/IN)	YIELD STRENGTH (KSI)	ULTIMATE STRENGTH (KSI)	YIELD STRAIN (IN/IN)
HCBL-11-13	3257	3460	169.5	67.5	107.5	0.0024	59.0	88.1	0.0021
15	3257	3460	169.5	67.5	107.5	0.0024	59.0	88.1	0.0021
17	2829	1764	91.3	56.7	85.8	-	63.5	99.3	-
18	2829	1764	91.3	59.5	90.0	-	63.5	99.3	-
19	2381	2010	99.0	56.7	85.8	-	63.5	99.3	-
20	2381	2010	99.0	56.7	85.8	-	63.5	99.3	-
21	2381	2010	99.0	59.5	90.0	-	63.5	99.3	-
22	2381	2010	99.0	56.7	85.8	-	63.5	99.3	-
23	2381	2010	99.0	56.7	85.8	-	63.5	99.3	-
24	2381	2010	99.0	56.7	85.8	-	63.5	99.3	-
25	2381	2010	99.0	56.7	85.8	-	63.5	99.3	-
26	2381	2010	99.0	56.7	85.8	-	63.5	99.3	-
HCBR-11-15	3781	3713	261.5	67.5	107.5	0.0024	67.5	107.5	0.0024
17	3781	3713	261.5	67.5	107.5	0.0024	67.5	107.5	0.0024
17S	3781	3713	261.5	67.5	107.5	0.0024	67.5	107.5	0.0024
19	2957	2879	91.9	56.7	85.8	-	63.5	99.3	-
20	2957	2879	91.9	56.7	85.8	-	63.5	99.3	-
21	2957	2879	91.9	56.7	85.8	-	63.5	99.3	-
22	2957	2879	91.9	63.5	99.3	-	63.5	99.3	-
23	2957	2879	91.9	59.5	99.0	-	63.5	99.3	-
24	2957	2879	91.9	59.5	99.0	-	63.5	99.3	-
25	2957	2879	91.9	56.7	85.8	-	63.5	99.3	-
26	2957	2879	91.9	56.7	85.8	-	63.5	99.3	-
27	2957	2879	91.9	56.7	85.8	-	59.5	99.0	-
28	2957	2879	91.9	59.5	99.3	-	60.5	99.0	-
30	4306	3709	136.5	56.7	85.8	-	63.5	99.3	-
CBRC-11- 8	2873	2093	184.0	67.5	107.5	0.0024	59.0	88.1	0.0021
8S	2873	2093	184.0	67.5	107.5	0.0024	59.0	88.1	0.0021
9	2873	2093	184.0	67.5	107.5	0.0024	67.5	107.5	0.0024
10	2873	2093	184.0	67.5	107.5	0.0024	59.0	88.1	0.0021
11	2873	2093	184.0	67.5	107.5	0.0024	67.5	107.5	0.0024
12	2873	2093	184.0	67.5	107.5	0.0024	57.8	85.6	0.0020

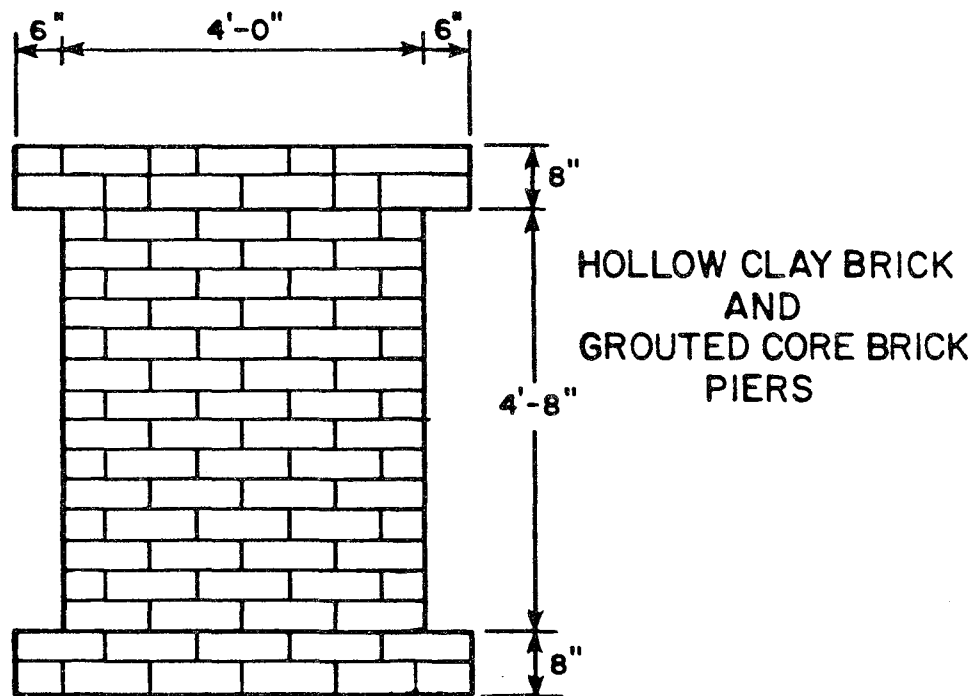
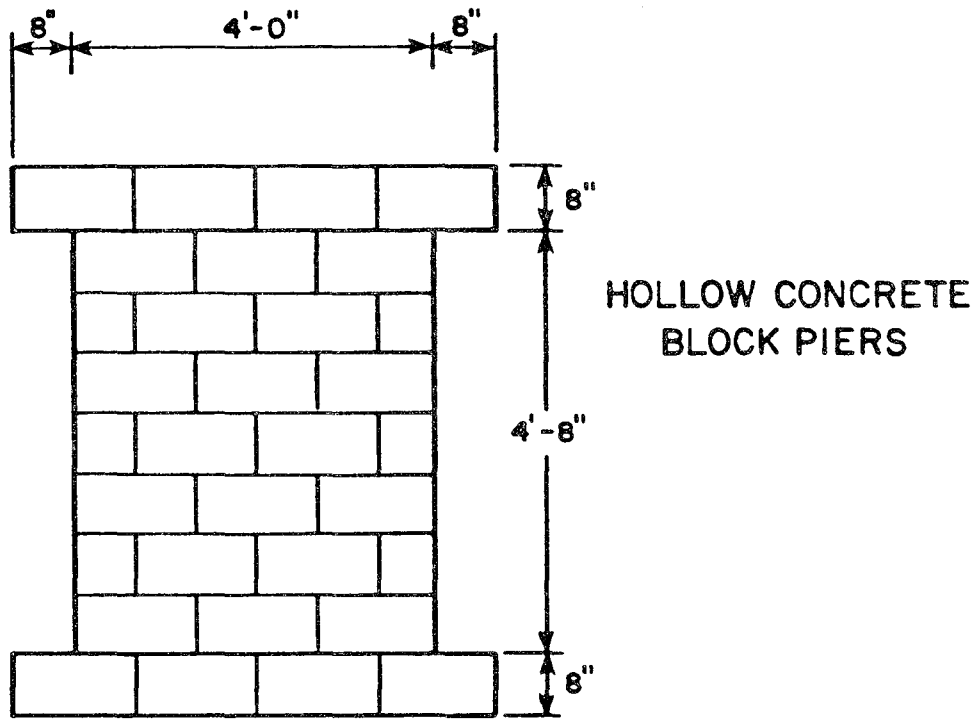
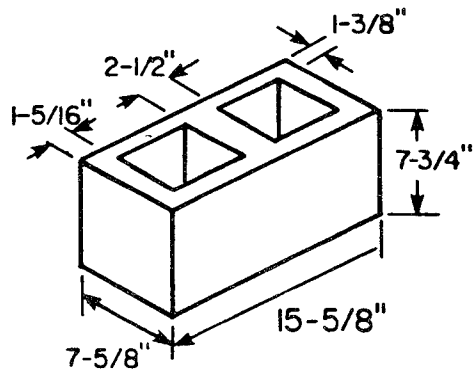
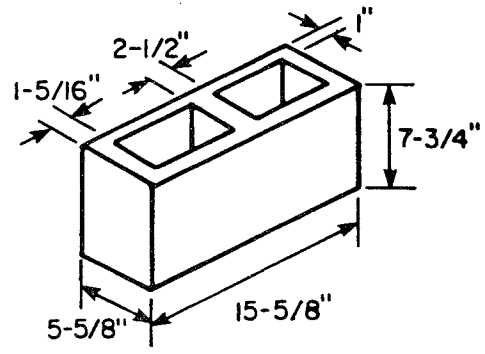


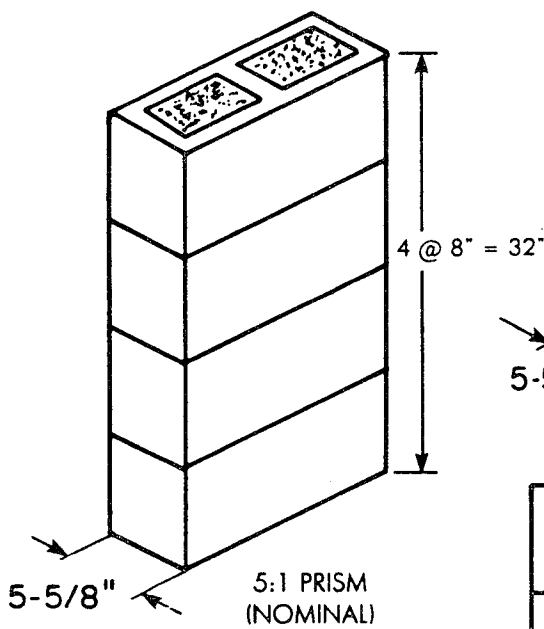
FIG. 2.1 PIER DIMENSIONS



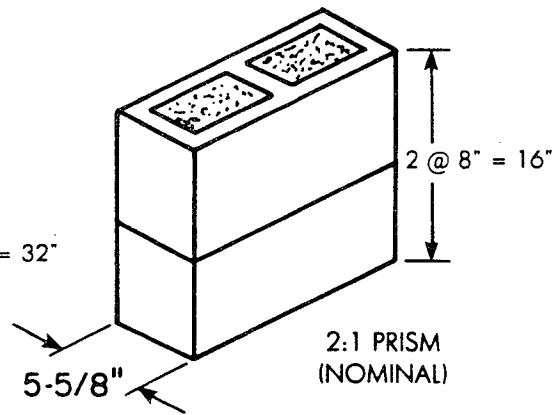
8 x 8 x 16 BLOCK



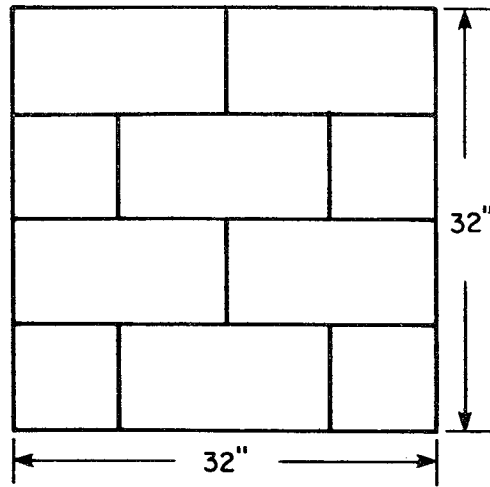
8 x 6 x 16 BLOCK



5:1 PRISM (NOMINAL)

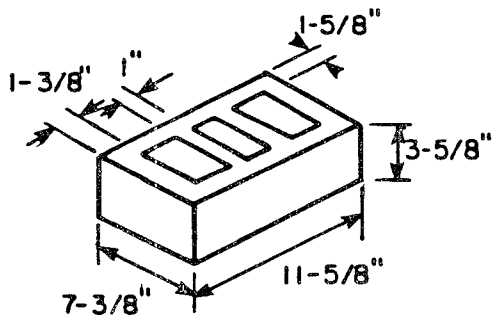


2:1 PRISM (NOMINAL)

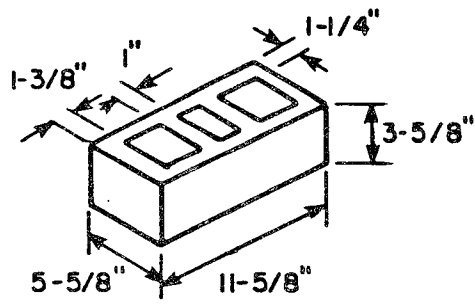


SQUARE PANEL (FRONT VIEW)

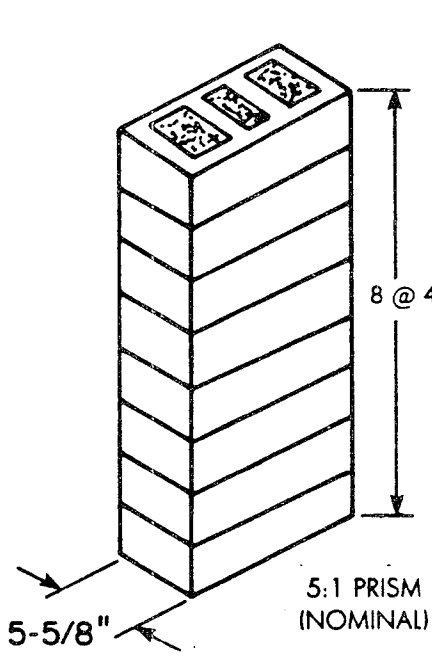
FIG. 2.2(a) BLOCK UNITS AND SPECIMEN TO DETERMINE MATERIAL PROPERTIES (HCBL)



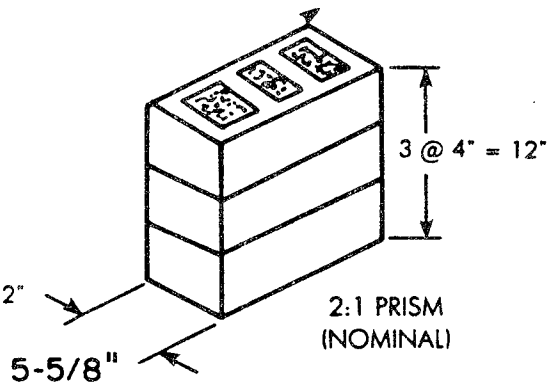
4 x 8 x 12 BRICK



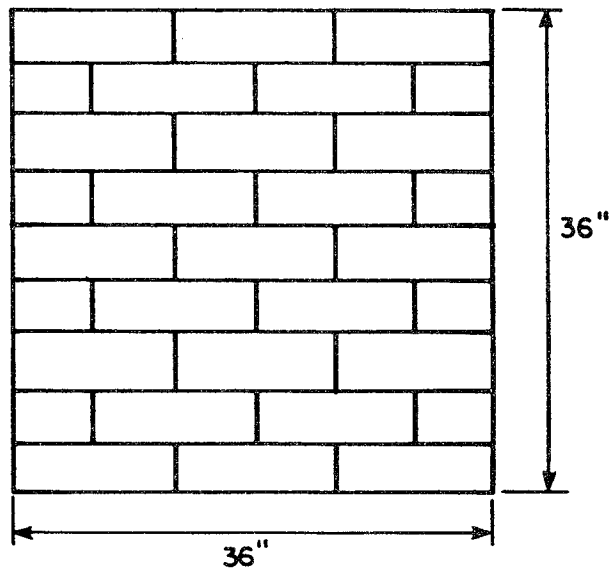
4 x 6 x 12 BRICK



5:1 PRISM
(NOMINAL)



2:1 PRISM
(NOMINAL)



SQUARE PANEL (Front View)

FIG. 2.2(b) BRICK UNITS AND SPECIMEN TO DETERMINE MATERIAL PROPERTIES (HCBR)

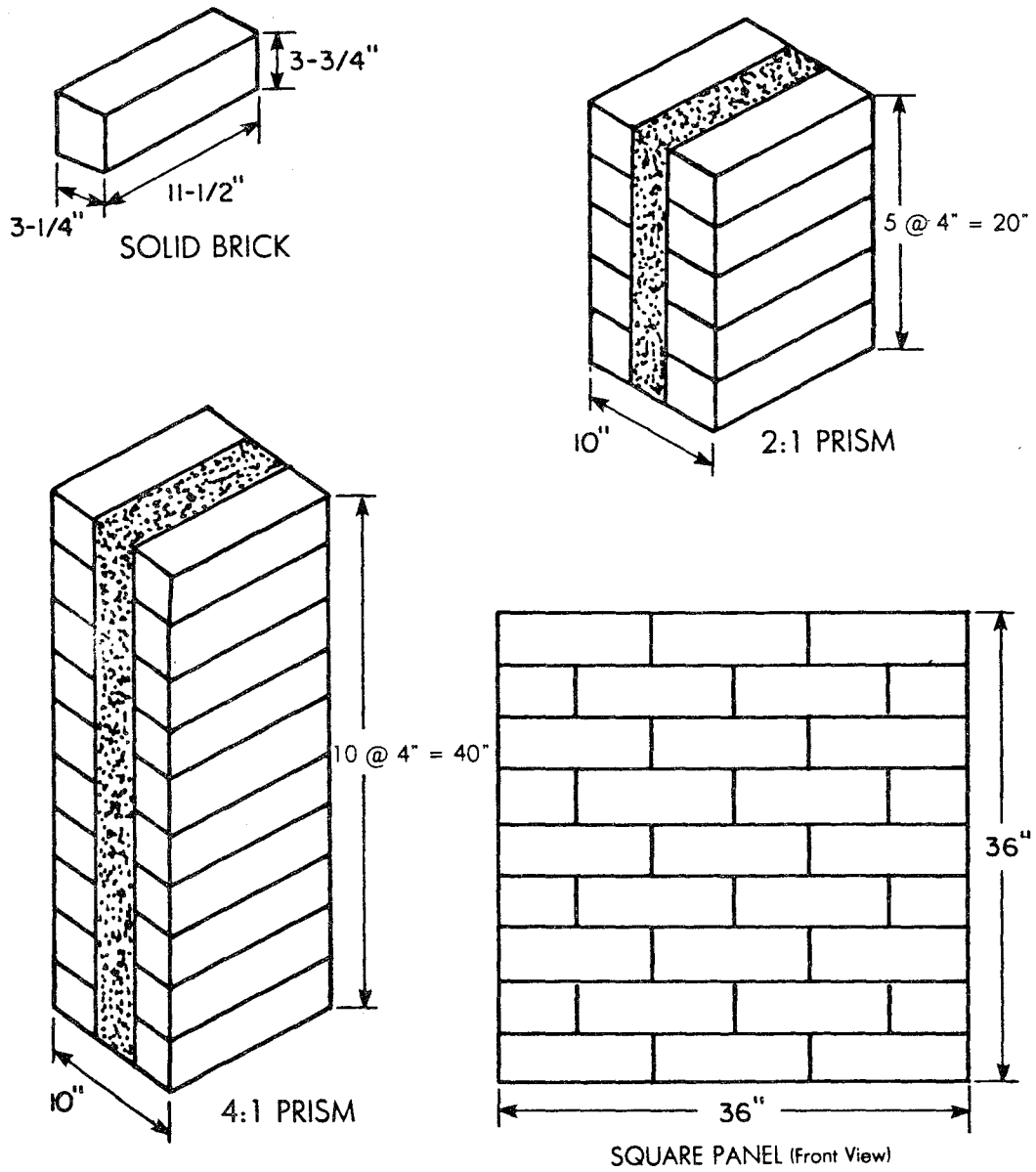


FIG. 2.2(c) BRICK UNITS AND SPECIMEN TO DETERMINE MATERIAL PROPERTIES (CBRC)



FIG. 2.3 CONSTRUCTION OF TEST SPECIMEN

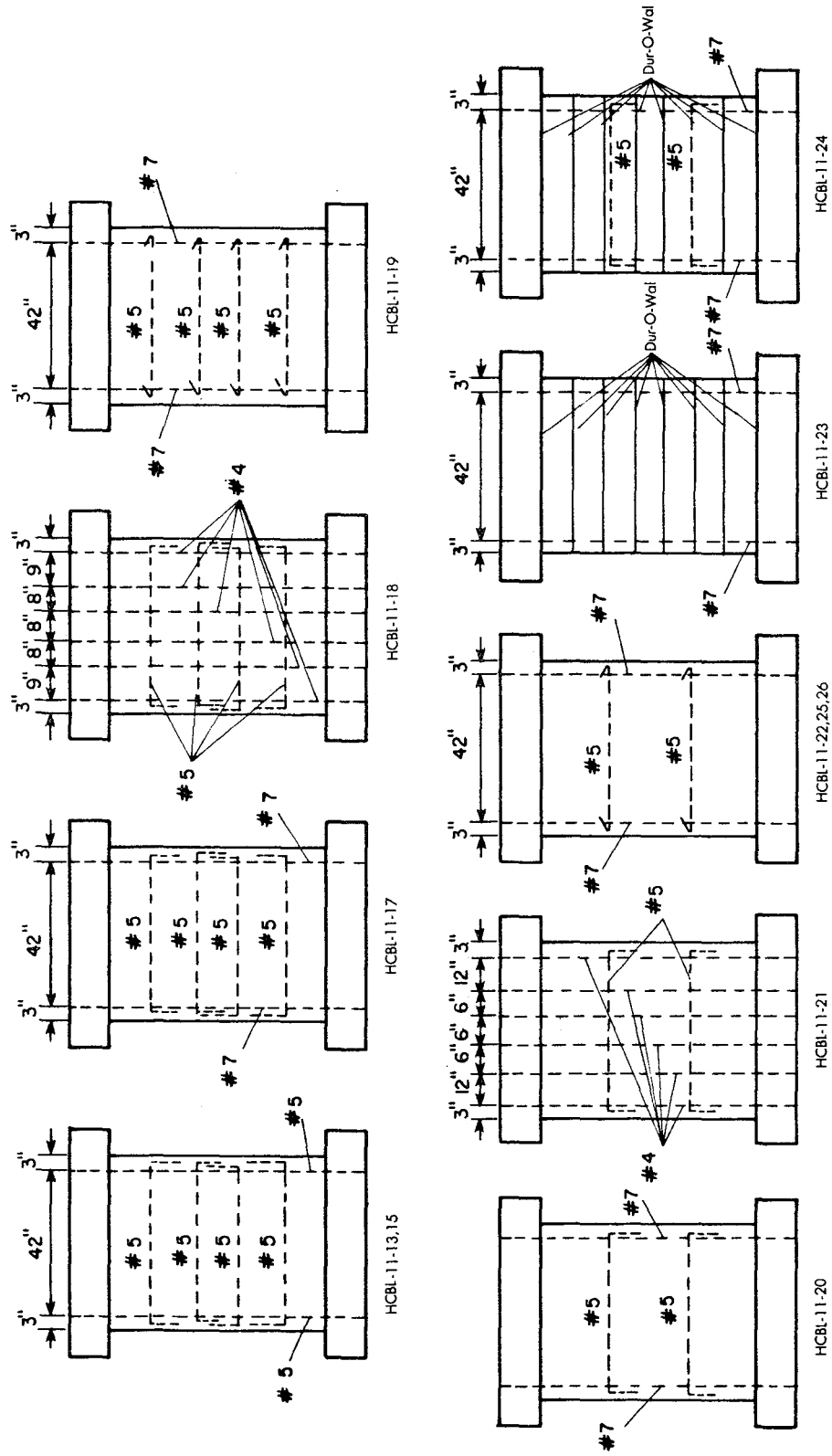


FIG. 2.4(a) REINFORCING STEEL ARRANGEMENTS FOR HOLLOW CONCRETE BLOCK PIERS (HCBL)

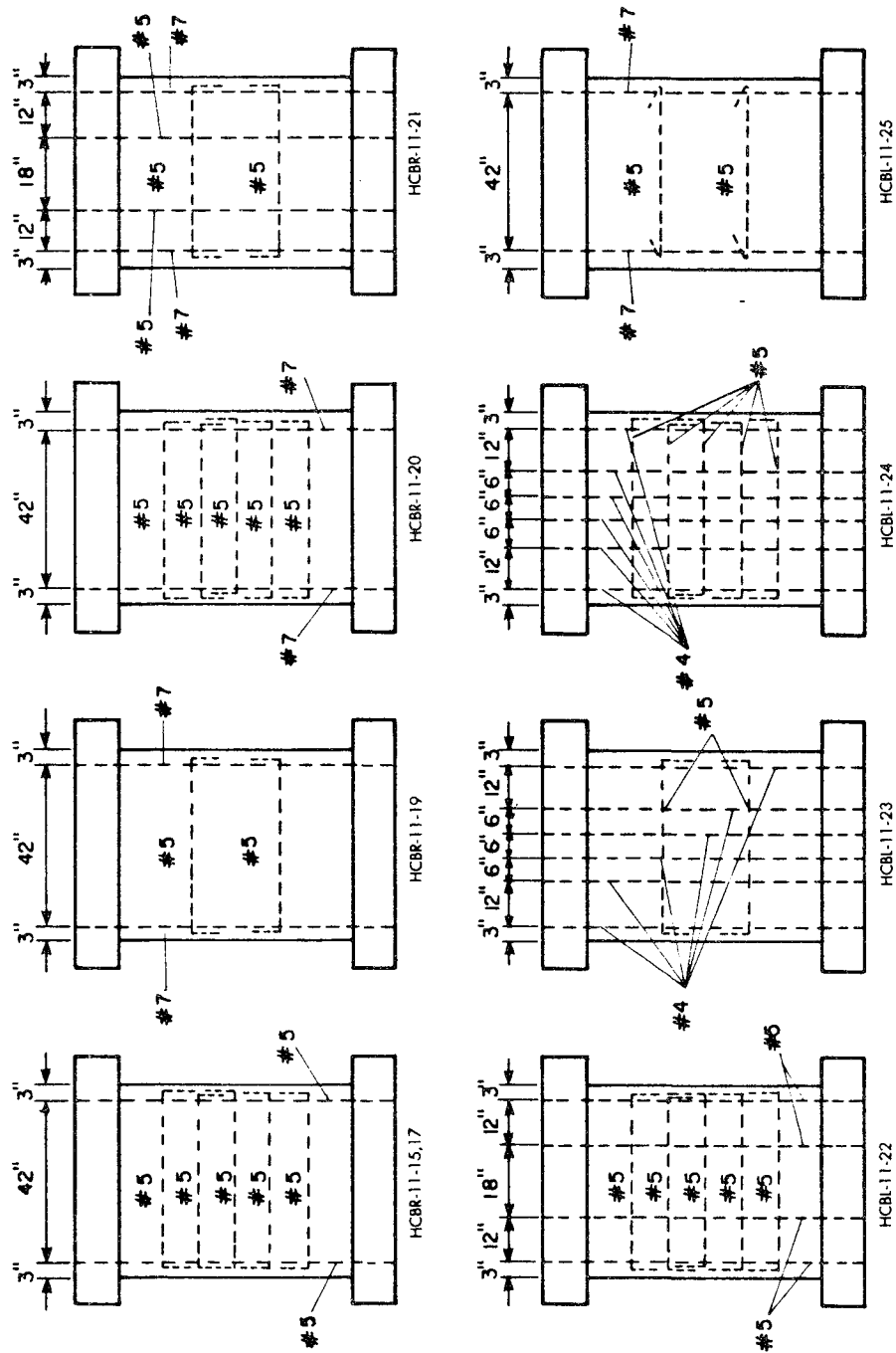


FIG. 2.4(b) REINFORCING STEEL ARRANGEMENTS FOR HOLLOW CLAY BRICK PIERS (HCBR)

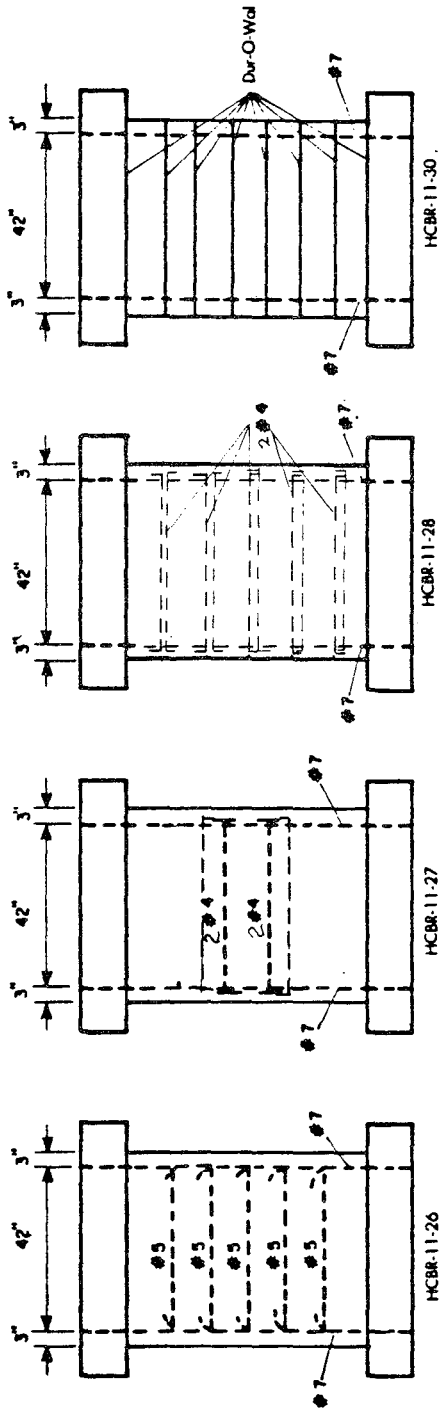


FIG. 2.4(b) (CON'T.) REINFORCING STEEL ARRANGEMENTS FOR HOLLOW CLAY BRICK PIERS (HCBR)

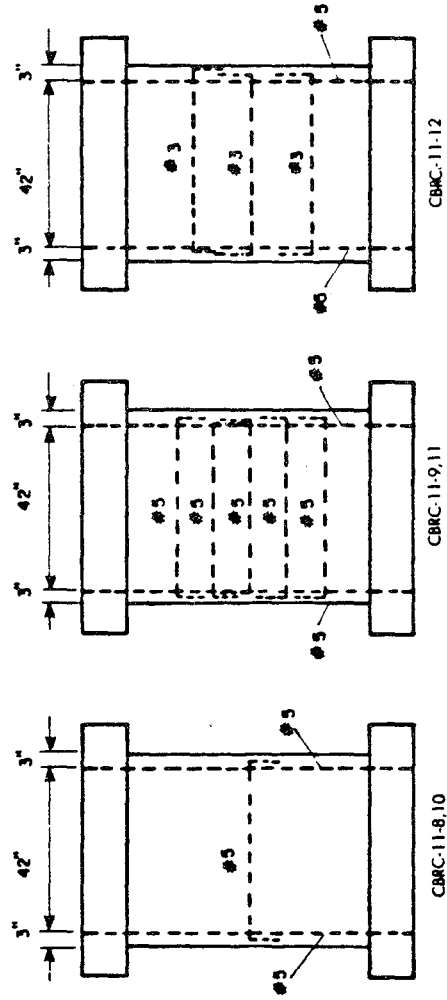


FIG. 2.4(c) REINFORCING STEEL ARRANGEMENTS FOR GROUTED CORE BRICK PIERS (CBRC)

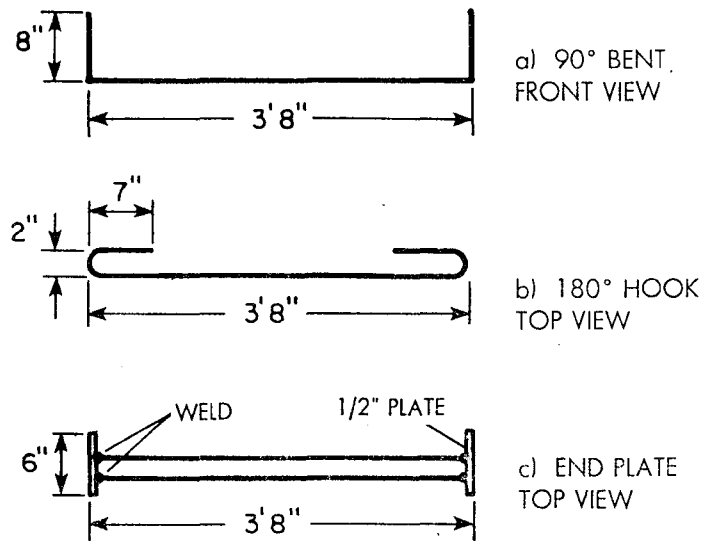


FIG. 2.5 TYPES OF ANCHORAGE OF HORIZONTAL BARS

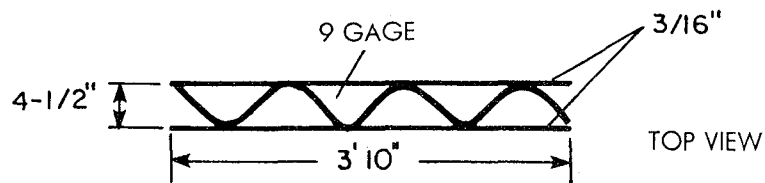


FIG. 2.6 WIRE-MESH REINFORCEMENT IN HORIZONTAL JOINTS (DUR-O-WAL)

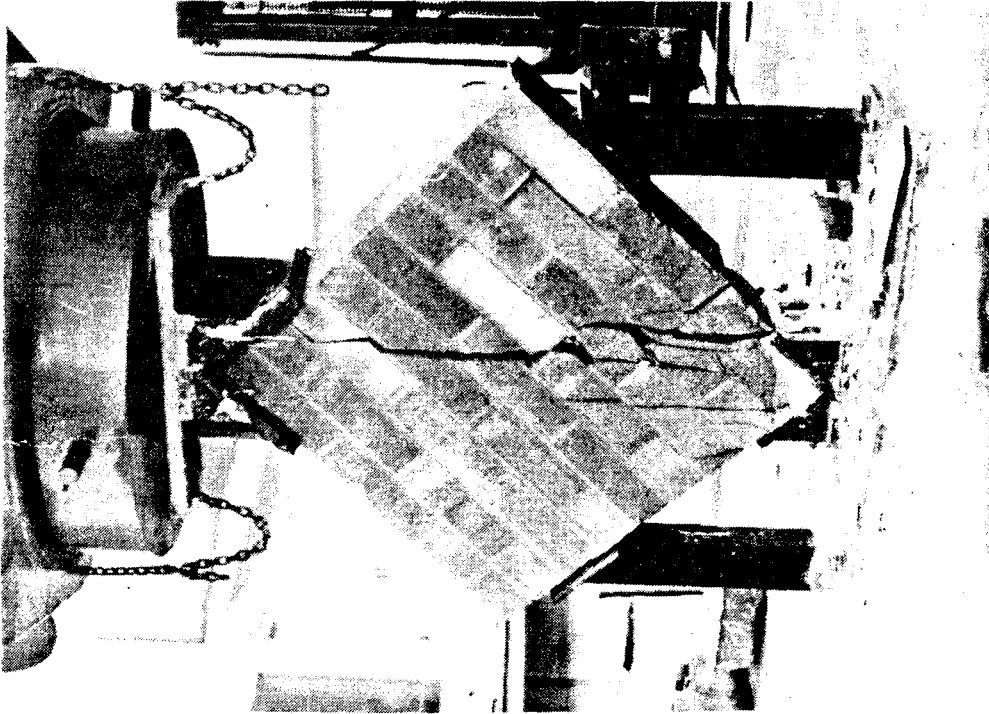


FIG. 2.8 SQUARE PANEL TEST

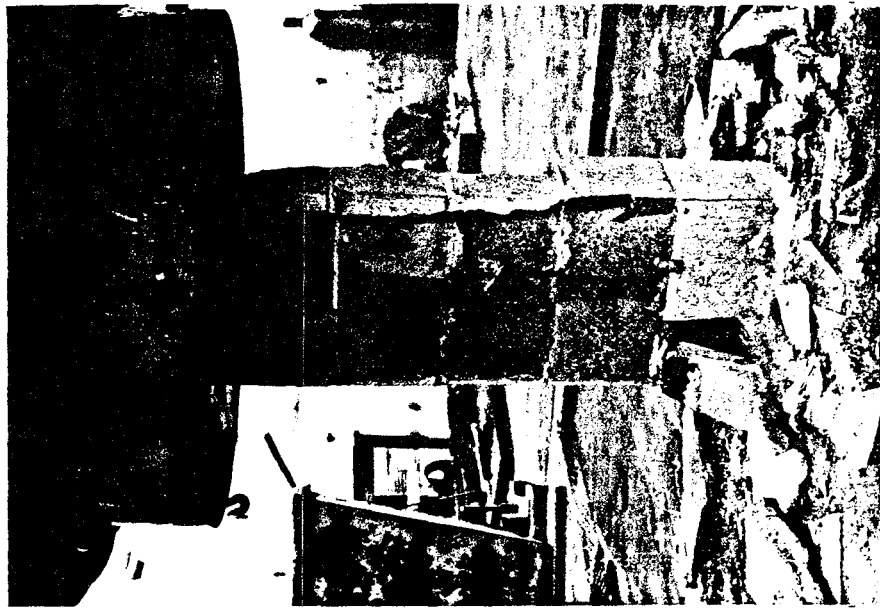


FIG. 2.7 PRISM TEST

SECTION 3 TEST EQUIPMENT AND TEST PROCEDURE

In this section a description of the test setup, the instrumentation, and the test control system is provided. The data acquisition and data processing systems are also described and the quasi-static loading sequence is discussed.

3.1 Test Setup

The test setup shown in Figs. 3.1 and 3.2 simulates the displacement and force boundary conditions imposed by floor diaphragms on the piers of a perforated shear wall during earthquake excitation. The test setup consists of a 20 ft. high, heavily braced reaction frame (A-frame) supporting a pair of horizontally acting actuators, a bottom beam and a top beam as shown in Fig. 3.1. The bottom beam is composed of a concrete base and a wide flange steel beam, and the top beam is fabricated from two wide flange steel beams. The top and bottom steel beams provide anchorage for the vertical reinforcing bars of the test specimens, and they have suitable connection holes for bolting the 0.75 inch thick steel plates at the top and bottom of the piers to the steel beams. Prior to the bolting process a layer of hydrostone was placed between the surfaces of the plates and beam flanges, as well as between the top plate and the top course of the pier.

The top and bottom beams simulate the action of rigid floor diaphragms in actual masonry construction. They are connected by two vertical actuators located 10 ft. - 7 in. apart (Fig. 3.1), which have a double purpose in the test setup. First, they provide vertical bearing loads similar to the gravity loads experienced by the piers in an actual structure, and also they develop a reaction couple which prevents

rotation of the top beam, thus providing a fixed-end condition during the test. The vertical actuators are a significant improvement to the test setup used in the prior single pier test program [1.2.3] in that the actuators are programmed to maintain a constant bearing load independent of the lateral displacement.

The maximum load that can be developed by each of the horizontal actuators is 75 kips, using a hydraulic pressure of 3,000 psi. The maximum stroke of the actuators is ± 6 inches. The servovalves of the horizontal actuators have a flow capacity of 200 gpm, which provides a maximum piston velocity of 26 in./sec.

Each of the vertical actuators can provide a maximum load of 125 kips and a maximum stroke of ± 18 inches. The flow capacity of the servovalves coupling with the vertical actuators is 5 gpm and the maximum piston velocity that can be developed at this flow rate is 0.36 in./sec. These values are adequate in view of the quasi-static conditions used to apply the horizontal displacements.

3.2 Instrumentation

The loads applied by the pairs of horizontal and vertical hydraulic actuators were measured by using pre-calibrated load cells. The stroke readings from the horizontal actuators were taken by LVDT's (linear variable differential transformers) built into the actuators.

Each pier was instrumented as indicated in Fig. 3.3. DCDT's (direct current differential transformers) H_1 , H_2 , H_3 and H_4 were attached to an external reference frame in order to measure the lateral deformation of the pier and the spandrel beams during each sequence of loading. The difference between the measured values H_2 and H_3 indicates the relative lateral deflection of each pier. The differences between the measured values H_1 and H_2 , and H_3 and H_4 indicate the deformation of the portions of masonry bounding, respectively, the top and bottom of each pier. In addition, wire-potentiometers were attached to the reference frame to read the lateral displacements at the top and bottom of the piers, and thus act as a back-up measurement system for H_2 and H_3 .

DCDT's D_1 and D_2 measured changes in the distance between points along the diagonals of the pier. DCDT's V_1 and V_2 measured the vertical displacement of the top spandrel beam along both edges of the pier and were used to control the rotation of the top spandrel beam as well as to measure the axial deflections of the piers during the loading sequences.

3.3 Control, Data Acquisition, and Data Processing Systems

The flowchart of the control and data acquisition systems is given in Fig. 3.4. The control system which is shown in Fig. 3.5 consists of two controllers for the horizontal actuators, two controllers for the vertical actuators and a transfer box. The components of the data acquisition system, shown in Fig. 3.6, are an analog to digital (A-D) converter, a high speed scanner and multiplexer and a computer with storage capability. The functions of the components constituting both systems (marked from 1 to 6 in Fig. 3.4) are explained briefly in the following paragraphs.

1. Signal Conditioners : These were used for conditioning the transducer signals. Their function is to impress an excitation voltage on the transducers (force and displacement), to receive their output voltage signals, and then to generate a high level signal by amplifying and filtering the output voltage from the transducers.
2. Controllers for the Horizontal Actuators : Both of these controllers were programmed to generate identical signals on the horizontal actuators. The main components are two MTS 443 controllers with control and counter panels, and a function generator. The system has a self-adjusting feedback system.

The actuators are commanded by the function generator which sends a displacement command signal to the electro-hydraulic servovalves which convert it to hydraulic pressure, and consequently to an actuator output stroke. The signal

conditioners in the controllers then receive the actual load and stroke readings from the load cells and LVDT's attached to the horizontal actuators. By selecting the actual actuator stroke as the feedback, the feedback system compares it to the command signal (input stroke) and, if they differ, generates a modified command signal to minimize this difference. The feedback loop operates until the feedback equals the program input command. Then the function generator sets a new program input and the procedure is repeated.

The load and stroke readings are sent to the A-D converter simultaneously from the signal conditioners of each controller.

3. Transfer Box : This box receives the current horizontal load readings from the conditioners of the horizontal actuator controllers, adds them and multiplies the sum by h'/a , where h' is the vertical distance between the horizontal actuators and the midheight of the pier, and a is the horizontal distance between the vertical actuators, as shown in Fig. 3.7. The value thus computed is the force component V_C of the reaction couple that is applied by the vertical actuators to the top beam to prevent its rotation (Fig. 3.7).

4. Controllers for the Vertical Actuators : In these tests the vertical actuators are load controlled using two MTS 406 controllers which control either the load or stroke of the actuators. The controllers have program inputs equal to $N/2 \pm V_C$ where N is the total bearing load acting on the pier. The positive sign on V_C indicates added tension in the actuators (compression on the pier) - see Fig. 3.7. The signal defining the current value of V_C is received from the transfer box and $N/2$ is set initially and kept constant throughout the test run. The operation of the feedback loop is similar to that of the horizontal actuator controllers, except the load is selected

as feedback instead of stroke.

The vertical load readings are simultaneously sent to the A-D converter from the signal conditioners in the controllers.

5. Analog to Digital Converter and High Speed Scanner : The A-D converter receives the high-level analog voltage signals from the instrumentation channels and converts them to digital values. The high speed scanner reads the digitized values from all channels one at a time with a burst reading rate of 100,000 readings per second. The scanner is then held inactive until it is required to make another sweep through all the channels and take readings. The overall scanning frequency, i.e. the burst reading and inactive period, during this test program was specified at two readings per second per channel. Higher scanning rate was not necessary because of the low excitation frequency (quasi-static) used to run the tests.

6. Computer and Storage Medium : The computer used for data acquisition and reduction is the DEC LSI-11 model. A screen terminal with graphic display capability is connected for interactive use (Fig. 3.6). Two storage media, a permanent hard disk unit of 20 megabytes storage capacity and a floppy disk recording unit, are controlled by the computer.

Three computer programs are used for data acquisition and reduction. The first one is the data acquisition program. This program is used in calibrating the instruments, it then sets up the sampling schedule and records the data at the specified scanning frequency and for the specified duration. The program has a graphics mode which enables the user to view, on the graphics display screen, the data recorded from any selected data channel immediately after acquisition is completed. The

other two programs are used to process the original bulk data, and to reduce them to a form suitable for interpretation (plots, tables, etc.).

3.4 Loading Sequence

Each pier was subjected to a series of displacement controlled, inplane shear loads. The full sequence of loading consisted of three sinusoidal cycles of loading at a specified horizontal actuator displacement amplitude. The amplitude was gradually increased; the full loading sequence is given in Table 3.1. During and after each stage (one set of three displacement cycles at the same amplitude), the walls were visually inspected, and the crack patterns identified and photographed. The sinusoidal cycles were applied at a frequency of 0.02 cycles per second throughout the test program.

The duration of each test was 3-4 hours. The tests were usually terminated when the shear strength of the piers had dropped sharply usually accompanied by excessive opening of major diagonal cracks.

Because of the flexibility of the reaction frame and other load transferring devices, the lateral displacements actually experienced by the pier were always less than the actuator stroke. This difference was smaller towards the end of the test when the lateral stiffness of the pier had attained its lowest value. There was also a slight difference between the maximum loads developed during the push and pull half cycles because of the different types of stress acting on the bolting system and the different pier stiffnesses associated with nonsymmetrical crack patterns.

**TABLE 3.1
LOADING SEQUENCE**

STAGE*	INPUT DISPLACEMENT AMPLITUDE (IN.)	STAGE*	INPUT DISPLACEMENT AMPLITUDE (IN.)
1	0.02	12	0.35
2	0.04	13	0.40
3	0.06	14	0.45
4	0.08	15	0.50
5	0.10	16	0.55
6	0.12	17	0.60
7	0.14		
8	0.16	18	0.70
		19	0.80
9	0.20	20	0.90
		21	1.00
10	0.25	22	1.10
11	0.30	23	1.20

* Each stage consists of three sinusoidal cycles at the amplitude shown

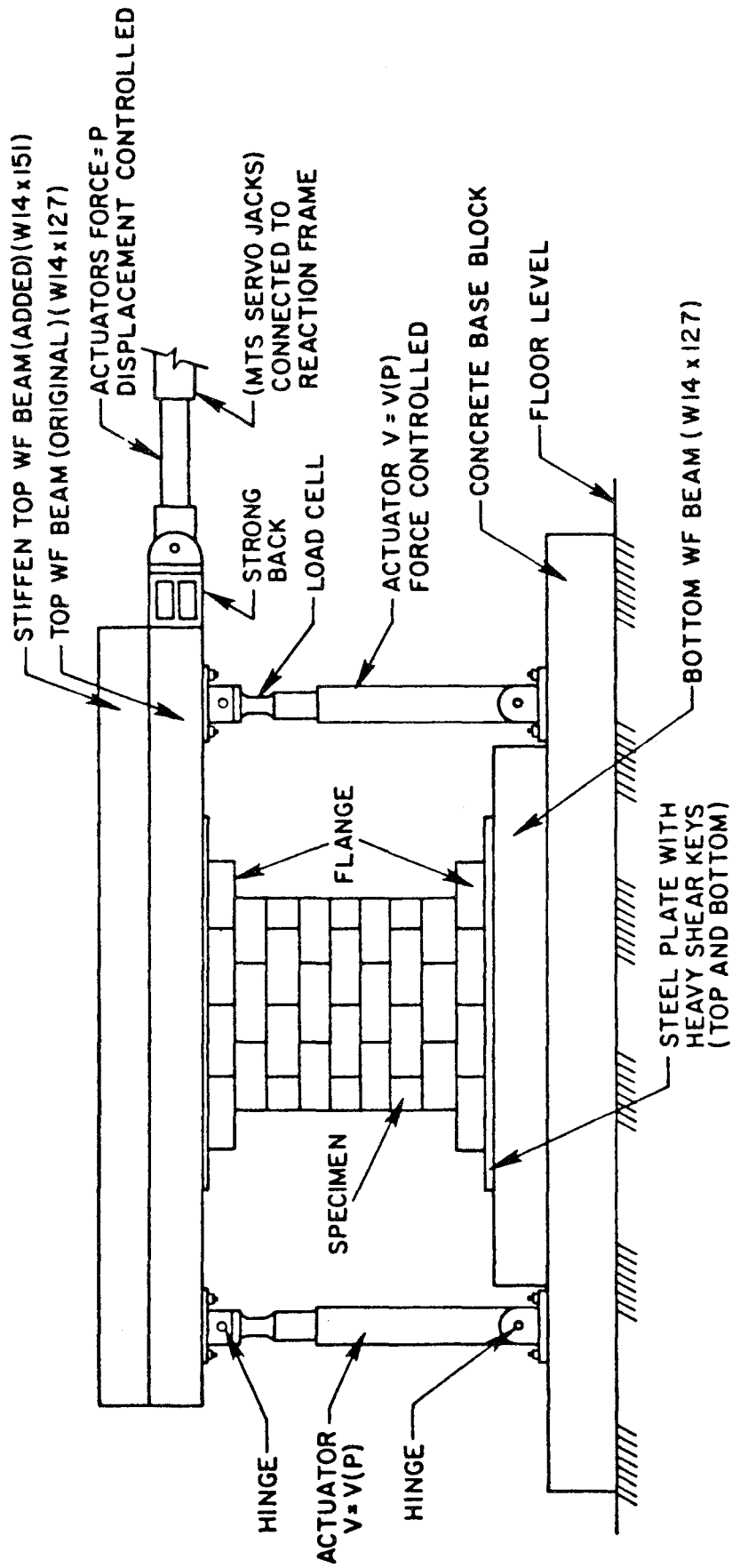


FIG. 3.1 SCHEMATIC ILLUSTRATION OF MASONRY PIER TEST SETUP

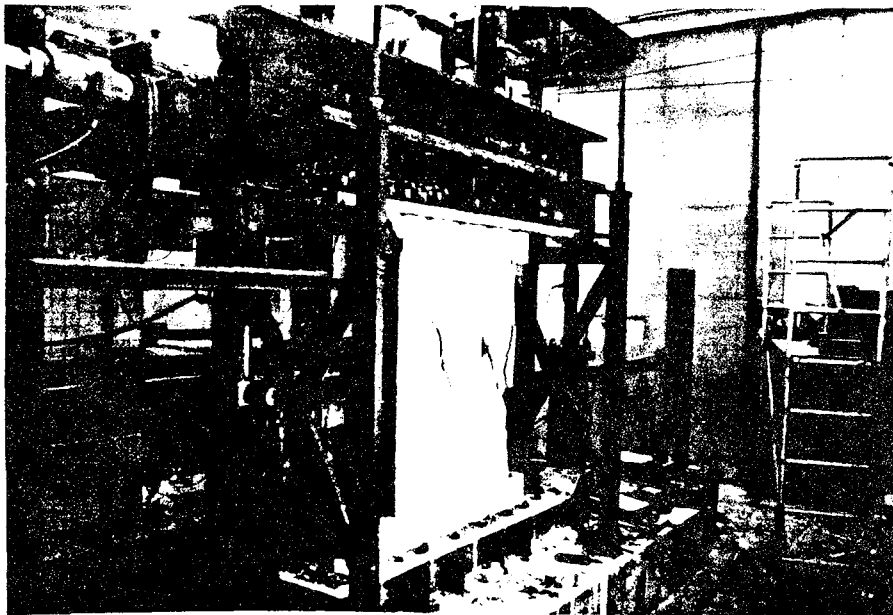
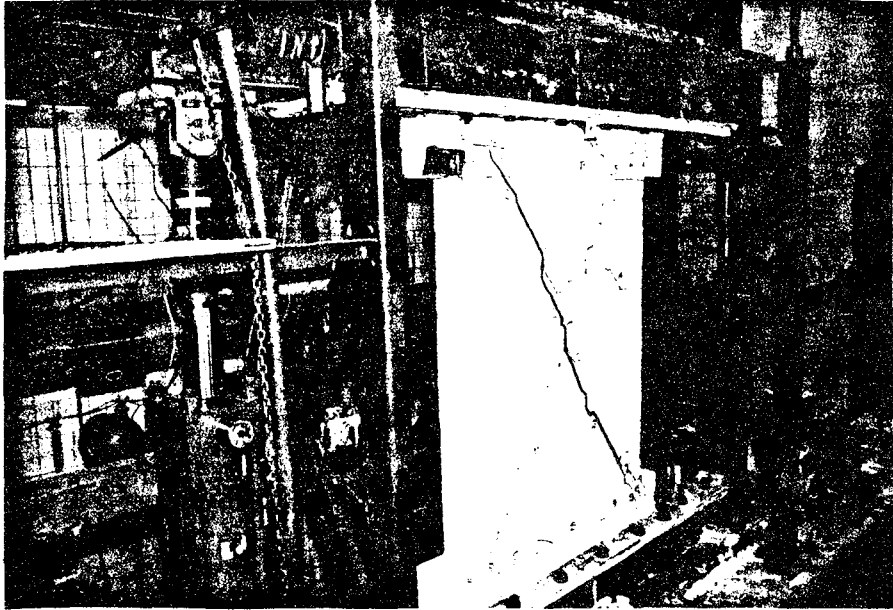
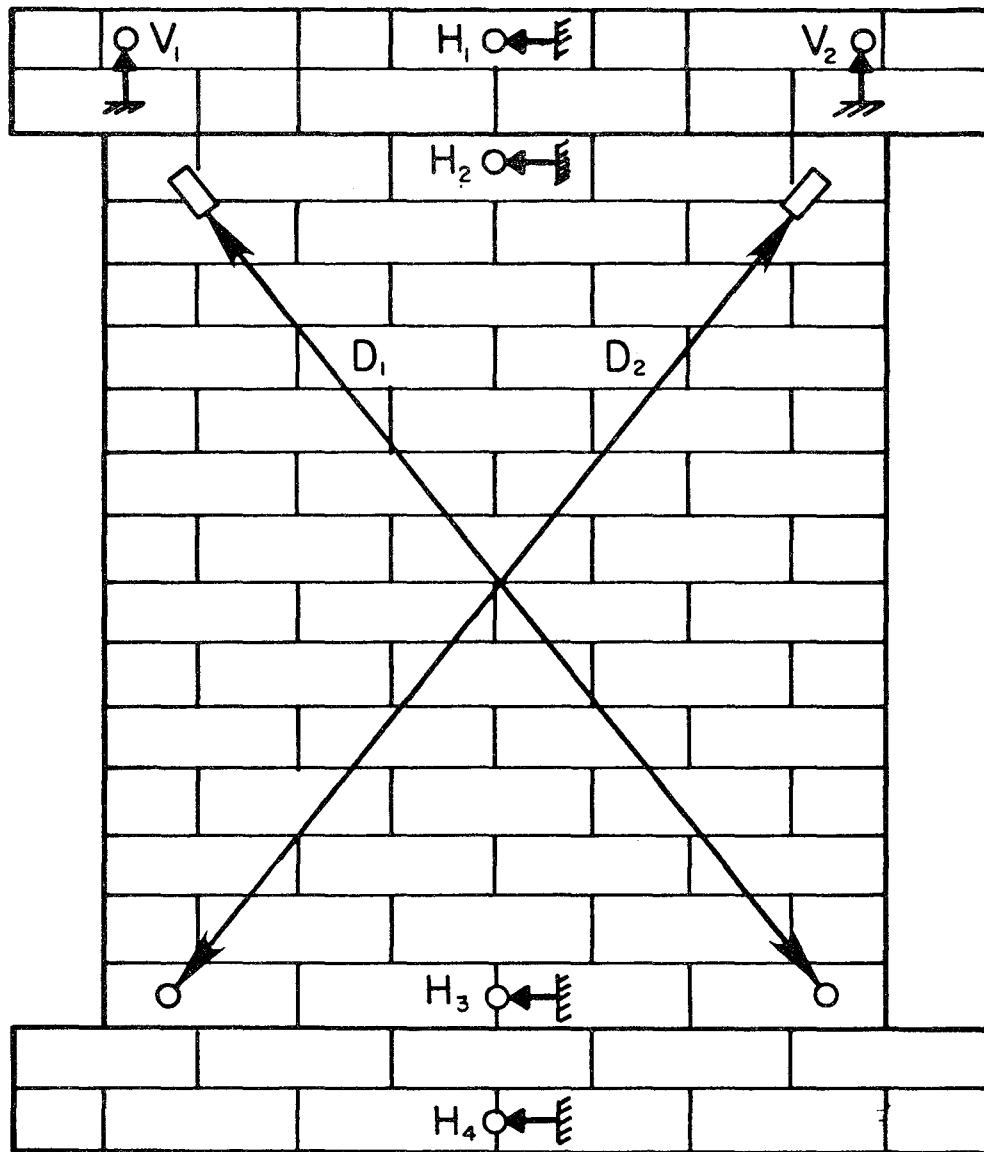


FIG. 3.2 PHOTOGRAPHS OF THE MASONRY PIER TEST SETUP



○ ← → □ INSTRUMENTATION ATTACHED TO PIER

○ ← → ▨ INSTRUMENTATION ATTACHED TO REFERENCE FRAME

FIG. 3.3 PIER INSTRUMENTATION

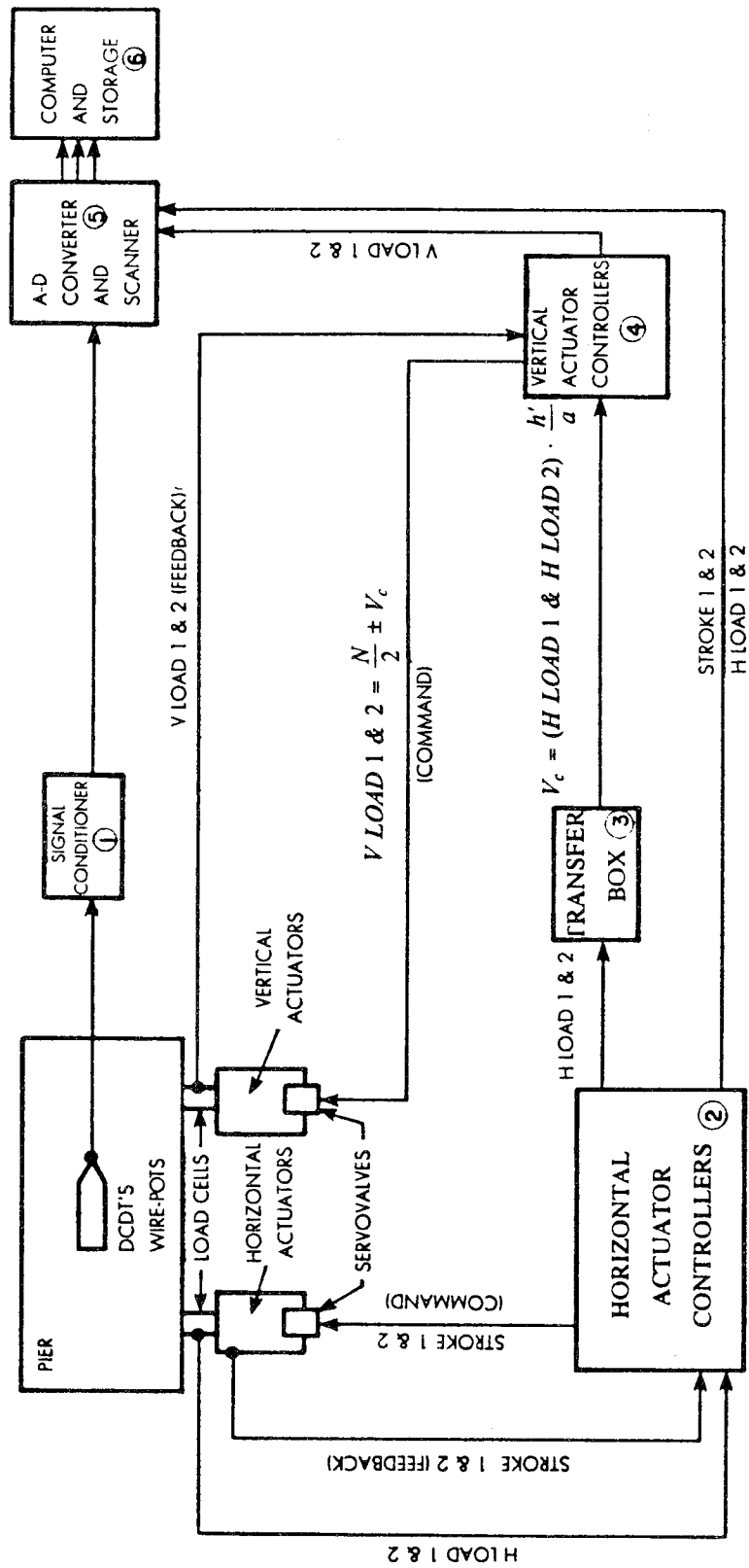


FIG. 3.4 FLOWCHART OF CONTROL AND DATA ACQUISITION PROCESSES

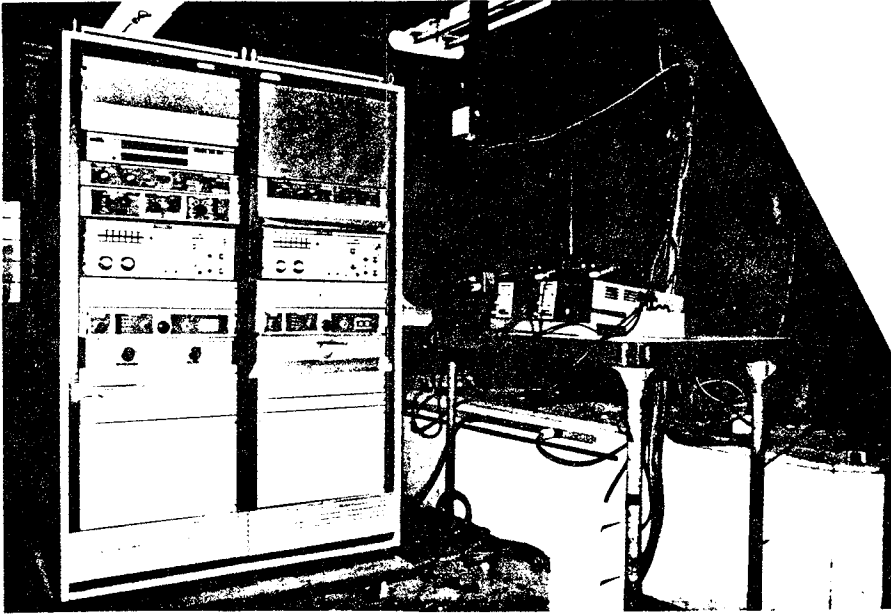


FIG. 3.5 TEST CONTROL CONSOLES

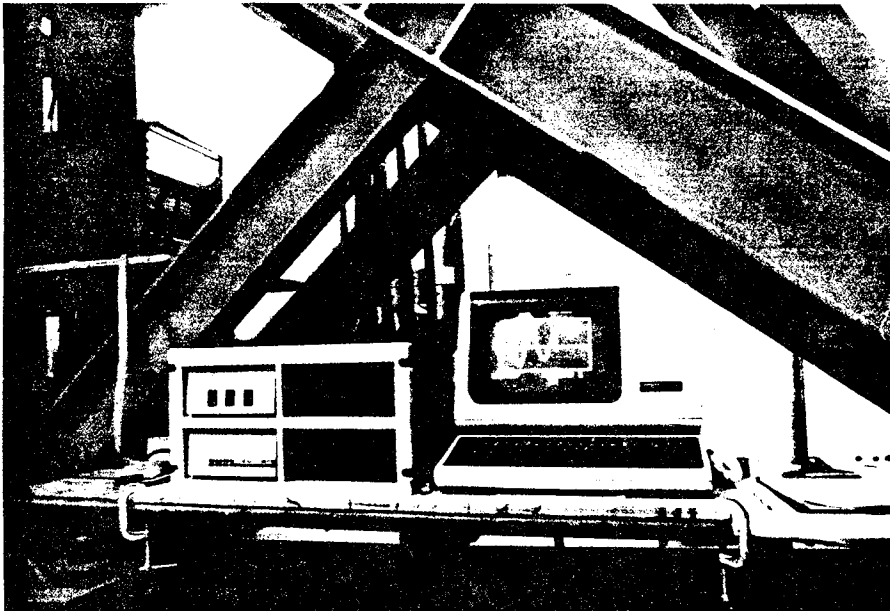
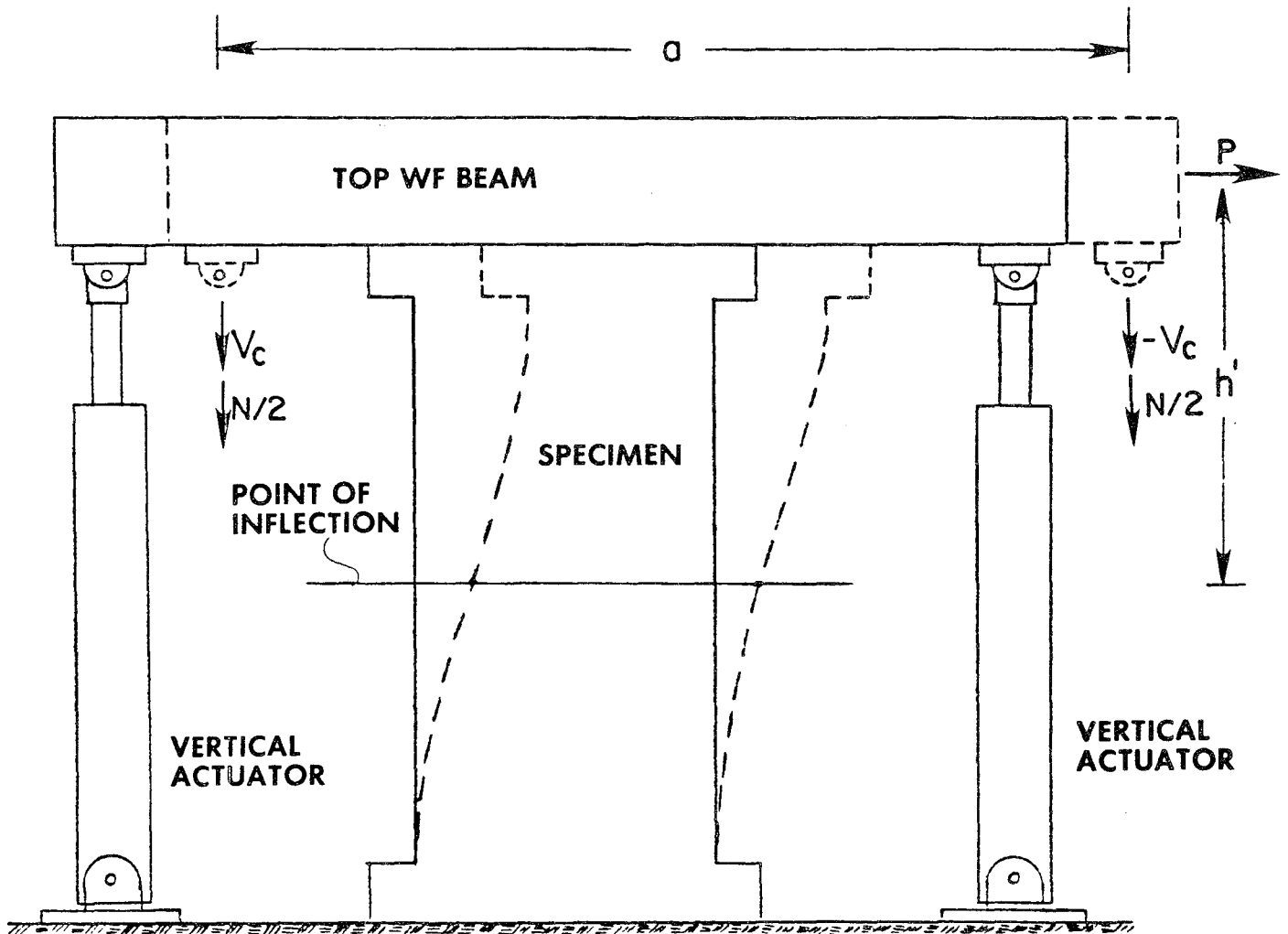
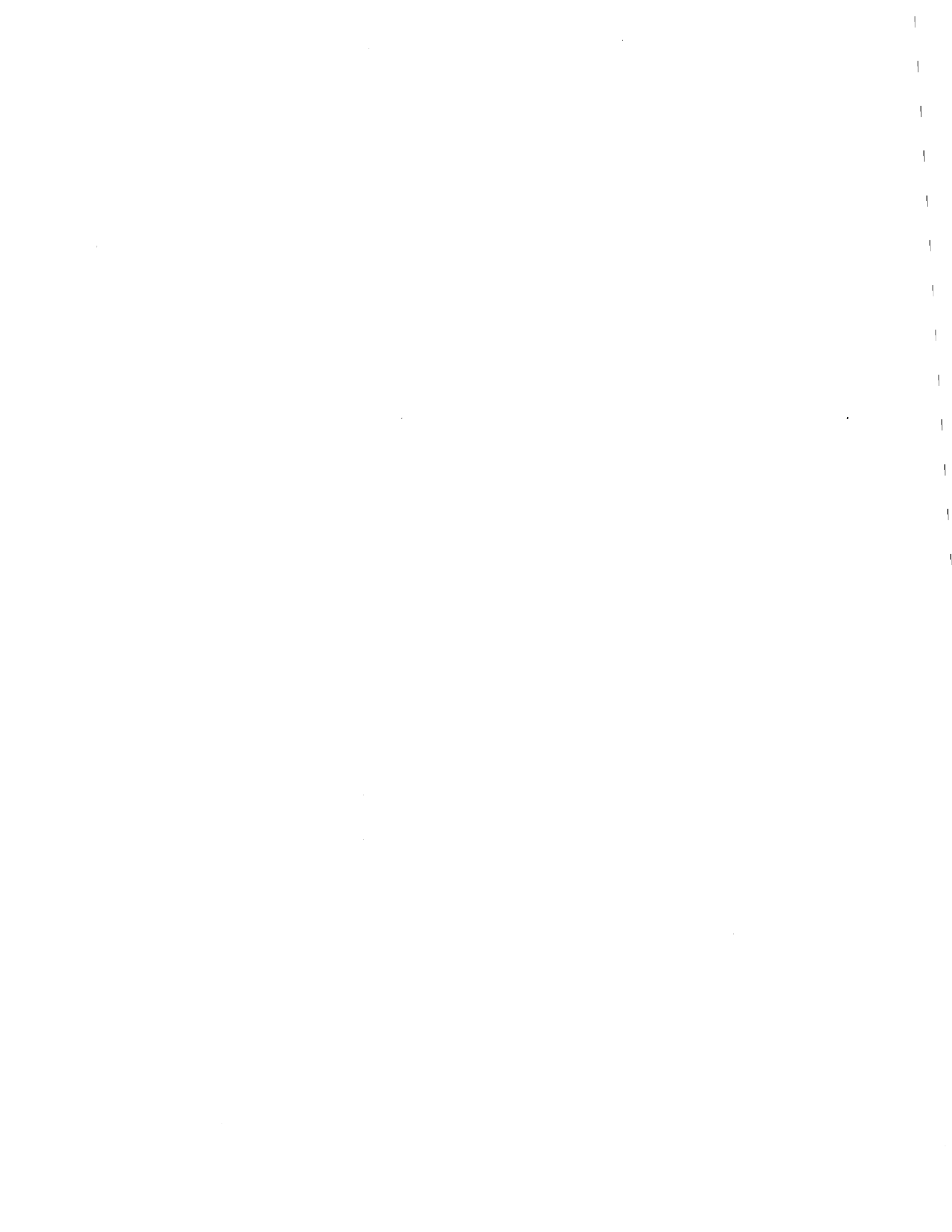


FIG. 3.6 DATA ACQUISITION SYSTEM



VERTICAL ACTUATORS ARE FORCE CONTROLLED: $V_c = \frac{Ph'}{a}$

FIG. 3.7 FREE BODY DIAGRAM FOR THE TOP BEAM



SECTION 4 TEST RESULTS

The experimental results concerning load-displacement characteristics of the thirty piers (thirty two tests) having height-to-width ratios of one are presented in the form of hysteresis envelopes, stiffness degradation and load degradation properties. In addition, a sequence of photographs of the successive crack patterns is given for each test. An explanation of how each of the graphs was obtained and the meaning of the terms used above is included in Section 4.2. A complete presentation of the figures and photographs not included in this section has been arranged by test numbers and is included in Appendix A.

Data on the cracking strength, ultimate strength, deformation and ductility indicators for each test are listed in Tables 4.1(a), 4.1(b) and 4.1(c). Information on the reinforcement and bearing load of the specimens during each test is also included in these tables so that correlations can be made between the results and the relevant parameters. Discussion of the test results is presented in Section 5.

4.1 Modes of Failure

The sequence of horizontal displacements was continued until failure stage for twenty seven of the thirty test specimens. These specimens displayed the following four different failure modes:

1. A shear mode (diagonal tension)
2. A shear-sliding mode
3. A sliding mode
4. A flexural mode.

The failure mode for each of the tests is indicated in the last column of Tables 4.1(a), 4.1(b) and 4.1(c). A direct relationship was observed between the failure mode, and the strength and inelastic response characteristics of each of these specimens. Fundamental characteristics of the above mentioned failure modes are defined in the subsections that follow.

The remaining three piers, HCBR-11-17, CBRC-11-8 and CBRC-11-11 were subjected to very low bearing loads to induce the flexural mode of failure; they were displaced until and slightly beyond yielding of the vertical reinforcing bars. The loading was then halted in order to preserve the specimens for another sequence of loading, which continued until failure, under a higher level of bearing loads. Unfortunately, specimen CBRC-11-11 was accidentally damaged in the interim between the low and high bearing load tests, and therefore was only tested under a low bearing load. It was observed that the failure characteristics of the re-loaded specimens, labeled as HCBR-11-17S and CBRC-11-8S, were significantly affected by the flexural cracking which occurred during the previous, low bearing load cycles.

4.1.1 Shear Failure

Shear failure of the piers was characterized by the initiation of visible cracking along the pier diagonals, when the principal tensile stresses exceeded the tensile strength of masonry under the increasing imposed horizontal displacements. Whenever there was adequate horizontal reinforcement with proper anchorage in the specimen, redistribution of the stresses throughout the pier diagonals was achieved after the initiation of diagonal cracking. Accordingly, the initial

diagonal cracks did not open under increasing horizontal loads, but instead new sets of diagonal cracks formed and gradually spread all over the pier diagonals, accompanied by high energy dissipation and ductile behavior. This type of shear failure is called "ductile shear failure". Failure occurred gradually in this case as the strength of the pier deteriorated under cyclic horizontal loading, and partial crushing of the masonry at severely cracked portions of the pier diagonals finally led to complete loss of strength. A typical specimen exhibiting ductile shear failure is shown in Fig. 4.1(a).

When the amount and/or anchorage of horizontal reinforcement was not adequate to provide the transfer of tensile stresses across the diagonal cracks initiating failure, these cracks opened extensively, resulting in a major X-shaped diagonal crack pair, leading to a relatively sudden and destructive failure (Fig. 4.1(b)). This type of failure is called "brittle shear failure". The piers experienced less significant post-cracking deformation and energy dissipation in the brittle shear mode.

The shear failure displayed by the grouted core clay brick (CBRC) piers was accompanied by a separation of the brick wythes from the core at the final stage of failure (Fig. 4.2).

4.1.2 Shear-Sliding Failure

In general a shear-sliding mode of failure was observed for specimens with higher horizontal reinforcement ratios. The cracking began at the ends of the top and bottom bedjoints where the tensile stresses due to flexure were greatest. Diagonal cracking also began at later stages as the horizontal load increased, and spread over the web while the earlier cracks at the bedjoints propagated and extended over the full cross-section of the specimen (Fig. 4.3(a)). Final failure was due to crushing of the masonry at the compression toes and sliding of the pier along the top or bottom bedjoint experiencing crushing under lateral load reversals. After the sliding started, the zone of crushing quickly spread over the full horizontal cross-section and crushed masonry spalled away from the pier leaving a wide horizontal opening, as shown

in Fig. 4.3(b).

There are similarities between the shear-sliding failure of the masonry piers tested, and the flexural failure of slender masonry shear walls. The basic difference, however, comes from the significant contribution of the diagonal cracks, extending through the top and bottom ends of the pier, to the weakening and further crushing of the masonry along the top or bottom horizontal cross-section. Figure 4.3(a) shows the concentration of diagonal and flexural tensile cracks at the bottom end prior to the crushing stage; this is followed by complete crushing at the base, shown in Fig. 4.3(b). It is also recognized that the ultimate strengths of those piers that failed in the shear-sliding mode were significantly less than their estimated ultimate flexural strengths, and the ductilities obtained were less than the expected ductilities of walls designed for flexure. In view of these observations, shear-sliding failure is considered to be an independent failure mode.

4.1.3 Sliding Failure

Pure sliding failure was observed for two specimens. These specimens were heavily reinforced horizontally but had relatively small amounts of vertical reinforcing. The main characteristics of the sliding mode of failure is the lack of diagonal tension (shear) cracks on the face of the specimens. The cracks, which are horizontal, initiate at the top and bottom of the piers and propagate through the full cross-section. Gradually the material grinds, and finally crushes, under the vertical load and spalls away at the top or bottom of the pier, leaving the rest of the specimen relatively undamaged.

Figure 4.4 shows the sliding mode of failure.

4.1.4 Flexural Failure

The flexural mode of failure was observed for two specimens although the flexural behavior was purposely present for an additional three piers, i.e. the piers not tested to failure the first time. The common parameter in these tests

was the low bearing load allowing the yielding of the vertical reinforcing bars to take place. Although diagonal shear cracks were prominent on the face of these specimens the ultimate failure mode was by crushing of the compression toes at relatively large displacements. This failure mode is accompanied by relatively high ductilities.

The flexural mode of failure is shown in Fig. 4.5.

4.2 Load-Displacement Characteristics

The strength and deformation characteristics of the piers are summarized in Tables 4.1(a), 4.1(b) and 4.1(c) and the complete test results are presented in Appendix A. The details of the derivation of each of the figures compiled in Appendix A are discussed in the following sections.

- a. Hysteresis Envelopes : Each point on the hysteresis envelope was obtained by averaging the absolute values of the three extreme positive and three extreme negative lateral forces and plotting this average against the average value of the corresponding absolute values of the relative lateral displacement for each displacement stage of the test (Section 3.4). For each stage (three sinusoidal displacement cycles), one point on the hysteresis envelope was obtained. The point corresponding to the stage during which diagonal cracking initiated is indicated with a black dot.

The average cracking strength and the average ultimate strength obtained from the hysteresis envelope are indicated in Tables 4.1(a), 4.1(b) and 4.1(c) in terms of the lateral (shear) forces and shear stresses. (The stress values are computed by dividing the associated force by the cross-section area of the pier.) The "average" ultimate lateral shear force was approximately 94% of the peak shear force which was always

attained at the first cycle of the ultimate displacement stage. The cracking displacement, designated by δ_{cr} , defines the average relative lateral displacement at the beginning of the formation of diagonal tensile cracks, and the maximum displacement, designated by δ_{max} , defines the maximum relative lateral displacement experienced by the pier before failure. The relative displacement at the ultimate shear force level is designated as δ_u . The last column of Tables 4.1(a), 4.1(b) and 4.1(c) lists the observed failure modes of the specimens. The hysteresis parameters are defined graphically in Fig. 4.6.

Hysteresis loops for the complete load-deflection history are not presented.

- b. Load Degradation : The average of the absolute values of the extreme positive and extreme negative lateral forces at the first, second and third consecutive load cycles at each stage were plotted against the corresponding average relative displacements. The family of three curves representing the envelopes of the first, second and third load-deflection cycles at all loading stages gives an indication of the load degradation at a given displacement level during three consecutive cycles of loading.
- c. Stiffness Degradation : The stiffness during a loading cycle was obtained by dividing the average of the absolute extreme positive and extreme negative lateral forces by the corresponding relative displacement. The three stiffness values obtained from the three cycles of loading were averaged and plotted against the corresponding average lateral force obtained from the hysteresis envelope. The stiffness values were also plotted against the average lateral displacement from the hysteresis envelopes. The stiffness degradation curves were truncated at the stage when the ultimate shear strength was attained.

TABLE 4.1 (a)
PIER CHARACTERISTICS AND TEST RESULTS - HCBL

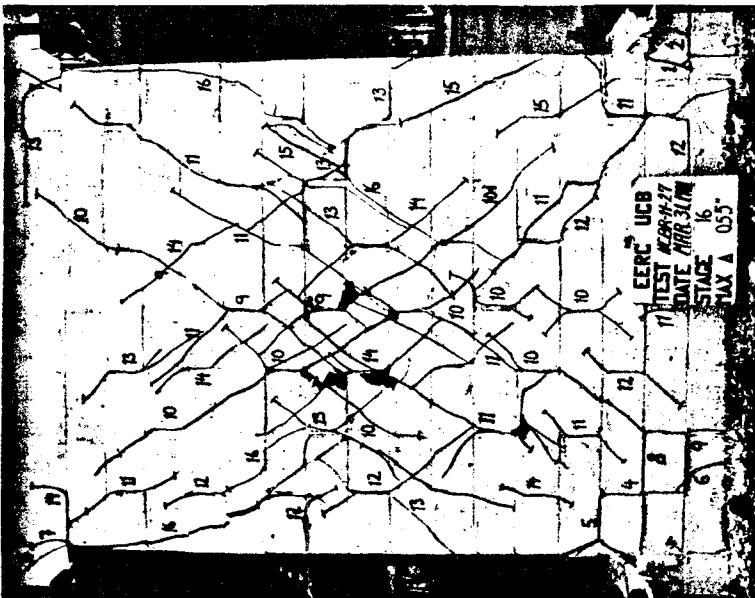
SPECIMEN	VERT REINFORCING		HOR REINFORCING			TOTAL REINF. RATIO $P_v + P_h$	VERTICAL LOAD (KIPS)	VERTICAL STRESS (PSI)
	NO. OF REBARS	$P_v = \frac{A_{vs}}{A_g}$	NO. OF REBARS	$P_h = \frac{A_h}{st}$	TYPE OF ANCHOR.			
HCBL-11-13	2 # 5	0.0017	4 # 5	0.0029	BENT	0.0046	100	273
15	2 # 5	0.0017	4 # 5	0.0029	BENT	0.0046	160	437
17	2 # 7	0.0045	4 # 5	0.0039	BENT	0.0084	108	400
18	6 # 4	0.0044	4 # 5	0.0039	BENT	0.0083	108	400
19	2 # 7	0.0045	4 # 5	0.0039	HOOK	0.0084	68	252
20	2 # 7	0.0045	2 # 5	0.0020	BENT	0.0064	108	400
21	6 # 4	0.0044	2 # 5	0.0020	BENT	0.0064	108	400
22	2 # 7	0.0045	2 # 5	0.0020	HOOK	0.0064	27	100
23	2 # 7	0.0045	D-O-W	0.0010	-	0.0055	108	400
24	2 # 7	0.0045	D-O-W	0.0030	-	0.0075	108	400
25	2 # 7	0.0045	2 # 5	0.0020	BENT	0.0064	68	252
26	2 # 7	0.0045	2 # 5	0.0020	HOOK	0.0064	108	400
SPECIMEN	AVERAGE CRACKING SHEAR FORCE (KIPS)	AVERAGE CRACKING SHEAR STRESS (PSI)	AVERAGE ULTIMATE SHEAR FORCE (KIPS)	AVERAGE ULTIMATE SHEAR STRESS (PSI)	δ_{cr} (INCH)	δ_u (INCH)	δ_m (INCH)	MODE OF FAILURE
HCBL-11-13	81.7	223	103.7	283	0.049	0.264	0.359	S
15	86.5	236	126.1	345	0.044	0.230	0.321	S
17	65.0	241	96.4	357	0.083	0.350	0.374	S
18	80.6	299	96.3	357	0.094	0.207	0.207	S
19	72.8	270	89.0	330	0.055	0.175	0.679	F
20	66.2	245	92.2	342	0.050	0.245	0.245	S
21	59.5	220	87.5	324	0.039	0.210	0.252	S
22	36.2	134	61.3	227	0.047	0.308	0.400	F
23	59.8	222	75.0	278	0.049	0.216	0.265	S
24	59.9	222	95.2	353	0.039	0.244	0.380	S
25	65.9	244	76.9	285	0.048	0.165	0.272	S
26	86.1	319	94.3	349	0.064	0.145	0.227	S

TABLE 4.1 (b)
PIER CHARACTERISTICS AND TEST RESULTS - HCDBR

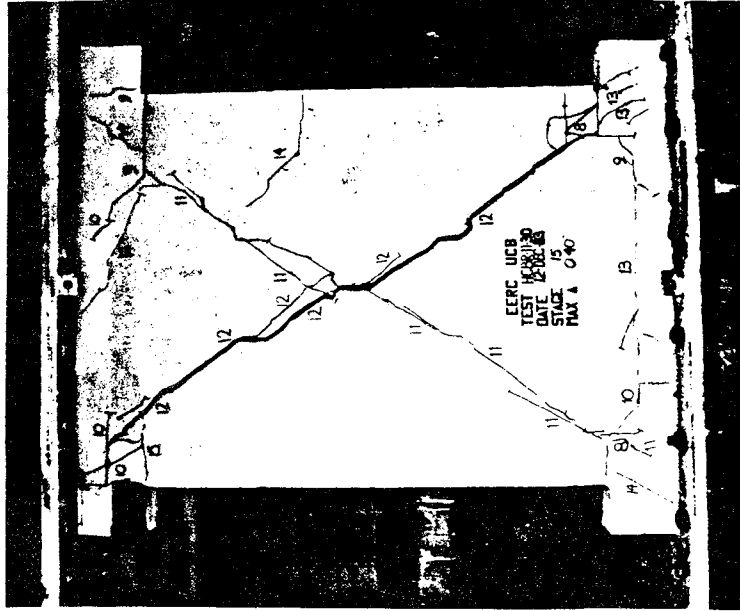
SPECIMEN	VERT REINFORCING		HOR REINFORCING		TOTAL REINF. RATIO $P_v + P_h$	VERTICAL LOAD (KIPS)	VERTICAL STRESS (PSI)
	NO. OF REBARS	$P_v = \frac{A_{vs}}{A_g}$	NO. OF REBARS	$P_h = \frac{A_h}{Sf}$			
HCDBR-11-15	2 # 5	0.0017	5 # 5	0.0037	0.0054	160	452
17	2 # 5	0.0017	5 # 5	0.0037	0.0054	20	56
17S	2 # 5	0.0017	5 # 5	0.0037	0.0054	100	282
19	2 # 7	0.0045	2 # 5	0.0020	0.0064	108	400
20	2 # 7	0.0045	5 # 5	0.0049	0.0093	108	400
21	4 # 5	0.0045	2 # 5	0.0020	0.0065	108	400
22	4 # 5	0.0045	5 # 5	0.0049	0.0094	108	400
23	6 # 4	0.0044	2 # 5	0.0020	0.0063	108	400
24	6 # 4	0.0044	5 # 5	0.0049	0.0093	108	400
25	2 # 7	0.0045	2 # 5	0.0020	0.0064	108	400
26	2 # 7	0.0045	5 # 5	0.0049	0.0093	108	400
27	2 # 7	0.0045	4 # 4	0.0025	0.0070	108	400
28	2 # 5	0.0023	10 # 4	0.0062	0.0085	108	400
30	2 # 7	0.0045	D-O-W	0.0010	0.0055	108	400
SPECIMEN	AVERAGE CRACKING SHEAR FORCE (KIPS)	AVERAGE CRACKING SHEAR STRESS (PSI)	AVERAGE ULTIMATE SHEAR FORCE (KIPS)	AVERAGE ULTIMATE SHEAR STRESS (PSI)	δ_u (INCH)	δ_m (INCH)	MODE OF FAILURE
HCDBR-11-15	100.6	284	118.1	334	0.142	0.169	SL
17	41.0	116	50.9	144	-	-	SL
17S	65.2	184	96.4	272	0.220	0.365	SL
19	58.4	216	72.2	267	0.260	0.313	S
20	54.2	201	75.1	278	0.266	0.357	S/S/L
21	69.1	256	92.2	341	0.330	0.427	S
22	76.8	284	94.0	348	0.306	0.345	S/S/L
23	57.7	214	79.6	295	0.426	0.467	S
24	57.6	213	86.3	320	0.342	0.376	S/S/L
25	76.5	283	85.4	316	0.287	0.609	S
26	68.5	254	84.1	311	0.240	0.379	S/S/L
27	65.0	240	88.4	327	0.270	0.414	S
28	82.7	306	89.2	330	0.444	0.572	S/S/L
30	105.5	391	105.5	391	0.260	0.260	S

TABLE 4.1 (c)
PIER CHARACTERISTICS AND TEST RESULTS - CBRC

SPECIMEN	VERT REINFORCING		HOR REINFORCING			TOTAL REINF. RATIO $P_v + P_h$	VERTICAL LOAD (KIPS)	VERTICAL STRESS (PSI)
	NO. OF REBARS	$P_v = \frac{A_{vs}}{A_g}$	NO. OF REBARS	$P_h = \frac{Ah}{st}$	TYPE OF ANCHOR.			
CBRC-11-8	2 # 5	0.0013	1 # 5	0.0006	BENT	0.0019	20	42
8S	2 # 5	0.0013	1 # 5	0.0006	BENT	0.0019	106	221
9	2 # 5	0.0013	5 # 5	0.0027	BENT	0.0040	160	333
10	2 # 5	0.0013	1 # 5	0.0006	BENT	0.0019	160	333
11	2 # 5	0.0013	5 # 5	0.0027	BENT	0.0040	20	42
12	2 # 5	0.0013	3 # 3	0.0006	BENT	0.0019	160	333
SPECIMEN	AVERAGE CRACKING SHEAR FORCE (KIPS)	AVERAGE CRACKING SHEAR STRESS (PSI)	AVERAGE ULTIMATE SHEAR FORCE (KIPS)	AVERAGE ULTIMATE SHEAR STRESS (PSI)	δ_{σ} (INCH)	δ_u (INCH)	δ_m (INCH)	MODE OF FAILURE
CBRC-11-8	43.6	91	53.8	112	0.035	-	-	-
8S	100.9	210	103.8	216	0.236	0.265	0.431	S
9	112.2	234	113.6	237	0.105	0.146	0.314	S
10	120.4	251	120.4	251	0.087	0.087	0.217	S
11	41.4	86	49.0	102	0.034	-	-	-
12	120.8	252	131.2	273	0.086	0.132	0.166	S



(a) DUCTILE SHEAR FAILURE

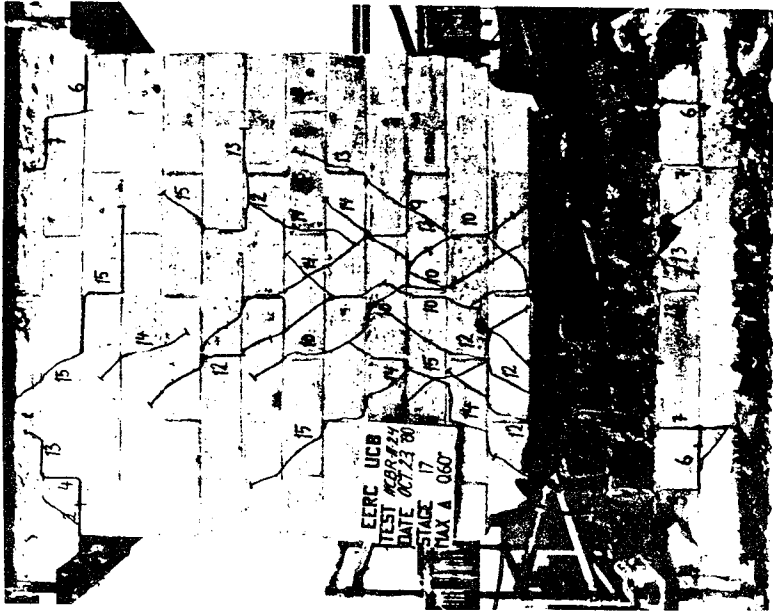


(b) BRITTLE SHEAR FAILURE

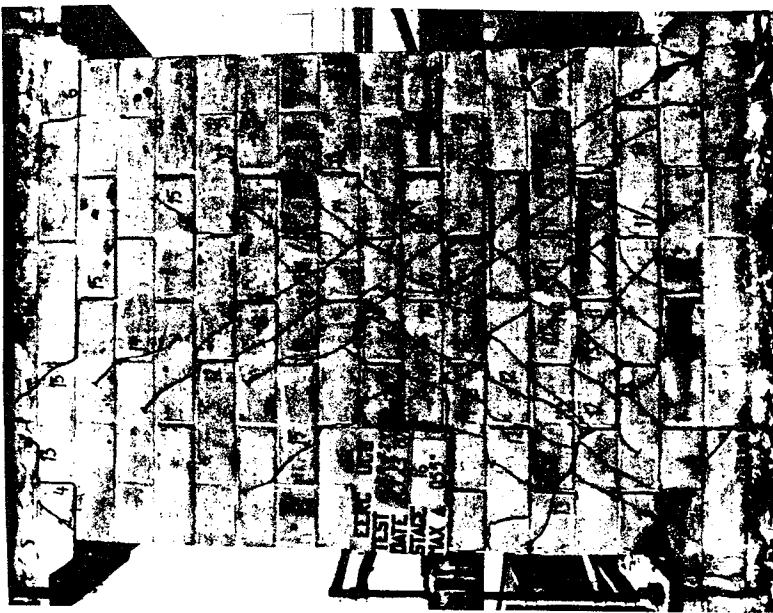
FIG. 4.1 SHEAR MODES OF FAILURE



FIG. 4.2 CORE SPLIT IN GROUTED CORE BRICK WALLS

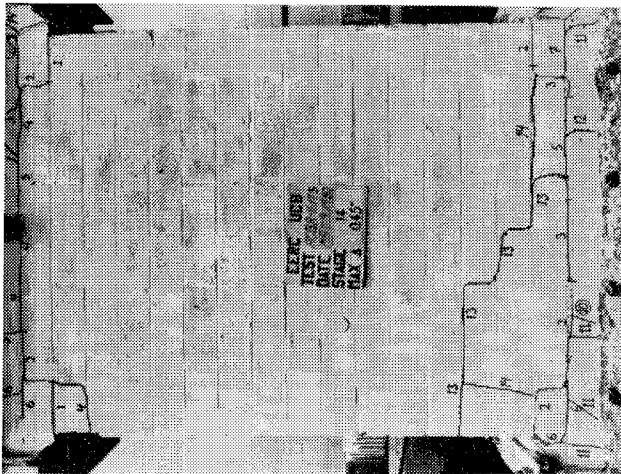


(a) BEFORE CRUSHING

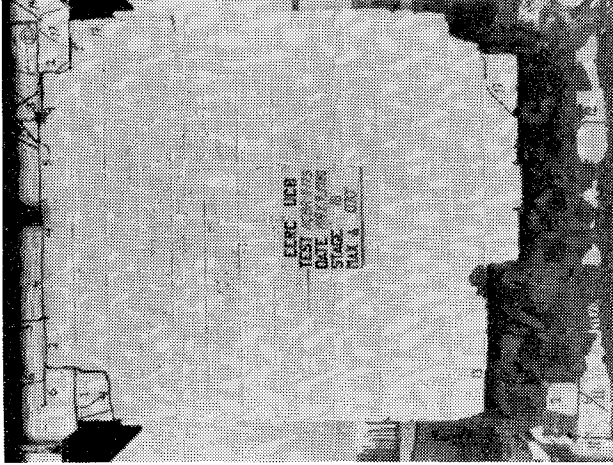


(b) AFTER CRUSHING

FIG. 4.3 SHEAR-SLIDING MODE OF FAILURE

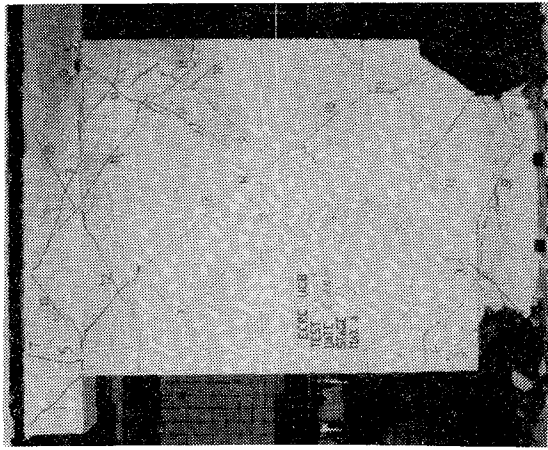


(a) Before Crushing

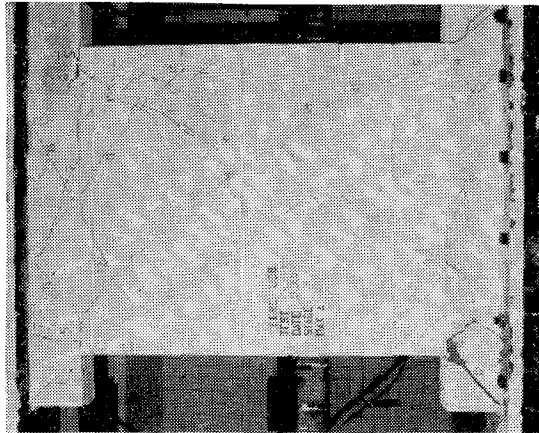


(b) After Crushing

FIG. 4.4 SLIDING MODE OF FAILURE



(b) Compression Toe Crushing



(a) Before Failure

FIG. 4.5 FLEXURAL MODE OF FAILURE

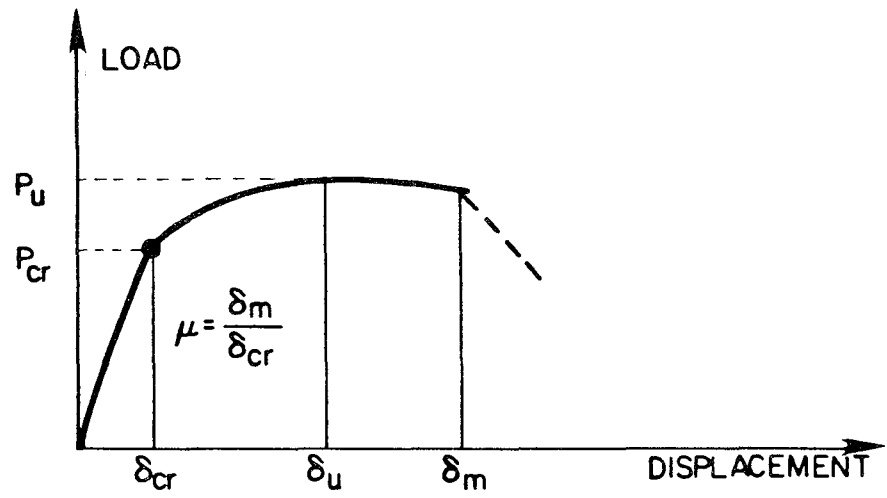


FIG. 4.6 DEFINITION OF HYSTERESIS ENVELOPE PARAMETERS



SECTION 5 DISCUSSION OF TEST RESULTS

Section 4 offered a discussion of the four observed failure modes and explained the presentation of the main load-displacement characteristics, summarized in Appendix A. Some of the major results were summarized in Tables 4.1(a), 4.1(b) and 4.1(c); in particular the lateral force and displacement at first visible cracking, the ultimate lateral force and corresponding displacement, the pier displacement at failure and the failure mode of each specimen.

In this section the test results are further discussed and the effect of each test parameter on the pier behavior is evaluated. These parameters were defined in Section 1.3 as:

1. The level of bearing stress
2. Amount of horizontal reinforcement
3. Anchorage of horizontal reinforcing bars (four different types including joint reinforcing).
4. Distribution of vertical reinforcement

The figures in this section are limited to hysteresis envelopes and stiffness degradation curves, arranged in groups to show the effect of a particular parameter. A full set of curves for each test is presented in Appendix A.

The main method of displaying the test results is by means of hysteresis envelopes. These are curves that relate the applied horizontal displacement and the lateral force with which the pier resists the displacement. A complete test on an individual pier supplies a family of hysteresis loops (load vs. displacement), one loop per cycle of imposed displacement. From these hysteresis loops the envelope is calculated as explained in Section 4.2. This envelope is the single most revealing evidence of the pier behavior throughout a complete test.

In addition curves are developed that show the stiffness degradation of the pier as the horizontal displacement (or lateral load) increases.

In the following subsections the influence of each test parameter on the hysteresis envelopes and stiffness degradation of the piers is discussed.

5.1 The Hysteresis Envelopes:

The hysteresis envelopes, evaluated for these test specimens, provide considerable information about the behavior of the specimens and how that behavior is affected by the various parameters under investigation. The ultimate load, the ultimate deflection and, in general, the shape of the hysteresis envelope are all dependent to a varying degree upon these parameters. These will be discussed in the following subsections.

5.1.1 Effect of Bearing Load

Examination of Figures 5.1, 5.2 and 5.3 shows that the vertical load affects the behavior considerably. As the vertical load increases, so does the ability of the pier to offer lateral resistance. This is particularly evident in the increase of the lateral load required to initiate cracking (indicated on the figures by a black dot) when the bearing load increases. The reason for this is clear. For the higher level of vertical bearing load being considered, the ultimate failure mode is usually shear or, to be more explicit, diagonal tension. As the lateral displacement increases the shear or shear-sliding failure modes begin

appearing in the form of diagonal cracks. The pier gradually begins to lose its resistance when the diagonal cracking appears and the cracks widen and spread as the horizontal displacement increases. In order for the masonry to fail in diagonal tension, the tensile stresses induced by the horizontal displacement must first overcome the compression field caused by the vertical load. The greater the vertical load, the greater the compressive stresses, so that the tensile stresses needed to surpass these compressive stresses, to the effect of causing failure, will also be much larger. Cracking is accordingly delayed until the resistance grows to a higher level, resulting in a larger load when cracking is visible.

Figures 5.1, 5.2 and 5.3 also show that with increasing vertical load the ductility of the piers decreases considerably as the failure becomes more brittle.

For the lower level of bearing load (20 – 30 kips) the initial behavior is the same as for the higher bearing load; this is shown in that, when the lateral displacement increases, some diagonal cracks form. However, before the diagonal cracks can propagate, the vertical reinforcement yields and the behavior becomes flexural and as a consequence ductile. The deflection increases with relatively minor increase in lateral load resistance, mostly due to strain hardening of the vertical reinforcing bars, until failure occurs.

5.1.2 Effect of Horizontal Reinforcement

In this study both the amount of horizontal reinforcing steel and the distribution of the steel throughout the height of the pier are varied. The general comment can be made that a change in the amount and distribution of horizontal reinforcement results in relatively little change in the hysteresis envelope of a pier. This was also found to be the case in the tests reported in [1,2,3,4]. Of the three types of piers only those made of concrete block (HCBL) seem to be affected. In Fig. 5.4(a) the ultimate load increased by 16% when the horizontal reinforcement was doubled from 2 to 4 #5 bars. However, the ductility increased considerably although this effect can also be attributed to an increased effectiveness of the horizontal reinforcement because of a proper

anchorage (hook).

Two concrete block walls used Dur-O-Wal wire trusses at every joint as the horizontal reinforcement. One had only Dur-O-Wal, the other Dur-O-Wal plus 2 #5 bars. Comparing the two Dur-O-Wal tests (Fig. 5.4(b)) shows that the addition of the 2 #5 rebars increased the ultimate load by 27%. However, comparing these tests with the test that had only 2 #5 rebars shows that the addition of the Dur-O-Wal is relatively ineffective in increasing ultimate strength but can significantly enhance the ductility of the pier. The more uniform distribution of the steel probably contributed to that effect.

The walls made of hollow clay brick (HCBR) had various amounts of horizontal reinforcement. Examination of Figures 5.5(a-e) shows that the hysteresis envelope is affected very little by the amount of horizontal reinforcement. In the comparative cases shown, more than doubling the amount of reinforcing results in very little change in the hysteresis envelopes.

For the double wythe grouted core clay brick piers (CBRC), the difference in the two sets of tests whose results are exhibited in Figures 5.6(a) and 5.6(b) is the amount of vertical load, (a) being lightly loaded, (b) heavily loaded. In the lightly loaded piers, increasing the number of #5 rebars from 1 to 5 had little effect on the envelope. In the heavily loaded piers the envelopes are slightly different but their character is the same. The behavior of the lightly loaded piers is flexural but neither pier was tested to failure under the light load. All four piers show that, after cracking, the horizontal reinforcement in all cases was unable to pick up any of the lateral load resistance lost by the masonry due to cracking.

5.1.3 Effect of Anchorage of Horizontal Reinforcement

In this test program the great majority of the piers displayed a shear or diagonal tension failure. In understanding the behavior of the pier it is advantageous to examine the same problem in reinforced concrete. Both masonry and concrete are brittle materials and weak in tension. Considering

a reinforced concrete beam under a large shear load it is realized that the failure of this beam can be prevented and its ductility considerably enhanced by using stirrups of reinforcing steel. In the masonry piers these stirrups correspond to the horizontal reinforcement. It is the difference of the two types of construction that reveals the weakness of the piers. In the reinforced concrete beam the stirrups are embedded in the concrete so sufficient anchorage is available to develop very high loads in the stirrups. In reinforced masonry piers, the horizontal bars are not able to realize their full capabilities, usually because of poor anchorage. If the bars are simply laid in the mortar and/or grout at determined intervals, the bars are of little help in picking up horizontal resistance following cracking and failure will occur soon afterwards and will be sudden.

Therefore, one of the most important aspects of using reinforcing bars to improve the ductility of masonry piers is to provide sufficient anchorage. With sufficient anchorage the horizontal bars can realize their full value in maintaining the integrity of the piers following cracking. Recognizing this the piers in these tests were constructed with three different types of anchorage of the horizontal reinforcing bars. These anchorages are described as follows (refer to Figure 2.5):

1. The ends of the horizontal reinforcing bars are bent 90 degrees downwards into the grout in the cavities containing the end vertical reinforcing bars.
2. The horizontal reinforcing bars are bent 180 degrees around the end vertical reinforcing bars.
3. Plates are welded onto the horizontal reinforcing bars and the assembly embedded in the grout.

The test results are exhibited in Figures 5.7, 5.8(a) and 5.8(b).

In the hollow concrete block piers (HCBL) only the 90 degree and the 180 degree anchorages were used. The results are compared in Fig. 5.7. Since with no anchorage the drop off in the load would follow soon after the initiation of cracking (the black dot in the figures), both anchorages are effective in improving the ductility. With the 90 degree bent bar, however, the failure was sudden, exhibited by the abrupt drop in load as the bars straightened and the anchorage failed. With the 180 degree hook, not only was the strength enhanced, but the failure was gradual, a very desirable quality.

For the hollow clay brick piers (HCBR), all three anchorages were tested. In Figure 5.8(a), where the horizontal reinforcement was light, the influence of this parameter is dramatic. All three were effective in increasing ductility, but it is evident that both the hook and the plate were more effective; both considerably increased the strength of the pier and there is little to choose between them. Similarly, for the piers with heavy horizontal reinforcing (Figure 5.8(b)) the end plate was the most effective whereas the 90 degree bent was the least effective.

5.1.4 Effect of Distribution of Vertical Reinforcement

To study the effect of the distribution of the vertical reinforcement three combinations of bars were used, each combination contributing the same total cross-sectional area. The three combinations were

1. 2 #7 bars - $A = 1.20 \text{ in}^2$
2. 4 #5 bars - $A = 1.24 \text{ in}^2$
3. 6 #4 bars - $A = 1.20 \text{ in}^2$

Two of the bars were placed in the outer cavities, the remainder were distributed evenly over the remaining width. The 1.20 in^2 represents about 0.45% of the gross area of a pier. The test results are shown in Figures 5.9(a), 5.9(b), 5.10(a) and 5.10(b).

The overall effect of distributing the vertical reinforcing bars over the width of a pier seems to be inconsistent. It would be expected that, since cracking in the shear modes of failure (shear and shear-sliding) initiates near midwidth of the piers, the reinforcing bars would be somewhat effective in inhibiting further cracking by dowel action and thus affect the hysteresis envelope.

For the hollow concrete block specimens (HCBL) the effect of the distribution is negligible. However, for the hollow clay brick specimens (HCBR) the effect is quite pronounced when the results with an intermediate number of bars are compared with the results for the minimum number of bars: the strength is increased by 25%. In contrast to this when the maximum number of bars is used the strength again reduces. The reasons for this are not known, but it could have something to do with the anchorage of the vertical reinforcing bars to the test rig.

5.2 Stiffness Degradation

The stiffness degradation properties of each pier are presented in Appendix A as stiffness vs. horizontal (shear) force, and stiffness vs. relative horizontal displacement curves. These relationships indicate the sensitivity of the stiffness of the masonry piers with respect to the level of horizontal force, or relative lateral displacement. Significant stiffness degradation was present even at the beginning stages of horizontal loading, much earlier than the development of the first visible cracks.

The stiffness values of all three types of piers at the cracking stage were about 50% of the initial stiffness. The stiffness degradation characteristics of the masonry piers observed through the experiments, show that they do not possess a linear lateral force vs. deflection relationship even at very low levels of horizontal load resistance.

5.2.1 Effect of Vertical Load.

Comparisons of stiffness degradation curves of specimens subjected to different levels of bearing load are shown in Figures 5.12, 5.13 and 5.14 for the three pier types. All the figures indicate the dependence of horizontal stiffness on vertical load level. Although not very significant, there is a tendency toward decreasing stiffness degradation rate with increasing level of vertical compression.

5.2.2 Effect of Horizontal Reinforcement

Stiffness degradation curves of the hollow concrete block (HCBL) and hollow clay brick (HCBR) piers are compared for different amounts of horizontal reinforcement in Figures 5.15 and 5.16. The specimens compared in each figure displayed very similar stiffness degradation characteristics regardless of their amounts of horizontal reinforcement. Although the stiffness values of the more highly reinforced specimens are slightly above those of the less reinforced ones, the differences are negligible.

Stiffness degradation curves of two double wythe grouted core clay brick (CBRC) specimens shown in Fig. 5.17(a) also indicate that the stiffness degradation is independent of the amount of horizontal reinforcement.

5.2.3 Effect of Type of Anchorage

No consistent correlation is observed from Figs. 5.18 and 5.19 between the stiffness degradation characteristics and the anchorage of horizontal bars of the hollow concrete block (HCBL) and hollow clay brick (HCBR) specimens. However, the stiffness value at any given horizontal load level is considerably higher when horizontal bars are hooked around the vertical bars or welded to the end plates, compared with the values for those bent vertically into the grout core.

5.2.4 Effect of Vertical Reinforcement Distribution

It can be observed from Figures 5.20 and 5.21 that stiffness degradation in masonry piers is not affected by the distribution of vertical reinforcement. The degrading stiffness value at a given level of horizontal load shows an increasing trend as the distribution changes from two to more reinforcing bars. However, these results are inconsistent.

5.3 Crack Width Measurement

During the testing of specimen HCBL-11-25, two additional displacement measurements were taken by the DCDT's attached to the pier. These DCDT's were measuring the relative horizontal displacements between the vertical edges at the middle and top levels of the piers. These displacement readings correspond to the horizontal projection of the cumulative crack width throughout the pier.

In Figure 5.22 cumulative crack widths measured during the peaks of each displacement cycle are compared with the peak values of relative horizontal displacement. No crack width measurements were recorded at the uncracked stage as expected. The figure shows that the opening of cracks under increasing horizontal displacements is controlled very well by the 0.2% horizontal reinforcement until crushing occurs.

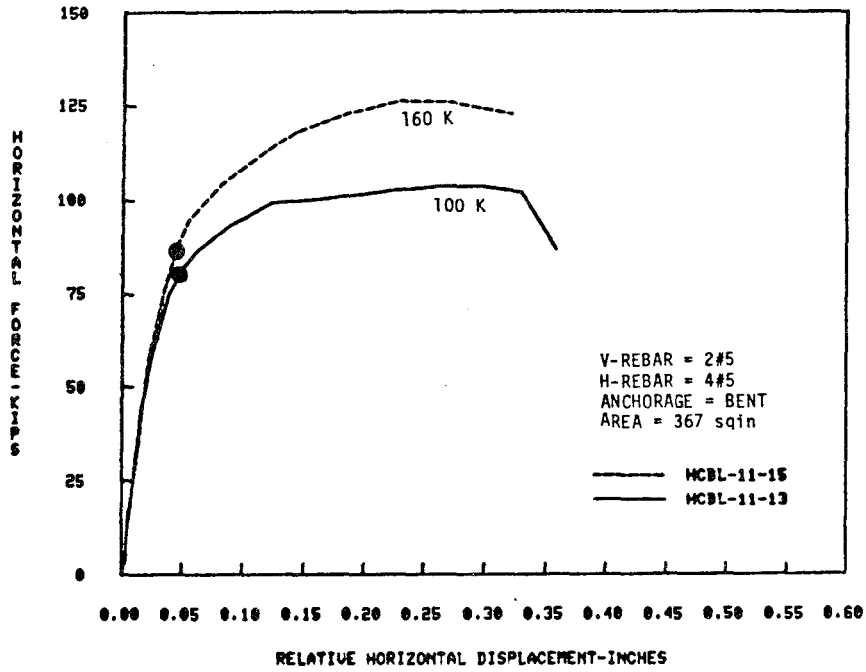


FIG. 5.1a EFFECT OF BEARING LOAD ON HYSTERESIS ENVELOPE (HCBL)

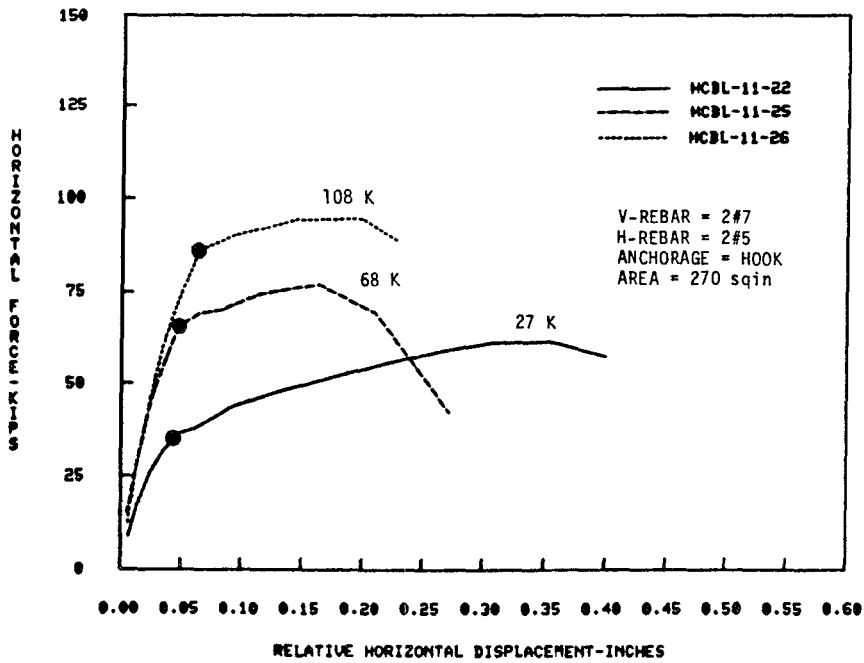


FIG. 5.1b EFFECT OF BEARING LOAD ON HYSTERESIS ENVELOPE (HCBL)

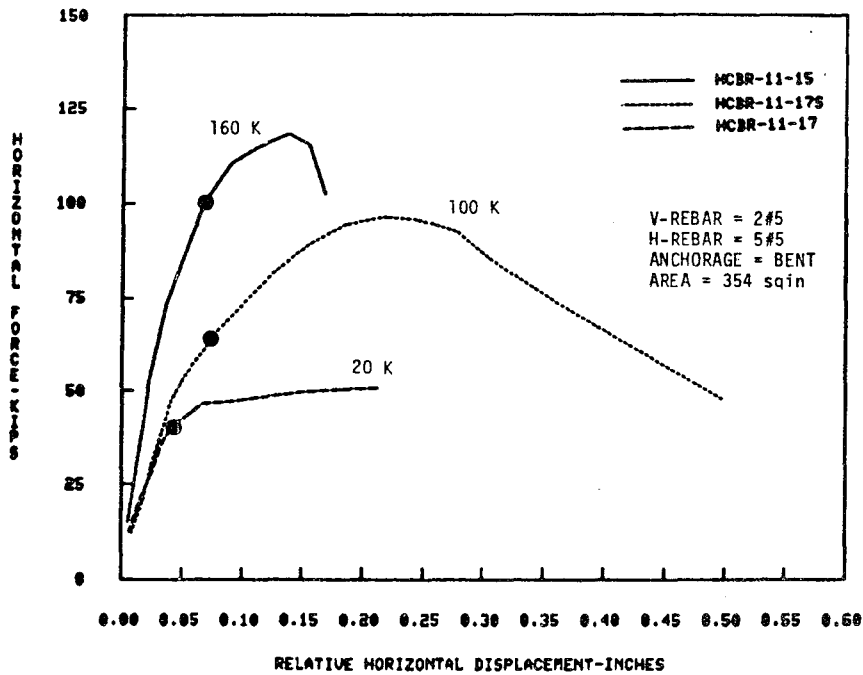


FIG. 5.2 EFFECT OF BEARING LOAD ON HYSTERESIS ENVELOPE (HCBR)

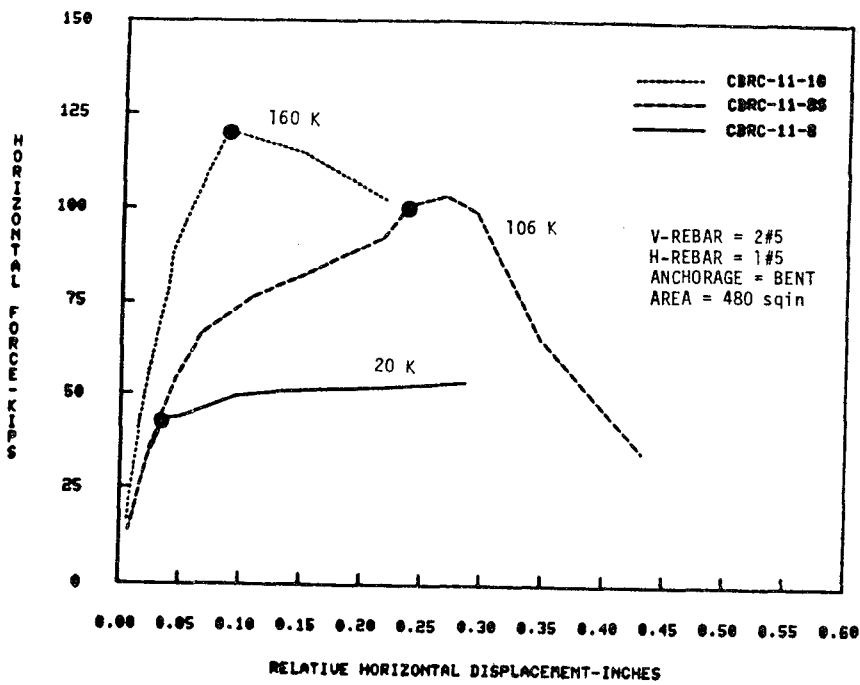


FIG. 5.3a EFFECT OF BEARING LOAD ON HYSTERESIS ENVELOPE (CBRC)

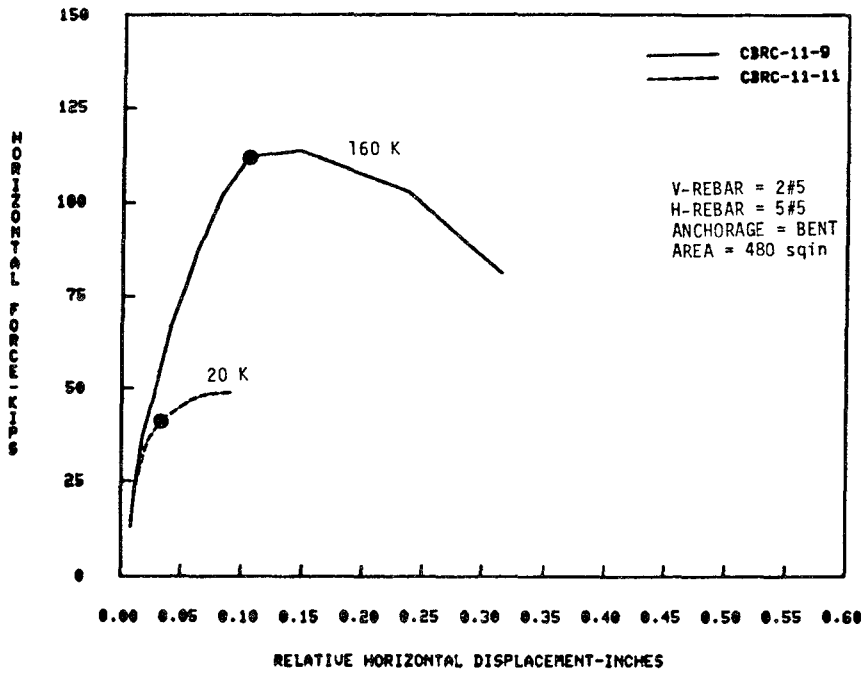


FIG. 5.3b EFFECT OF BEARING LOAD ON HYSTERESIS ENVELOPE (CBRC)

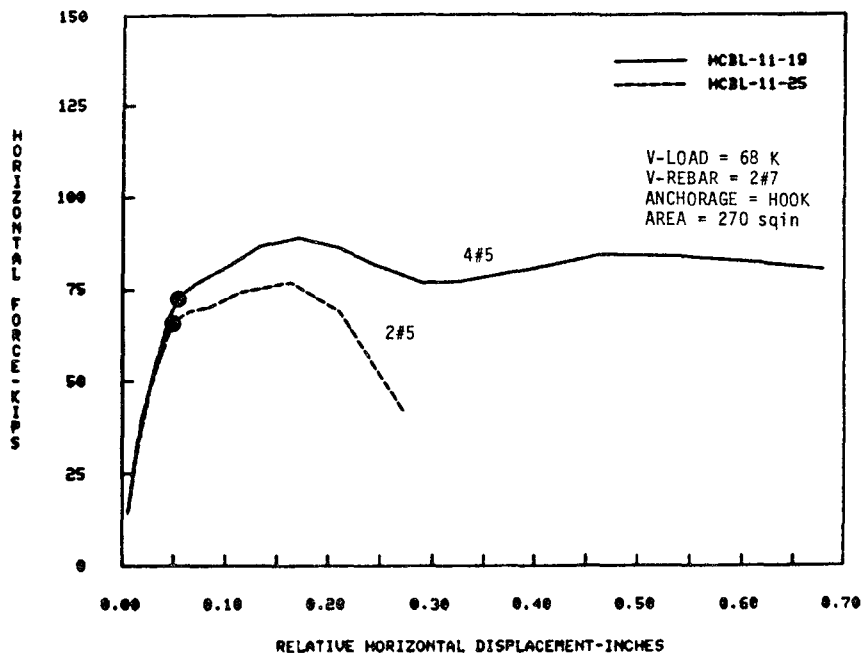


FIG. 5.4a EFFECT OF HORIZONTAL REINFORCEMENT ON HYSTERESIS ENVELOPE (HCBL)

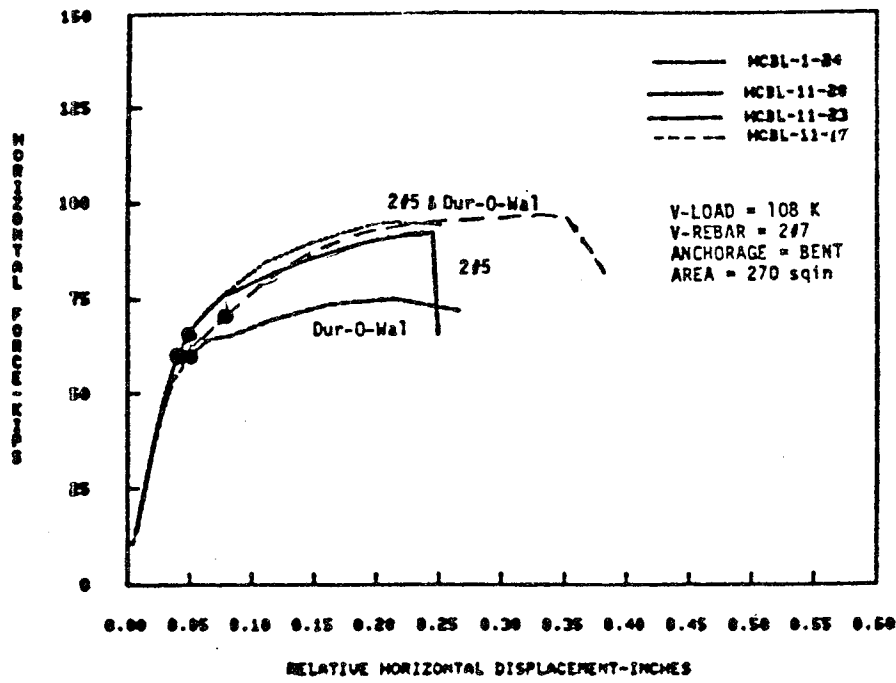


FIG. 5.4b EFFECT OF HORIZONTAL REINFORCEMENT ON HYSTERESIS ENVELOPE (HCBL)

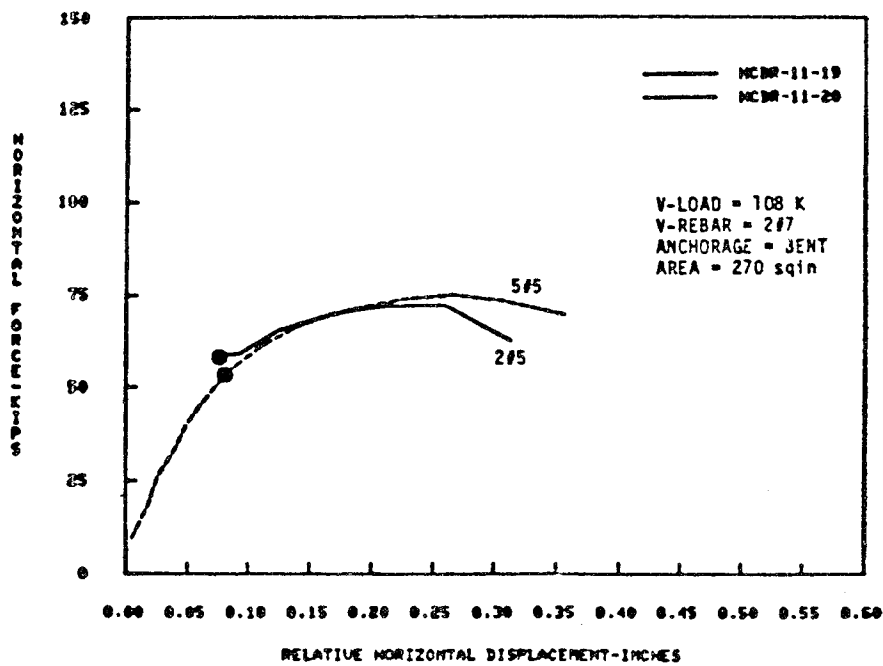


FIG. 5.5a EFFECT OF HORIZONTAL REINFORCEMENT ON HYSTERESIS ENVELOPE (HCBR)

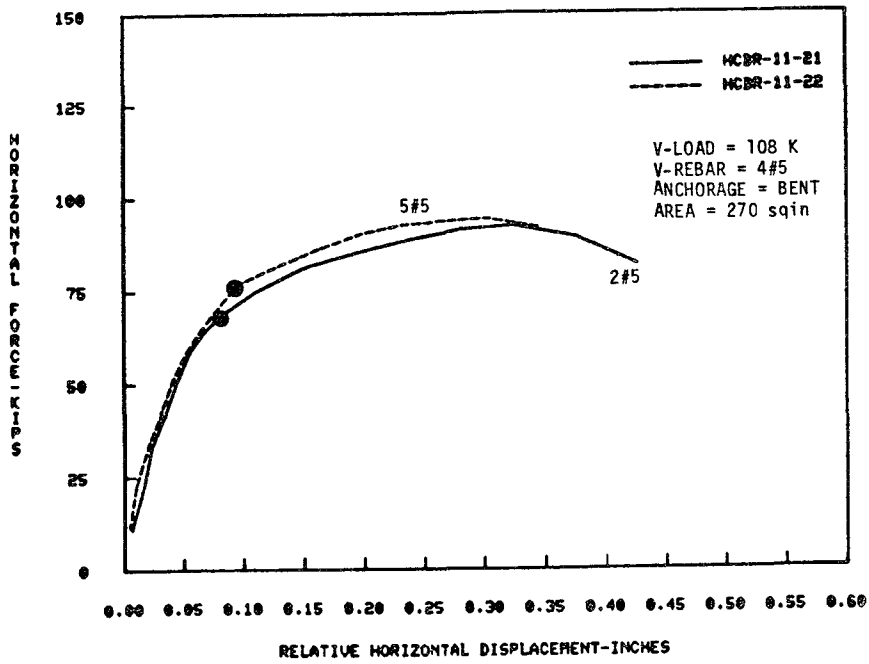


FIG. 5.5b EFFECT OF HORIZONTAL REINFORCEMENT ON HYSTERESIS ENVELOPE (HCBR)

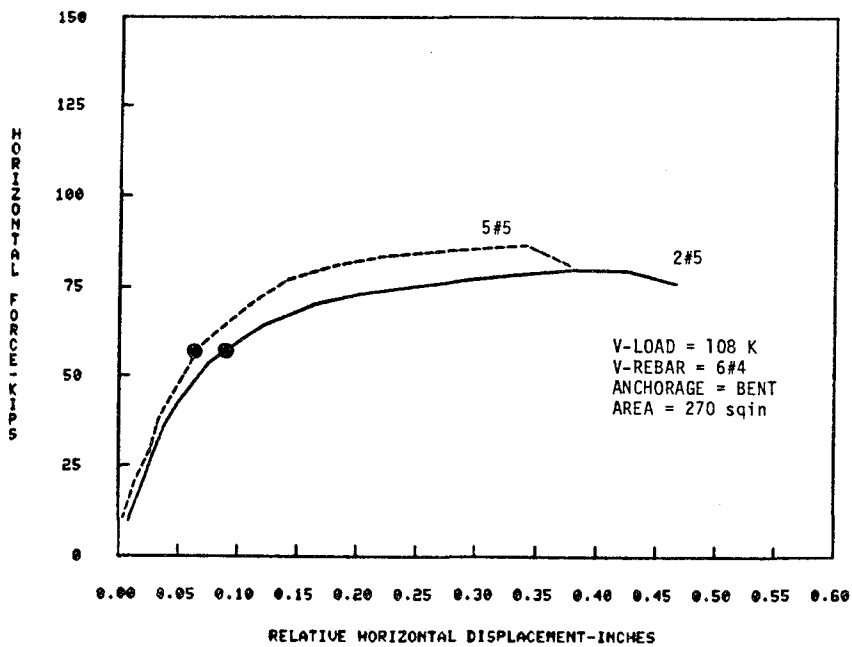


FIG. 5.5c EFFECT OF HORIZONTAL REINFORCEMENT ON HYSTERESIS ENVELOPE (HCBR)

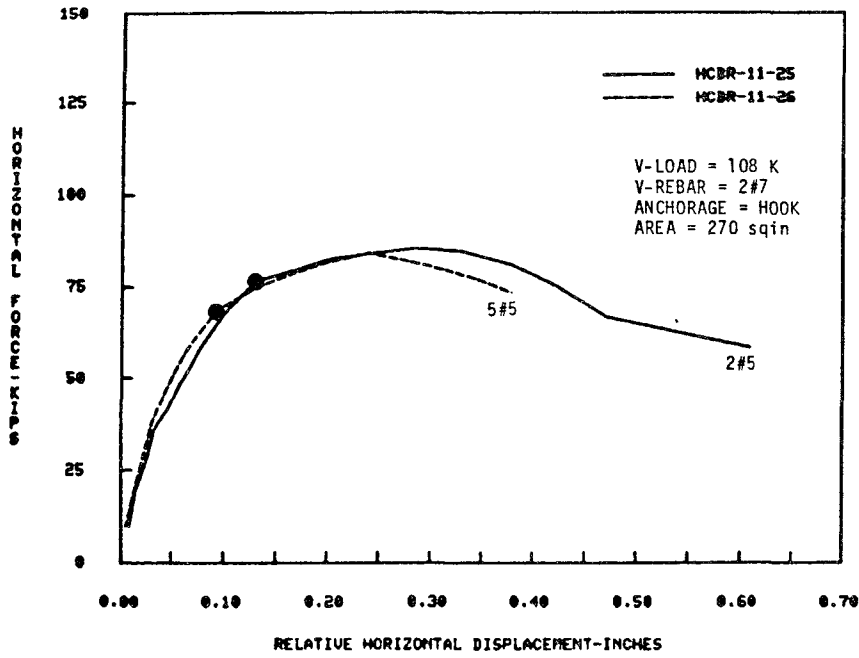


FIG. 5.5d EFFECT OF HORIZONTAL REINFORCEMENT ON HYSTERESIS ENVELOPE (HCBR)

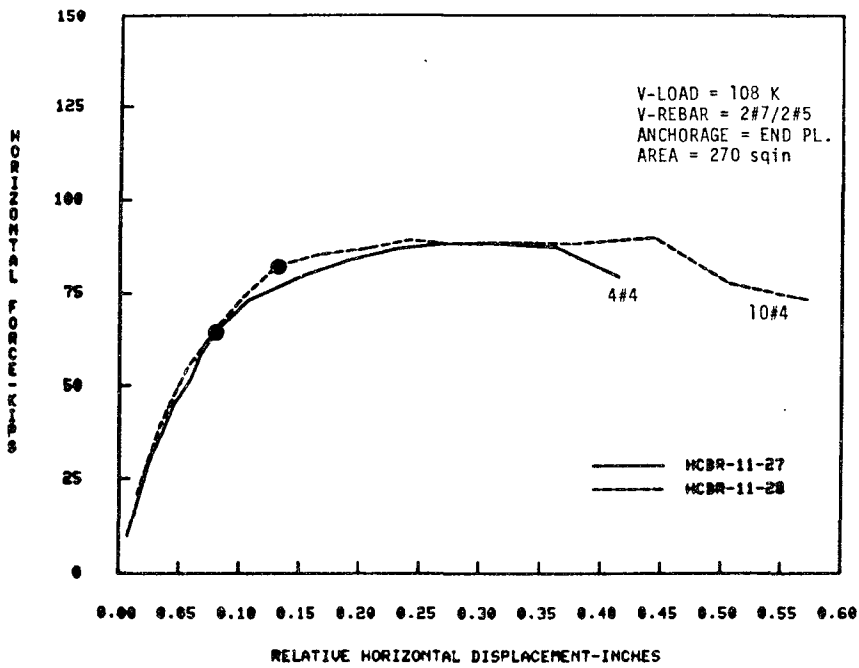


FIG. 5.5e EFFECT OF HORIZONTAL REINFORCEMENT ON HYSTERESIS ENVELOPE (HCBR)

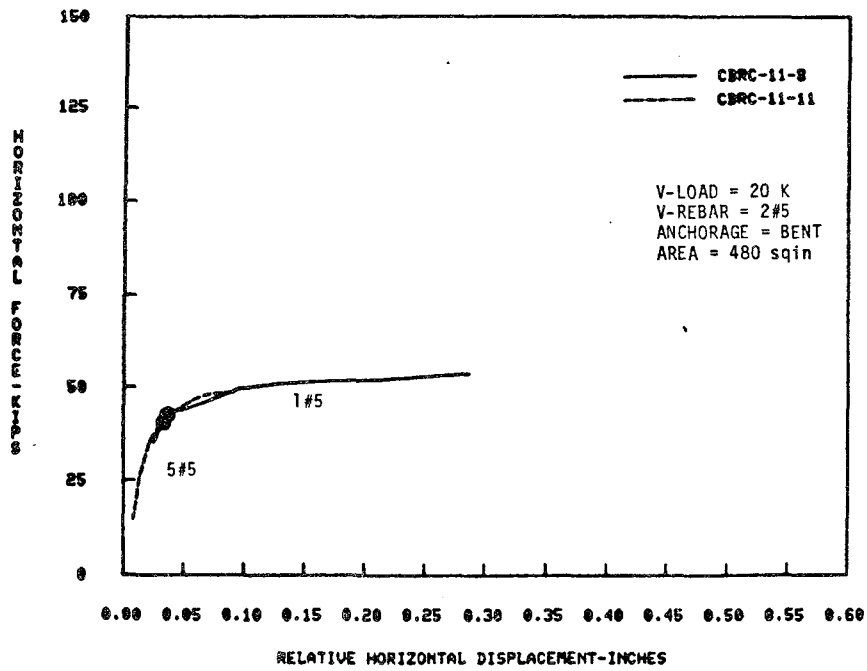


FIG. 5.6a EFFECT OF HORIZONTAL REINFORCEMENT ON HYSTERESIS ENVELOPE (CBRC)

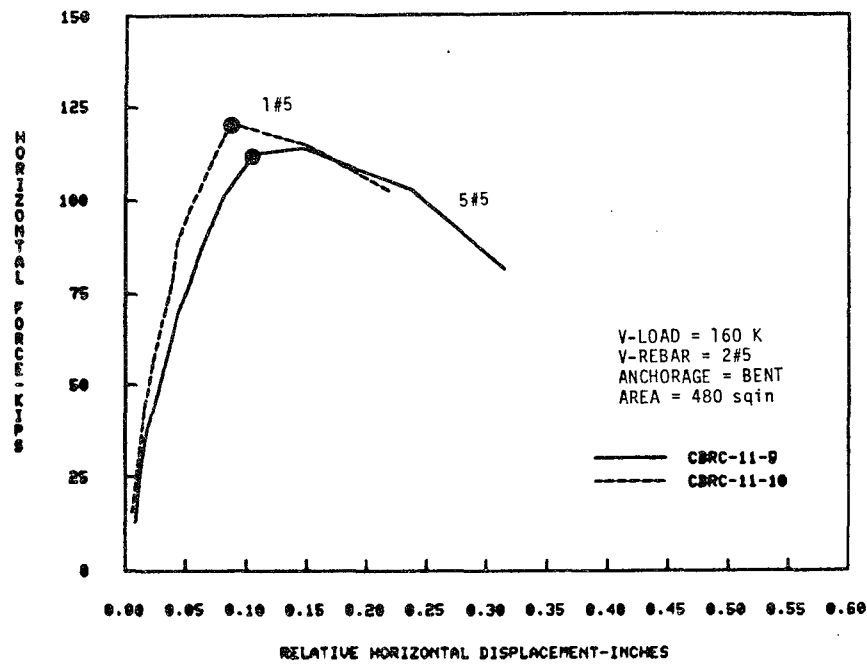


FIG. 5.6b EFFECT OF HORIZONTAL REINFORCEMENT ON HYSTERESIS ENVELOPE (CBRC)

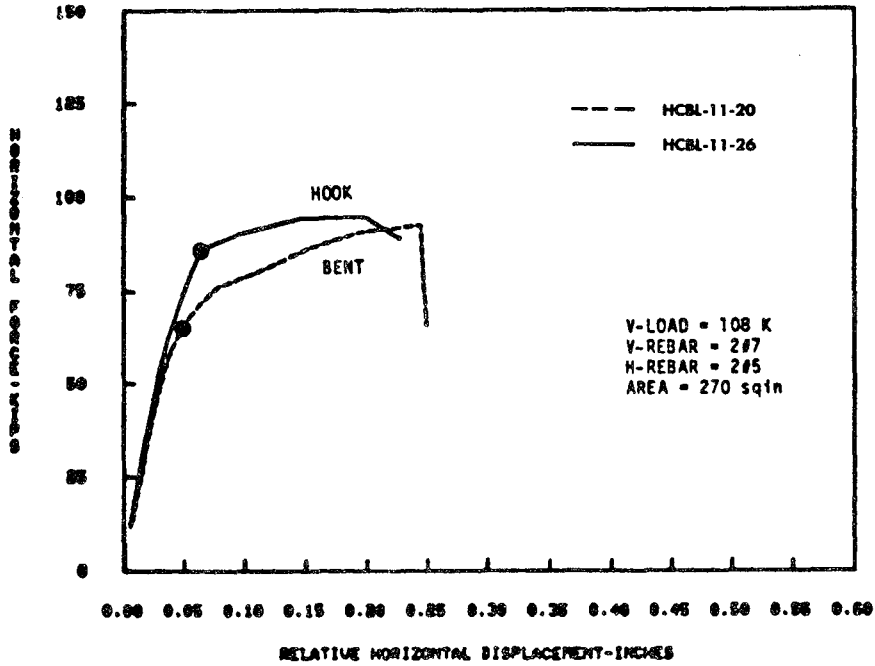


FIG. 5.7 EFFECT OF TYPE OF ANCHORAGE ON HYSTERESIS ENVELOPE (HCBL)

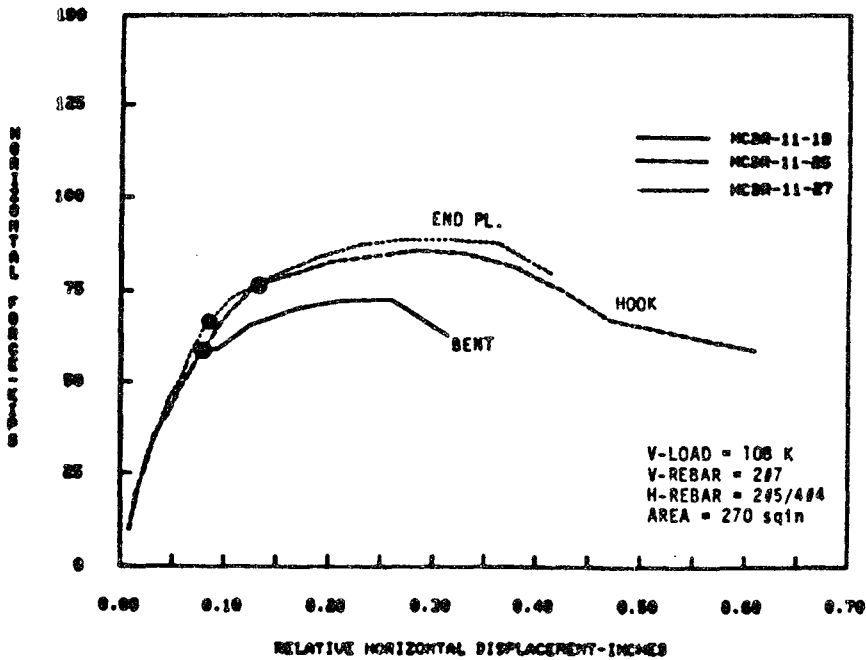


FIG. 5.8a EFFECT OF TYPE OF ANCHORAGE ON HYSTERESIS ENVELOPE (HCBL)

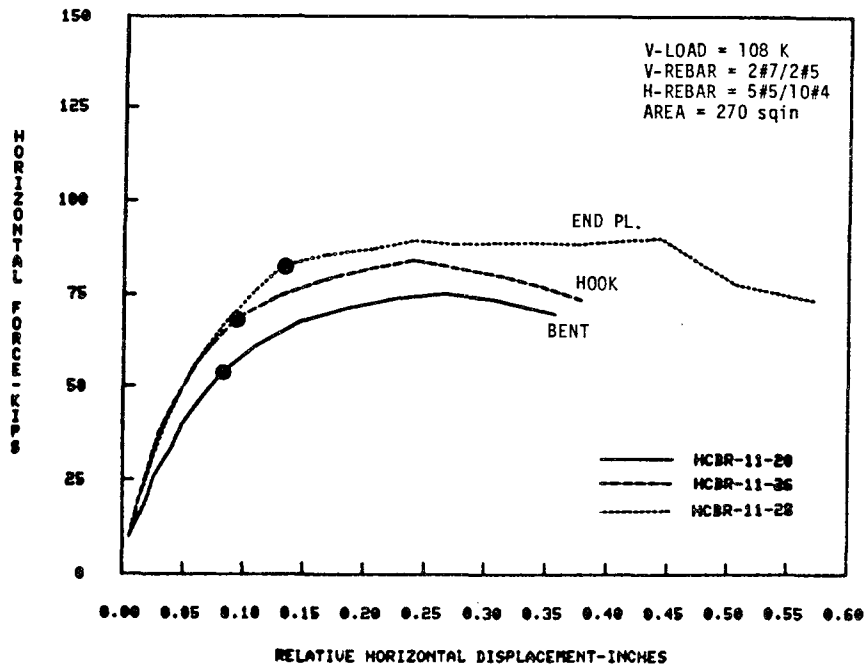


FIG. 5.8b EFFECT OF TYPE OF ANCHORAGE ON HYSTERESIS ENVELOPE (HCBR)

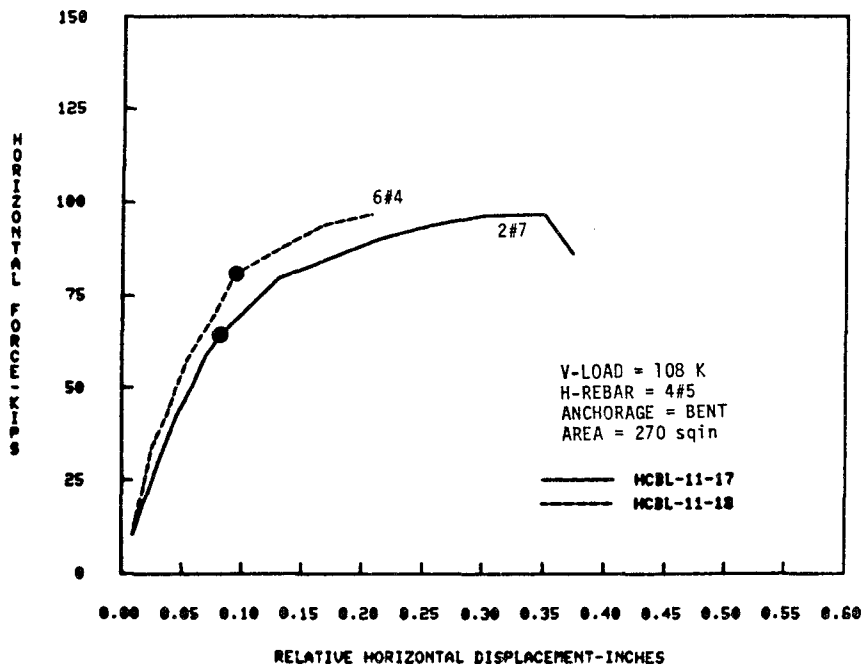


FIG. 5.9a EFFECT OF V-REBAR DISTRIBUTION ON HYSTERESIS ENVELOPE (HCBL)

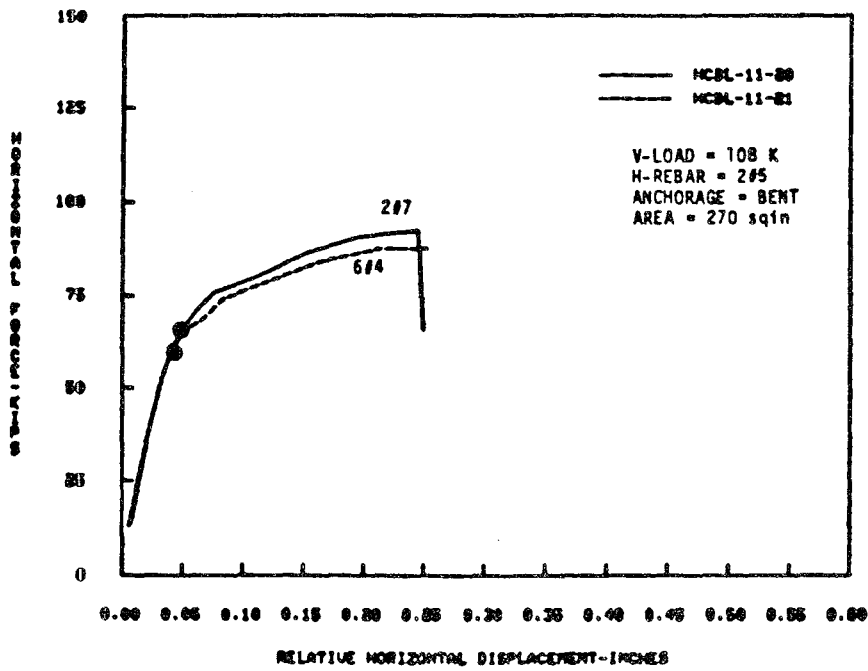


FIG. 5.9b EFFECT OF V-REBAR DISTRIBUTION ON HYSTERESIS ENVELOPE (HCBL)

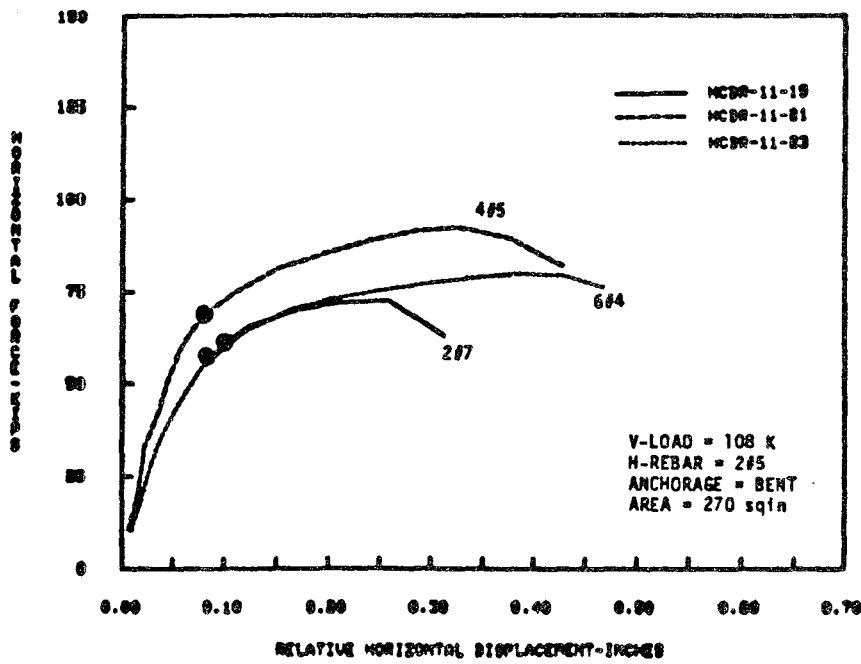


FIG. 5.10a EFFECT OF V-REBAR DISTRIBUTION ON HYSTERESIS ENVELOPE (HCBR)

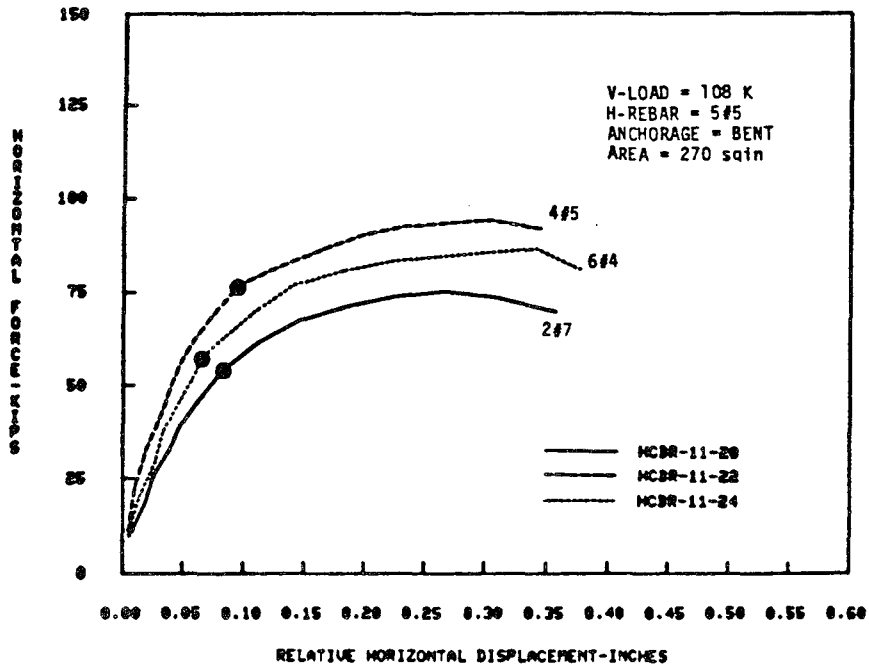


FIG. 5.10b EFFECT OF V-REBAR DISTRIBUTION ON HYSTERESIS ENVELOPE (HCBR)

THERE IS NO FIGURE 5.11

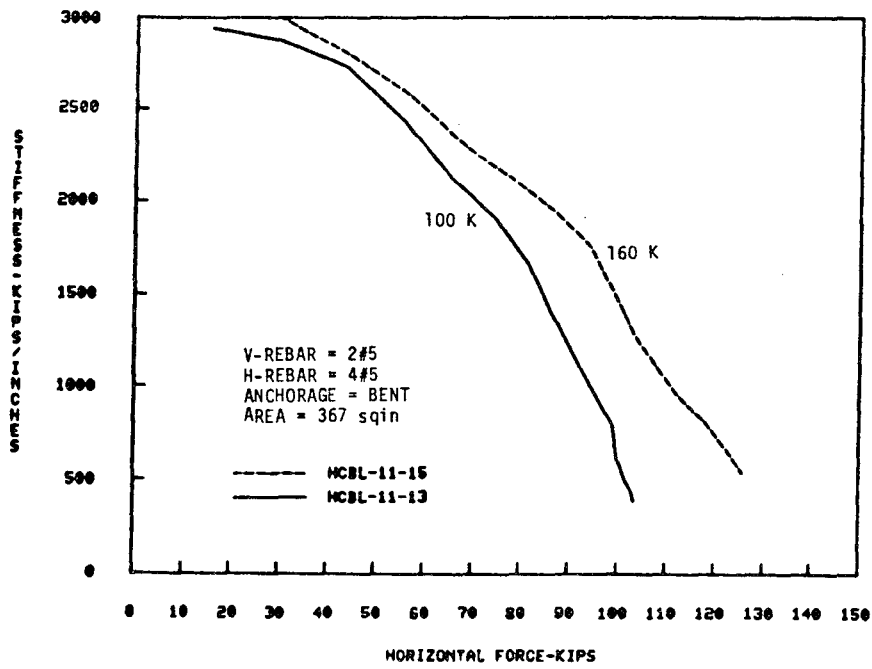


FIG. 5.12a EFFECT OF BEARING LOAD ON STIFFNESS DEGRADATION (HCBL)

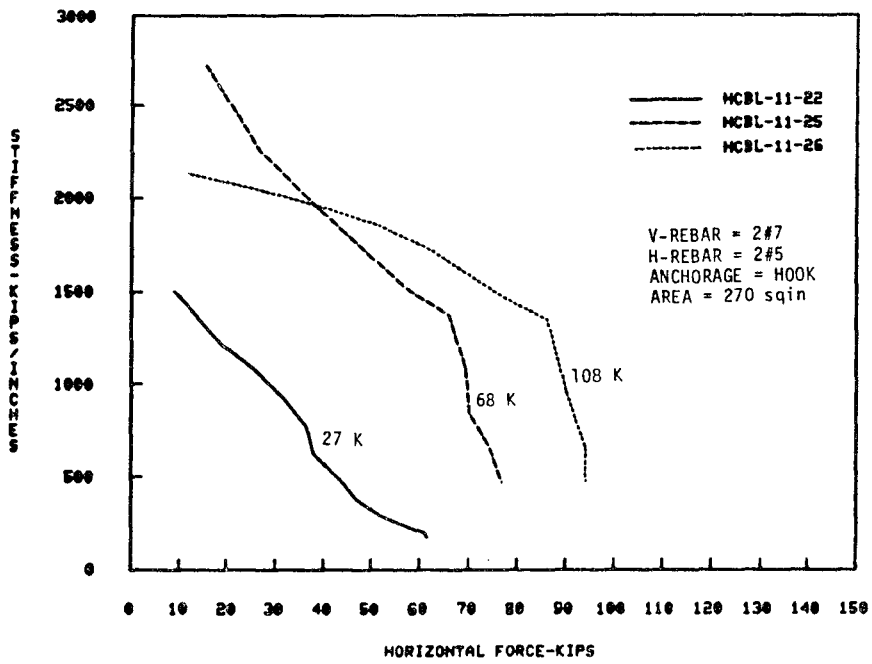


FIG. 5.12b EFFECT OF BEARING LOAD ON STIFFNESS DEGRADATION (HCBL)

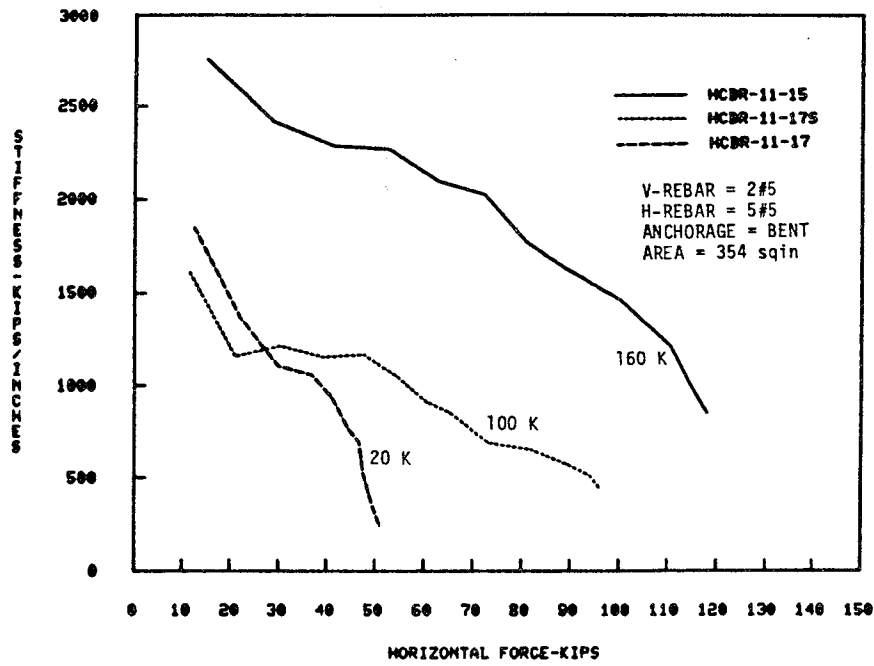


FIG. 5.13 EFFECT OF BEARING LOAD ON STIFFNESS DEGRADATION (HCBR)

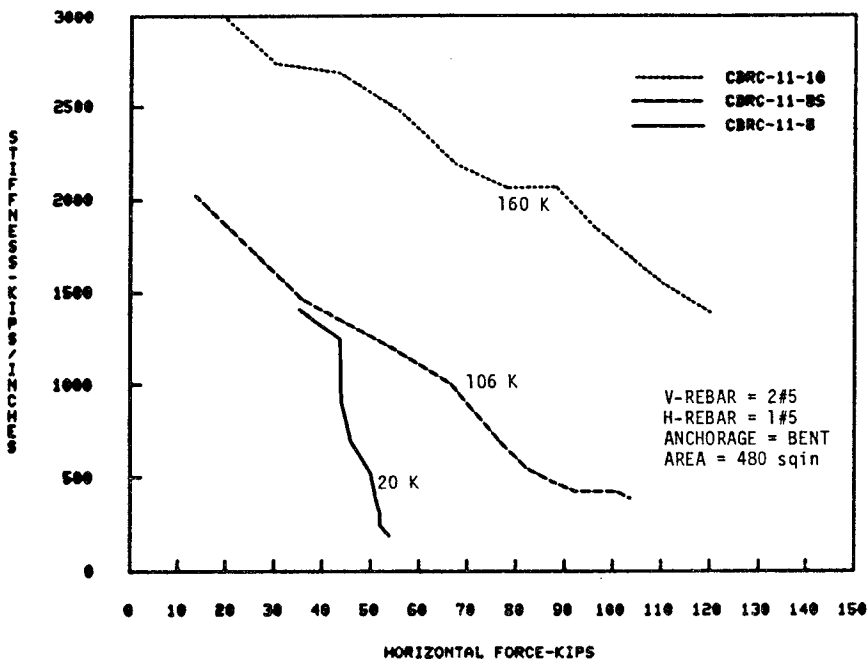


FIG. 5.14a EFFECT OF BEARING LOAD ON STIFFNESS DEGRADATION (CBRC)

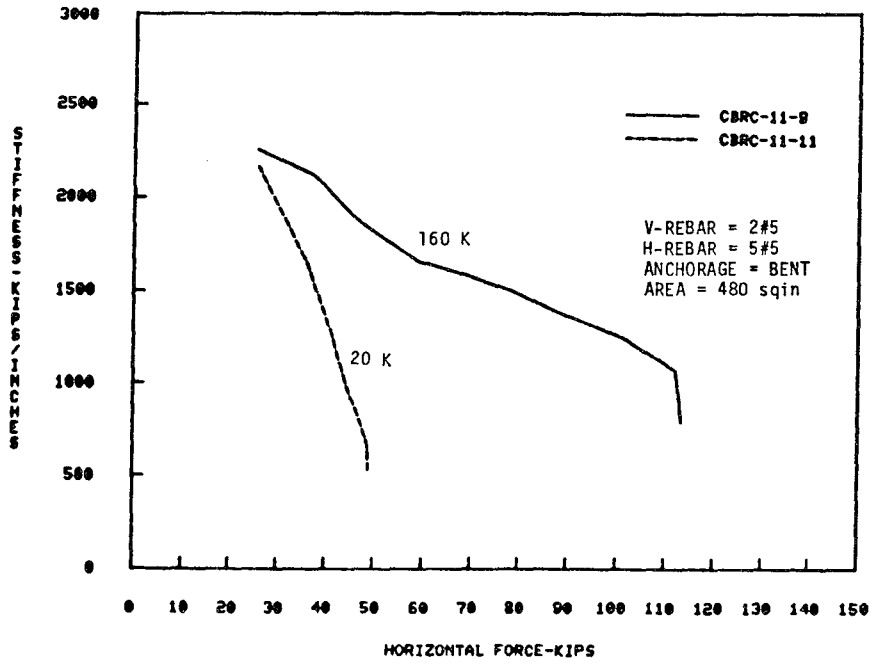


FIG. 5.14b EFFECT OF BEARING LOAD ON STIFFNESS ENVELOPE (CBRC)

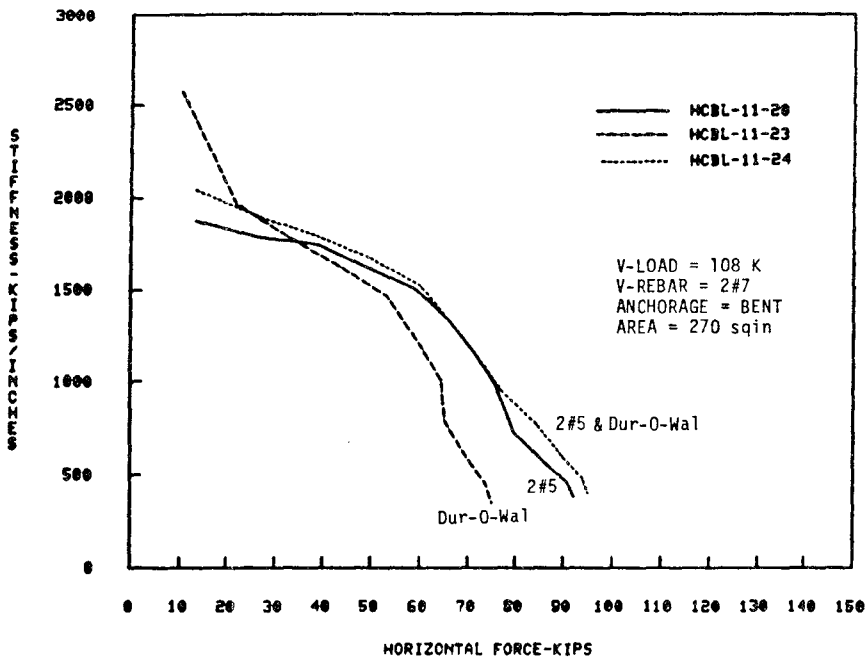


FIG. 5.15a EFFECT OF HORIZONTAL REINFORCEMENT ON STIFFNESS DEGRADATION (HCBL)

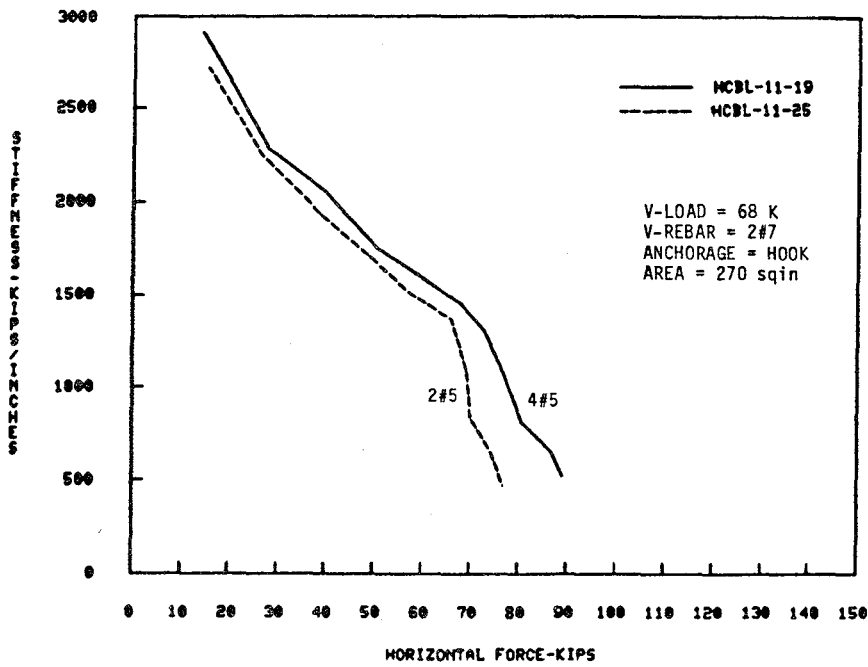


FIG. 5.15b EFFECT OF HORIZONTAL REINFORCEMENT ON STIFFNESS DEGRADATION (HCBL)

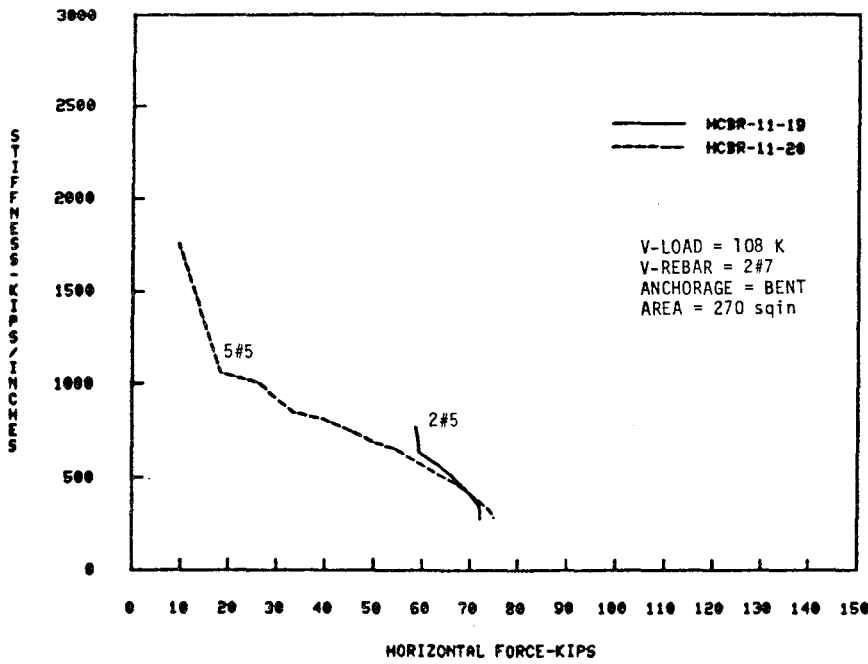


FIG. 5.16a EFFECT OF HORIZONTAL REINFORCEMENT ON STIFFNESS DEGRADATION (HCBR)

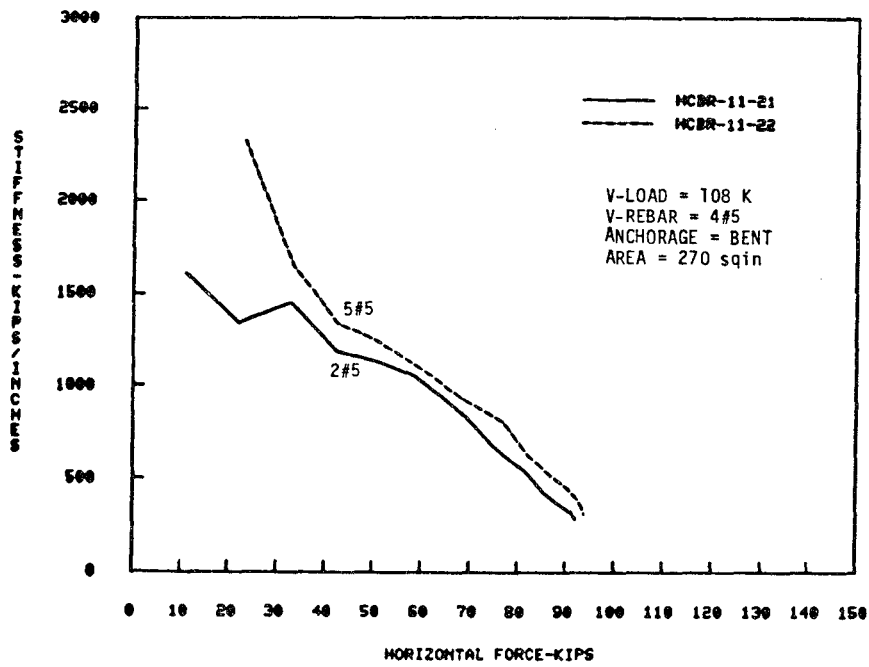


FIG. 5.16b EFFECT OF HORIZONTAL REINFORCEMENT ON STIFFNESS DEGRADATION (HCBR)

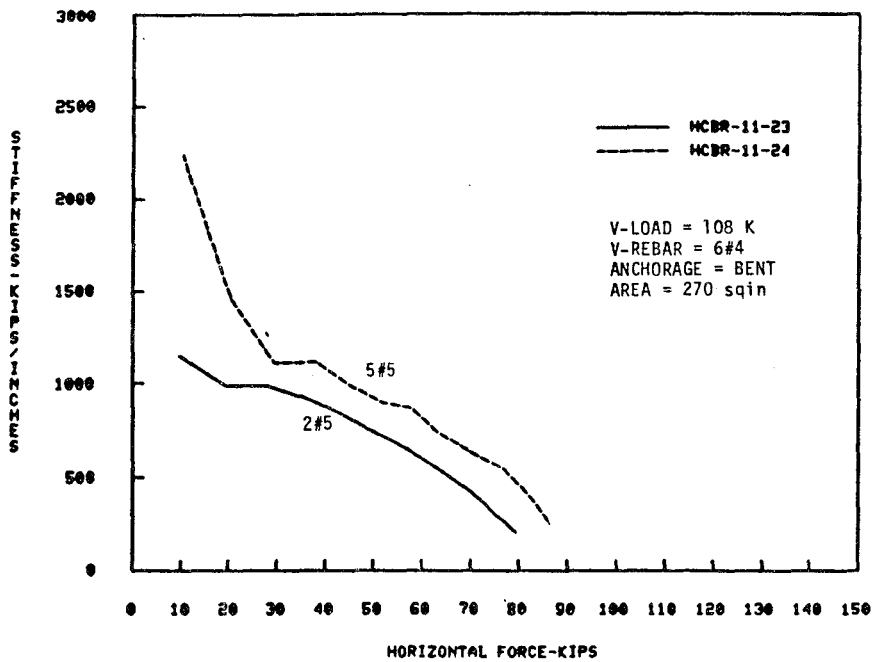


FIG. 5.16c EFFECT OF HORIZONTAL REINFORCEMENT ON STIFFNESS DEGRADATION (HCBR)

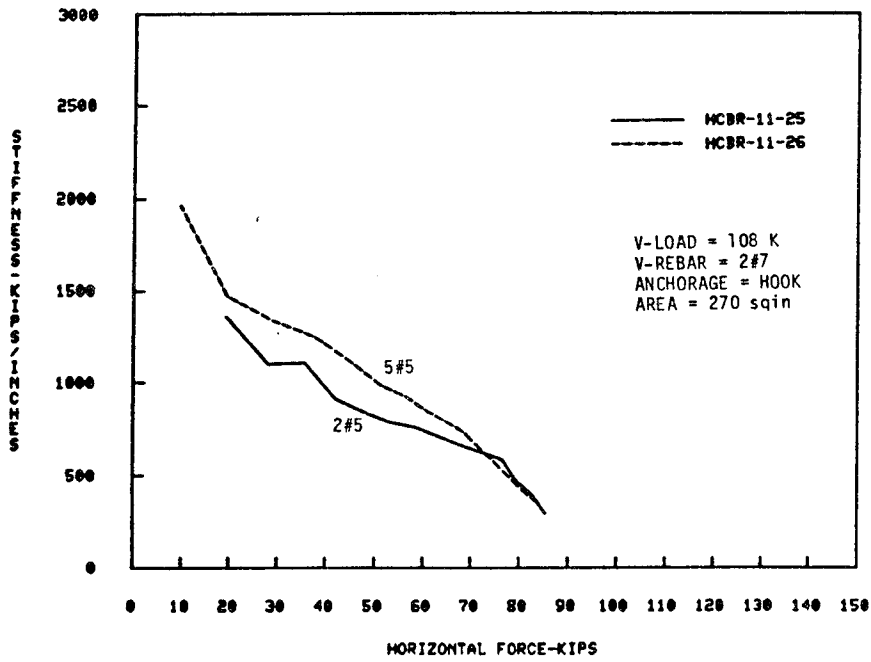


FIG. 5.16d EFFECT OF HORIZONTAL REINFORCEMENT ON STIFFNESS DEGRADATION (HCBR)

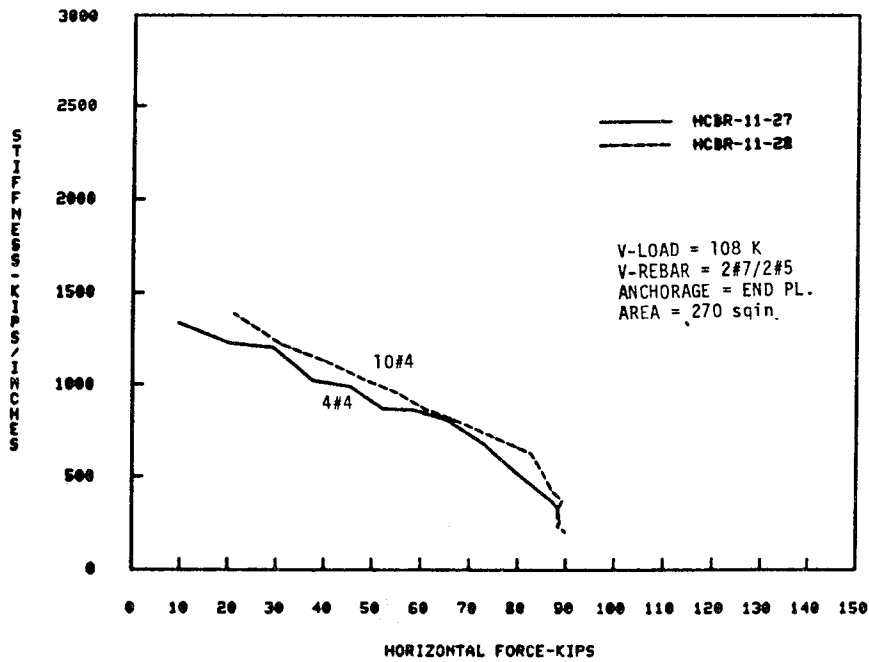


FIG. 5.16e EFFECT OF HORIZONTAL REINFORCEMENT ON STIFFNESS DEGRADATION (HCBR)

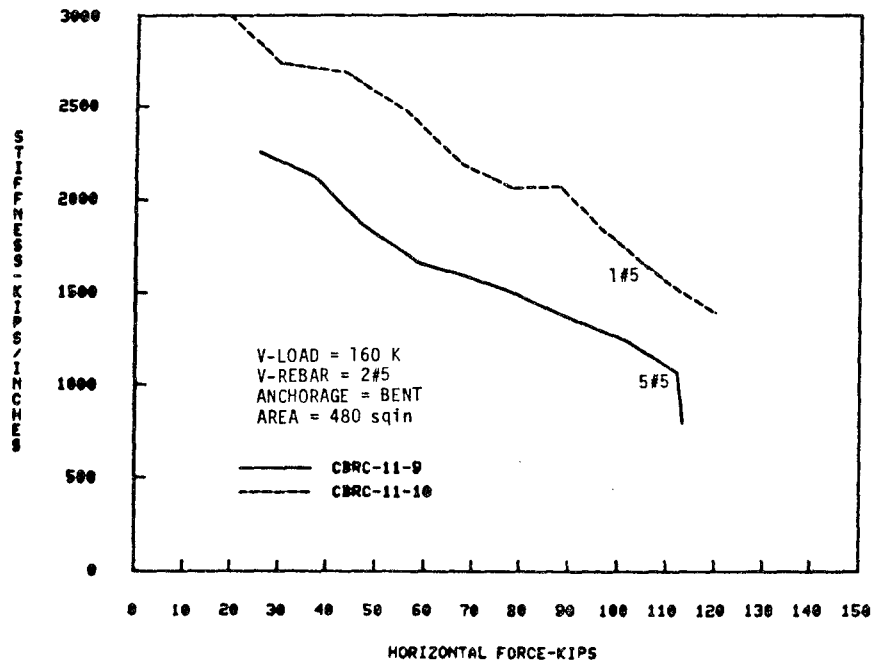


FIG. 5.17a EFFECT OF HORIZONTAL REINFORCEMENT ON STIFFNESS DEGRADATION (CBRC)

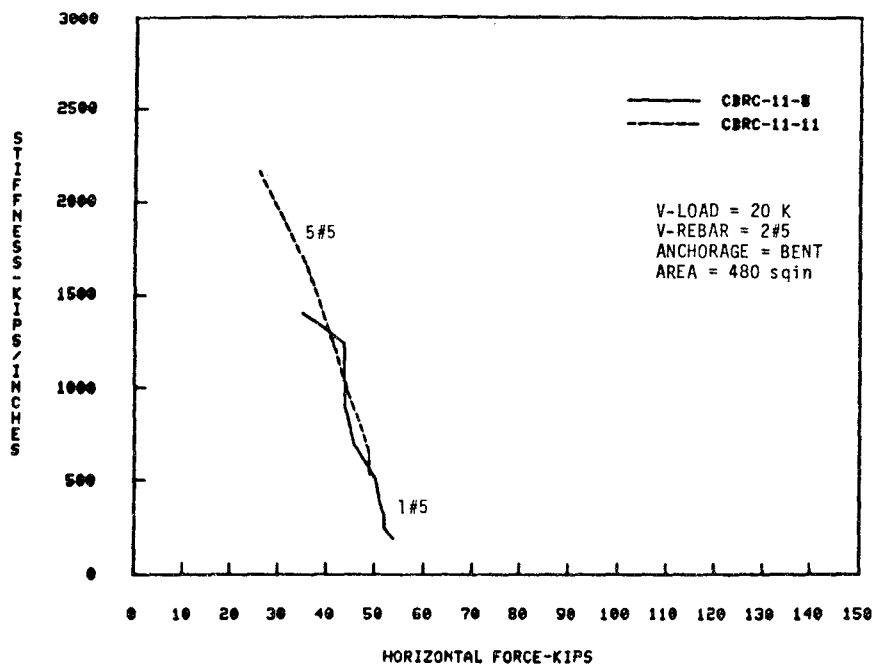


FIG. 5.17b EFFECT OF HORIZONTAL REINFORCEMENT ON STIFFNESS DEGRADATION (CBRC)

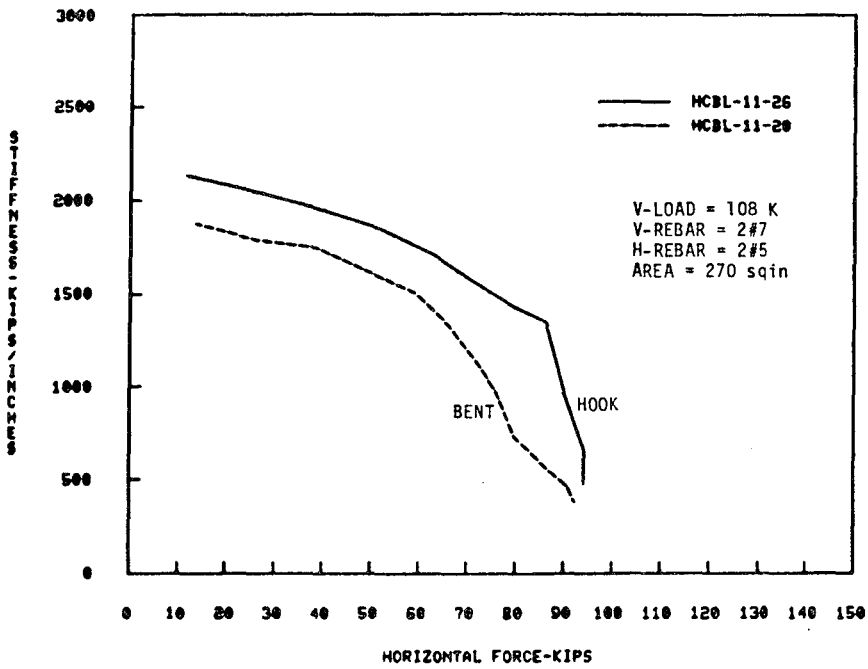


FIG. 5.18 EFFECT OF TYPE OF ANCHORAGE ON STIFFNESS DEGRADATION (HCBL)

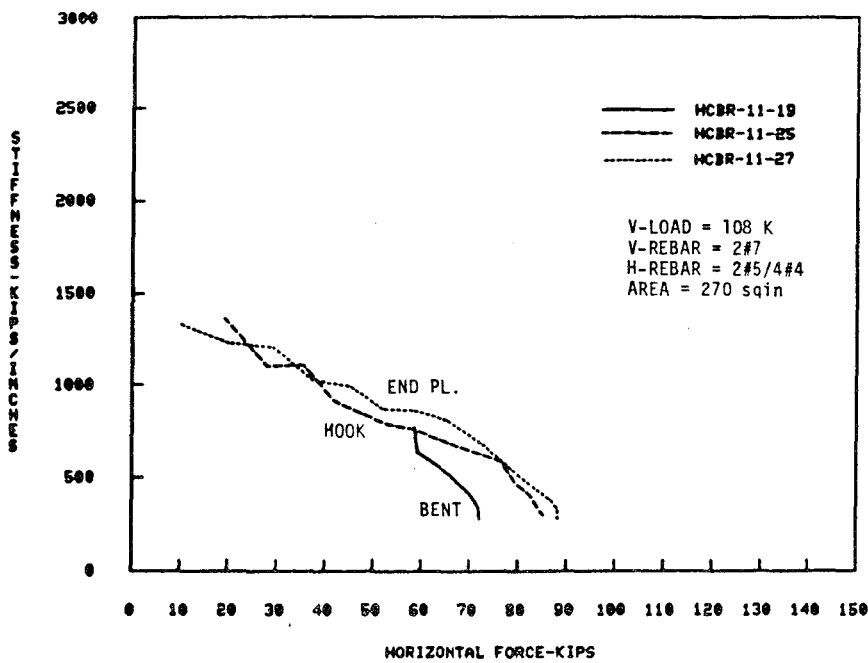


FIG. 5.19a EFFECT OF TYPE OF ANCHORAGE ON STIFFNESS DEGRADATION (HCBR)

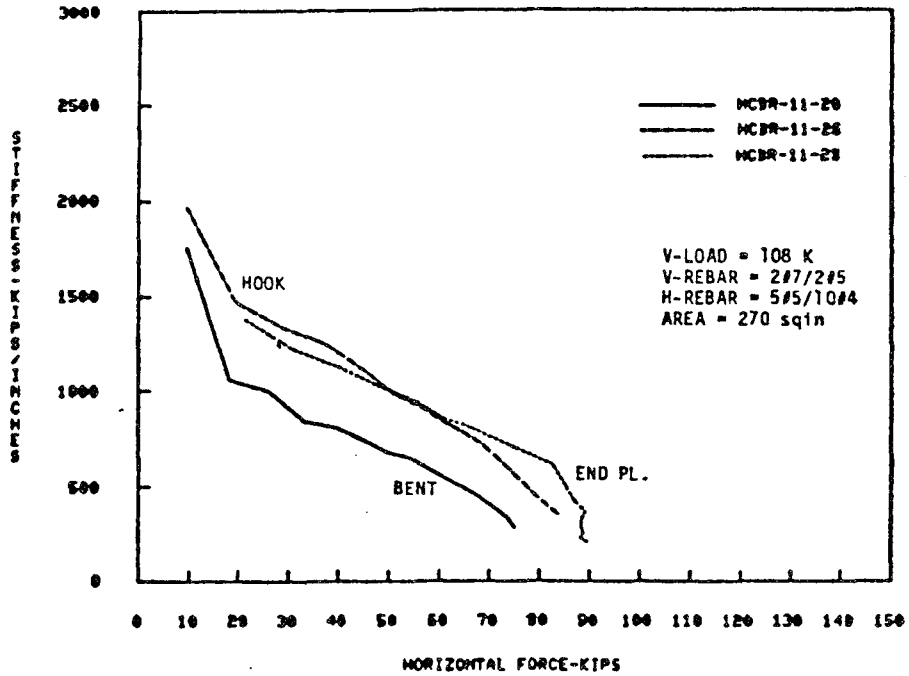


FIG. 5.19b EFFECT OF TYPE OF ANCHORAGE ON STIFFNESS DEGRADATION (HCBR)

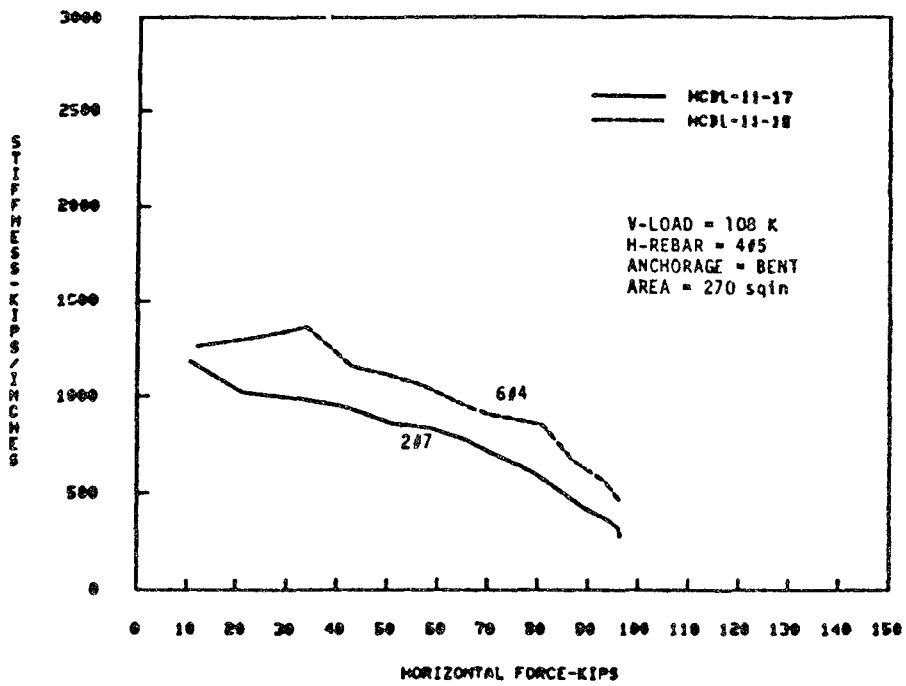


FIG. 5.20a EFFECT OF V-REBAR DISTRIBUTION OF STIFFNESS DEGRADATION (HCBL)

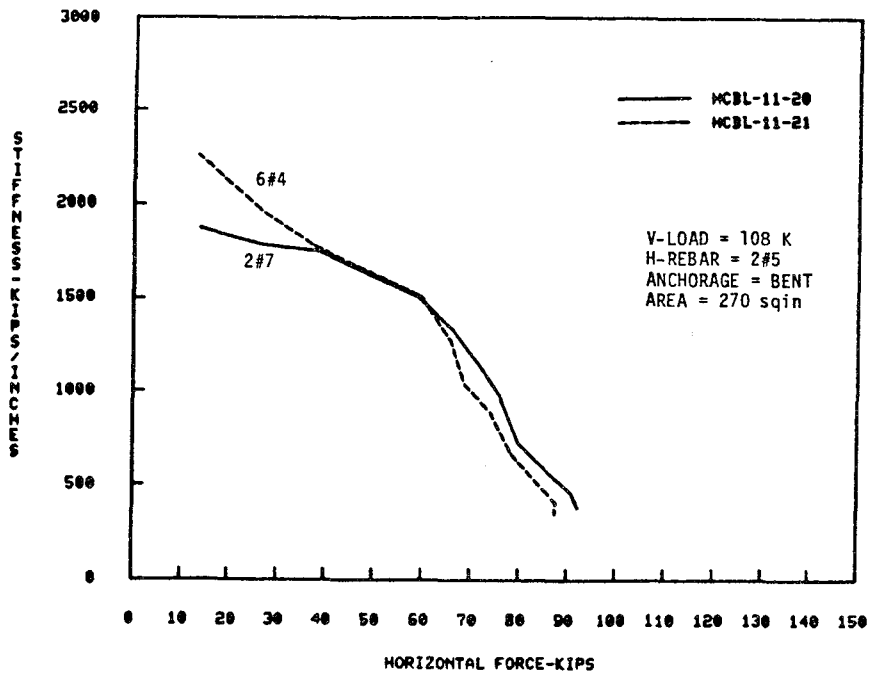


FIG. 5.20b EFFECT OF V-REBAR DISTRIBUTION ON STIFFNESS DEGRADATION (HCBL)

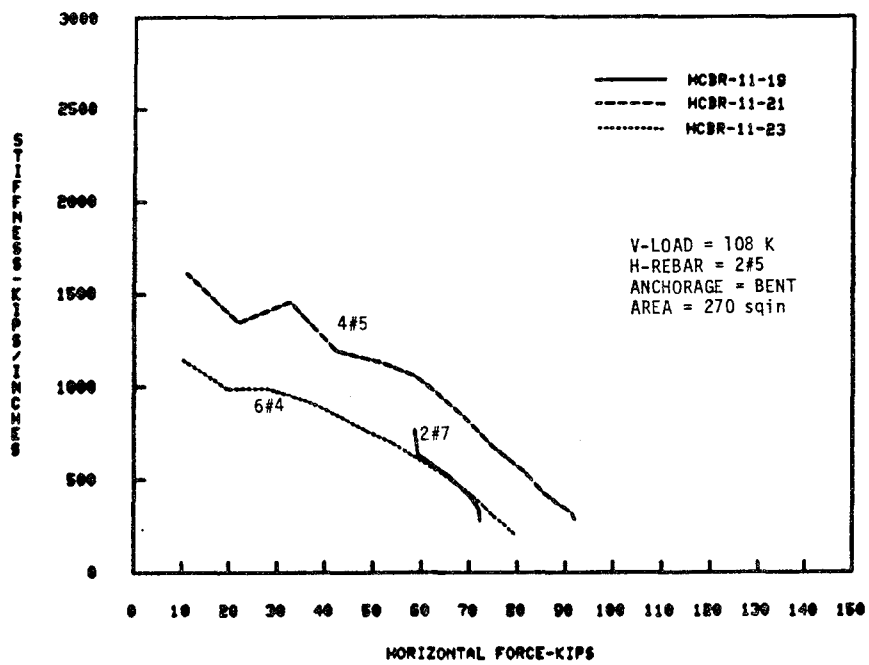


FIG. 5.21a EFFECT OF V-REBAR DISTRIBUTION ON STIFFNESS DEGRADATION (HCBR)

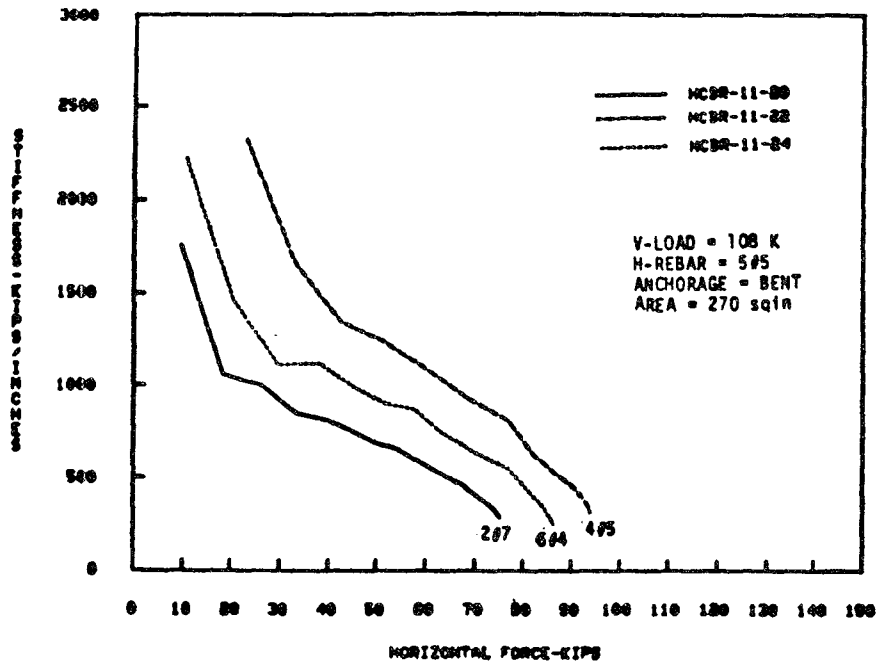


FIG. 5.21b EFFECT OF V-REBAR DISTRIBUTION ON STIFFNESS DEGRADATION (HCBR)

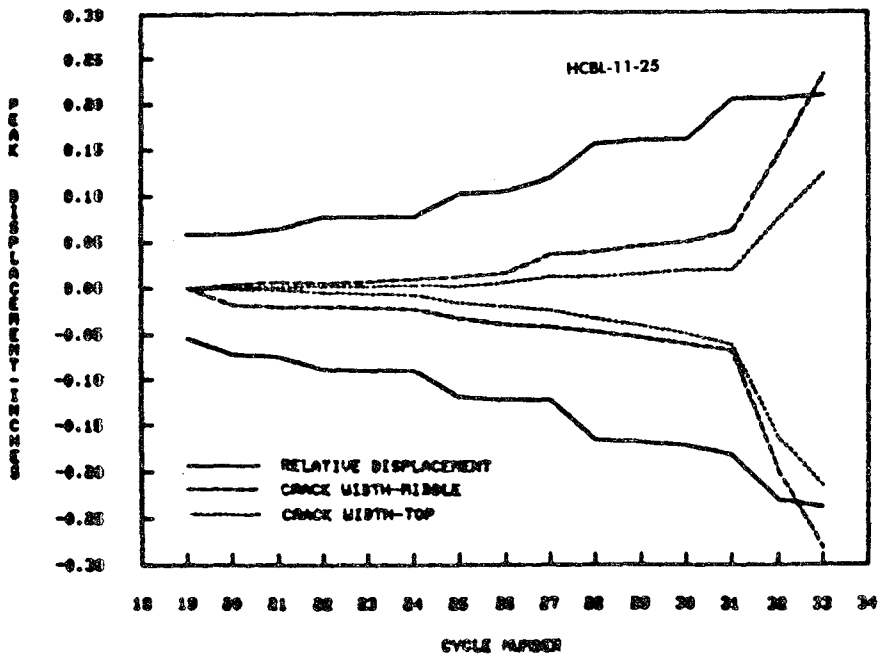


FIG. 5.22 COMPARISON OF CRACK WIDTH AND RELATIVE DISPLACEMENT IN HORIZONTAL DIRECTION

SECTION 6 SUMMARY AND CONCLUSIONS

In the introduction of this report it was pointed out that this particular study was directed at the influence of four parameters on the seismic behavior of thirty masonry piers. These parameters were

1. The level of bearing stress
2. Amount of horizontal reinforcement
3. Anchorage of horizontal reinforcing bars (four different types including joint reinforcement).
4. Distribution of vertical reinforcement

From the many different types of masonry structural elements used in actual masonry construction, this test program focused on the behavior of piers commonly found in perforated shear walls. The test specimens were constructed from three different, but commonly used materials. These were

1. Hollow concrete block piers (HCBL)
2. Hollow clay brick piers (HCBR)
3. Double wythe grouted core clay brick piers (CBRC).

All the piers had the same planar geometry and were fully grouted.

In Section 5 of this report the influence of each of the four parameters on the behavior of the piers was discussed. The discussion focused mainly on the influence of the parameters on the hysteresis envelopes of the piers, as determined from the resistance to the successively increasing displacement imposed on the piers. The effect of the parameters on stiffness degradation was also discussed. The following is a summary of the major findings.

1. Bearing Load : The magnitude of the bearing load was found to have a significant effect on the hysteretic behavior of the piers. The larger the bearing load, the greater the horizontal resistance, i.e. larger lateral force is required to induce cracking and cause failure of the piers. This is explained from principal stresses; a larger lateral load is required to exceed the compressive field resulting from the larger bearing load. This compressive field must be overcome and tension stresses introduced before cracking can begin.

The bearing load also influenced the behavior mode of the piers. For low bearing loads the piers deformed in flexure with high ductility, whereas for high bearing loads the behavior was characterized by shear deformations (diagonal cracking) and reduction in ductility.

The effect of bearing load on stiffness degradation was also noted although not very significant; the stiffness degradation was less pronounced with higher bearing loads.

2. Amount of Horizontal Reinforcement : The amount of horizontal reinforcement was not found to be a significant factor in the hysteretic behavior of the piers. In tests reported in [1,2,3,4] a positive correlation was observed between increase in horizontal reinforcement and improvement in inelastic behavior. It was noted,

however, that only some of the piers showed such improvement and that the improvement was not proportional to the increase in reinforcement. This study confirms those findings.

The effect of the amount of horizontal reinforcement on stiffness degradation was also found to be negligible.

3. Anchorage of Horizontal Reinforcement : This study showed that the most significant improvement in the hysteretic behavior of piers failing in shear is provided by adequate anchorage of the horizontal reinforcement. Without anchorage the ultimate strength is relatively low and failure follows immediately after the ultimate strength is reached. The failure is sudden and complete.

Anchorage provided by 90 degree bends grouted into the vertical end cavities increases the ultimate strength and provides some ductility.

Significant improvement in the hysteretic behavior was accomplished in two ways: by hooking the horizontal rebars 180 degrees around the vertical end reinforcing bars, and by welding plates to the ends of the horizontal reinforcing bars and embedding the assembly in the grout. These types of anchorage increase the ultimate strength above that for the 90 degree bends but, more important, significantly increase the pier ductility.

Dur-O-Wal trusses embedded in the bedjoints were not as effective in increasing the pier strength as the conventional horizontal reinforcing bars. However, the use of Dur-O-Wal appeared to improve the ductility of the piers, possibly because of a more uniform distribution of the horizontal steel.

No consistent correlation was observed between the anchorage of horizontal reinforcement and the stiffness degradation.

4. Distribution of Vertical Reinforcement : Three different configurations of vertical steel were used in this test program. The configurations employed identical steel ratios, but different distributions. The distribution of the vertical reinforcement was not found to be effective in improving the hysteretic behavior of the piers. Slight improvements were noted in the strength of the piers, but ductility was not improved.

The distribution of vertical reinforcement had no effect on the stiffness degradation of the piers.

Considering all the results from the thirty-two tests reported in this report the following can be concluded:

1. Bearing load significantly influences the seismic behavior of masonry piers commonly found in perforated shear walls. Most important, the level of bearing load can change the mode of failure. Low bearing loads favor the flexural mode of failure whereas high bearing loads favor the shear mode of failure.
2. Horizontal reinforcement is effective in inhibiting the opening of shear cracks, but with diminishing returns as the amount of reinforcing steel is increased. Also, improved ductility appears to be accomplished by distributing the horizontal reinforcing bars more uniformly over the pier by using smaller bar sizes or even Dur-O-Wal or a combination thereof. Typically, improvement can be expected for horizontal reinforcement ratios up to three to five times the minimum ratio specified by the 1985 UBC (0.07%). Horizontal reinforcement ratios beyond that are not expected to improve the ultimate strength of the masonry piers significantly, but a more uniform distribution of this steel area will probably improve the ductility of the piers.

3. Anchorage of horizontal reinforcement is very important for improved hysteretic behavior of piers. It is recommended that all horizontal bars with insufficient bond area be hooked 180 degrees around a vertical reinforcing bar. This increases the strength and ductility of the piers in the shear mode of failure.

SECTION 7 REFERENCES

- [1] Hidalgo, P.A., Mayes, R.L., McNiven, H.D. and Clough, R.W., "Cyclic Loading Tests of Masonry Single Piers, Vol. 1 - Height to Width Ratio of 2", EERC Report No. UCB/EERC-78/27, University of California, Berkeley, California, 1978.
- [2] Chen, S.W., Hidalgo, P.A., Mayes, R.L., Clough, R.W. and McNiven, H.D., "Cyclic Loading Tests of Masonry Single Piers, Vol. 2 - Height to Width Ratio of 1", EERC Report No. UCB/EERC-78/28, University of California, Berkeley, California, 1978.
- [3] Hidalgo, P.A., Mayes, R.L., McNiven, H.D. and Clough, R.W., "Cyclic Loading Tests of Masonry Single Piers, Vol. 3 - Height to Width Ratio of 0.5", EERC Report No. UCB/EERC-79/12, University of California, Berkeley, California, 1979.
- [4] Sveinsson, B.I., Mayes, R.L. and McNiven, H.D., "Evaluation of Seismic Design Provisions for Masonry in the United States", EERC Report No. UCB/EERC-81/10, University of California, Berkeley, California, 1981.
- [5] Meli, R. "Behaviour of Masonry Walls under Lateral Loads", Proceedings of the Fifth World Conference on Earthquake Engineering, Rome, 1973.
- [6] Priestley, M.J.N., "Seismic Resistance of Reinforced Concrete Masonry Shear Walls with High Steel Percentages", Bulletin of the New Zealand National Society for Earthquake Engineering, Vol. 10, No. 1, 1977.
- [7] Priestley, M.J.N. and Bridgeman, D.O., "Seismic Resistance of Brick Masonry Walls", Bulletin of the New Zealand National Society for Earthquake Engineering, Vol. 7, No. 4, 1974.
- [8] Priestley, M.J.N., "Cyclic Testing of Heavily Reinforced Concrete Masonry Shear Walls", University of Canterbury Research Report 76-12, New Zealand, 1976.
- [9] Mayes, R.L., Omote, Y. and Clough, R.W., "Cyclic Shear Tests of Masonry Piers, Vol. I - Test Results", EERC Report No. 76-8, University of California, Berkeley, California, 1976.

- [10] Mayes, R.L., Omote, Y. and Clough, R.W., "Cyclic Shear Tests of Masonry Piers. Vol. II - Analysis of Test Results", EERC Report No. 76-16, University of California, Berkeley, California, 1976.
- [11] Hidalgo, P and McNiven, H.D., "Seismic Behavior of Masonry Buildings", Proceedings of the 7th World Conference on Earthquake Engineering, Istanbul, Turkey, September 1980.

APPENDIX A PRESENTATION OF THE TEST RESULTS

The experimental results are arranged on two pages for each test, four graphs obtained from the test data and photographs showing the successive crack patterns. The graphs include the hysteresis envelope, strength degradation and stiffness degradation relationships.

The strength degradation is presented in terms of the envelope curves of the first cycles, second cycles and the third cycles in each loading stage, which were applied at a constant input displacement.

Stiffness degradation is given as a function of both the horizontal force and the relative lateral displacement.

Detailed information on the graphs is presented in Section 4.

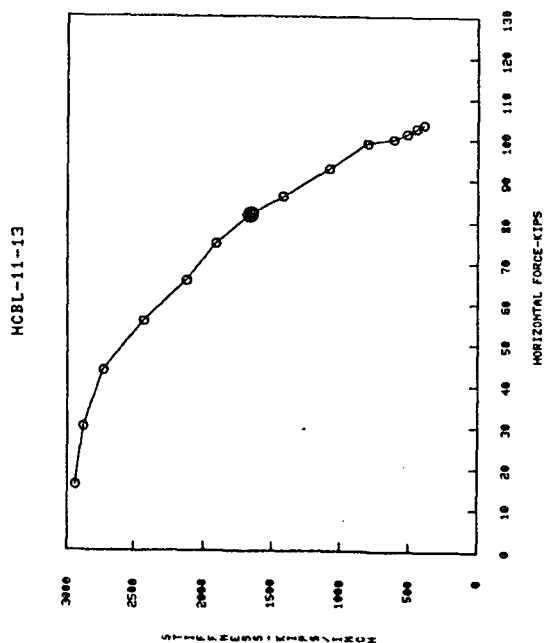
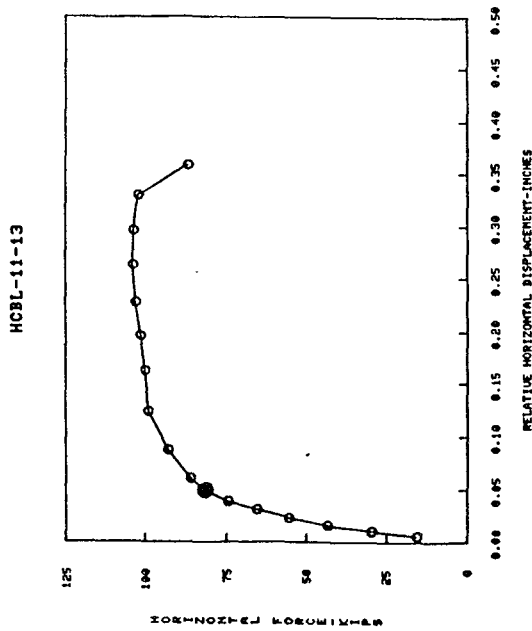
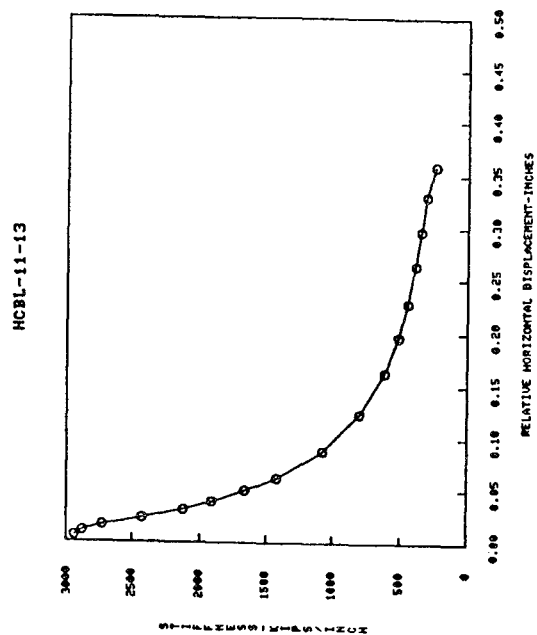
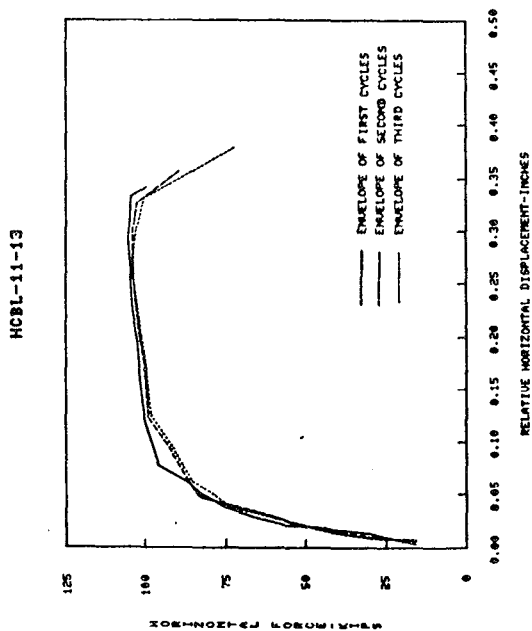


FIG. A.1a EXPERIMENTAL RESULTS (HCBL-11-13)

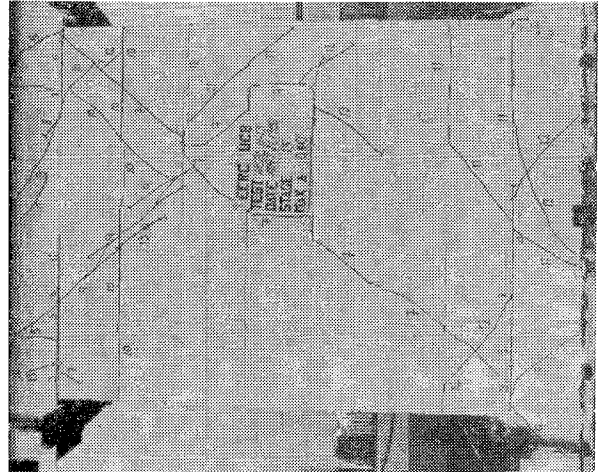
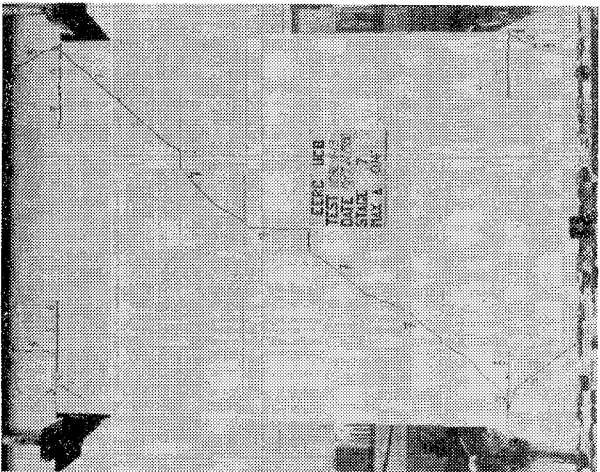
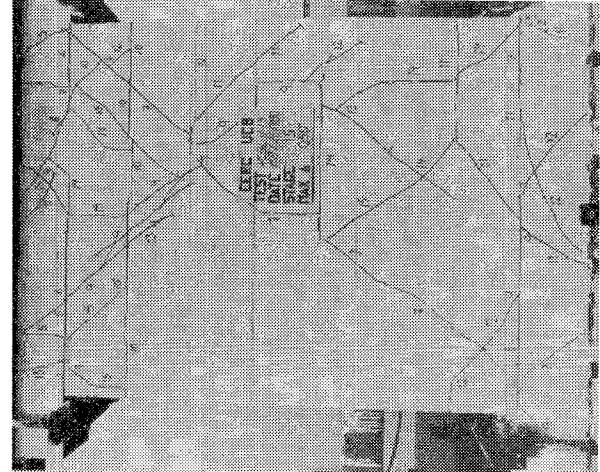
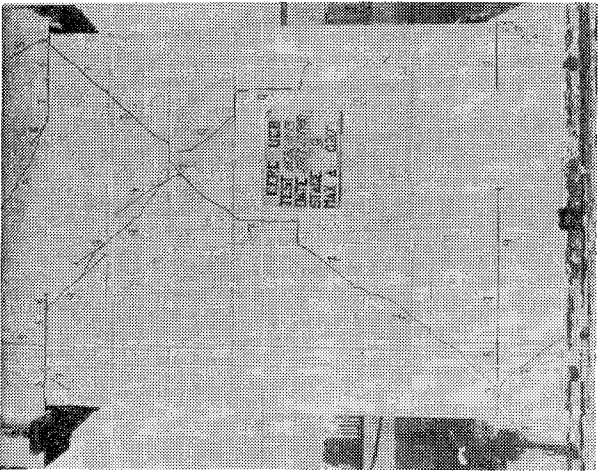
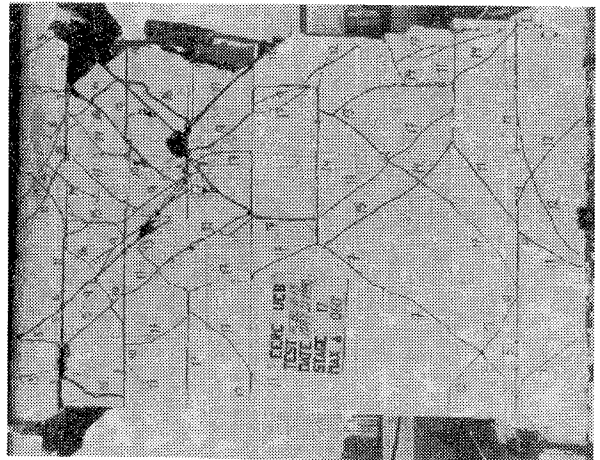
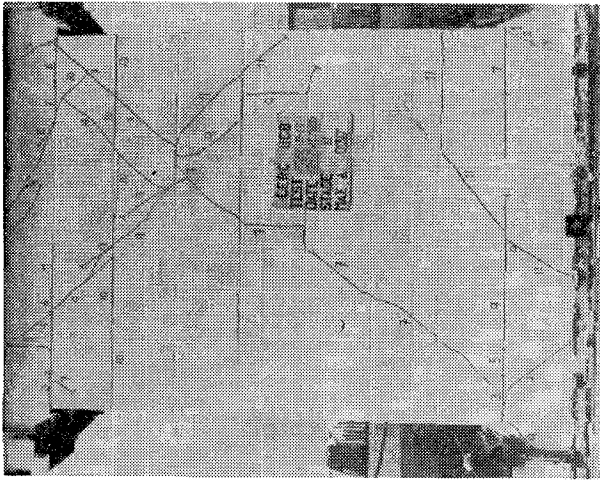


FIG. A.1b SUCCESSIVE CRACK FORMATION (HCBL-11-13)

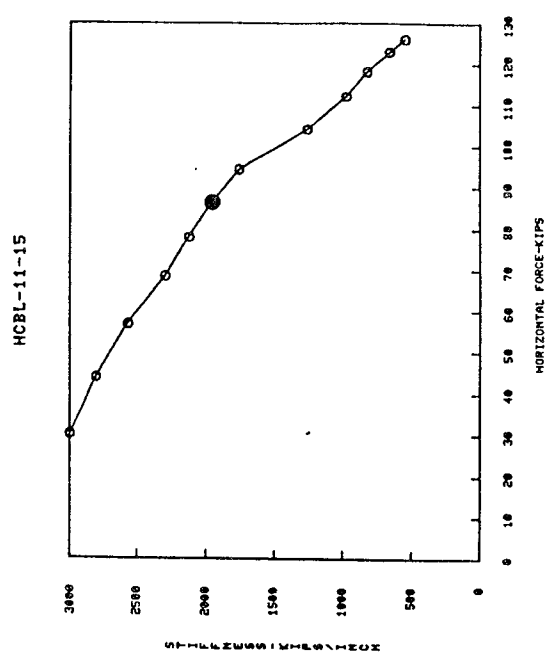
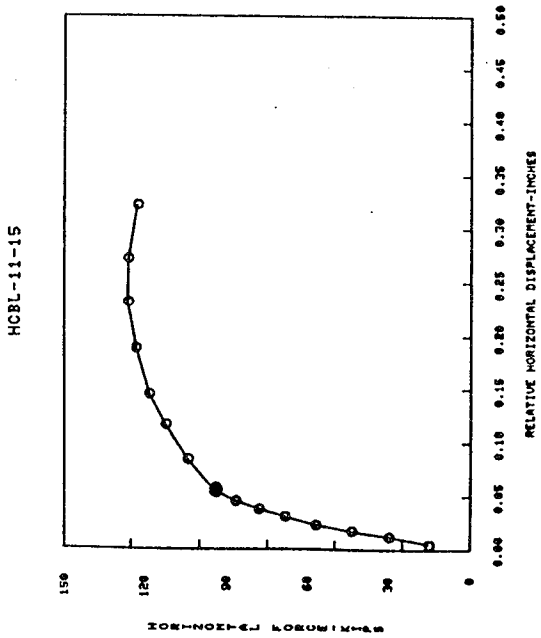
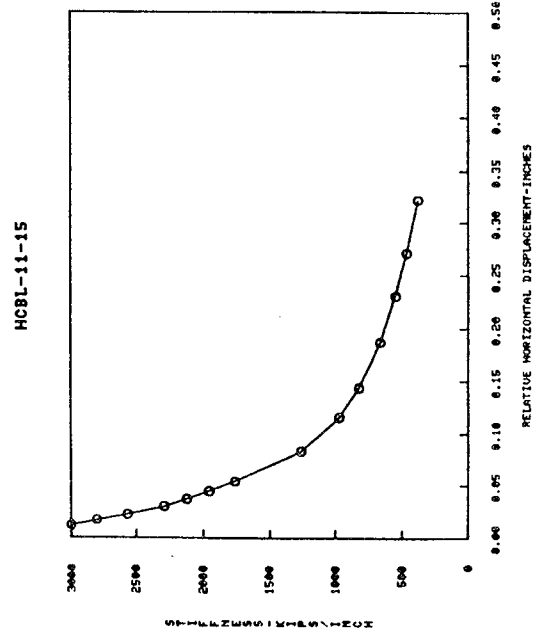
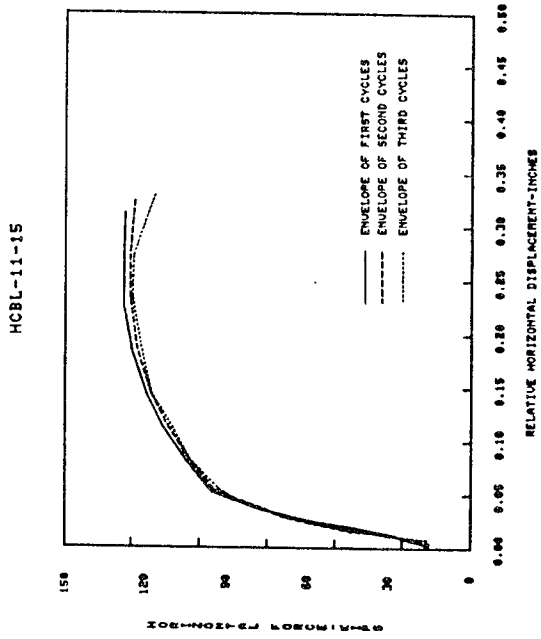


FIG. A.2a EXPERIMENTAL RESULTS (HCBL-11-15)

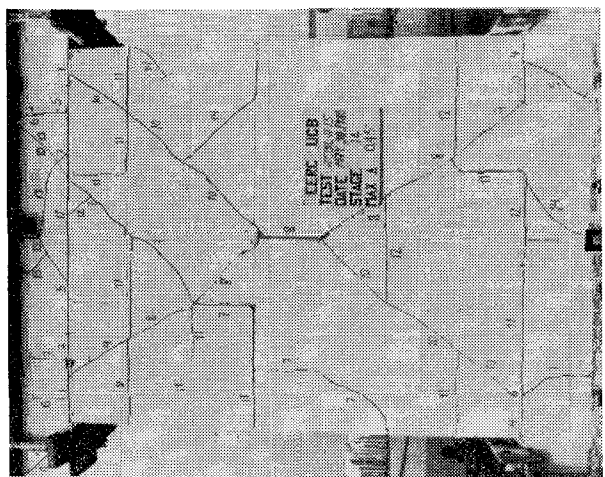
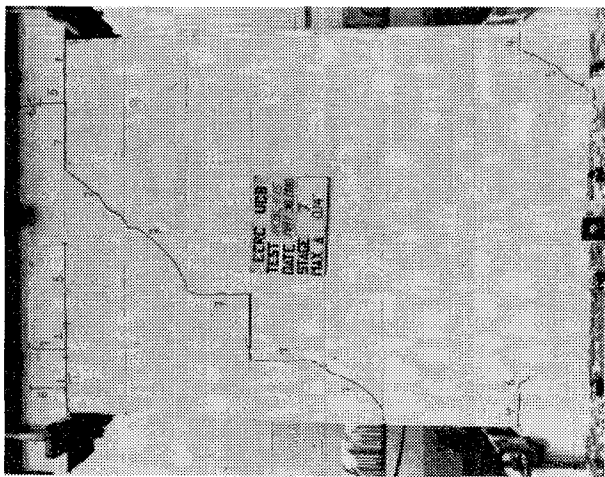
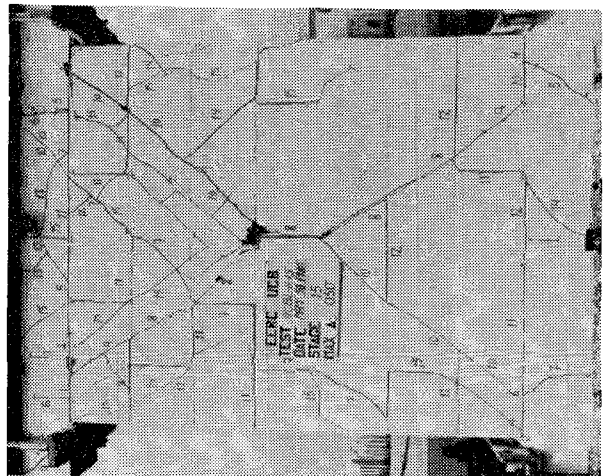
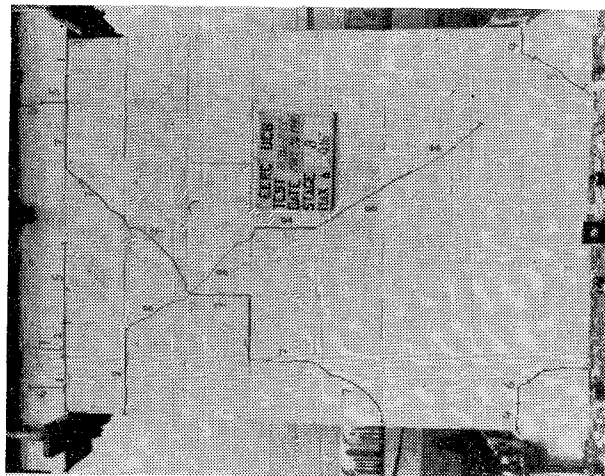
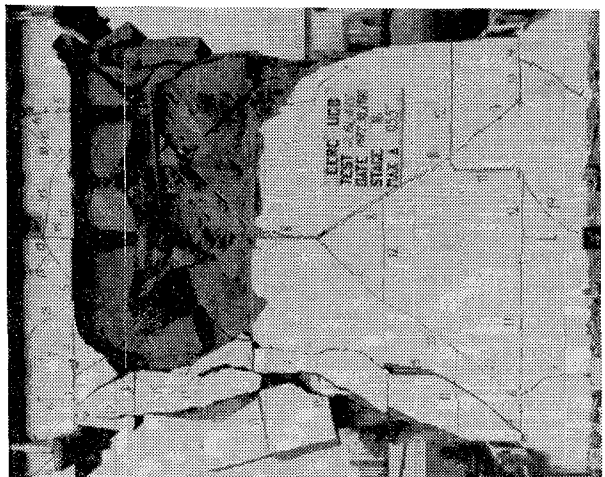
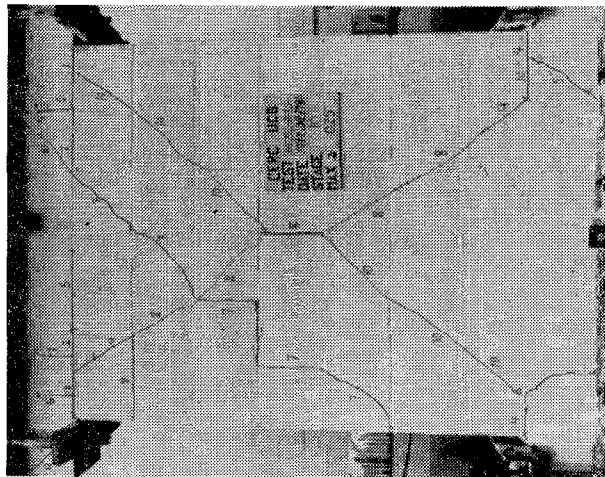


FIG. A.2b SUCCESSIVE CRACK FORMATION (HCBL-11-15)

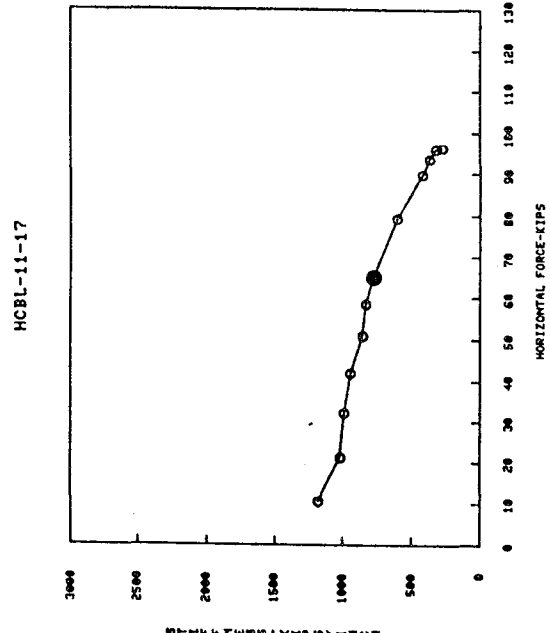
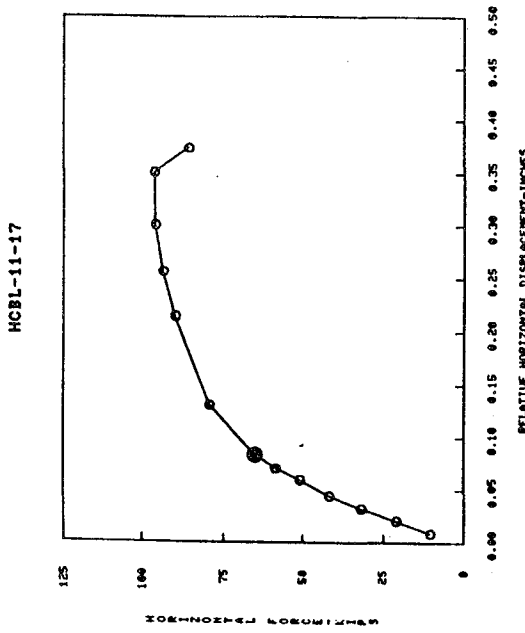
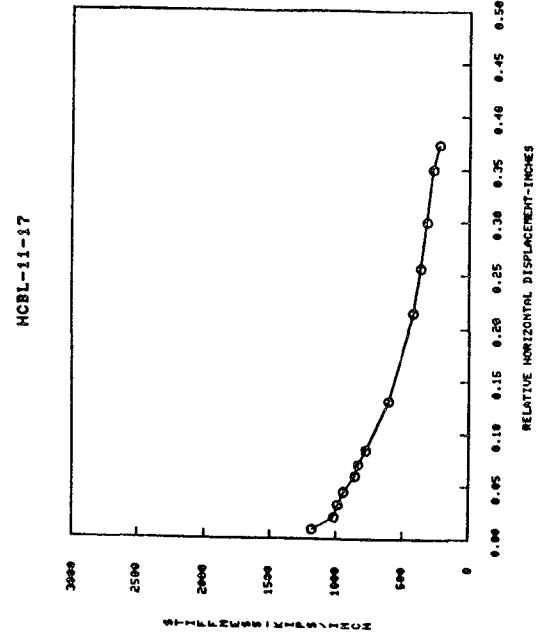
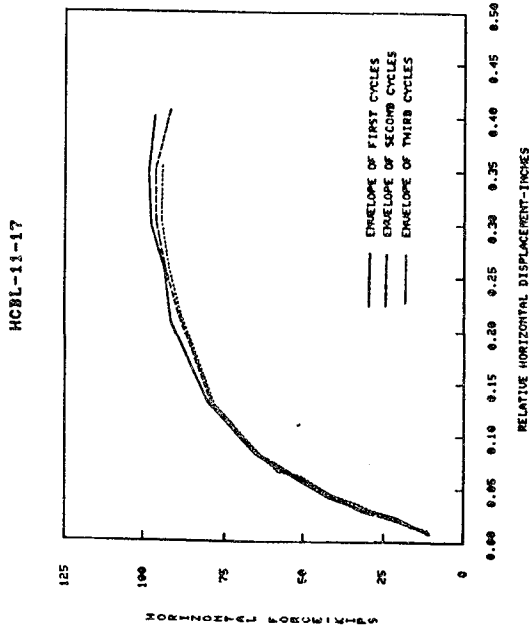


FIG. A.3a EXPERIMENTAL RESULTS (HCBL-11-17)

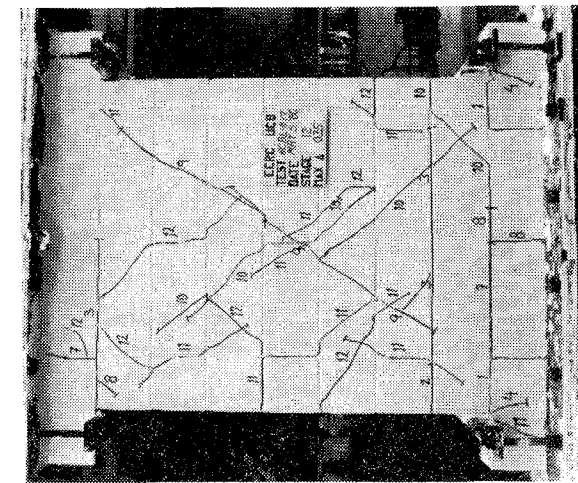
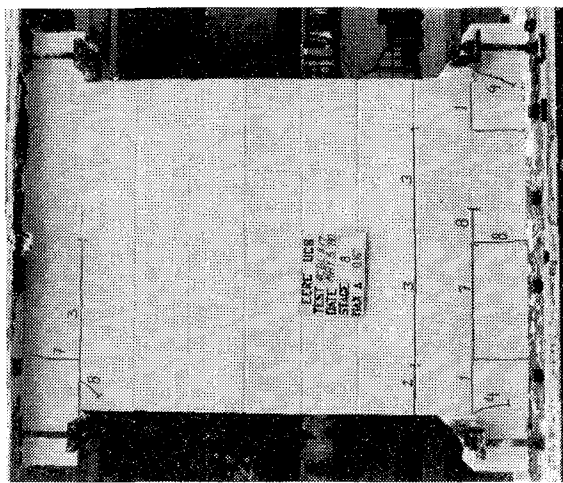
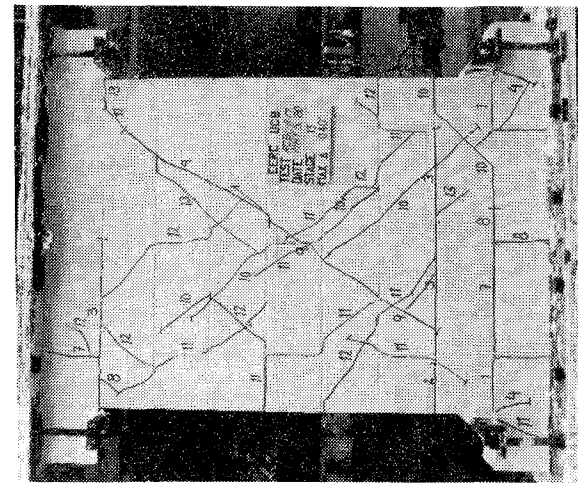
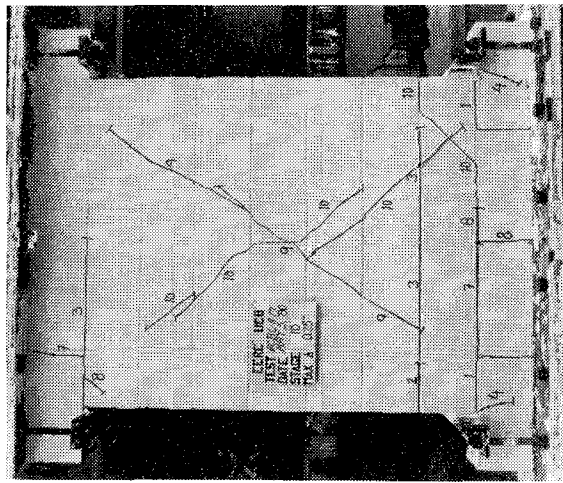
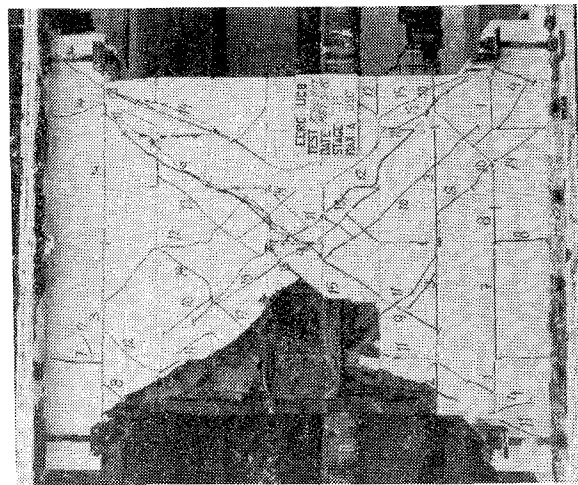
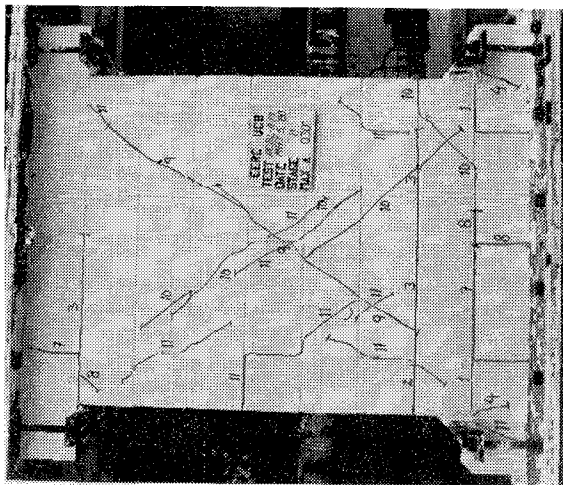
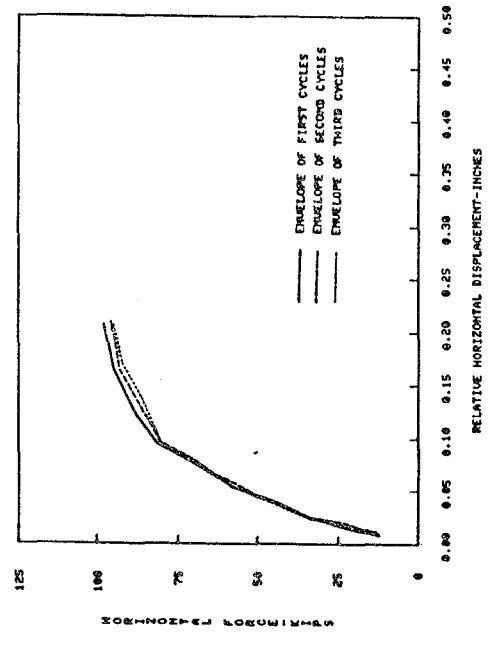
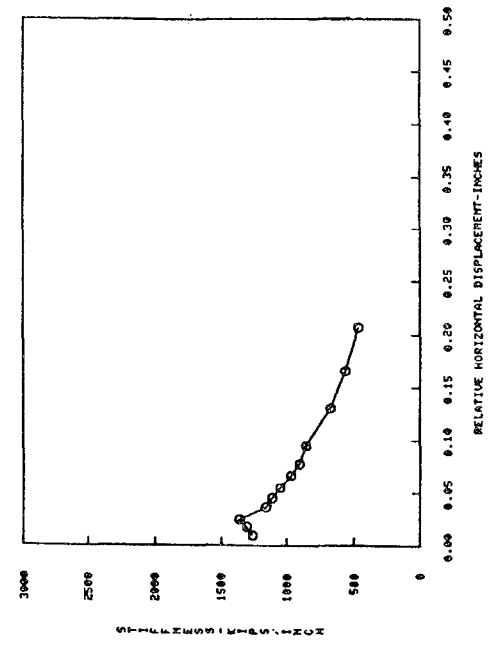


FIG. A.3b SUCCESSIVE CRACK FORMATION (HCL-11-17)

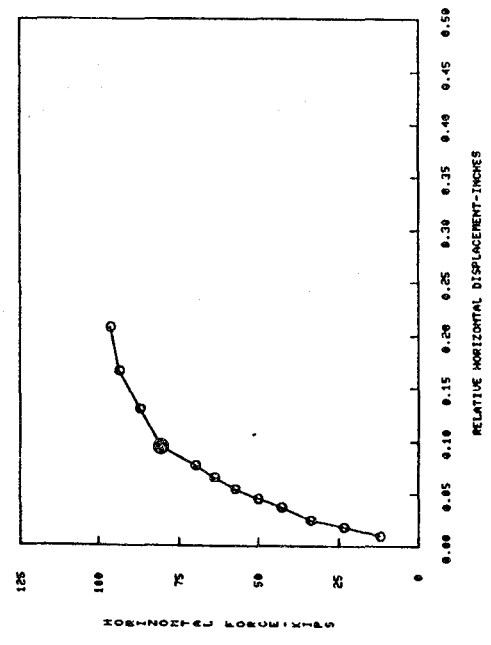
MCBL-11-18



MCBL-11-18



MCBL-11-18



MCBL-11-18

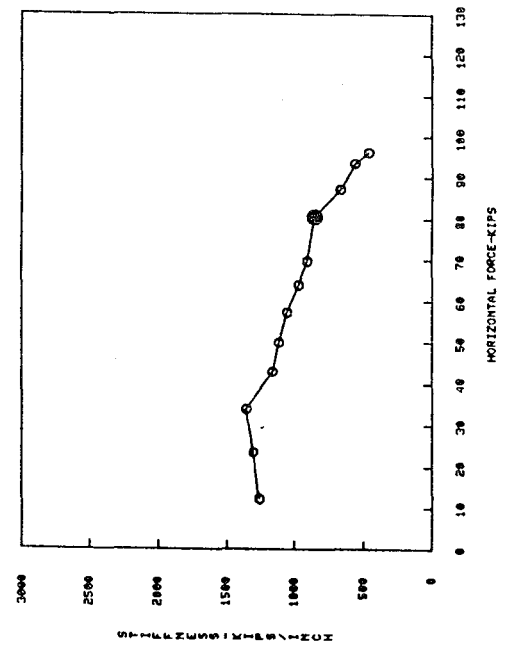


FIG. A.4 EXPERIMENTAL RESULTS (MCBL-11-18)

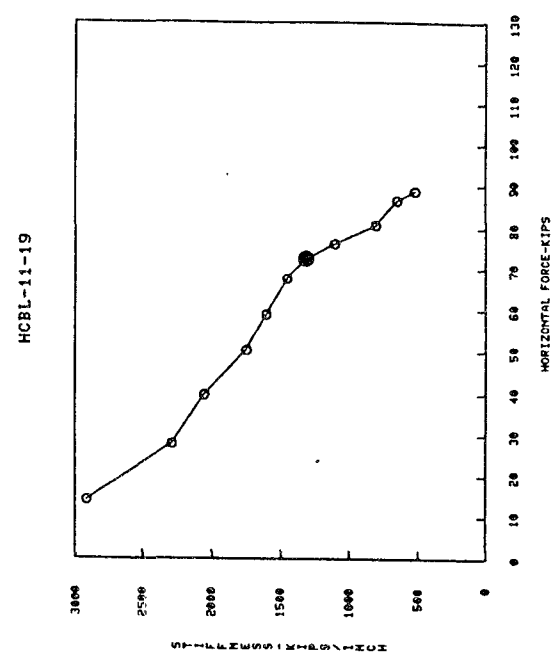
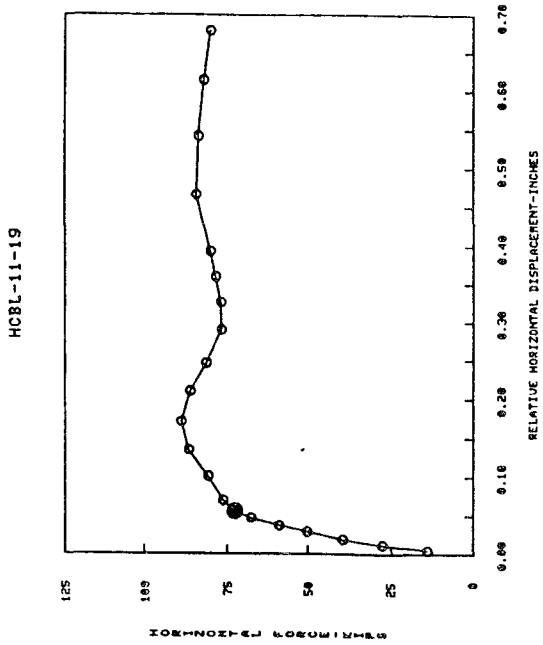
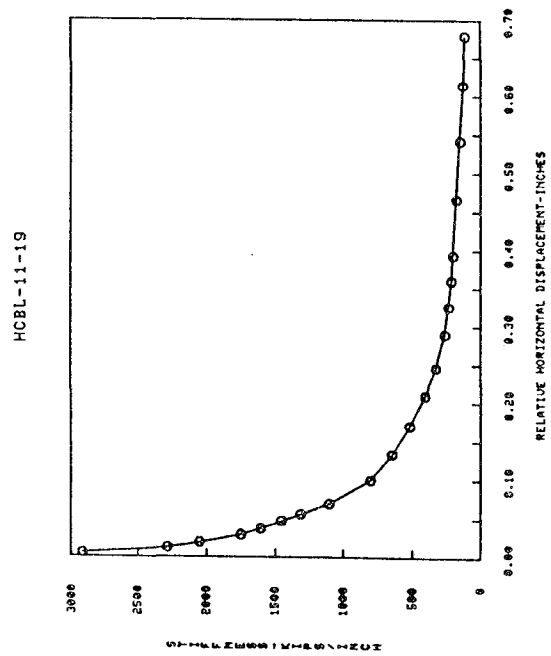
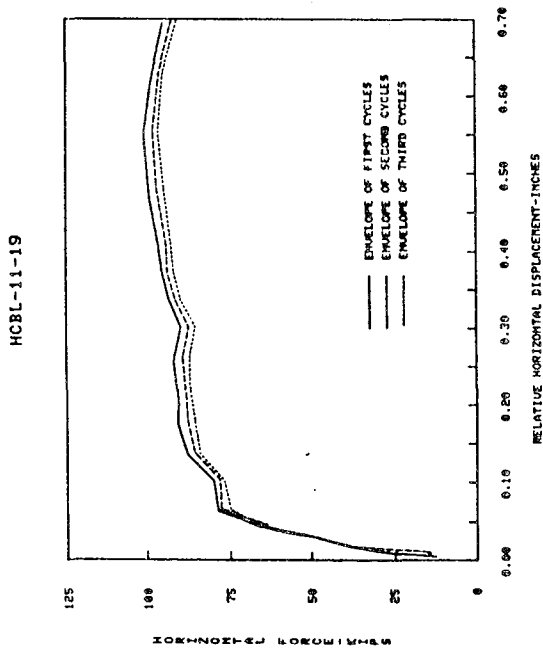


FIG. A.5a EXPERIMENTAL RESULTS (HCBL-11-19)

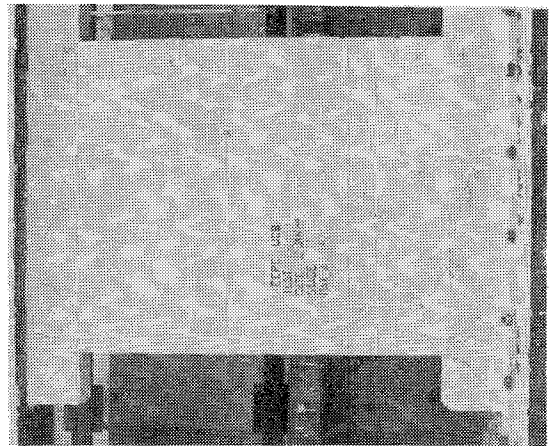
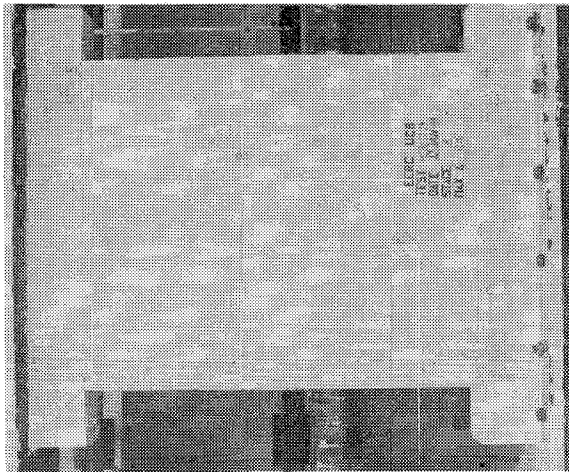
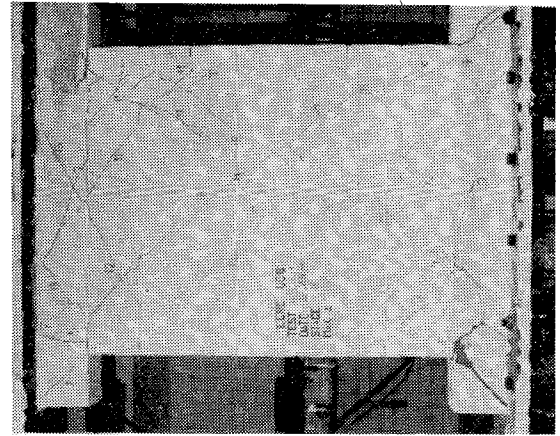
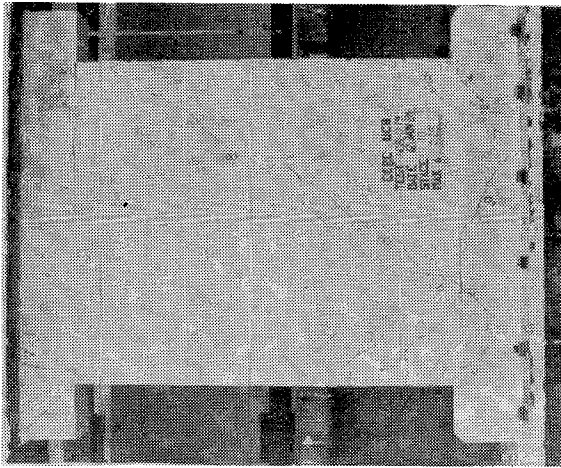
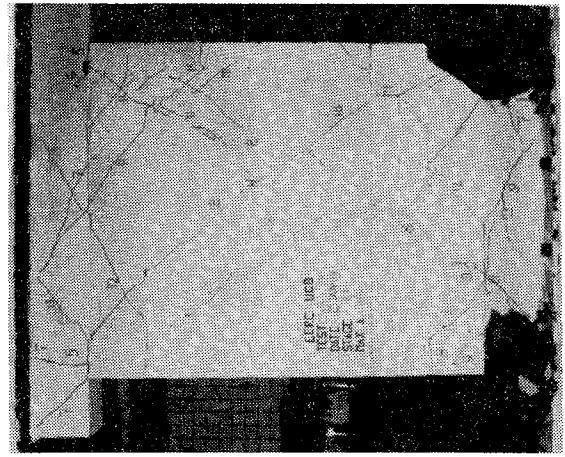
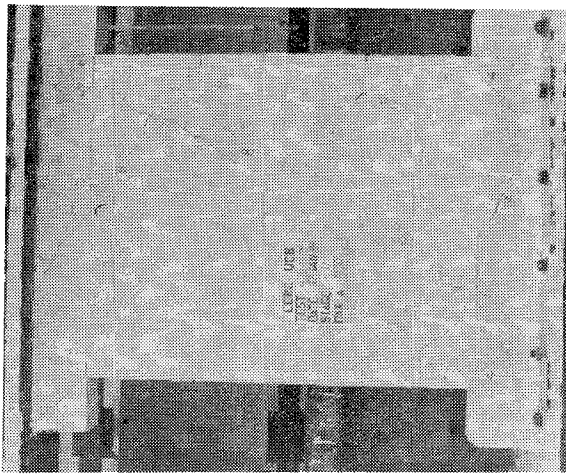
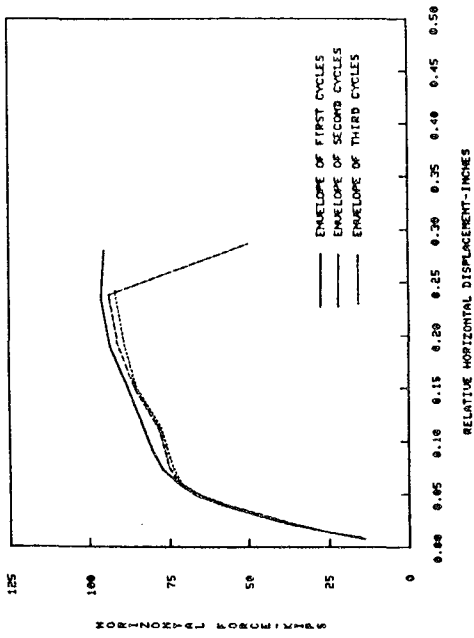
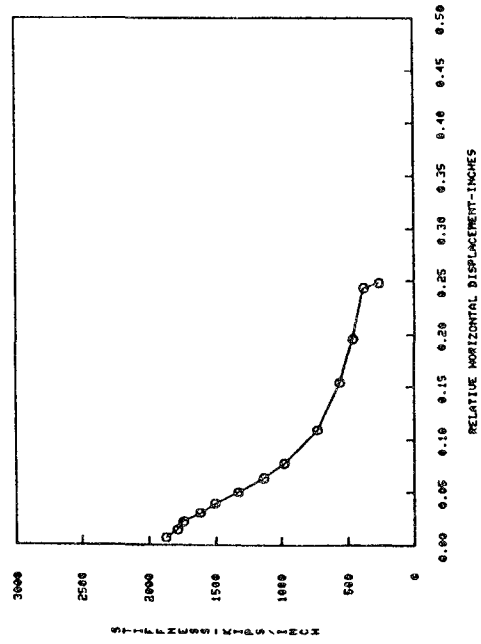


FIG. A.5b SUCCESSIVE CRACK FORMATION (HCBL-11-19)

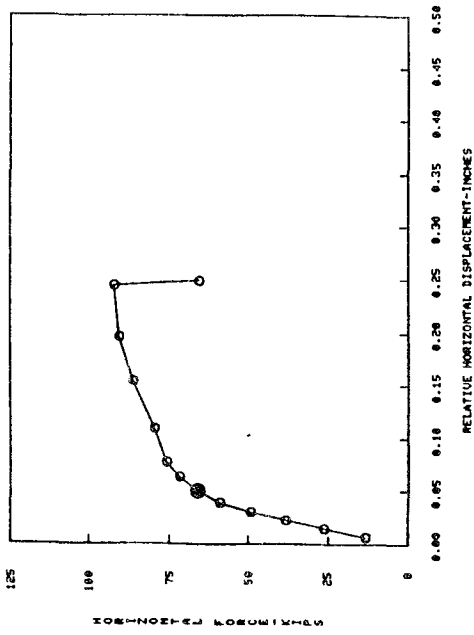
HCBL-11-20



HCBL-11-20



HCBL-11-20



HCBL-11-20

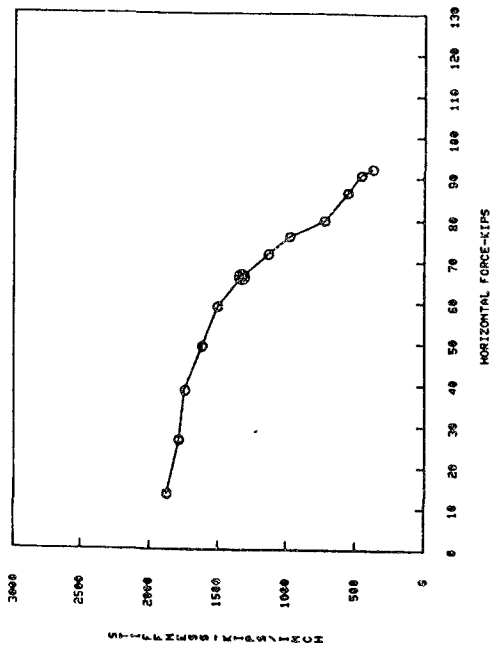


FIG. A.6a EXPERIMENTAL RESULTS (HCBL-11-20)

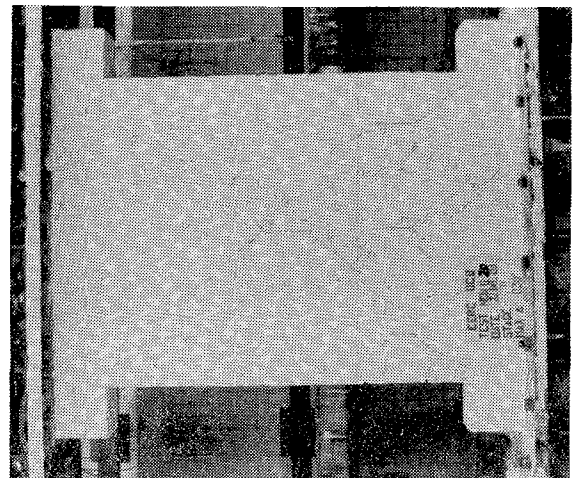
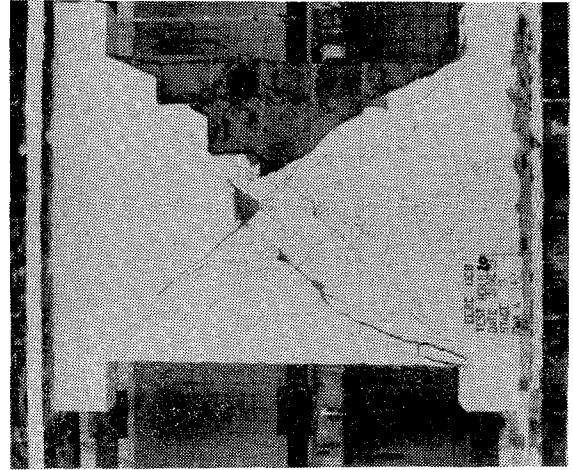
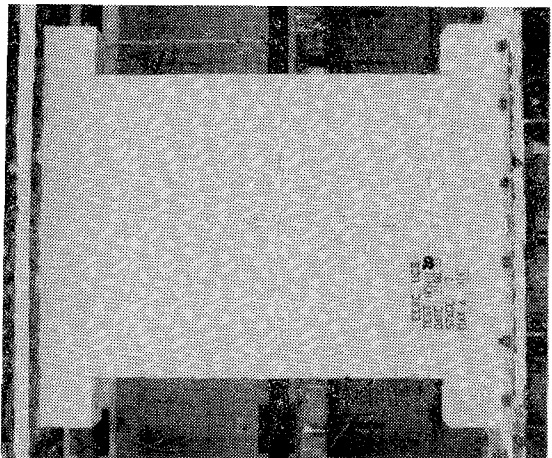
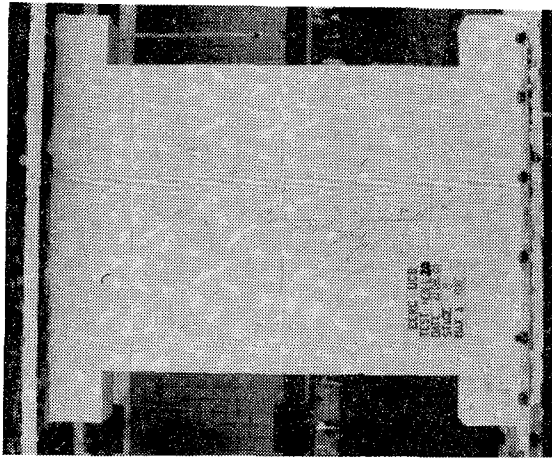
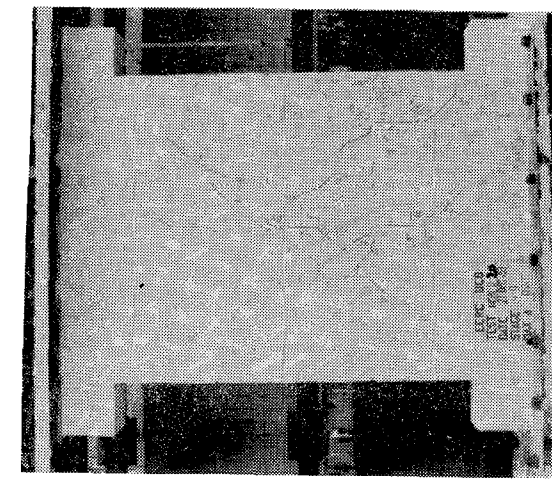


FIG. A.6b SUCCESSIVE CRACK FORMATION (HCBL-11-20)

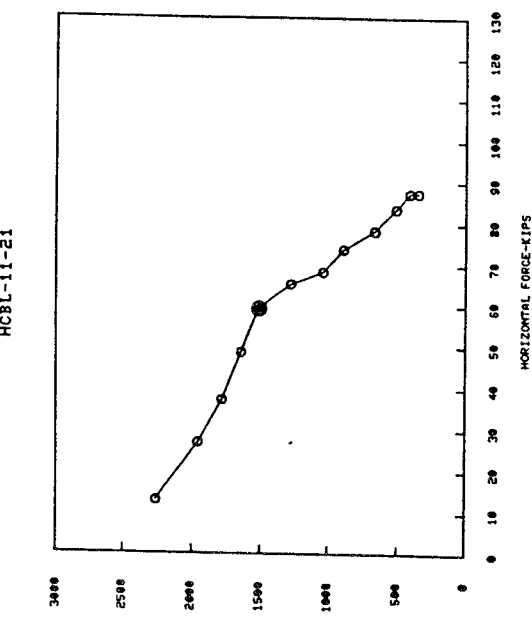
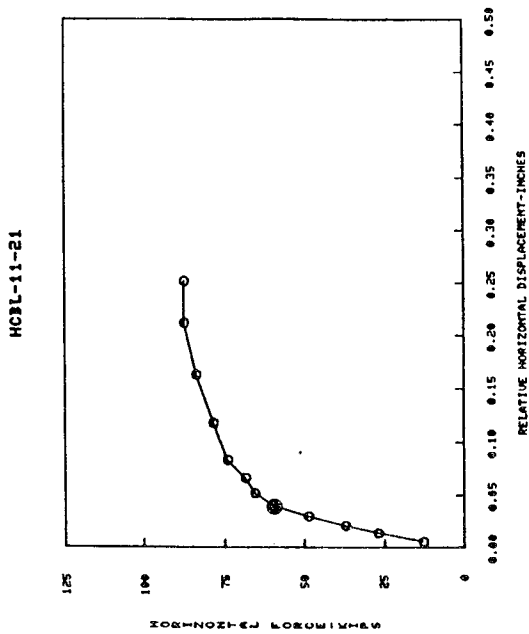
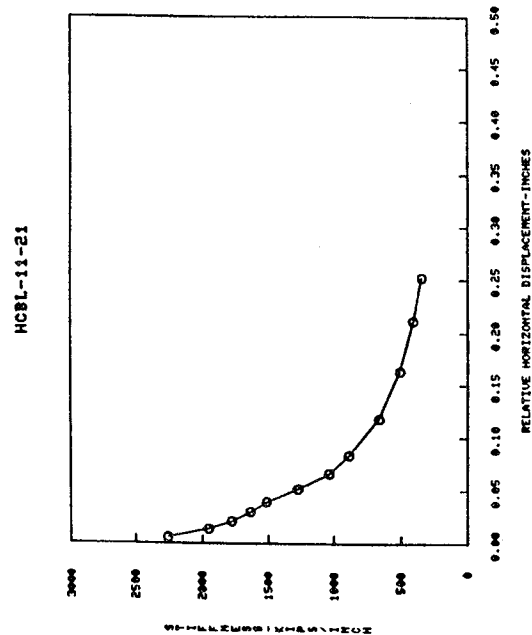
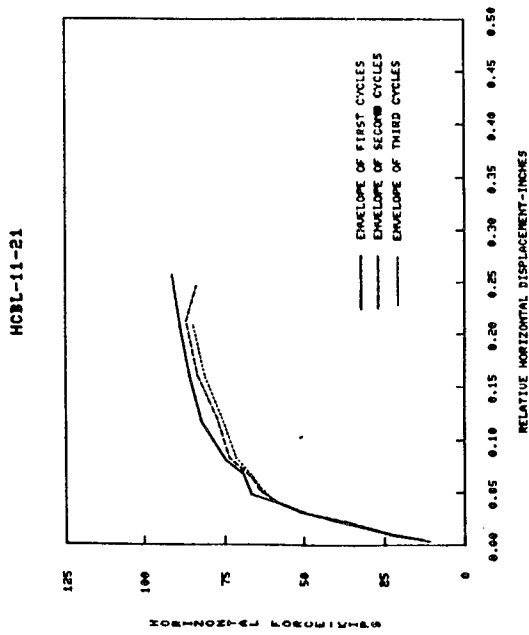


FIG. A.7a EXPERIMENTAL RESULTS (HCBL-11-21)

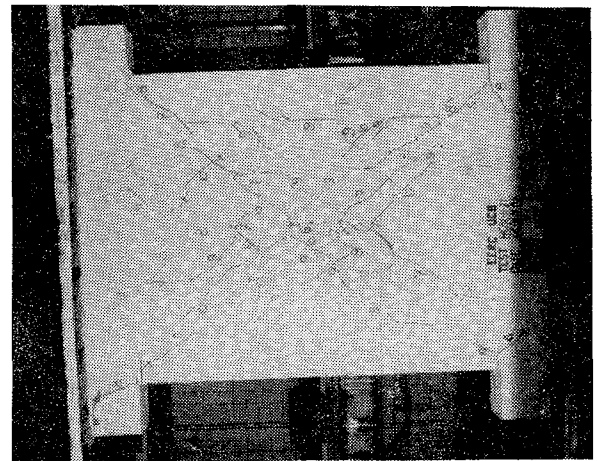
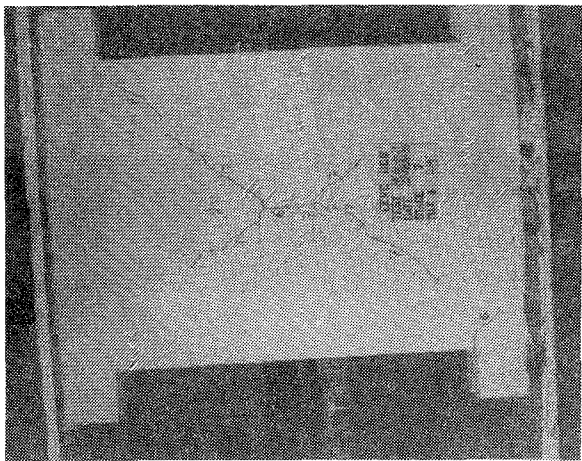
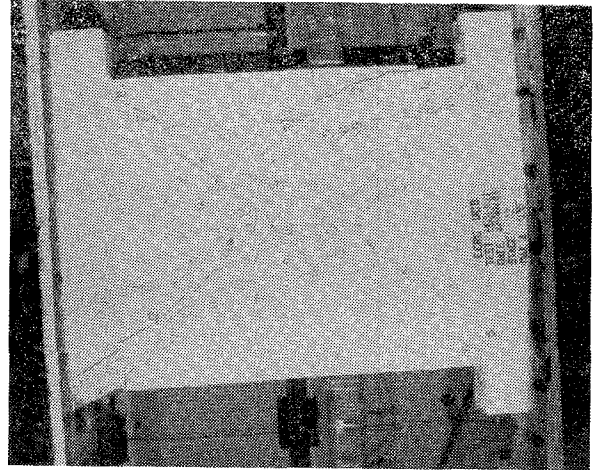
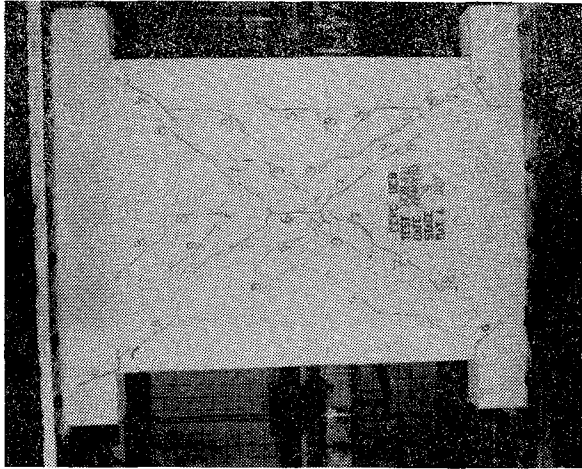
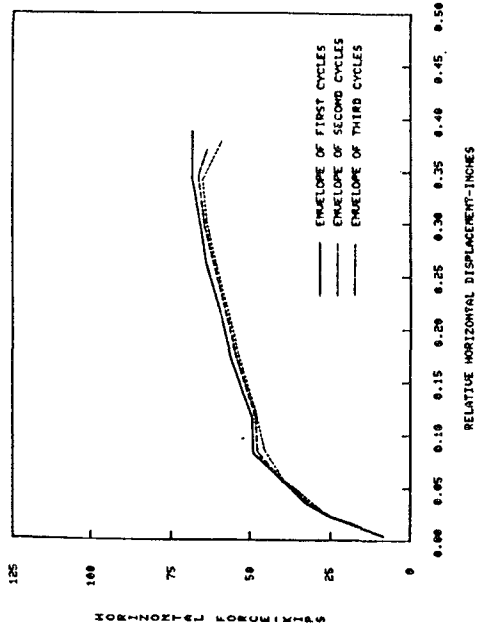
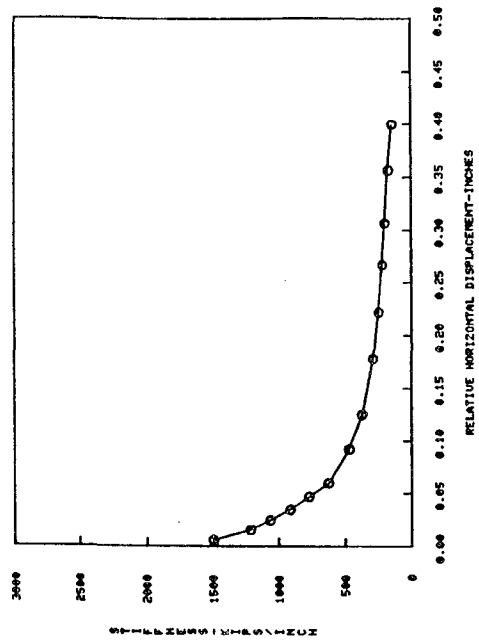


FIG. A. 7b SUCCESSIVE CRACK FORMATION (HCBL-11-21)

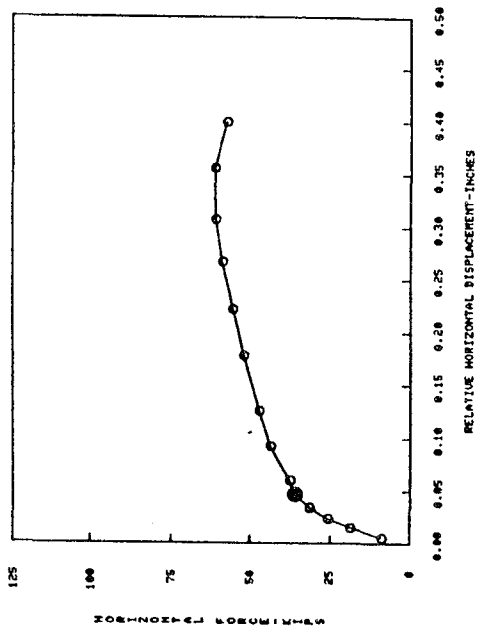
HCBL-11-22



HCBL-11-22



HCBL-11-22



HCBL-11-22

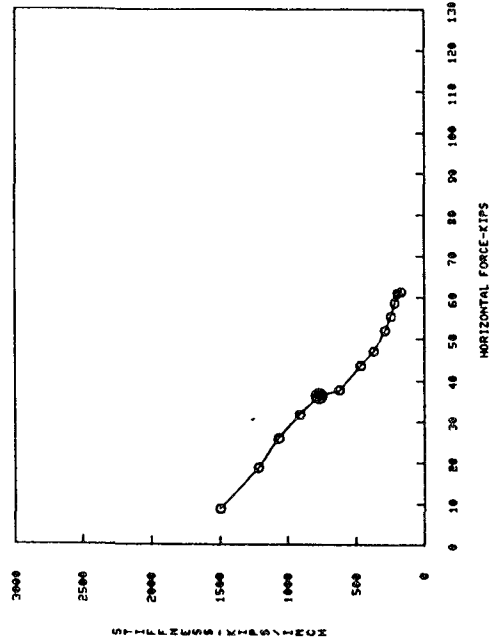


FIG. A.8a EXPERIMENTAL RESULTS (HCBL-11-22)

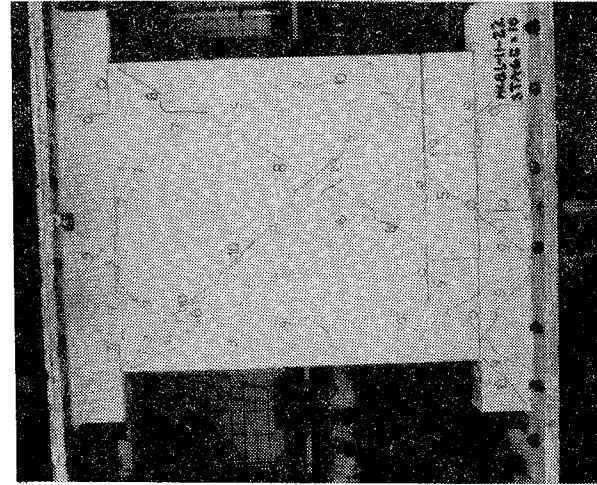
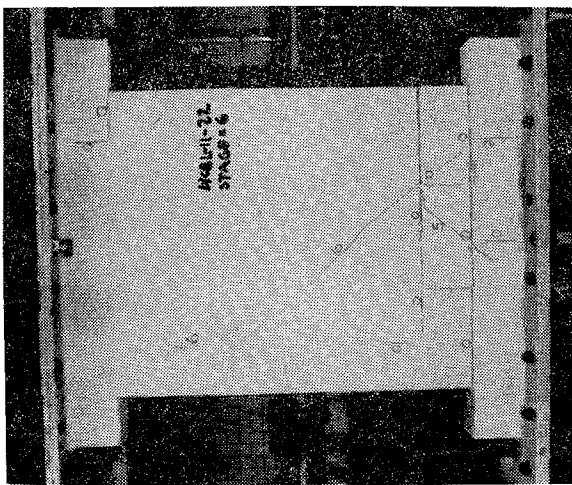
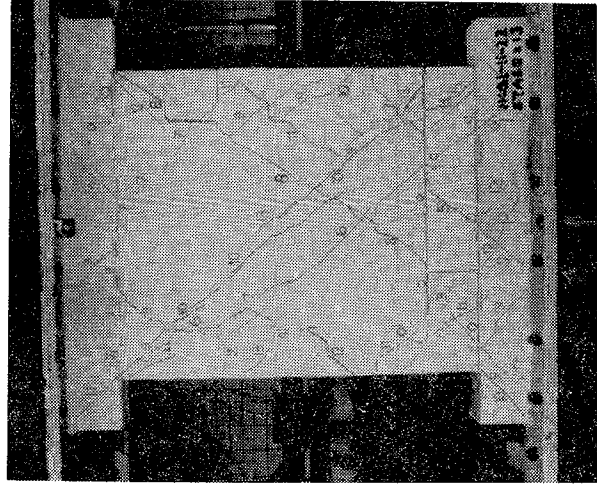
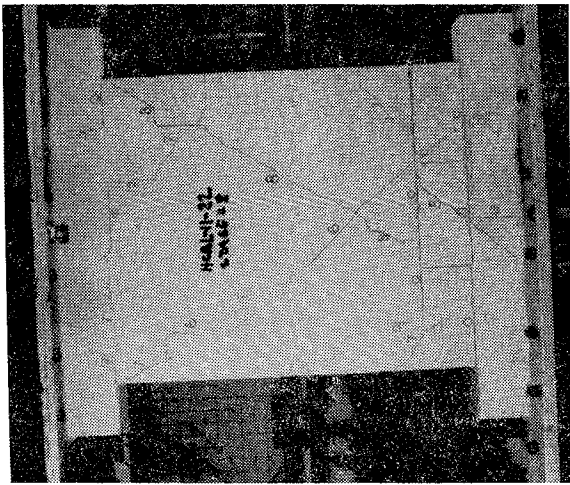
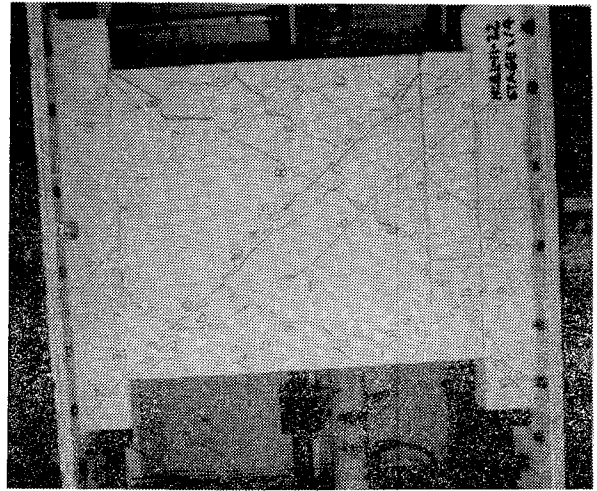
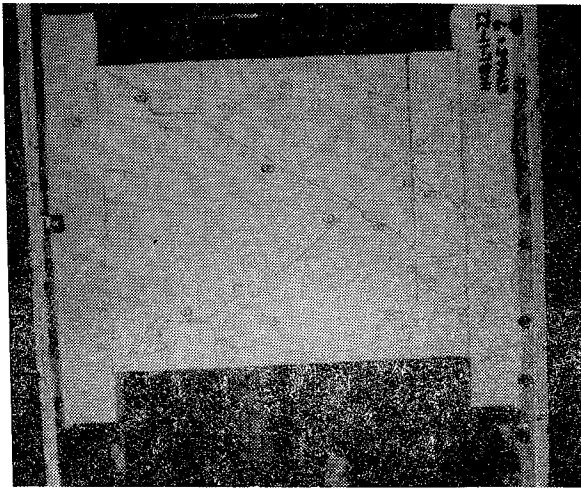


FIG. A. 8b SUCCESSIVE CRACK FORMATION (HCBL-11-22)

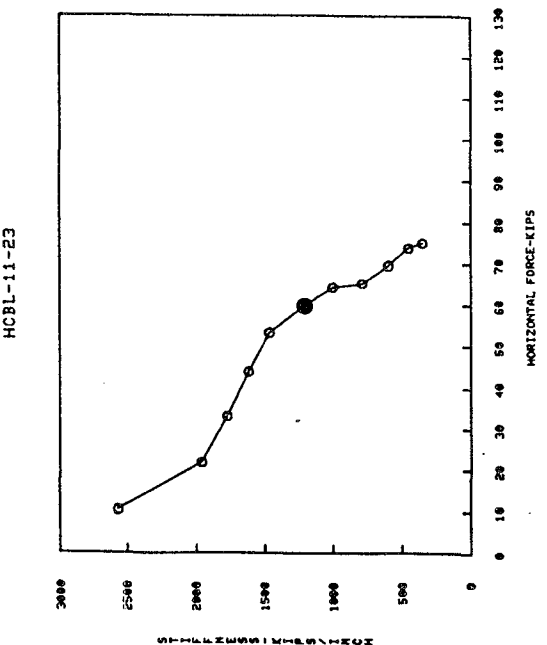
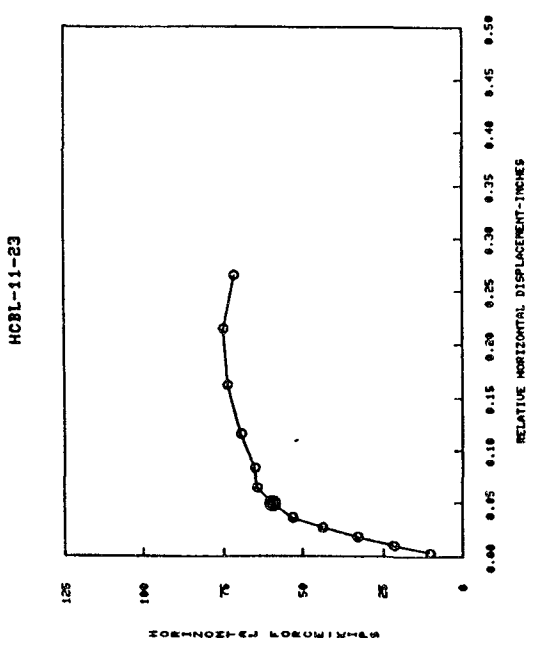
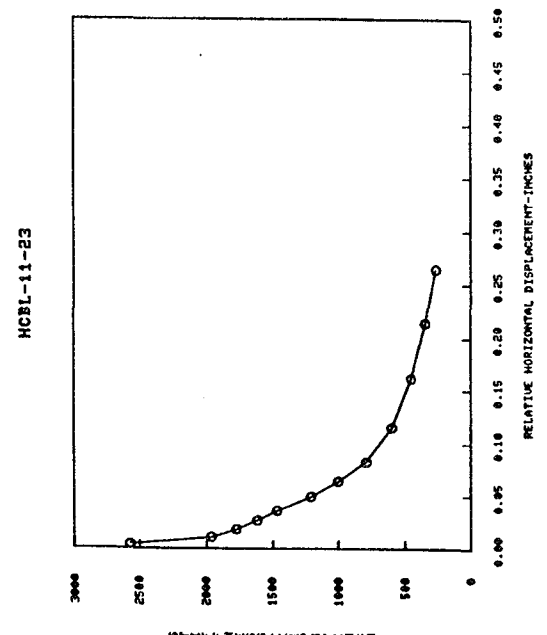
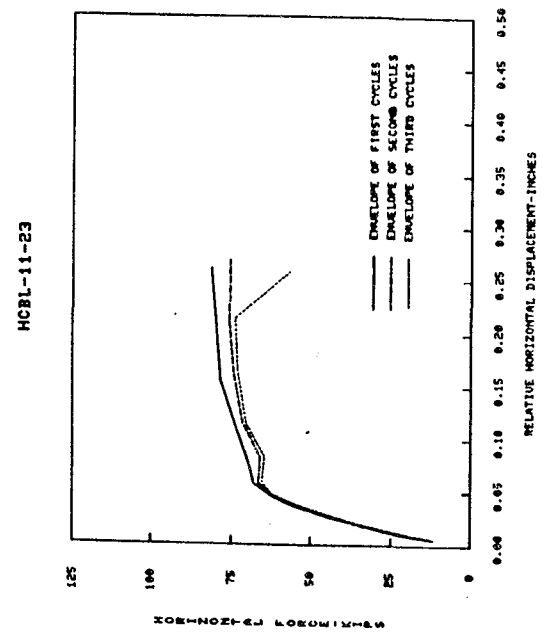


FIG. A.9a EXPERIMENTAL RESULTS (HCBL-11-23)

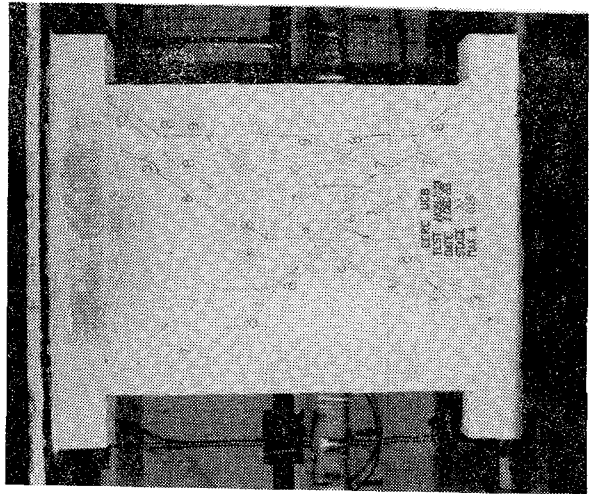
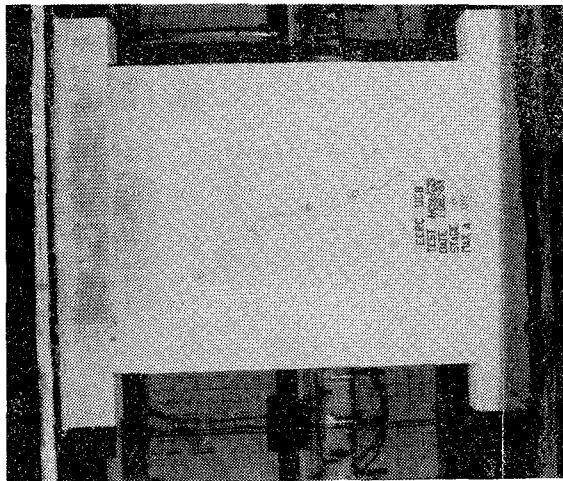
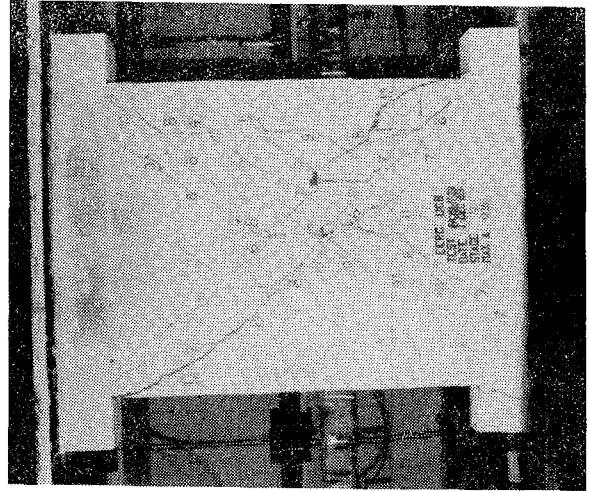
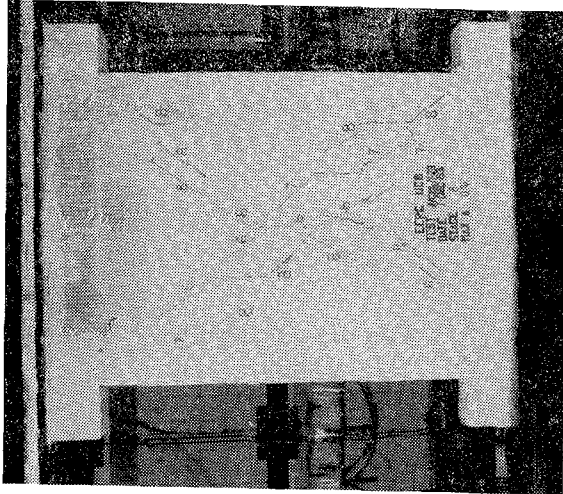
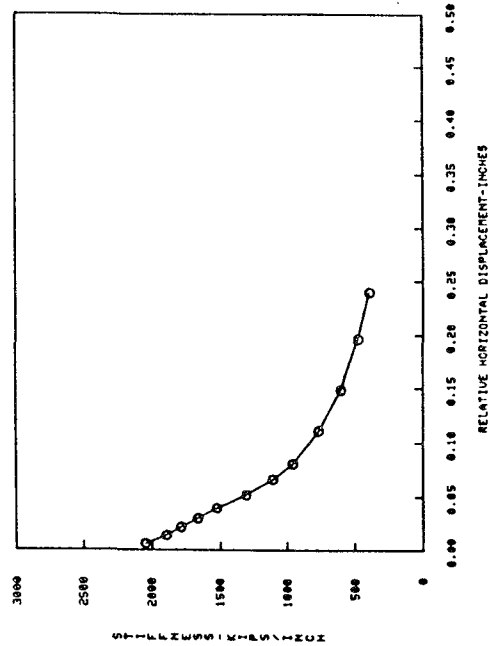
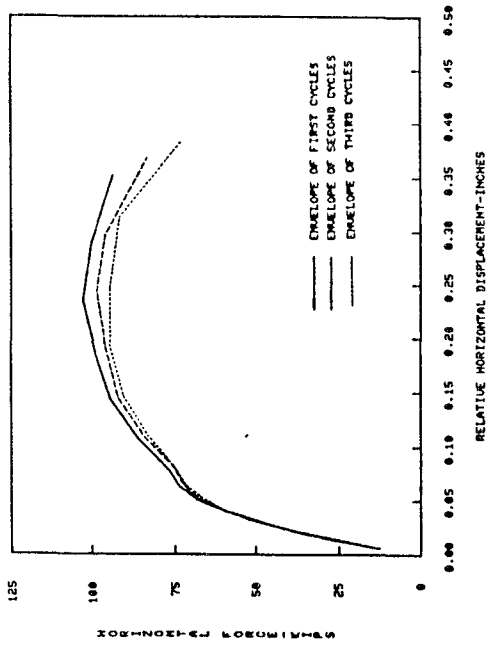
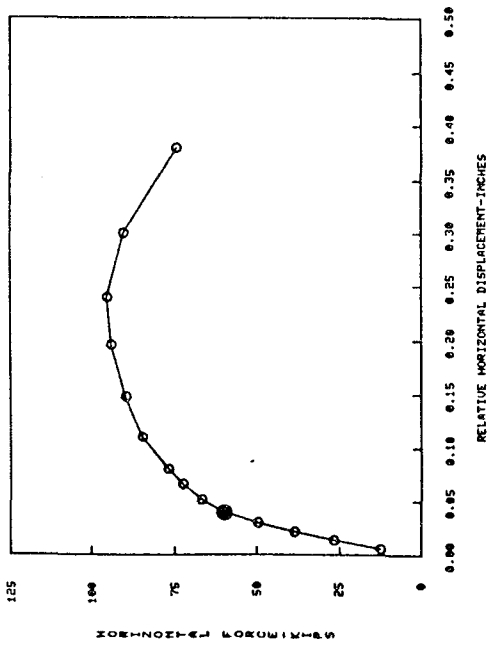


FIG. A. 9b SUCCESSIVE CRACK FORMATION (HCBL-11-23)

HCBL-11-24



HCBL-11-24



HCBL-11-24

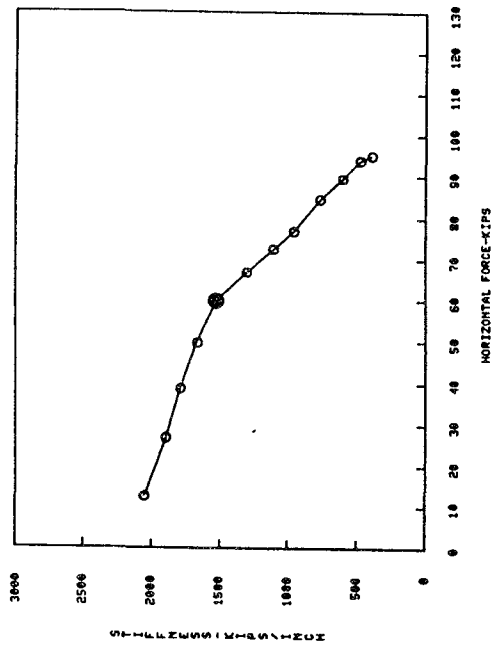


FIG. A.10a EXPERIMENTAL RESULTS (HCBL-11-24)

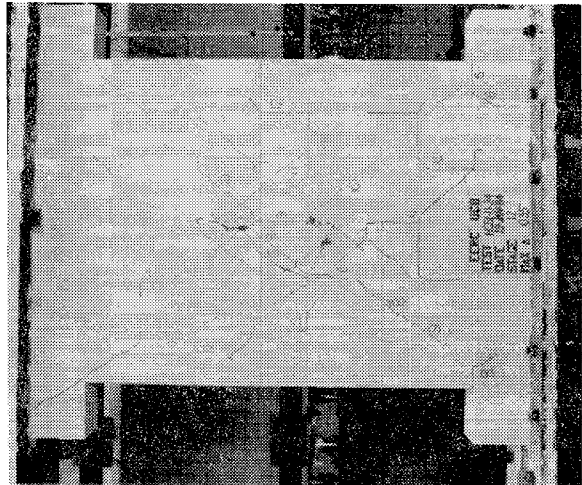
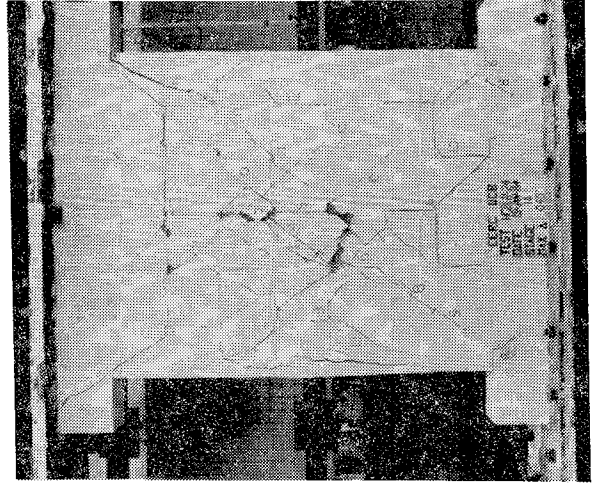
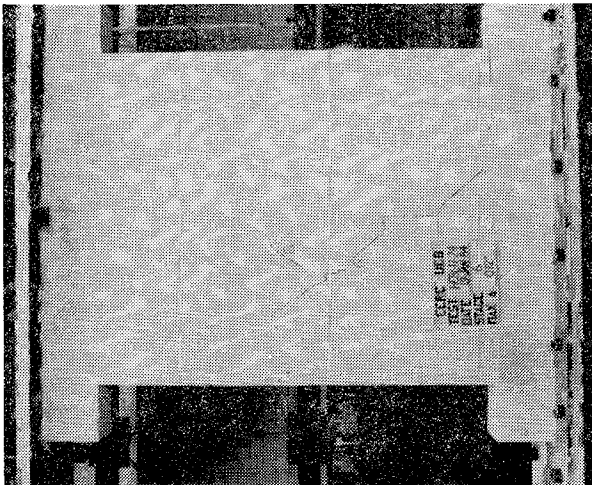
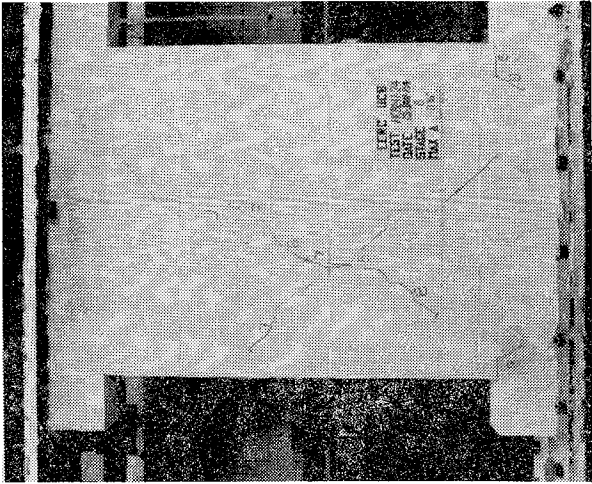
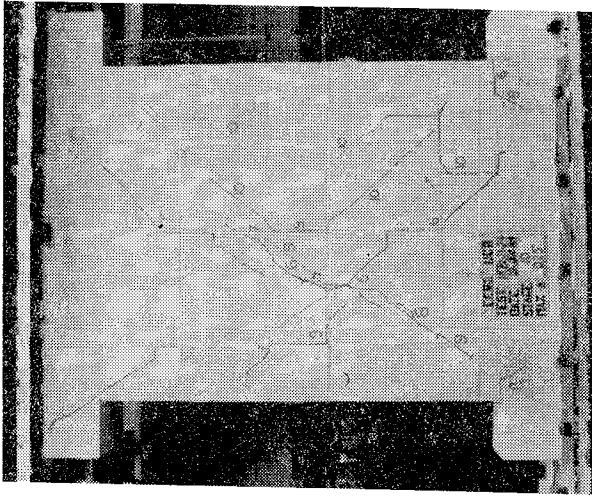
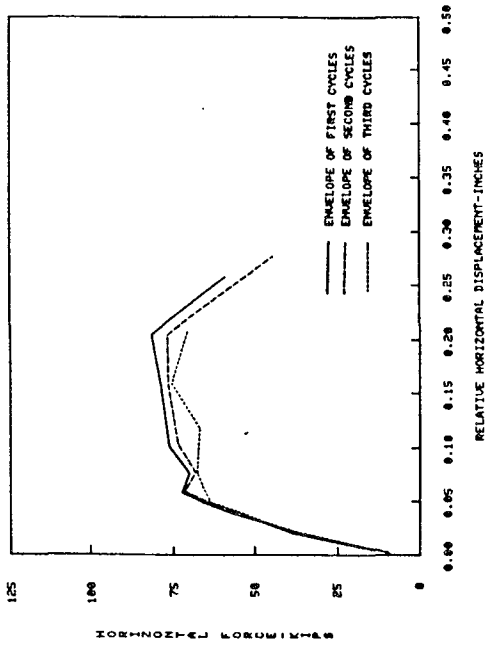
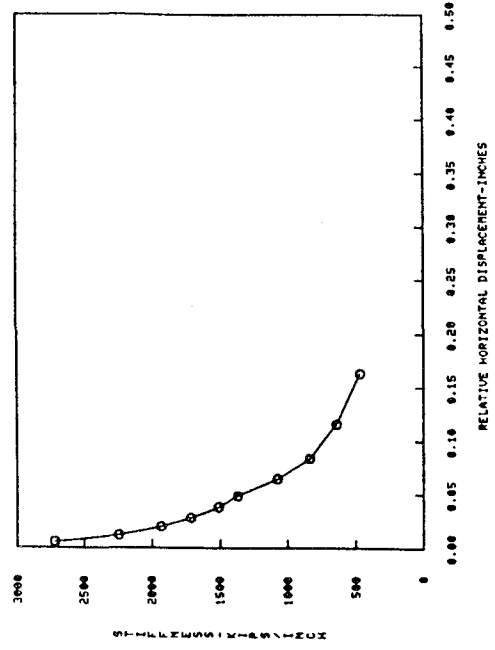


FIG. A.10b SUCCESSIVE CRACK FORMATION (HCBL-11-24)

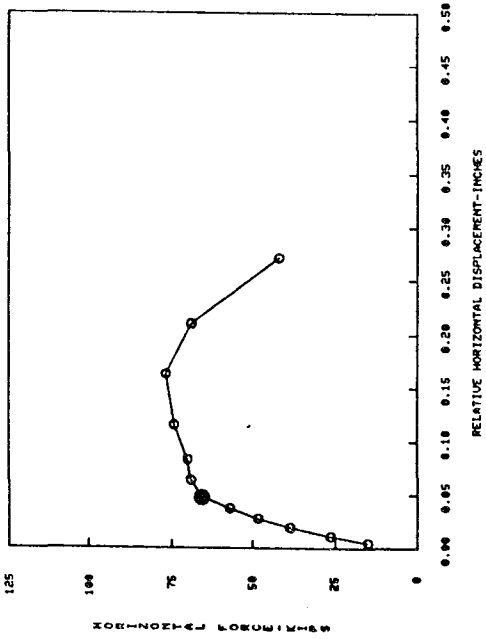
HCBL-11-25



HCBL-11-25



HCBL-11-25



HCBL-11-25

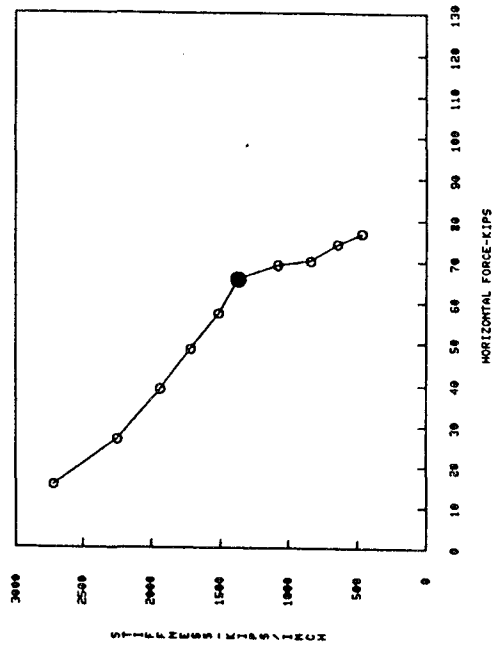


FIG. A.11a EXPERIMENTAL RESULTS (HCBL-11-25)

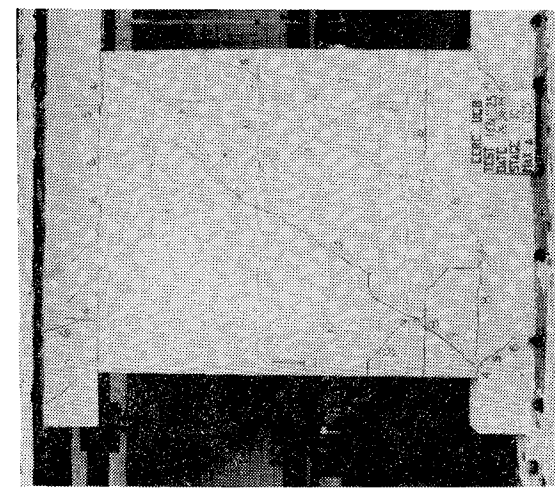
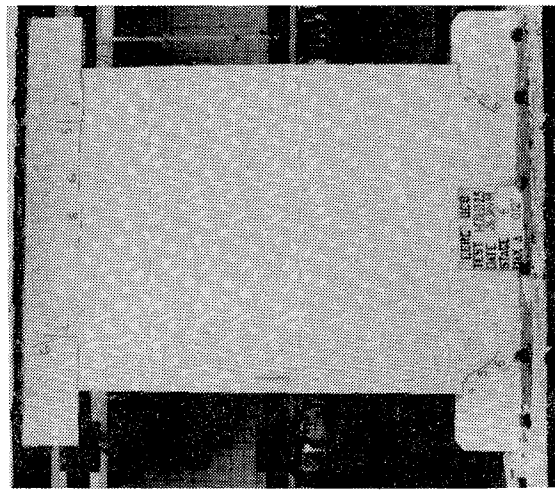
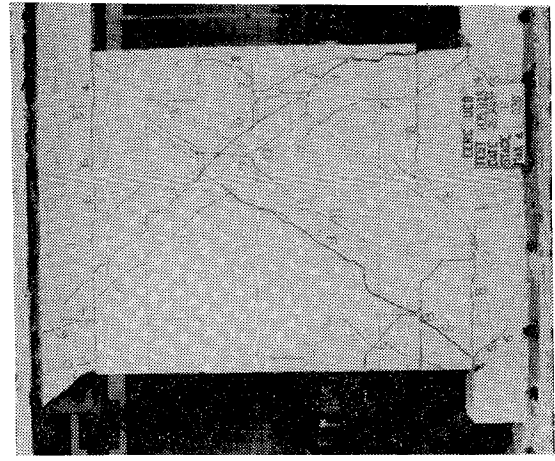
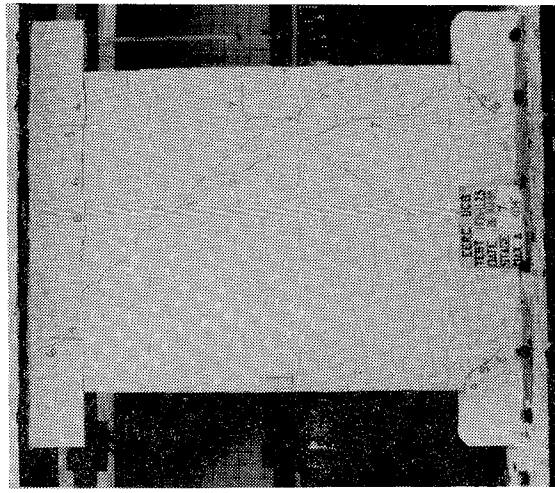
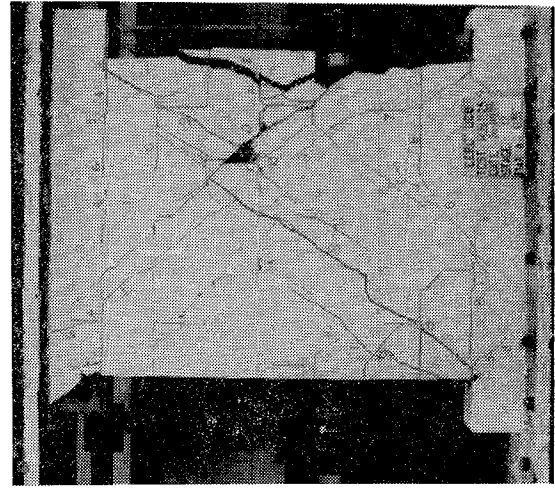
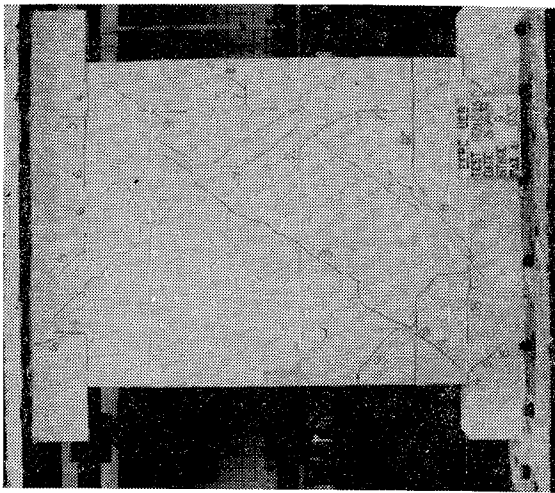


FIG. A.11b SUCCESSIVE CRACK FORMATION (HCBL-11-25)

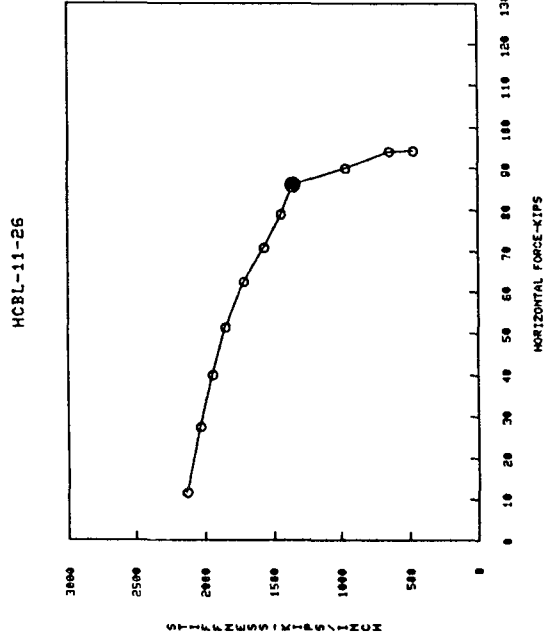
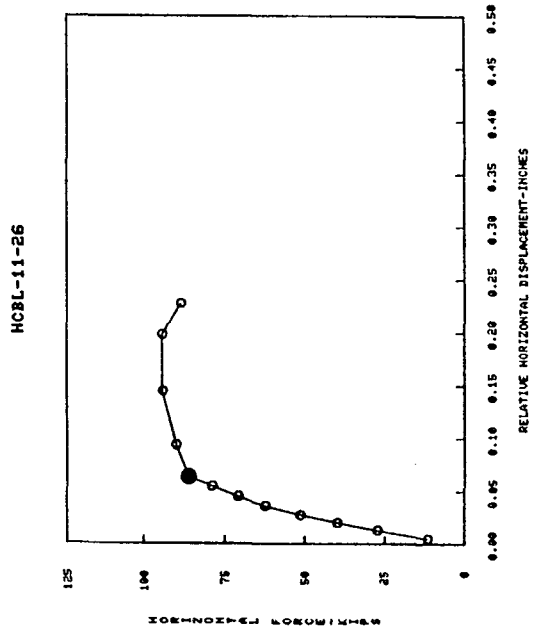
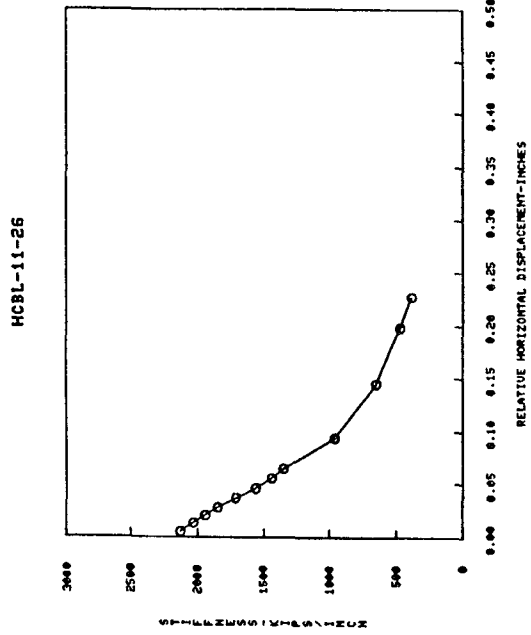
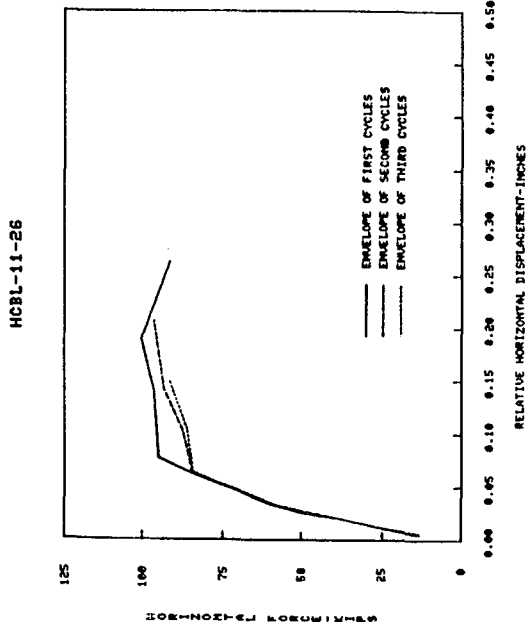


FIG. A.12a EXPERIMENTAL RESULTS (HCBL-11-26)

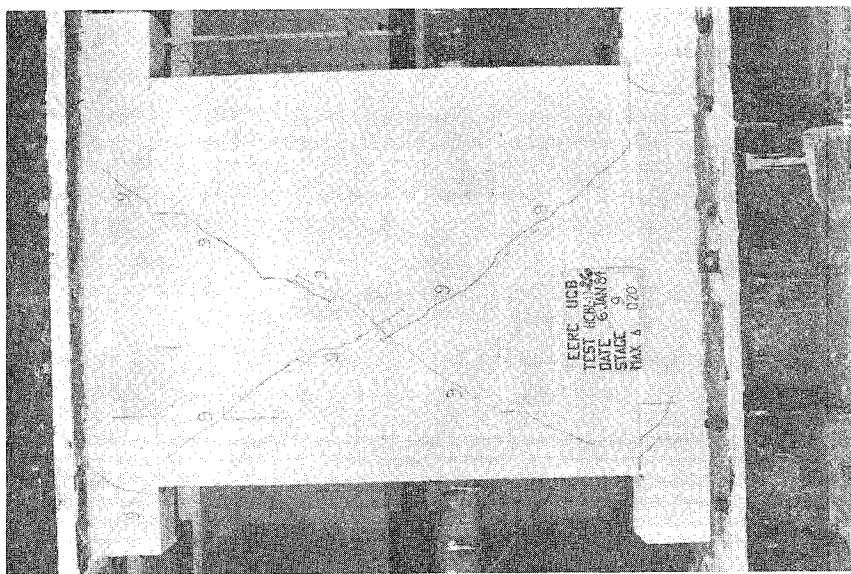
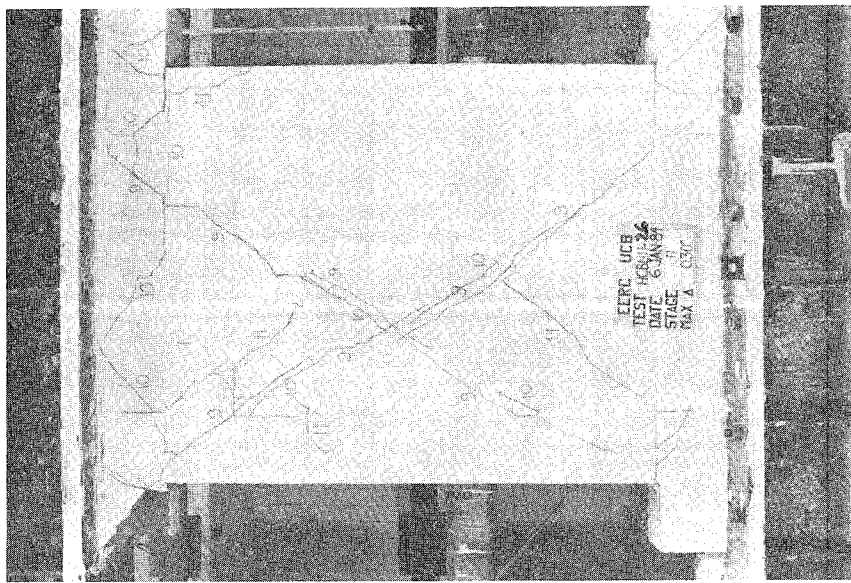
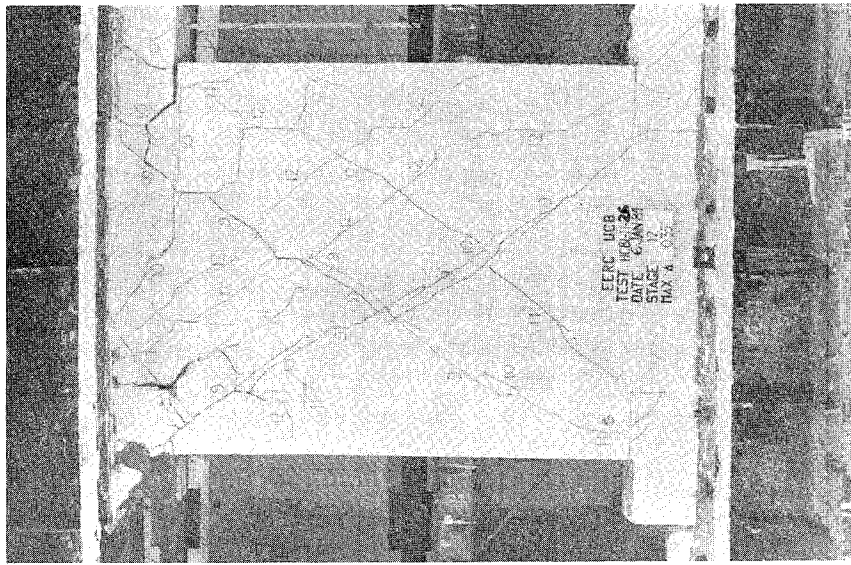


FIG. A.12b SUCCESSIVE CRACK FORMATION (HCBL-11-26)

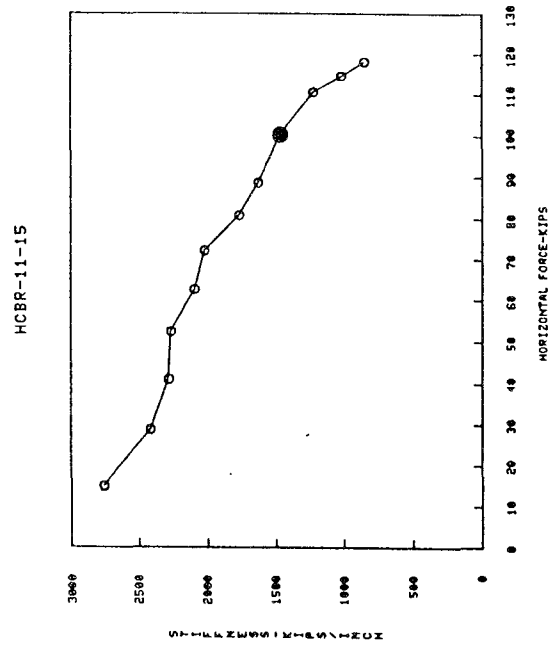
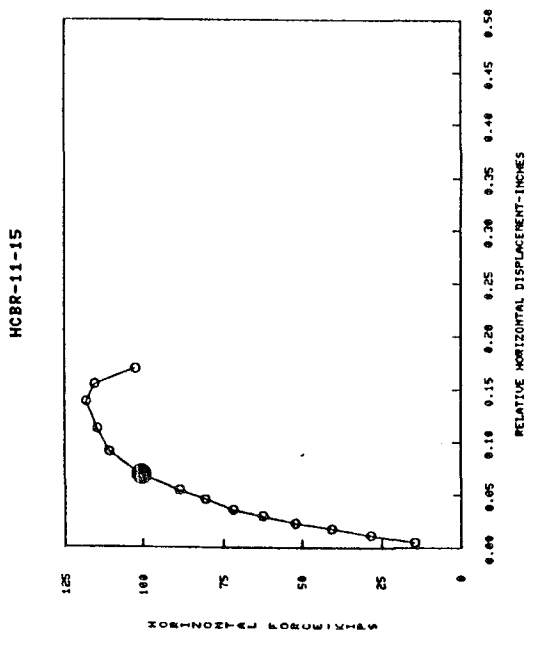
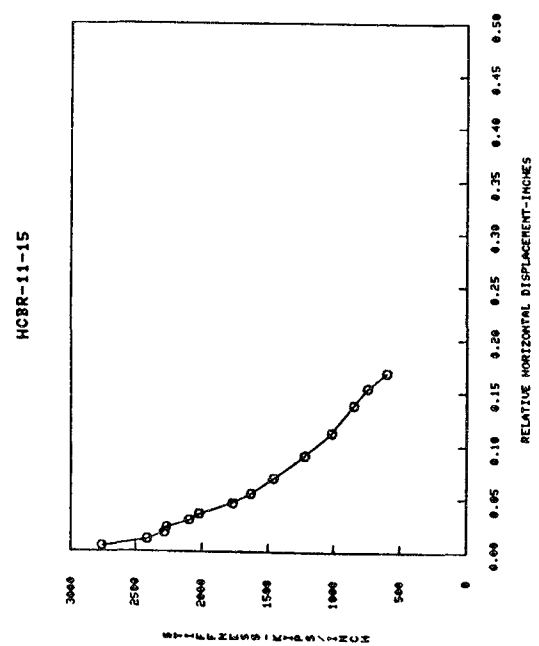
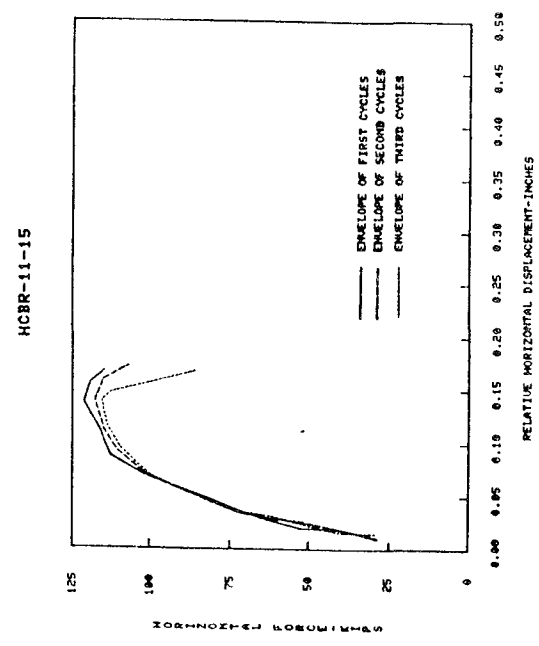


FIG. A.13a EXPERIMENTAL RESULTS (HCBR-11-15)

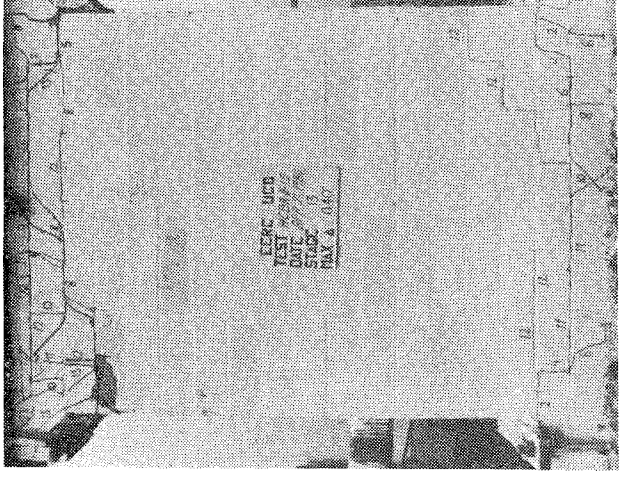
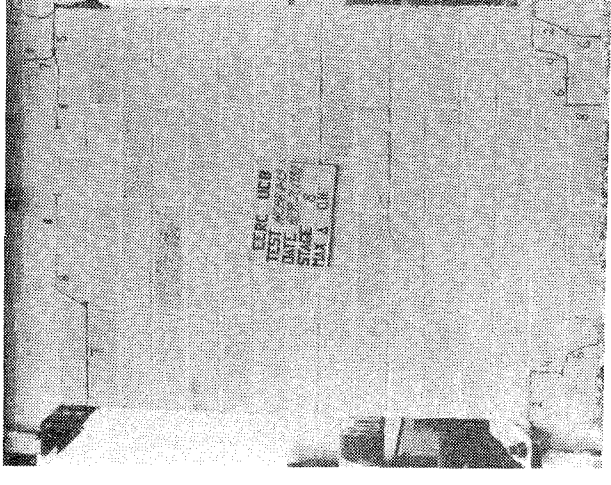
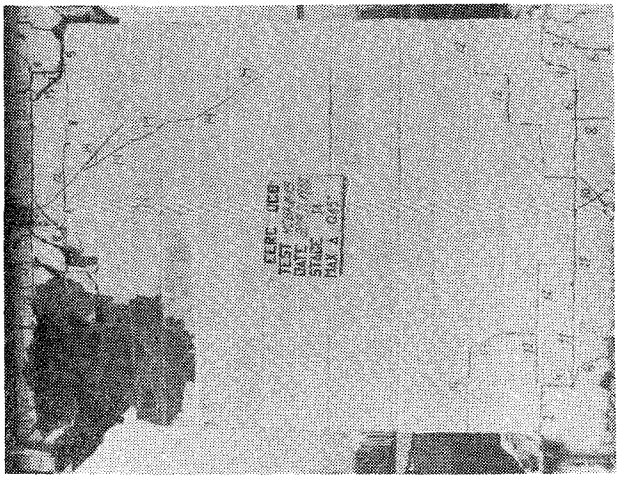
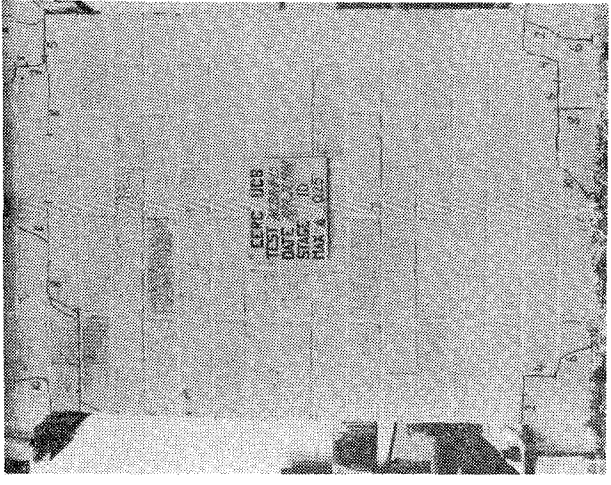
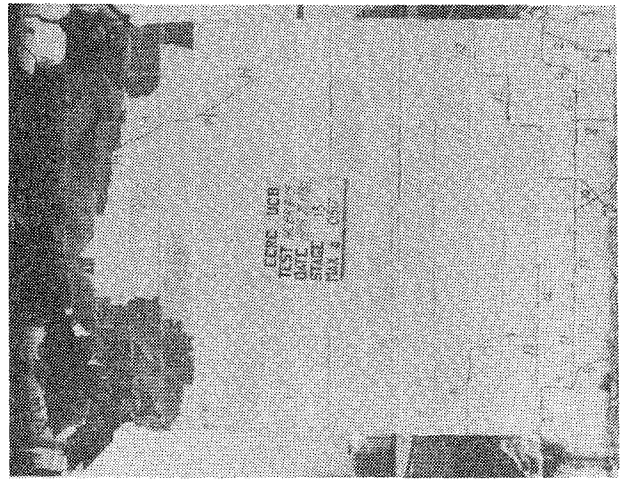
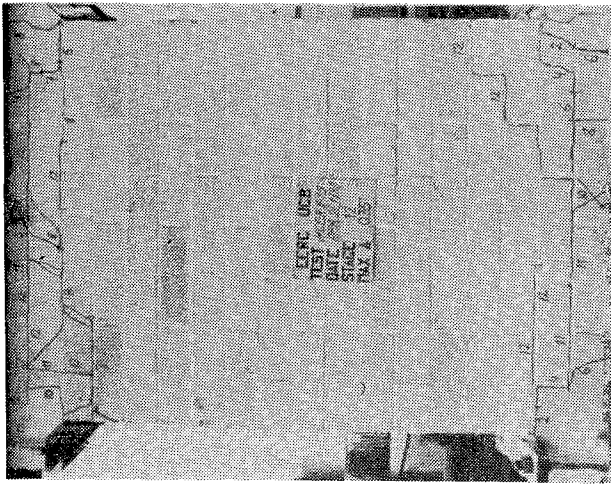


FIG. A.13b SUCCESSIVE CRACK FORMATION (HCBR-11-15)

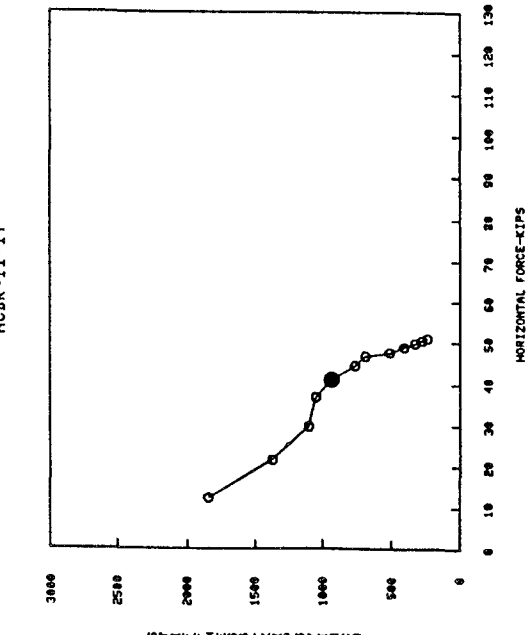
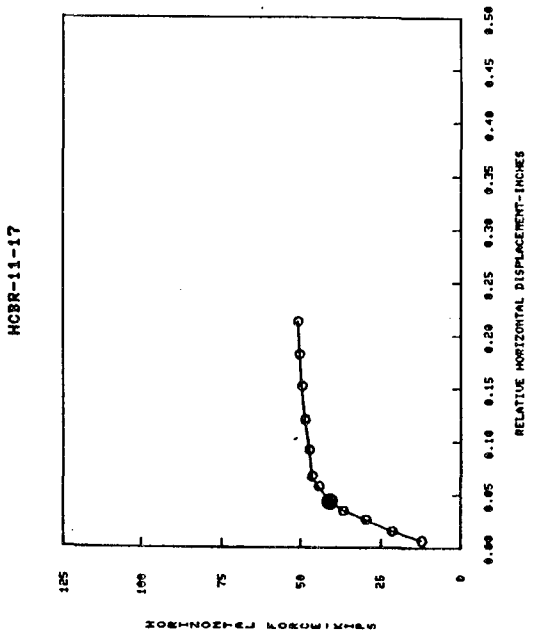
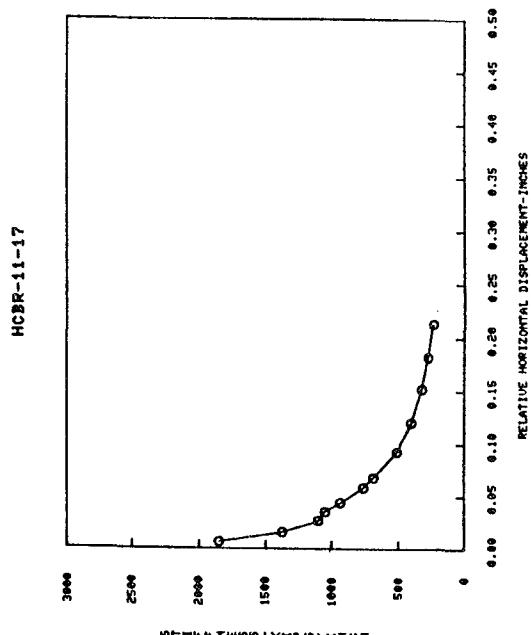
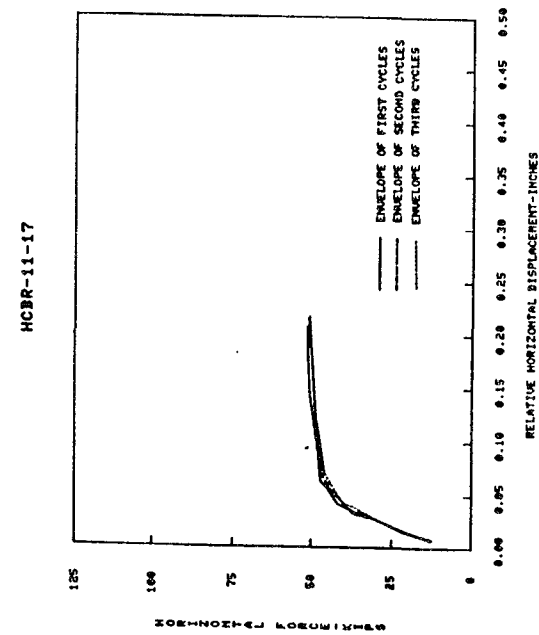


FIG. A.14a EXPERIMENTAL RESULTS (HCBR-11-17)

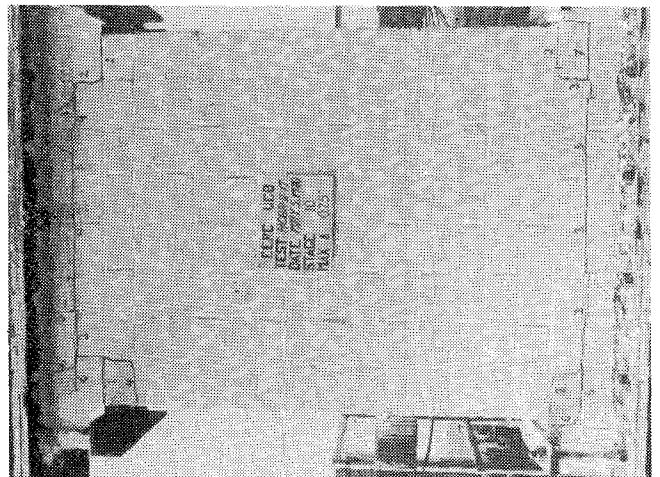
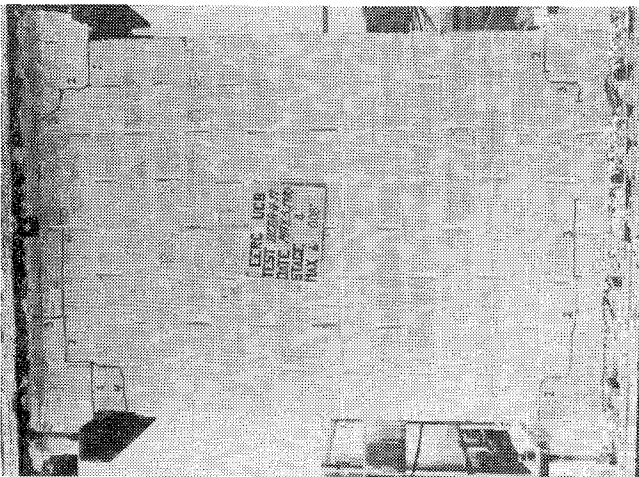
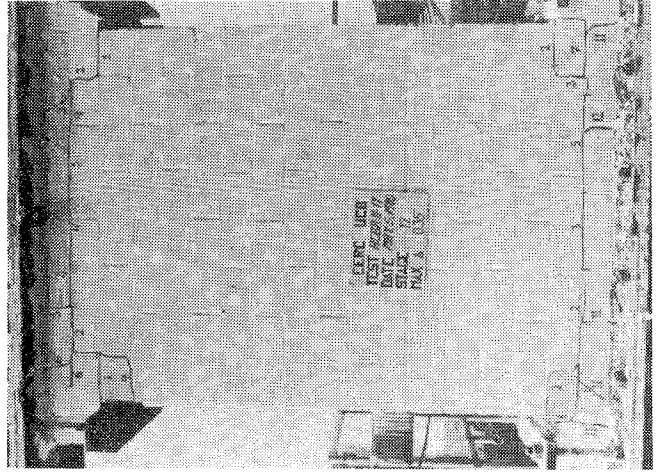
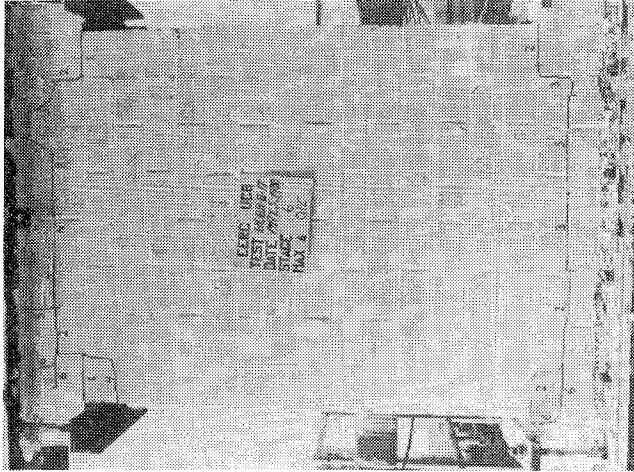
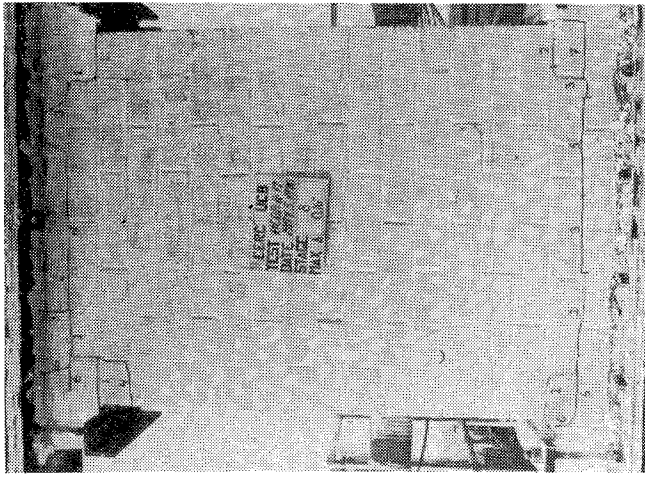


FIG. A.14b SUCCESSIVE CRACK FORMATION (HCBR-11-17)

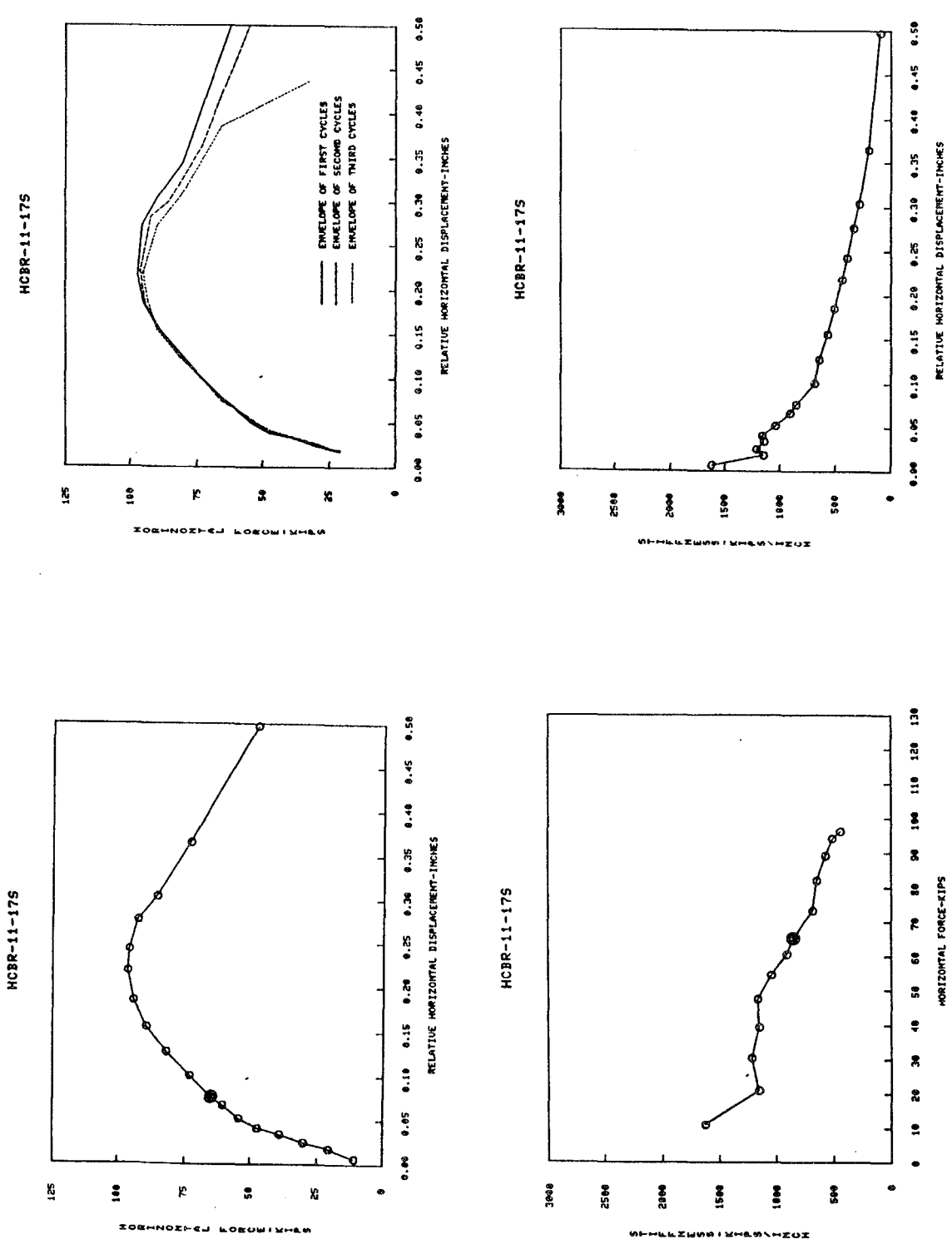


FIG. A.15a EXPERIMENTAL RESULTS (HCBR-11-17S)

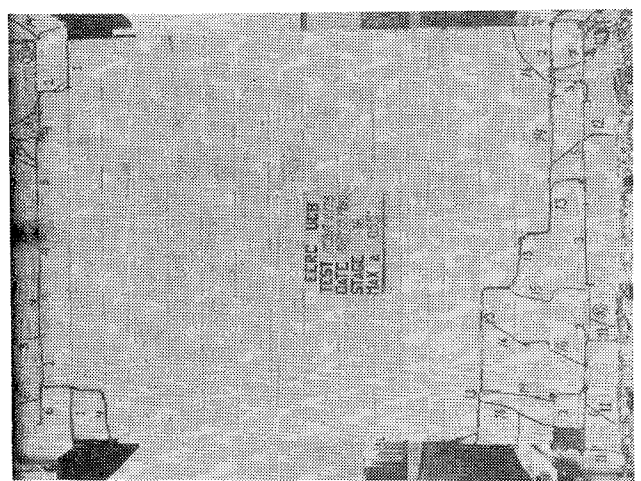
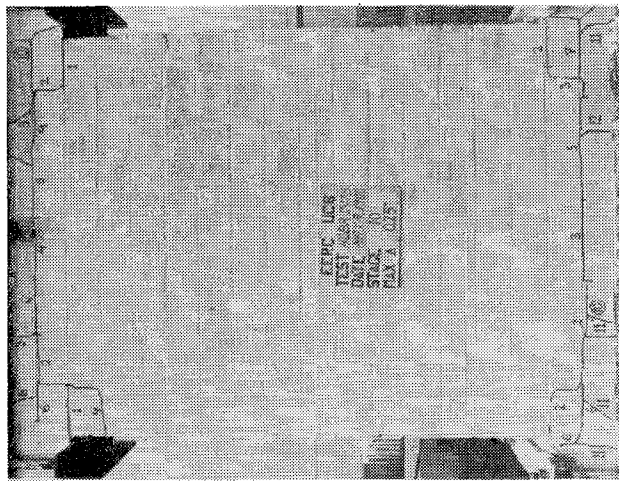
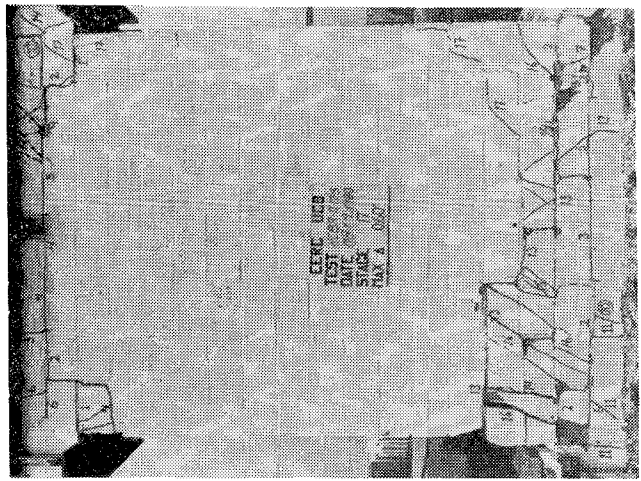
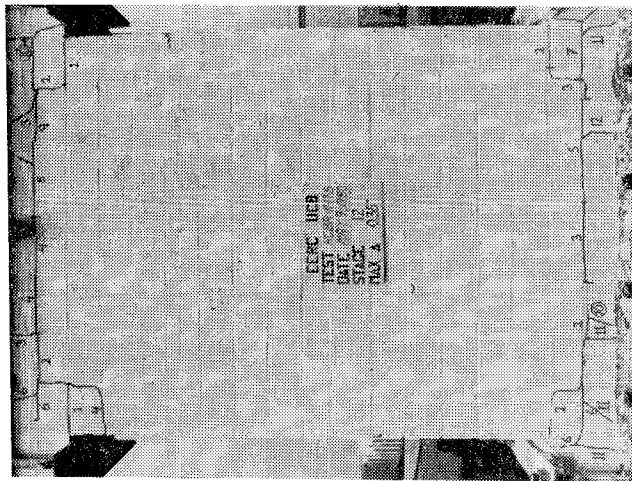
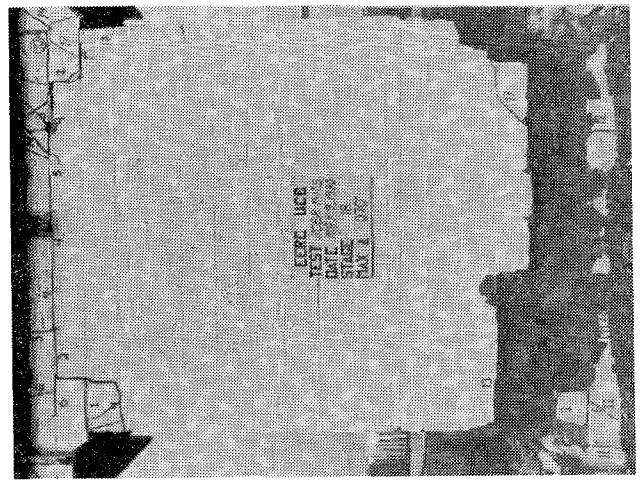
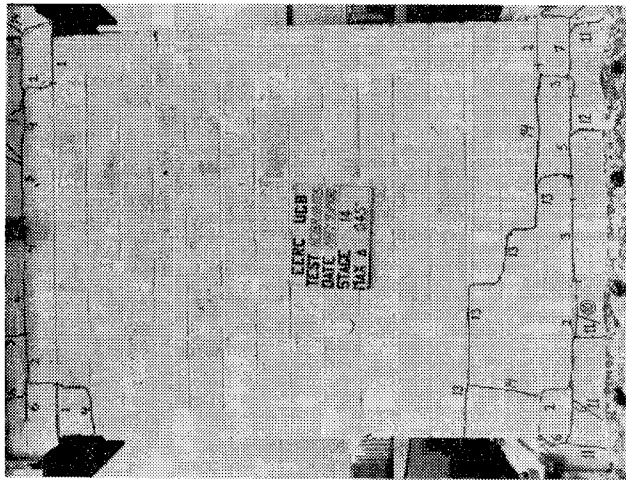


FIG. A. 15b SUCCESSIVE CRACK FORMATION (HCBR-11-17S)

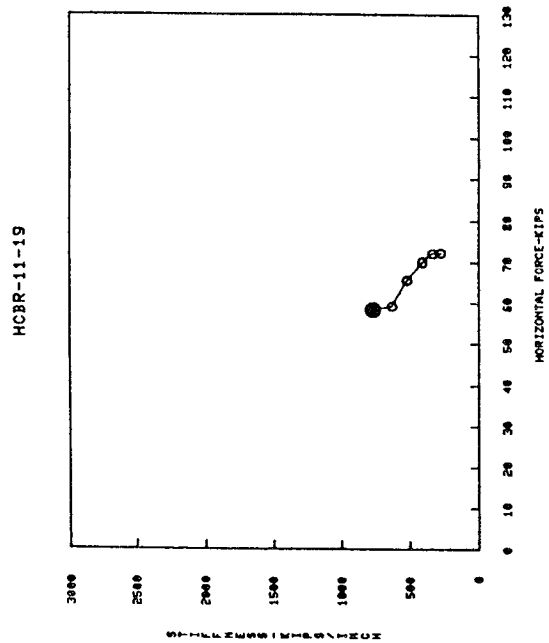
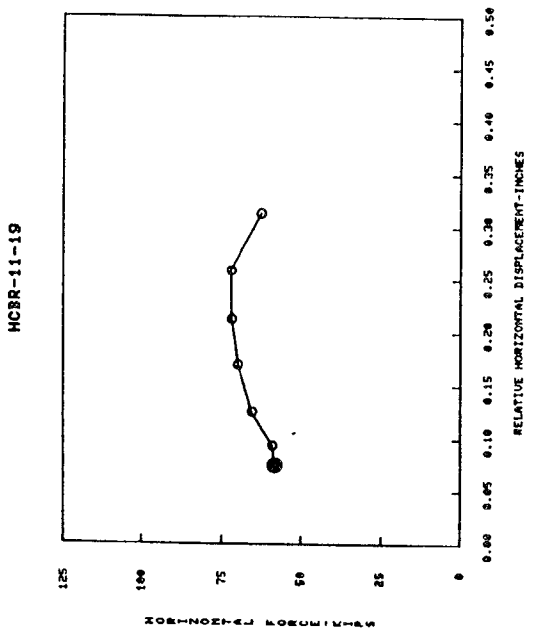
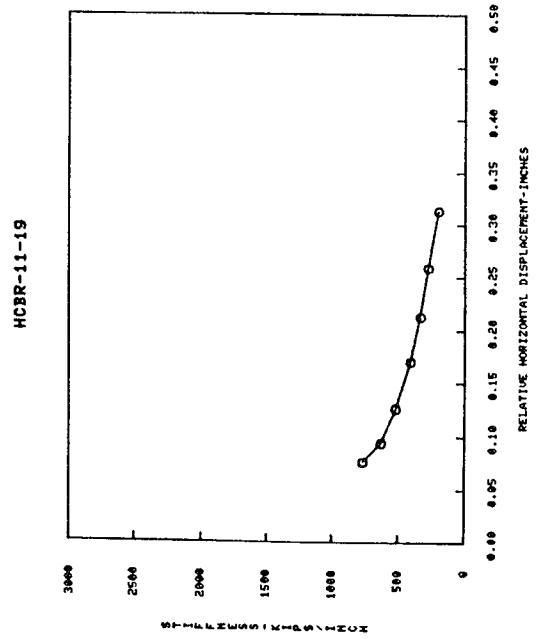
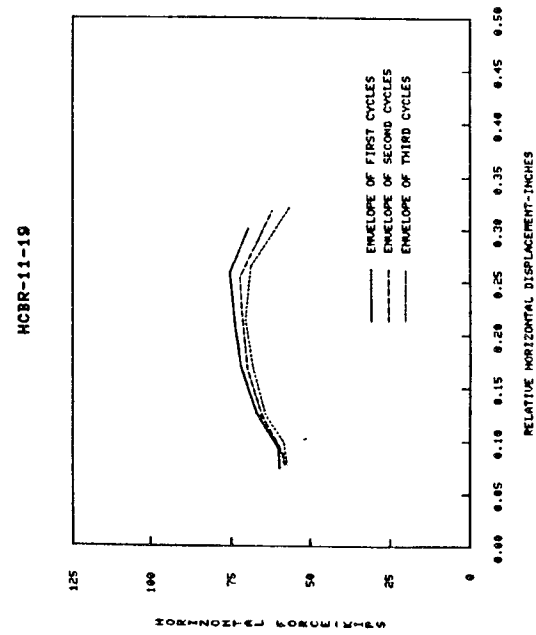


FIG. A.16a EXPERIMENTAL RESULTS (HCBR-11-19)

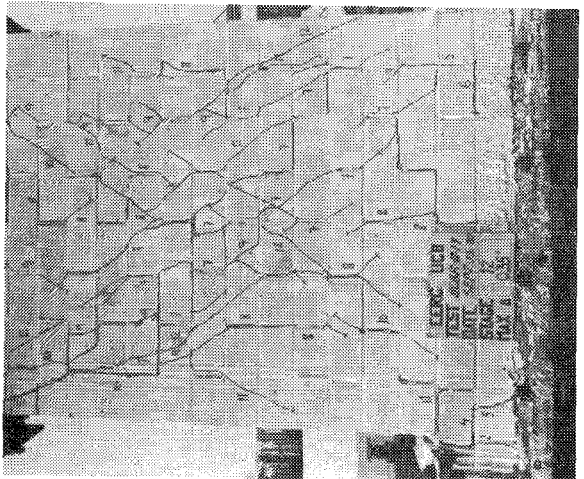
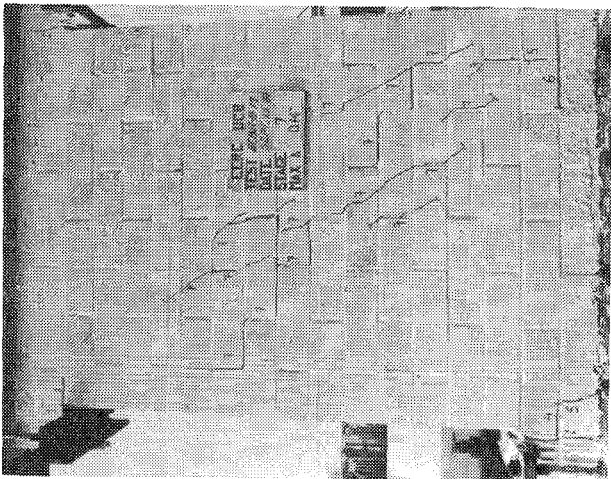
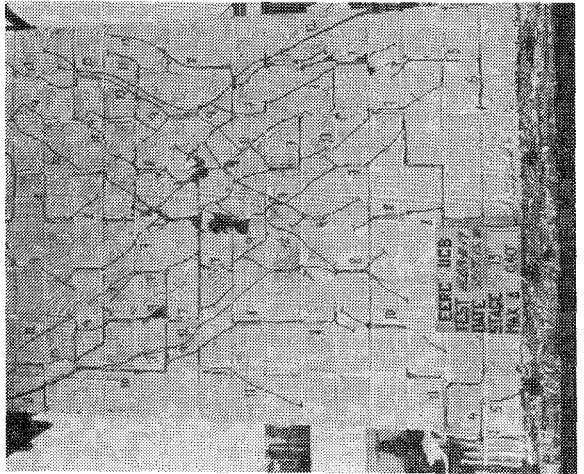
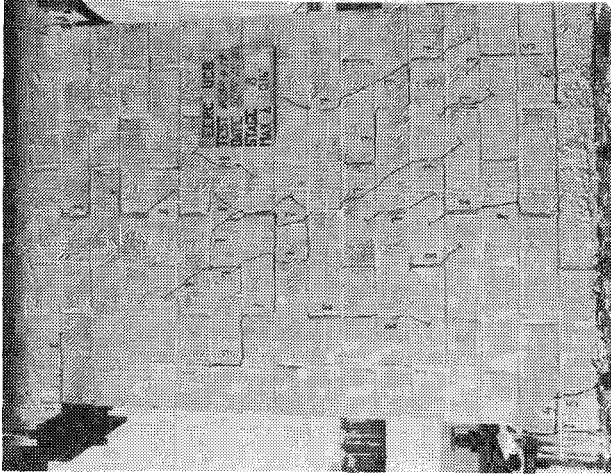
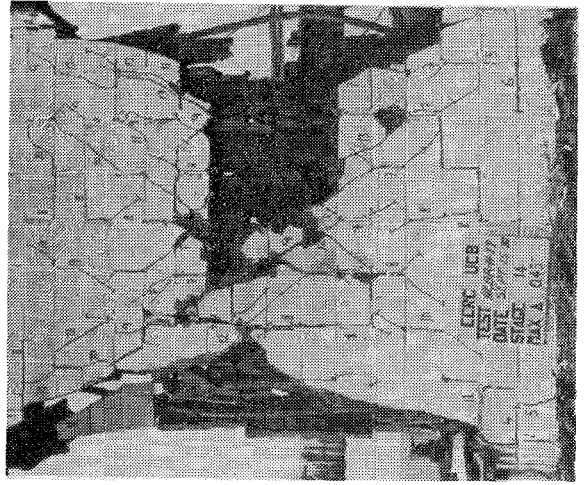
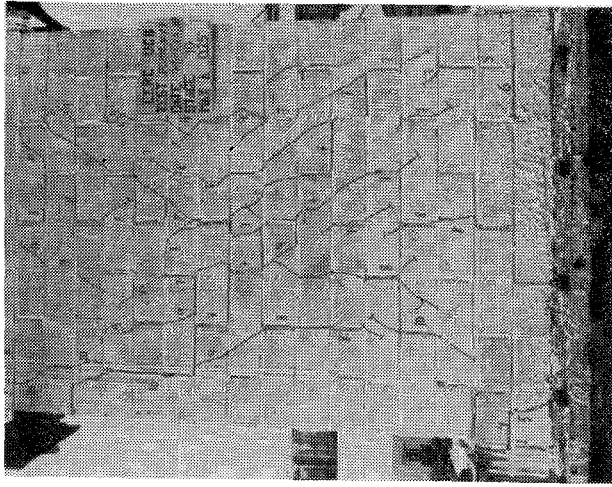


FIG. A.16b SUCCESSIVE CRACK FORMATION (HCBR-11-19)

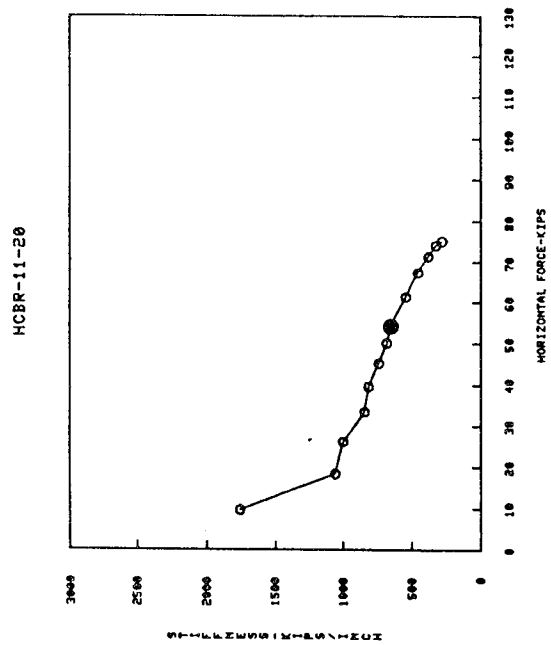
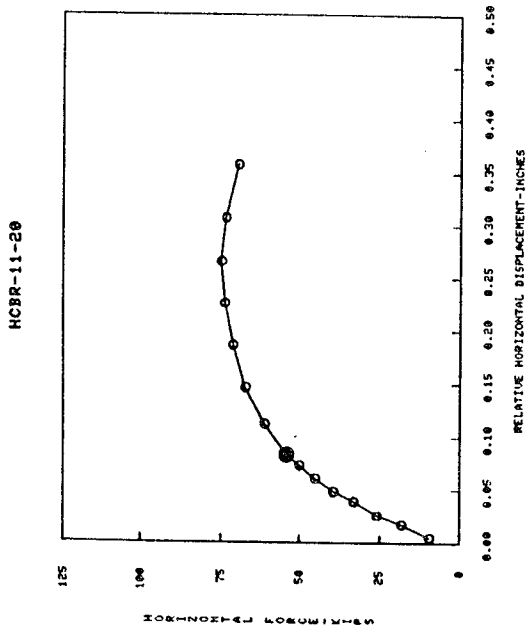
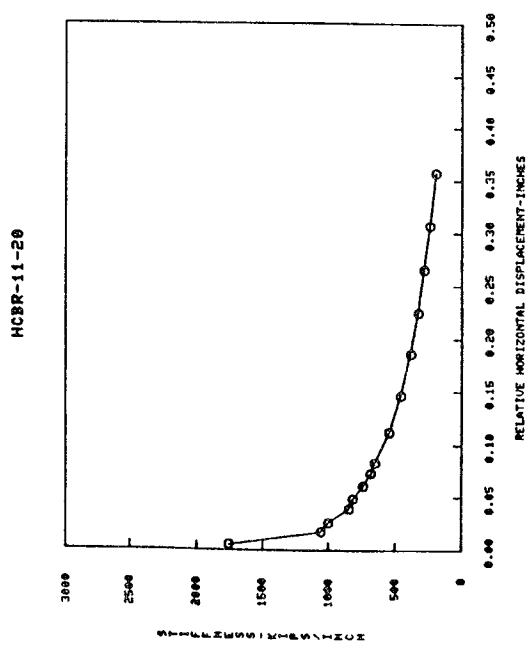
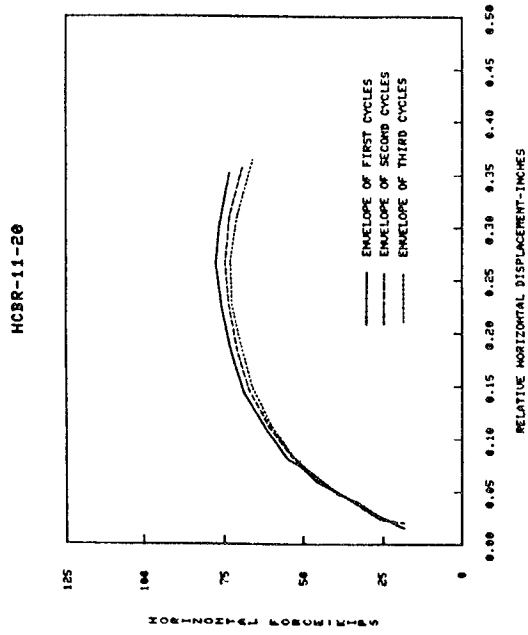


FIG. A.17a EXPERIMENTAL RESULTS (HCBR-11-20)

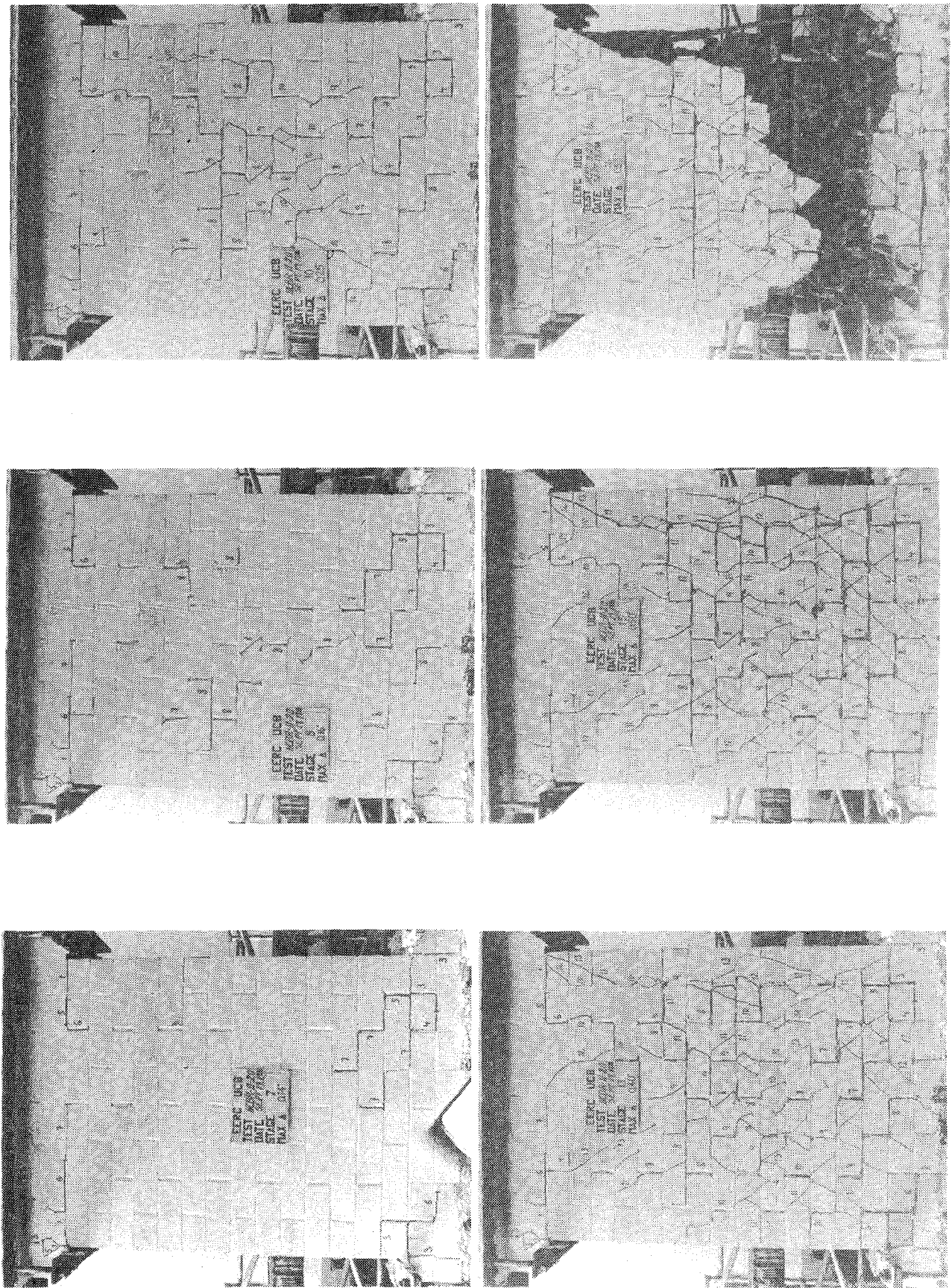
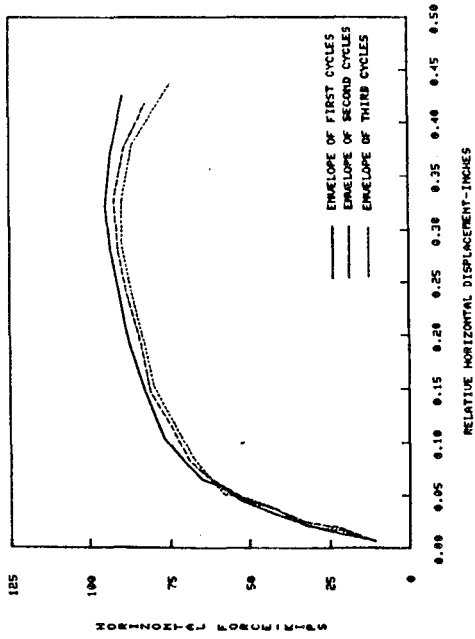
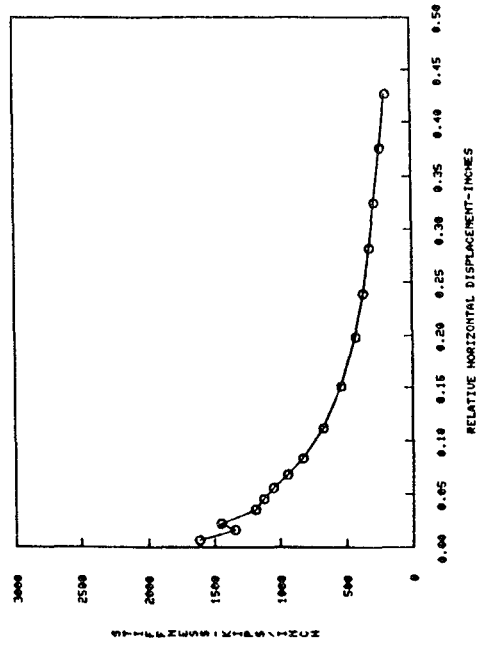


FIG. A.17b SUCCESSIVE CRACK FORMATION (HCBR-11-20)

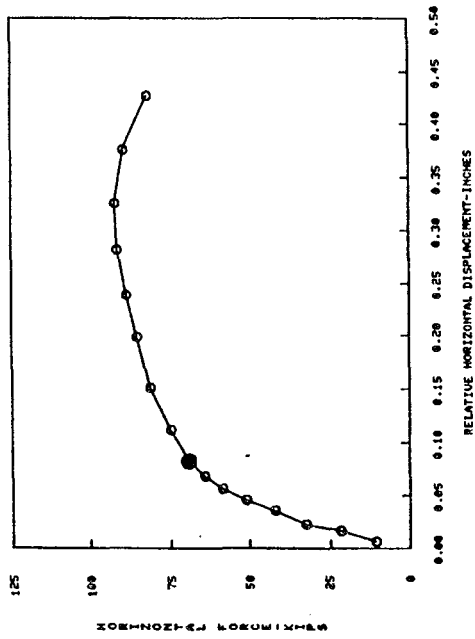
HCBR-11-21



HCBR-11-21



HCBR-11-21



HCBR-11-21

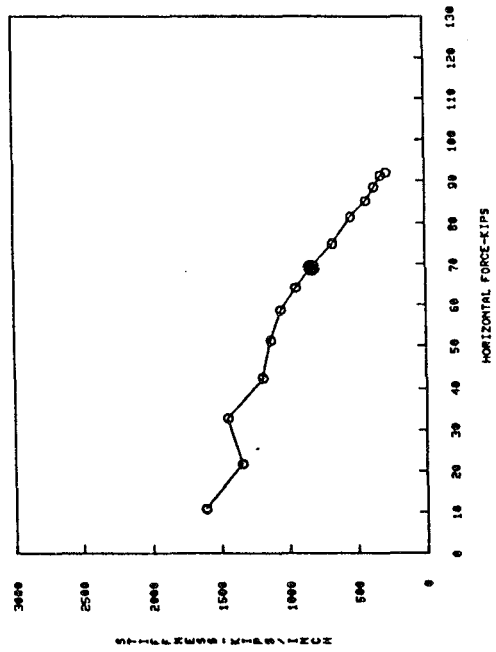


FIG. A.18a EXPERIMENTAL RESULTS (HCBR-11-21)

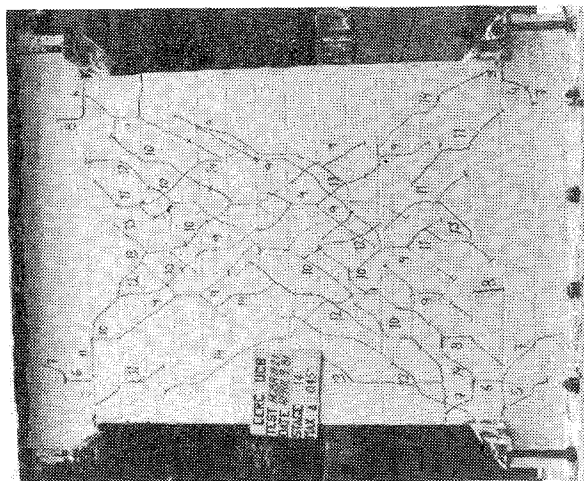
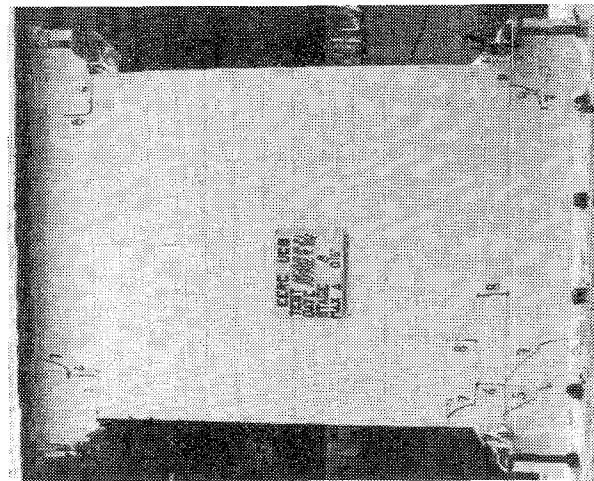
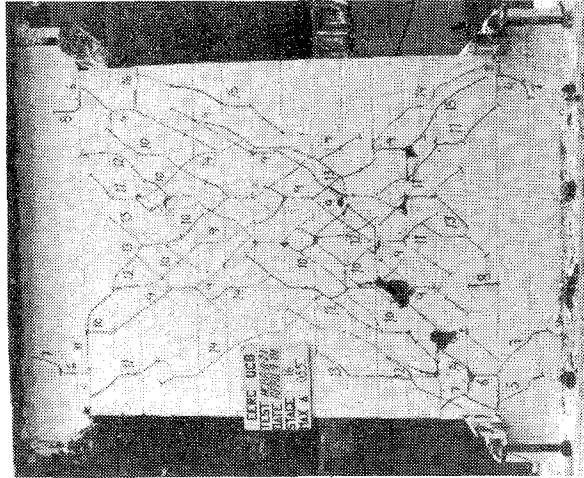
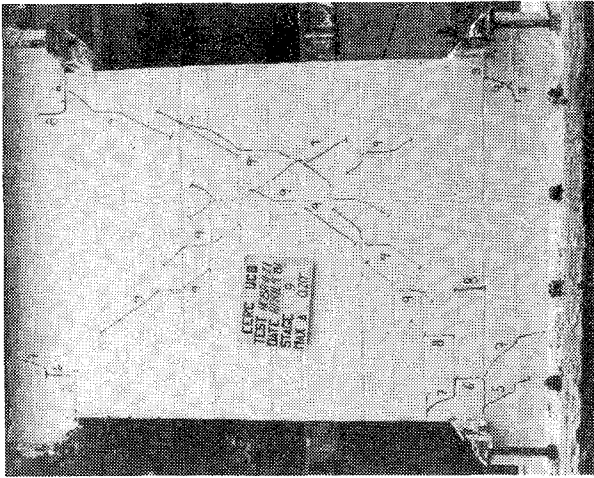
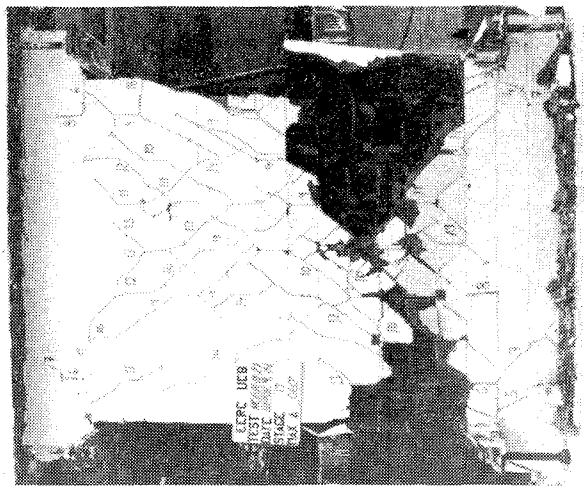
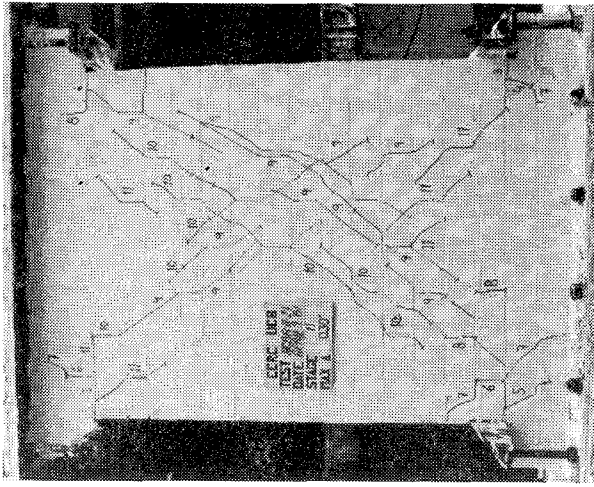


FIG. A.18b SUCCESSIVE CRACK FORMATION (HCBR-11-21)

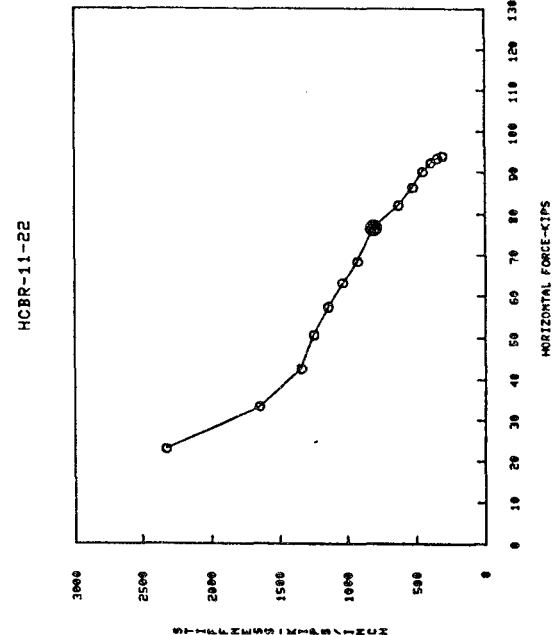
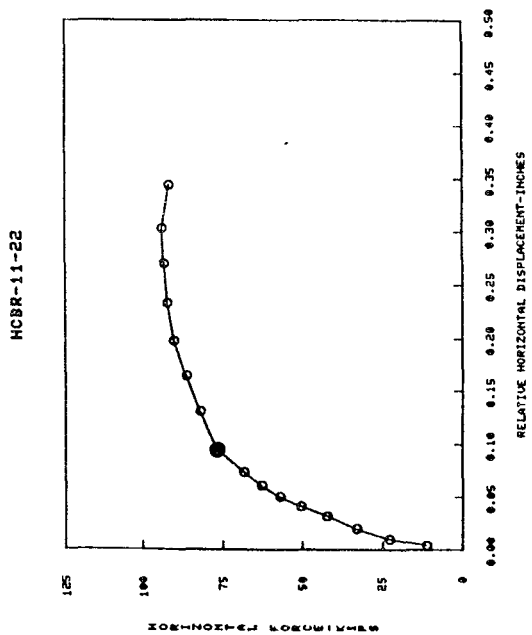
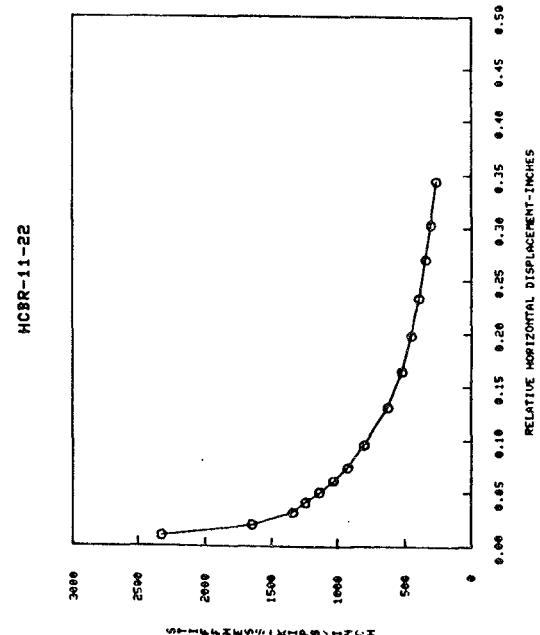
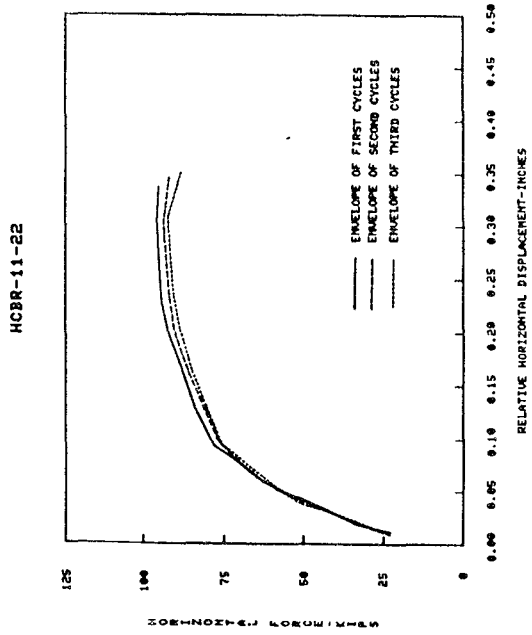


FIG. A.19a EXPERIMENTAL RESULTS (HCBR-11-22)

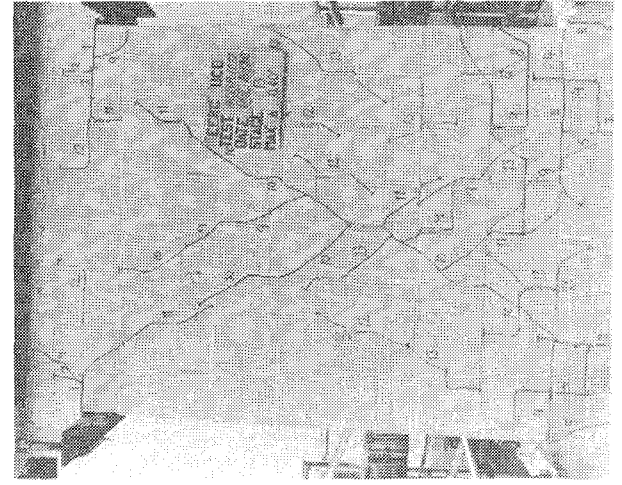
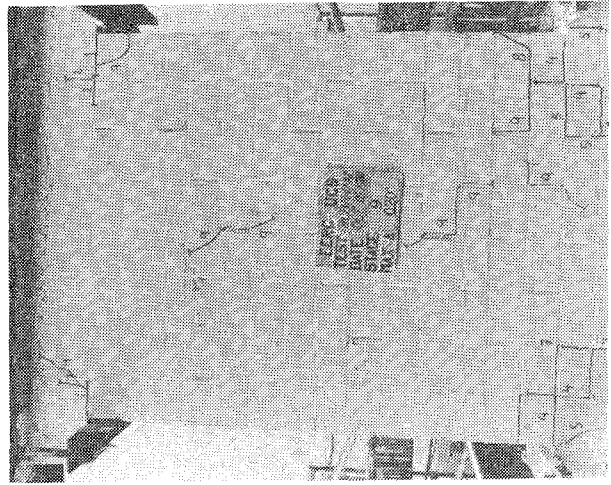
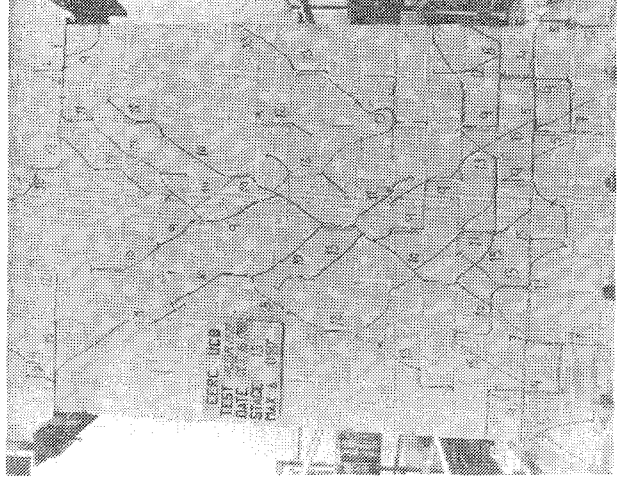
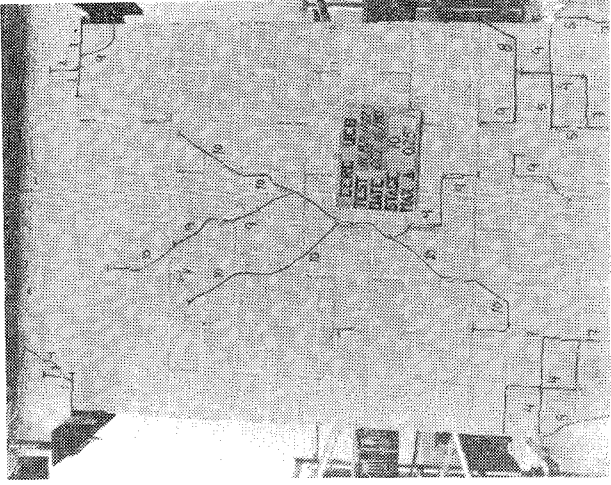
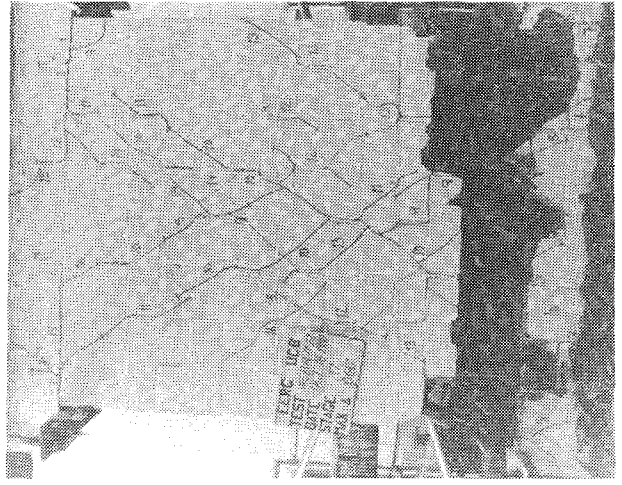
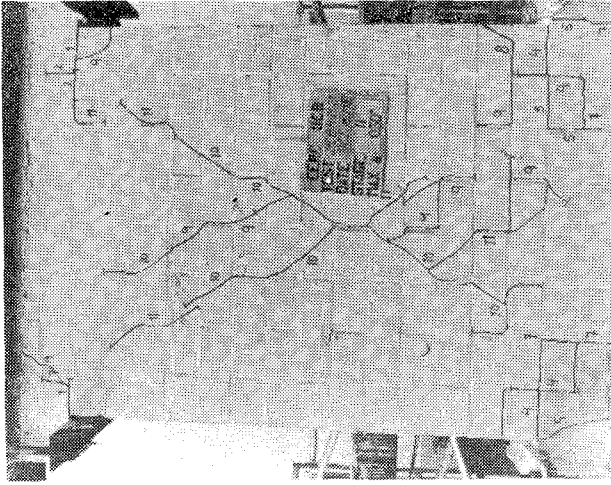
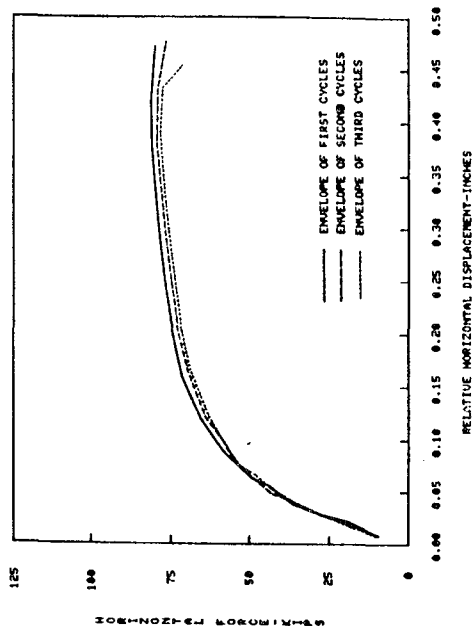
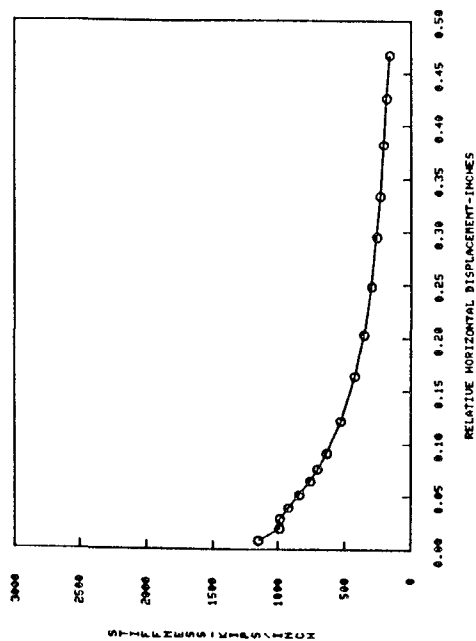


FIG. A.19b SUCCESSIVE CRACK FORMATION (HCBR-11-22)

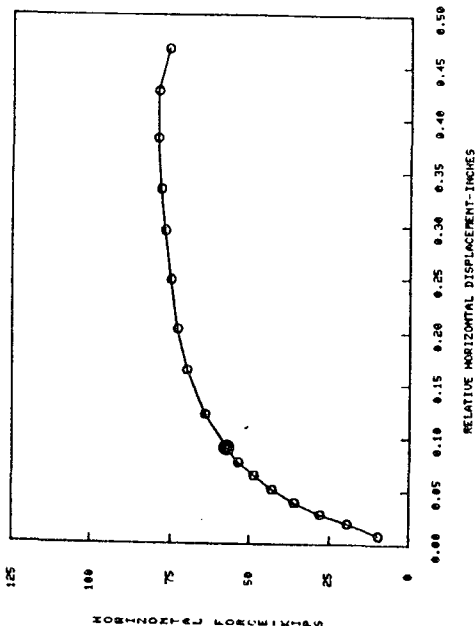
HCBR-11-23



HCBR-11-23



HCBR-11-23



HCBR-11-23

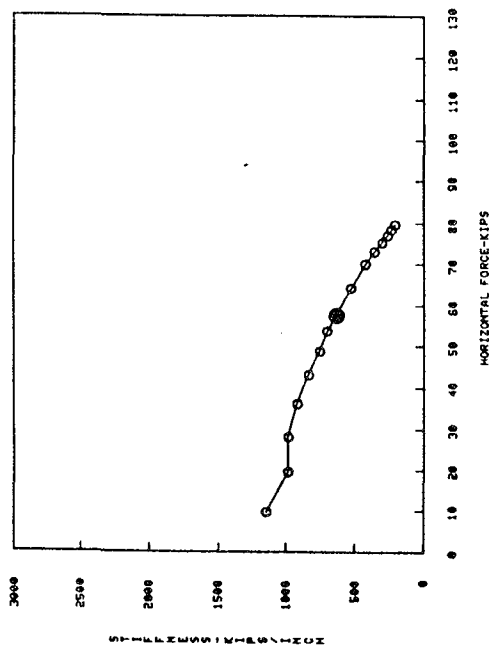


FIG. A.20a EXPERIMENTAL RESULTS (HCBR-11-23)

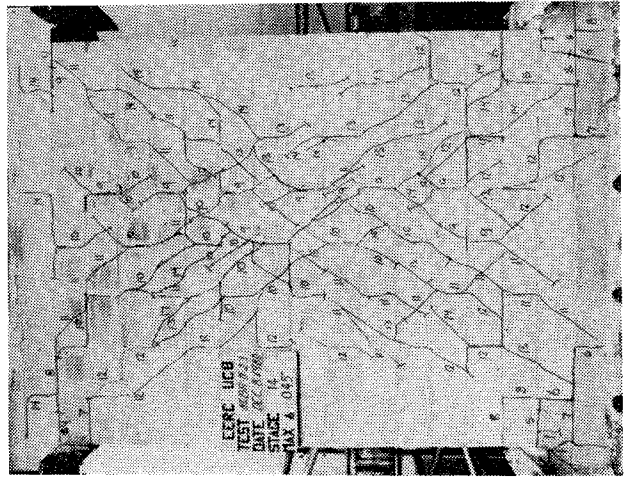
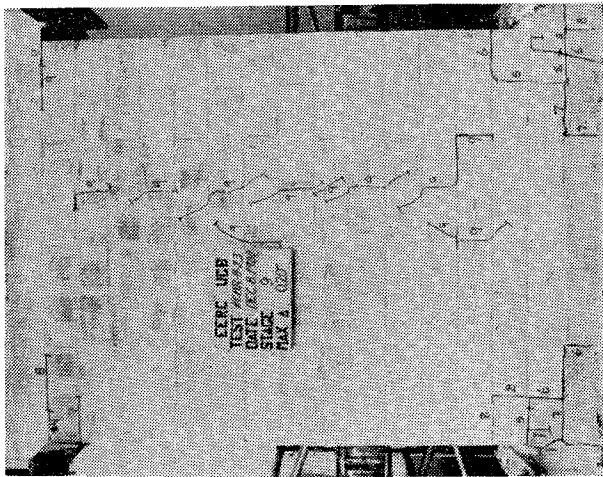
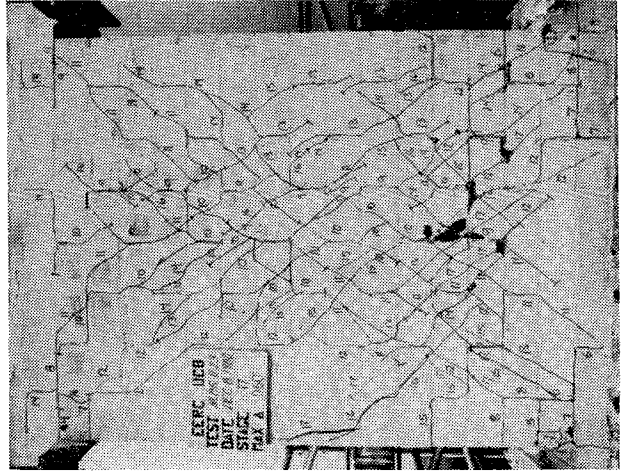
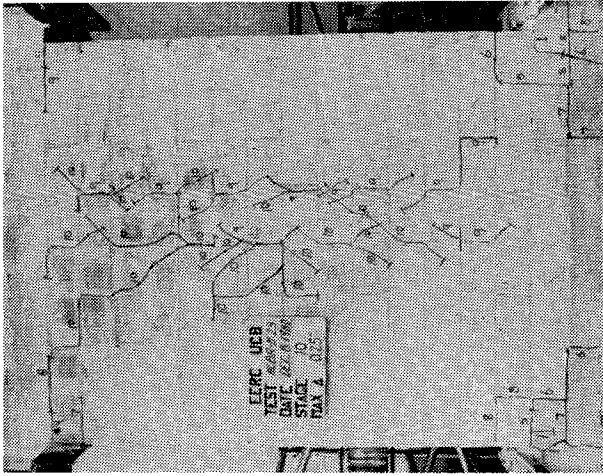
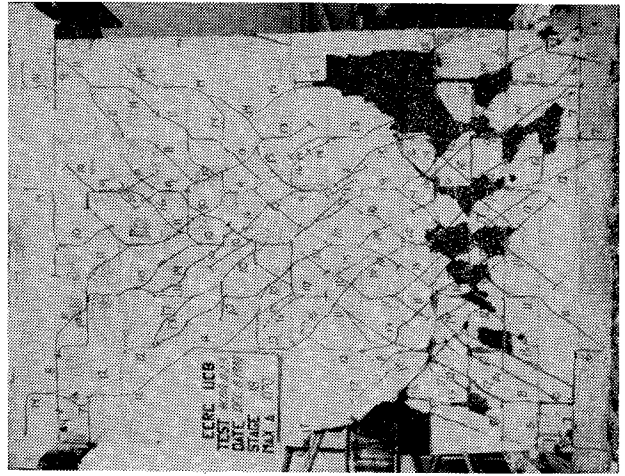
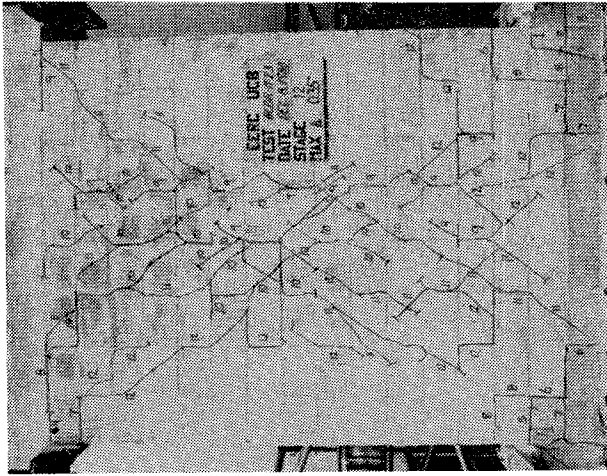


FIG. A.20b SUCCESSIVE CRACK FORMATION (HCBR-11-23)

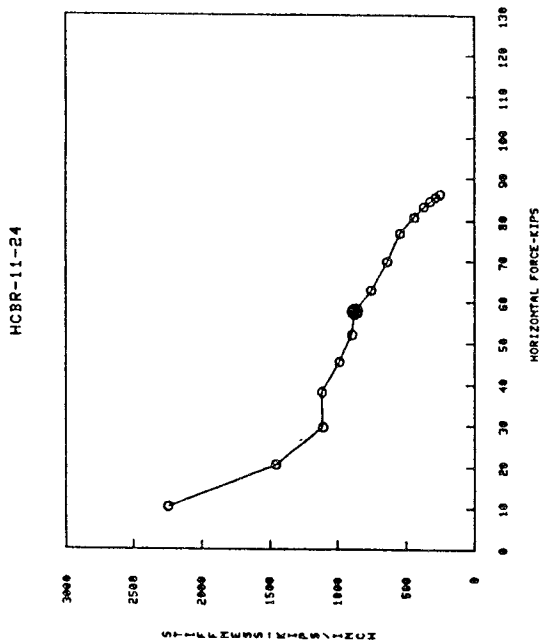
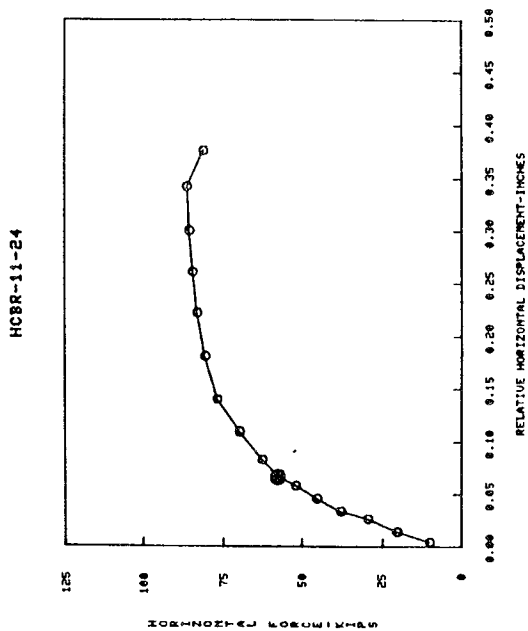
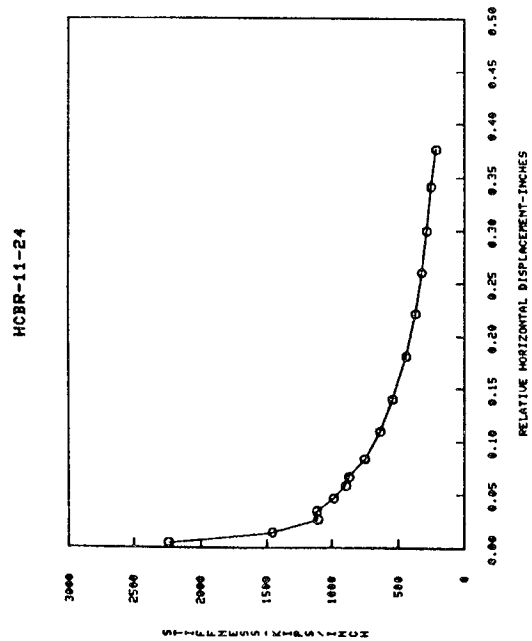
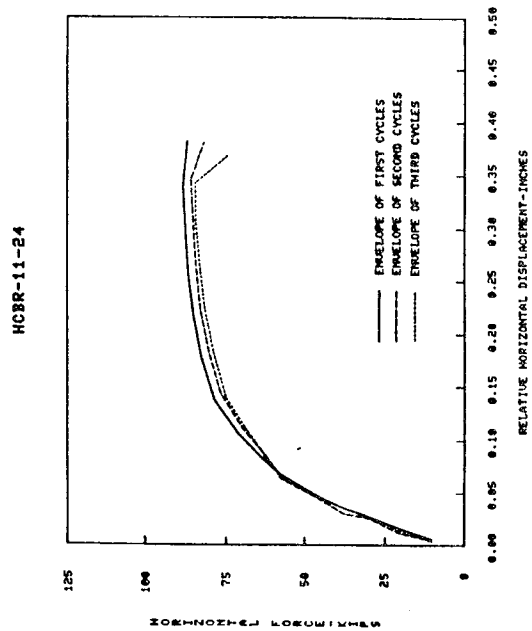


FIG. A.21a EXPERIMENTAL RESULTS (HCBR-11-24)

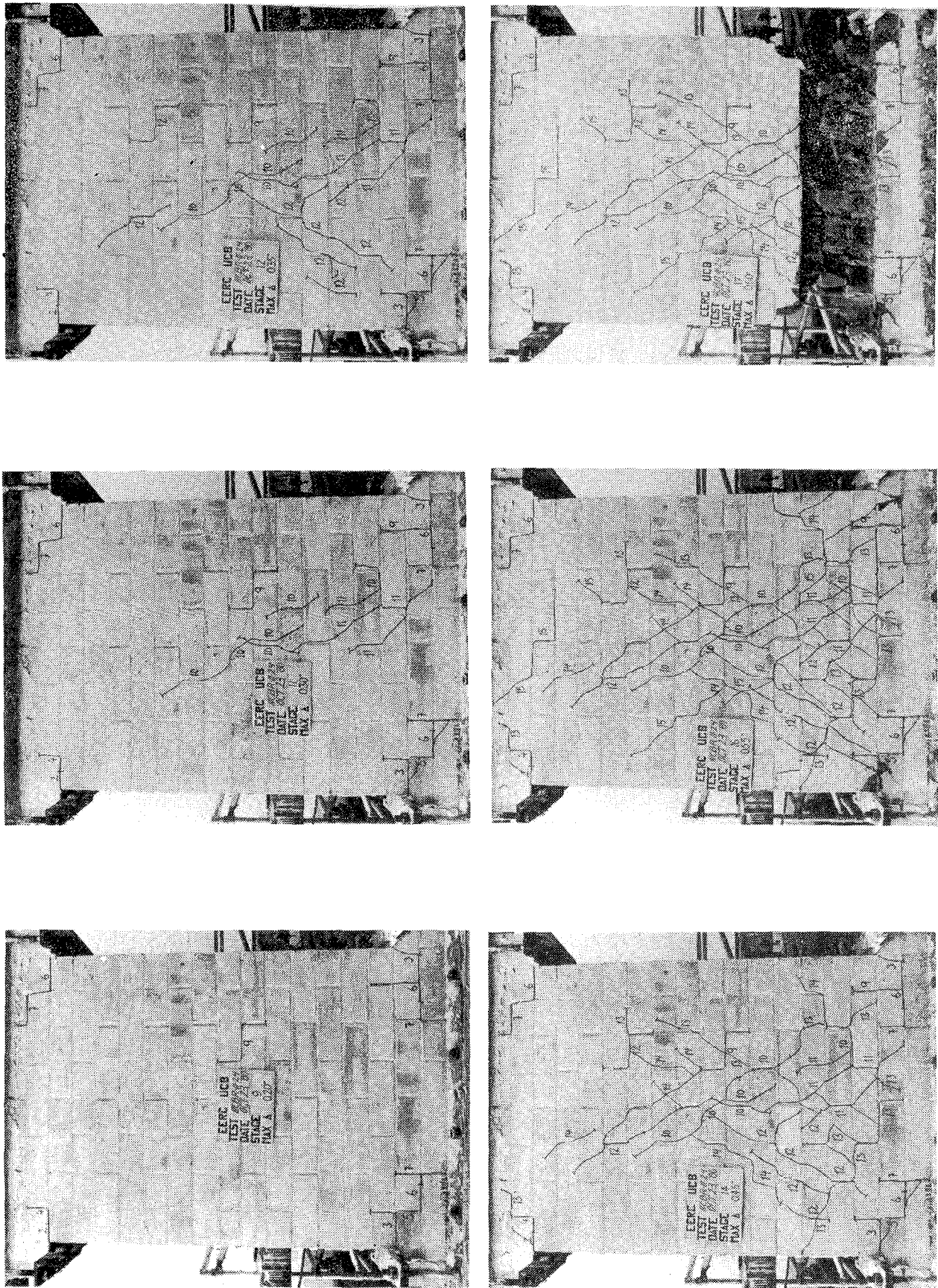


FIG. A.21b SUCCESSIVE CRACK FORMATION (HCBR-11-24)

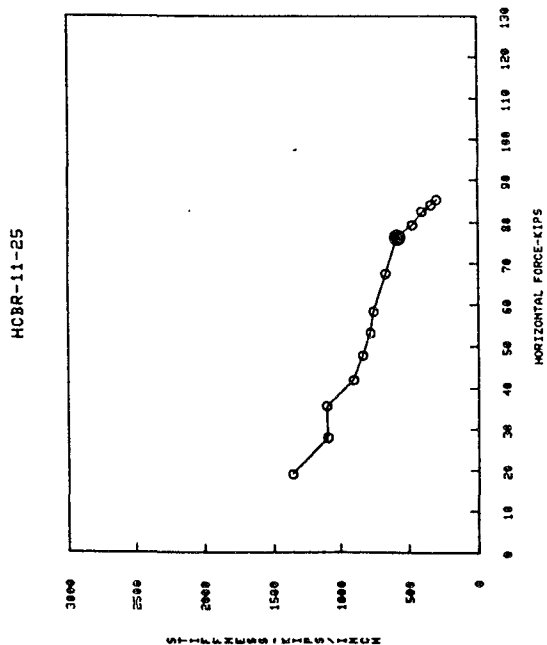
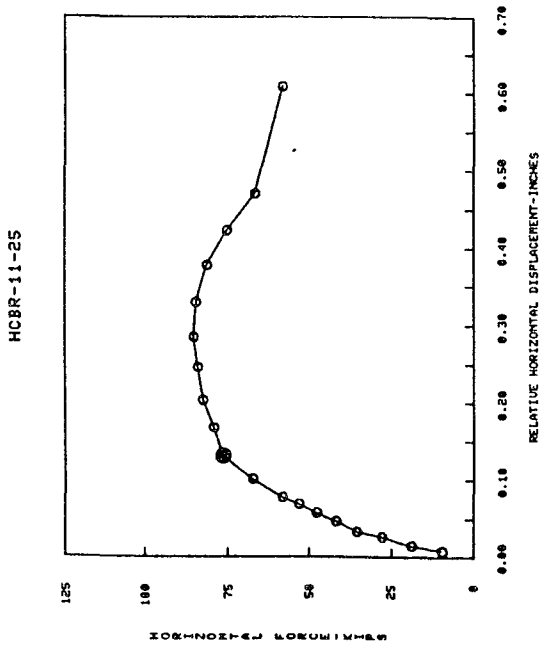
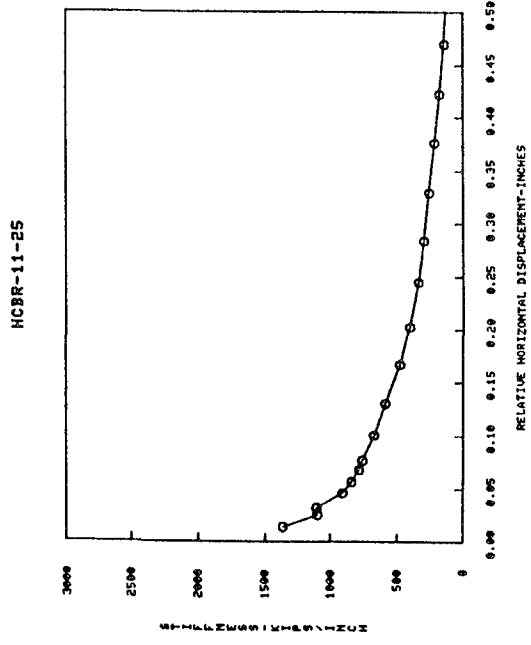
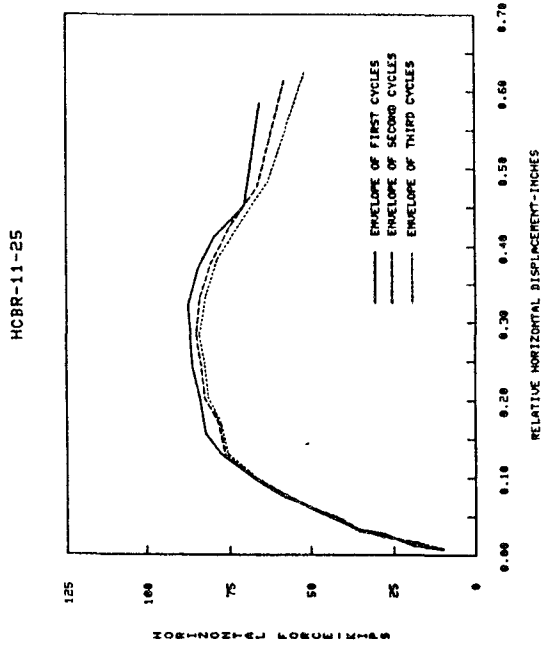


FIG. A.22a EXPERIMENTAL RESULTS (HCBR-11-25)

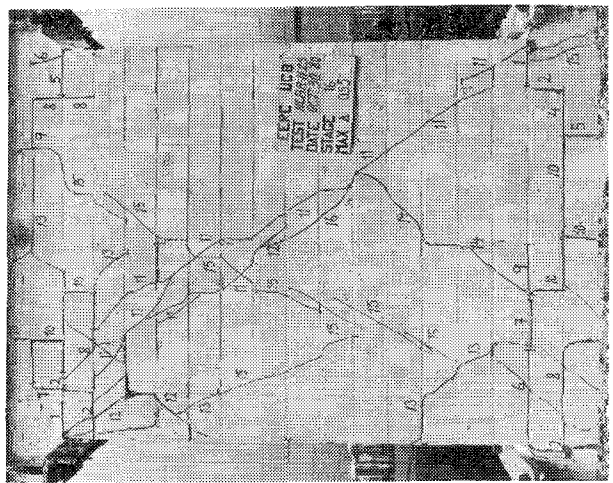
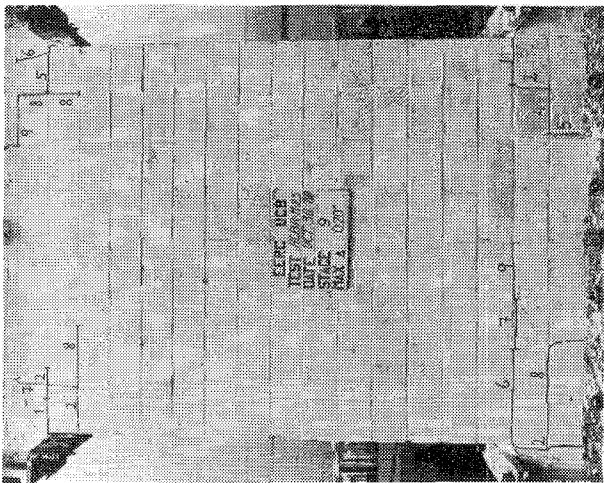
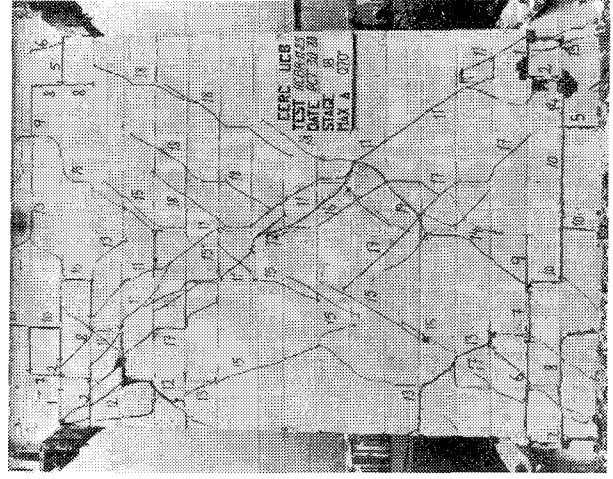
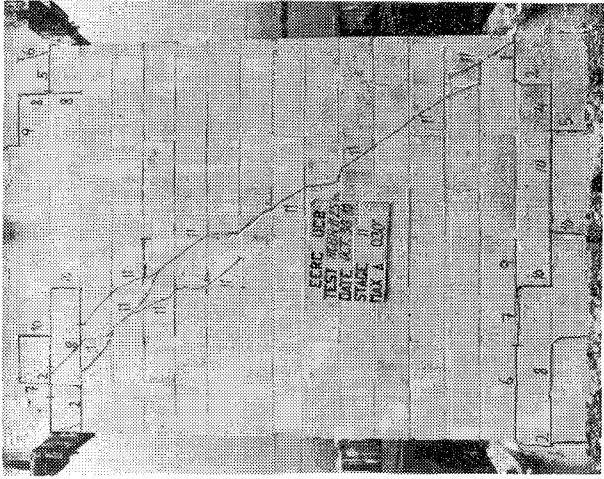
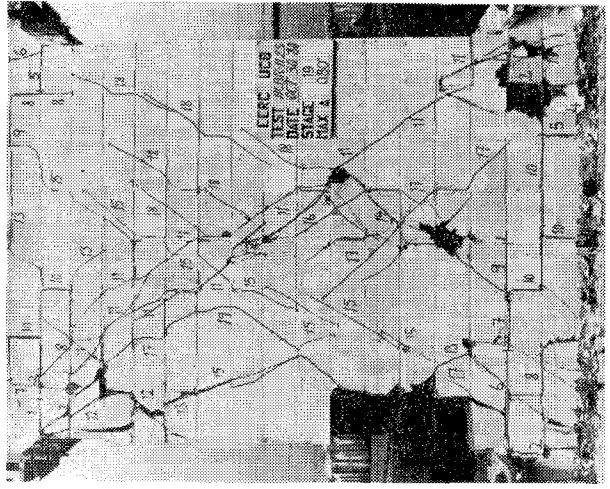
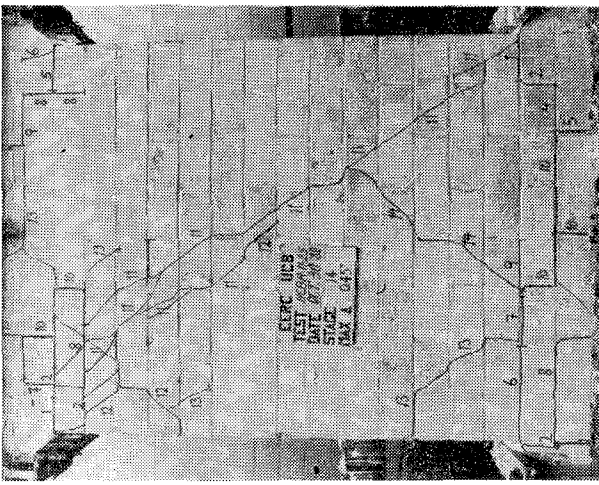


FIG. A.22b SUCCESSIVE CRACK FORMATION (HCBR-11-25)

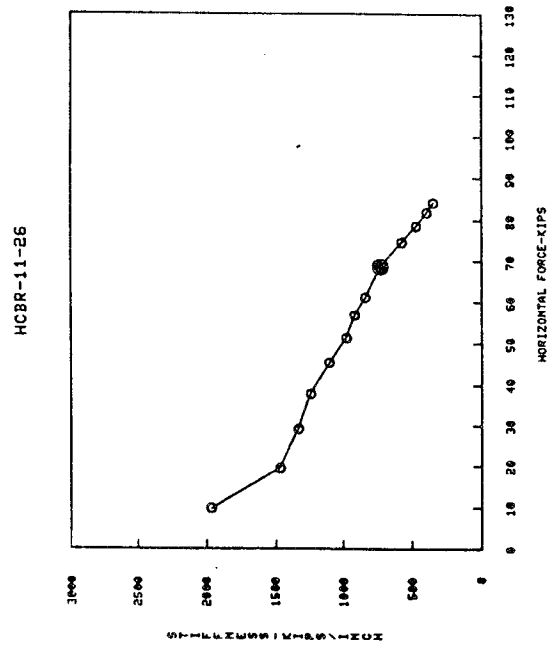
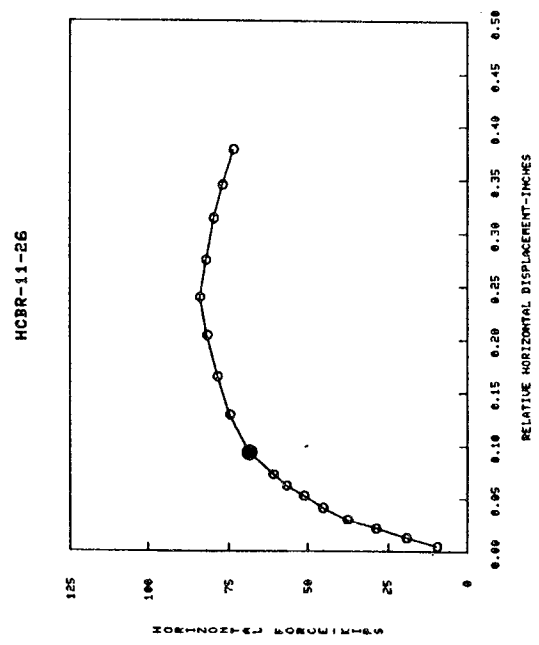
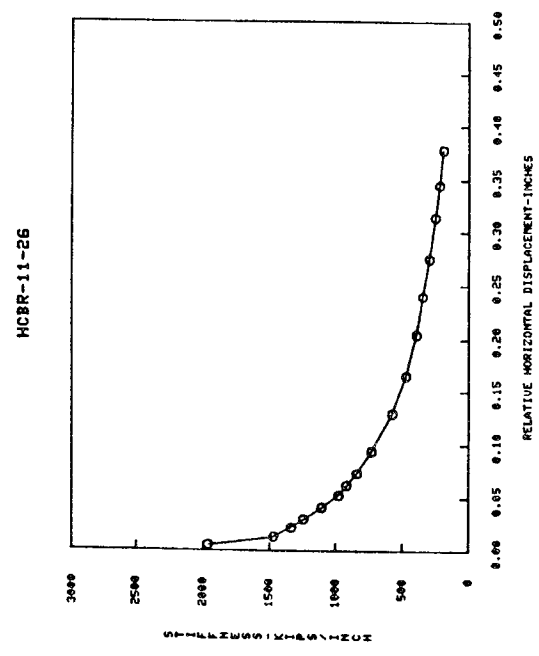
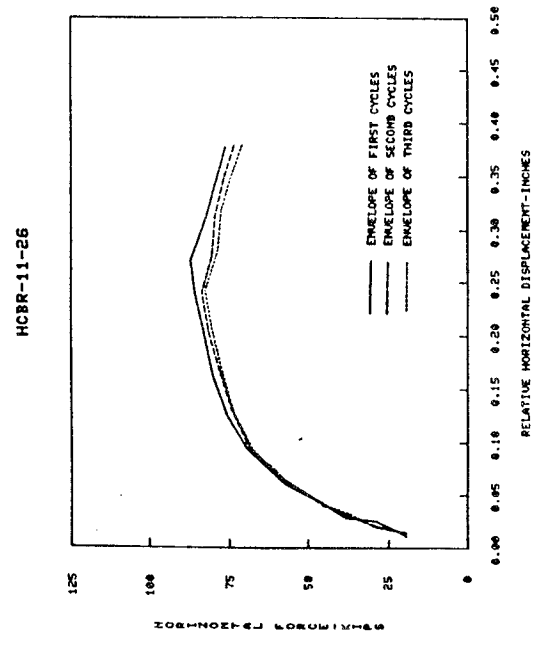


FIG. A.23a EXPERIMENTAL RESULTS (HCBR-11-26)

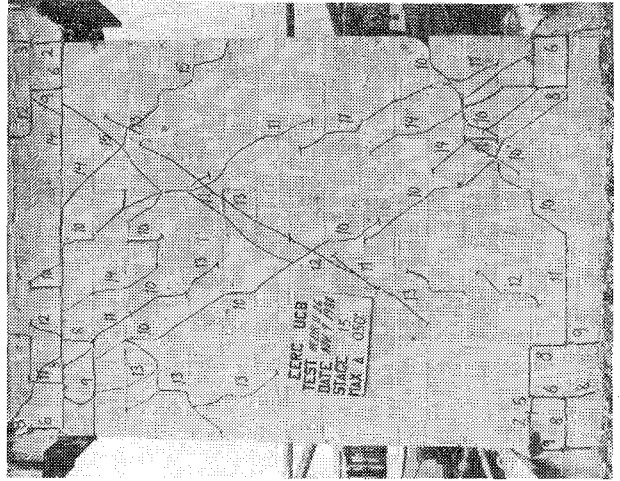
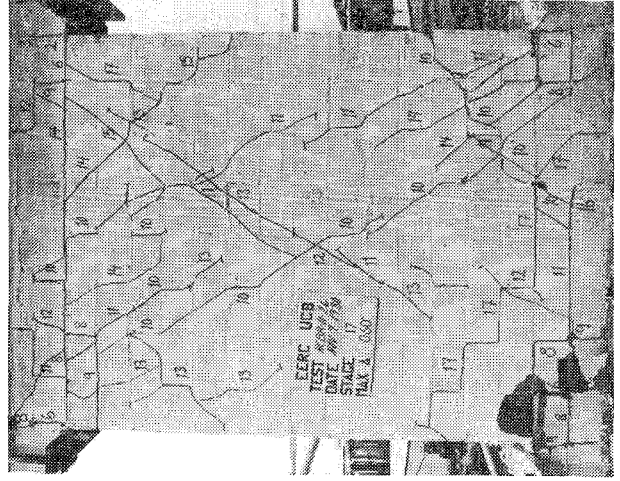
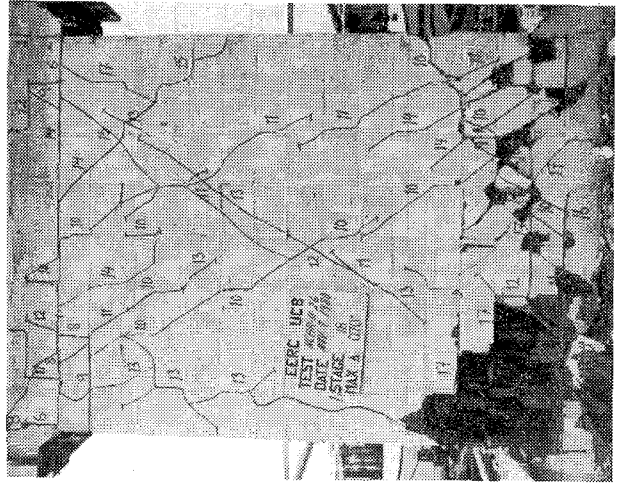
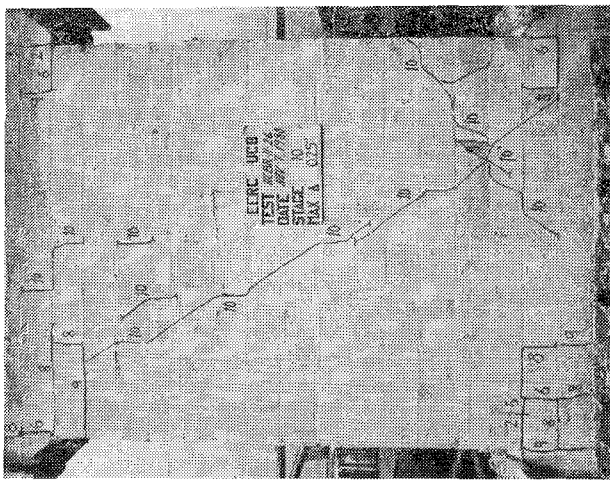
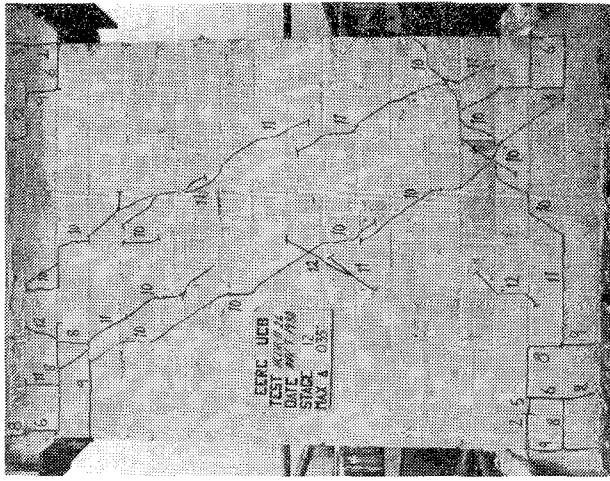
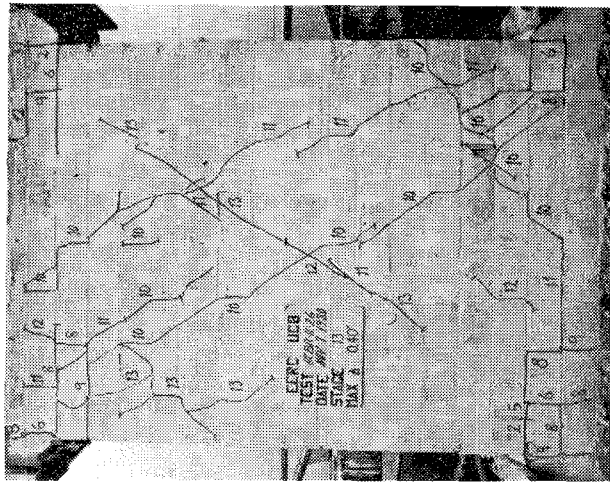


FIG. A.23b SUCCESSIVE CRACK FORMATION (HCBR-11-26)

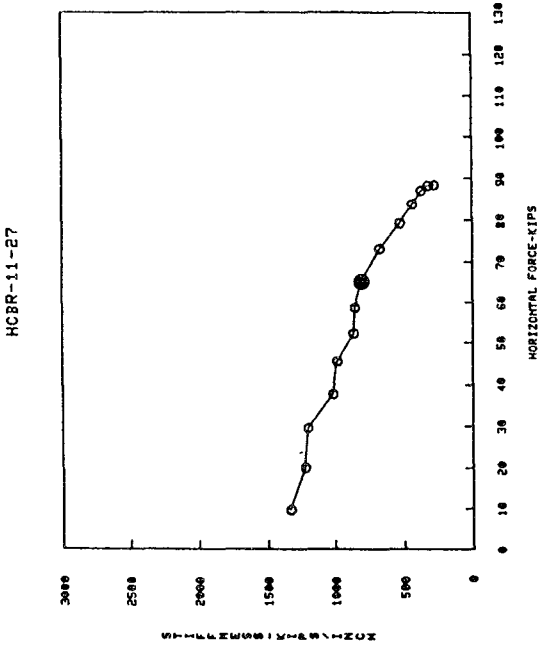
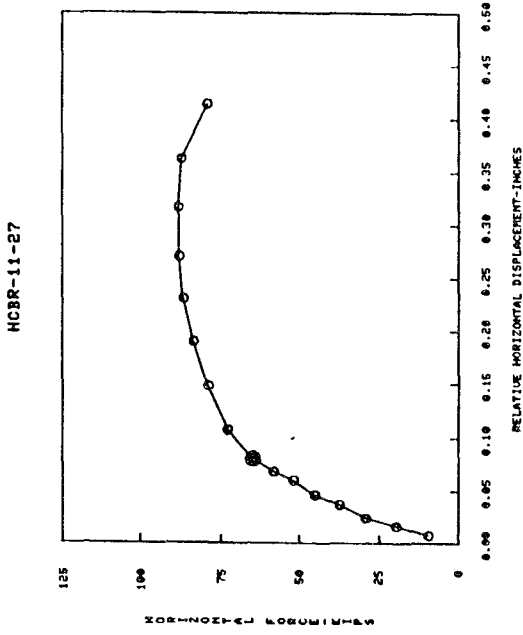
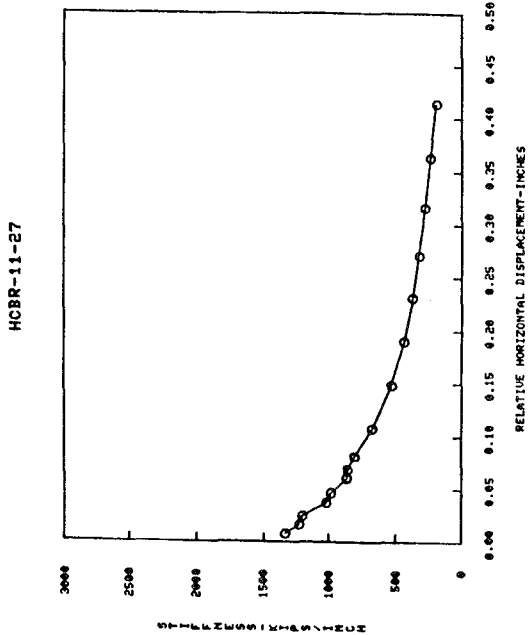
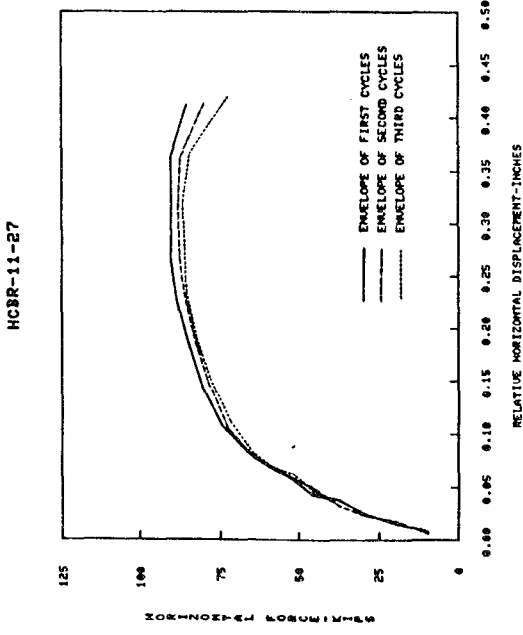


FIG. A.24a EXPERIMENTAL RESULTS (HCBR-11-27)

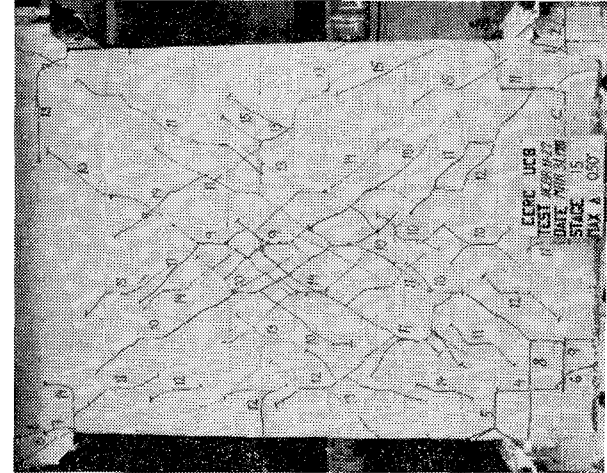
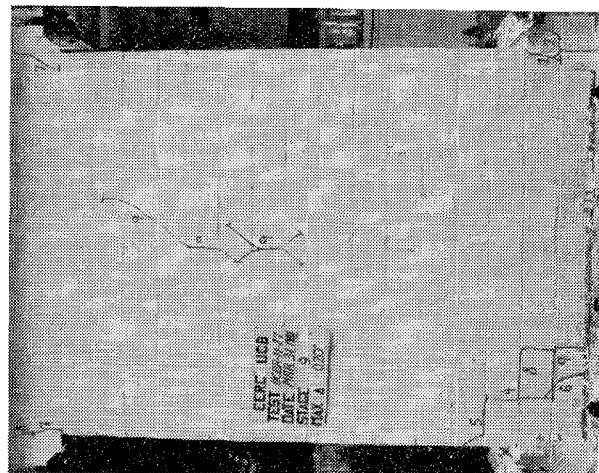
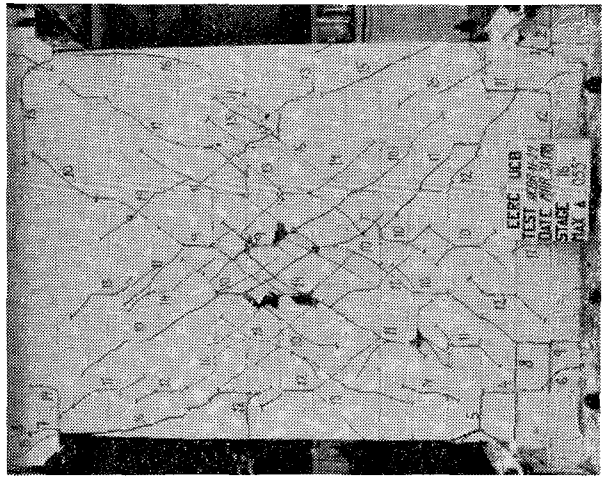
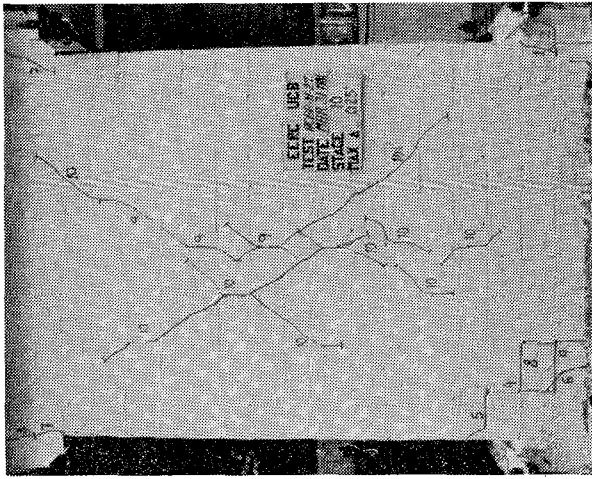
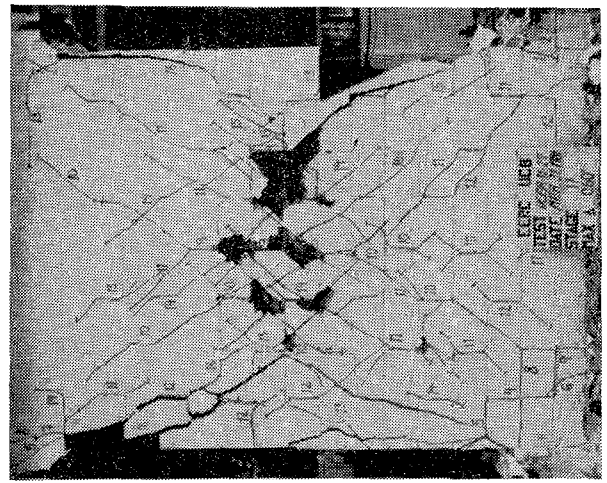
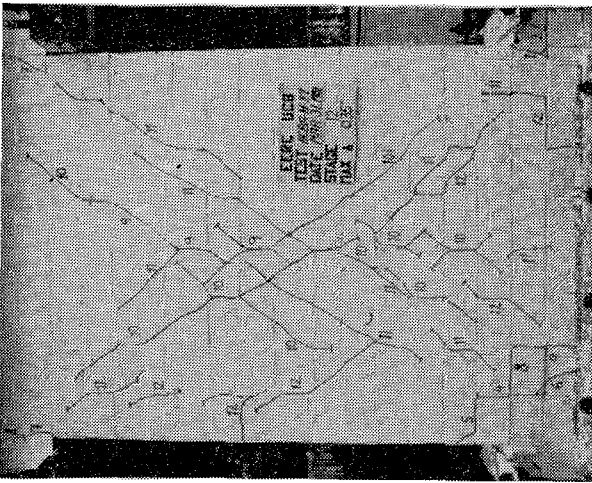


FIG. A. 24b SUCCESSIVE CRACK FORMATION (HCBR-11-27)

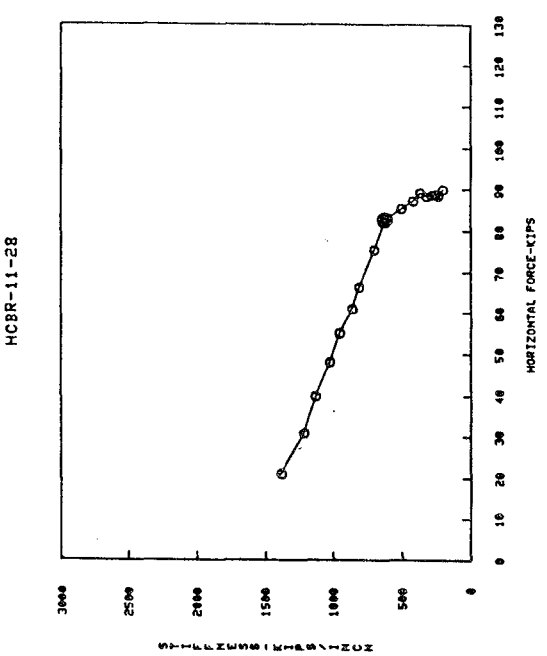
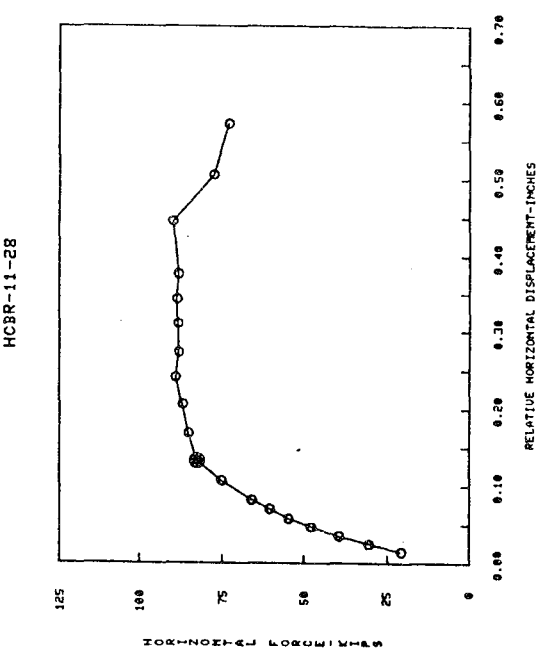
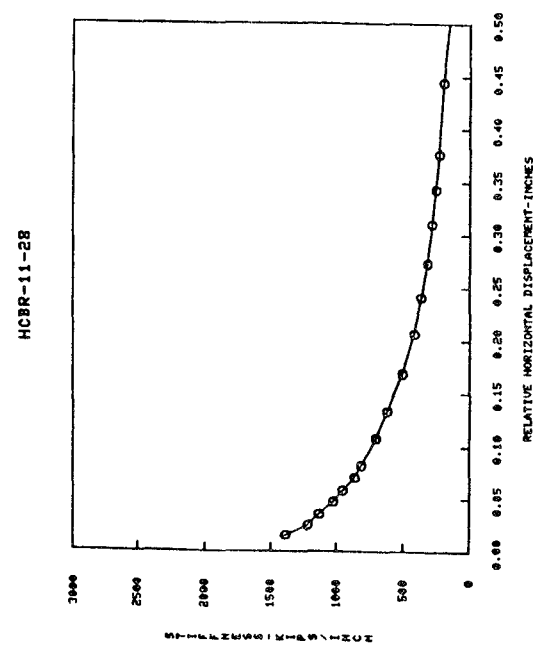
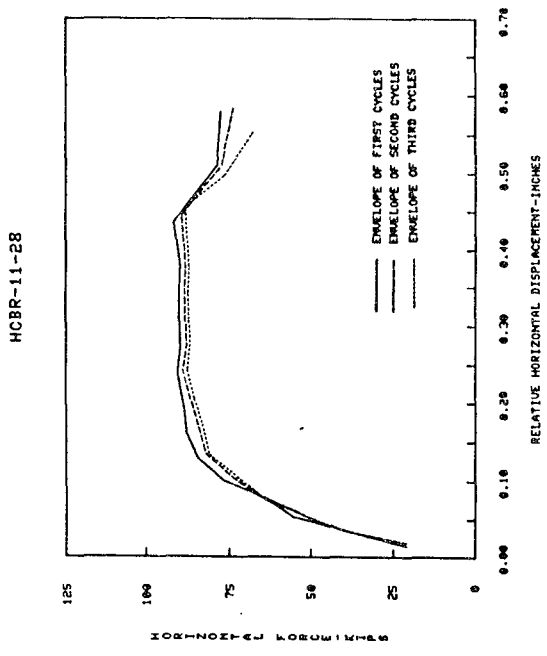


FIG. A.25a EXPERIMENTAL RESULTS (HCBR-11-28)

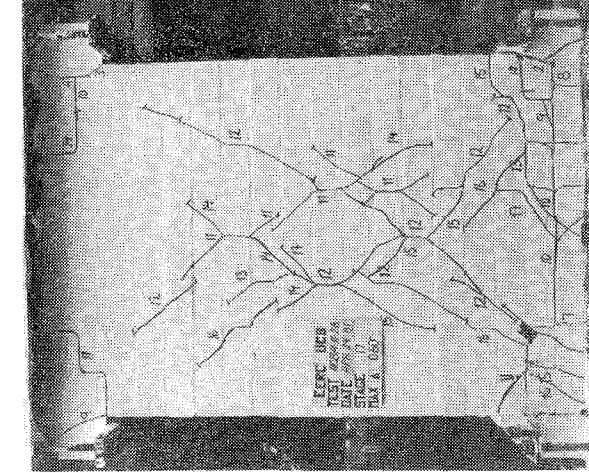
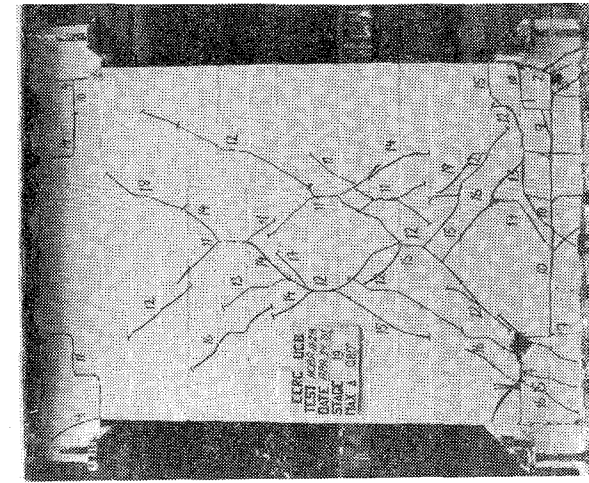
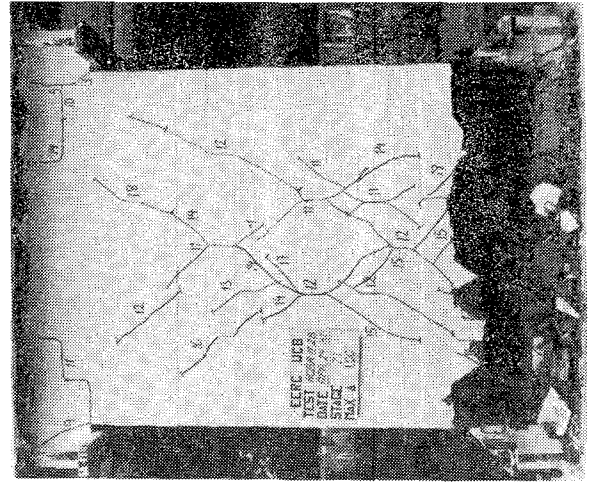
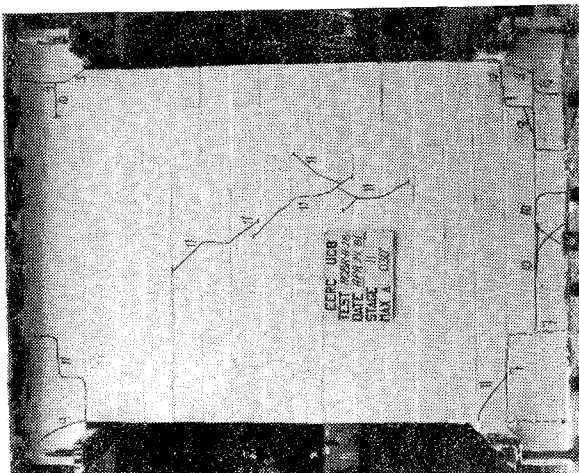
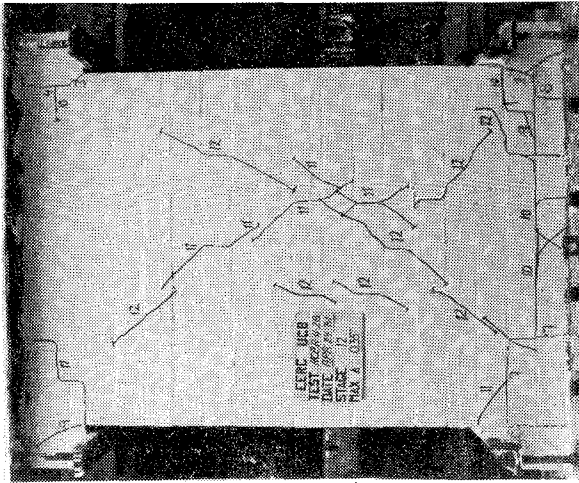
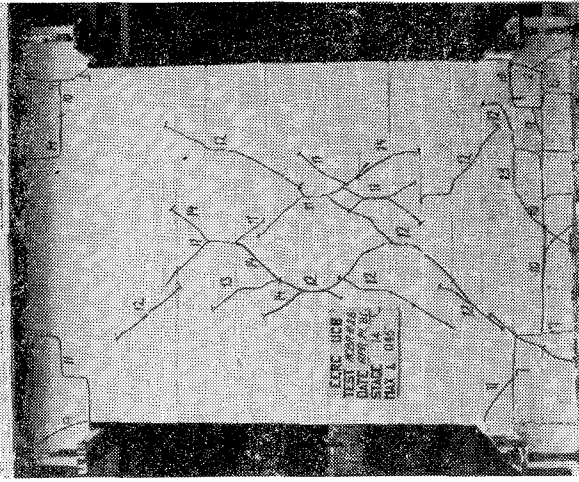


FIG. A.25b SUCCESSIVE CRACK FORMATION (HCBR-11-28)

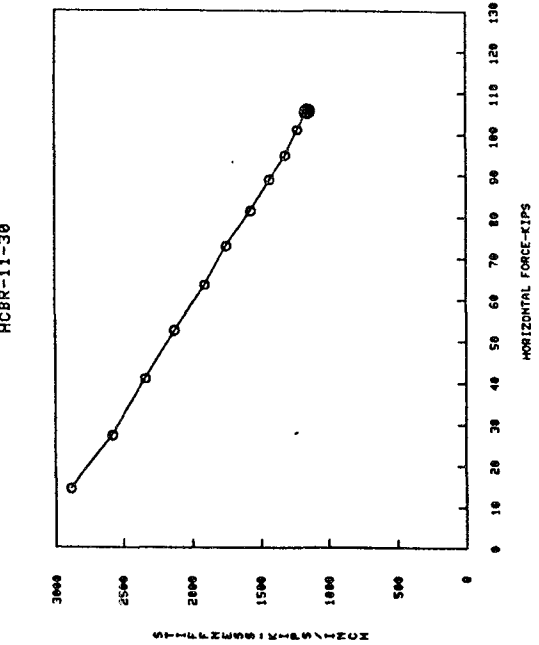
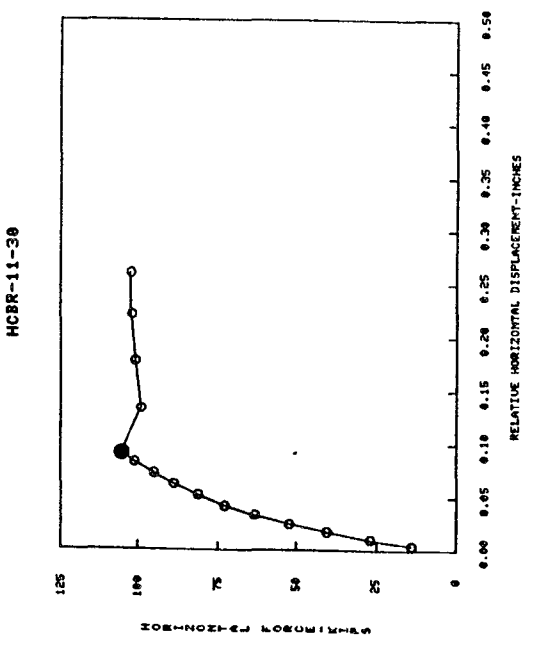
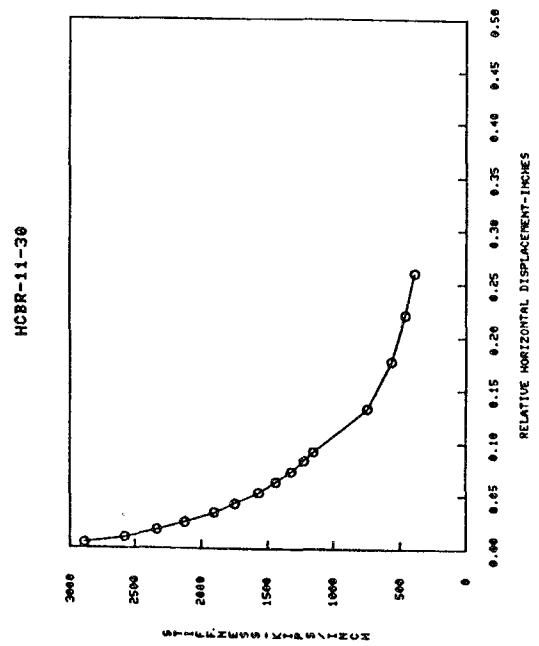
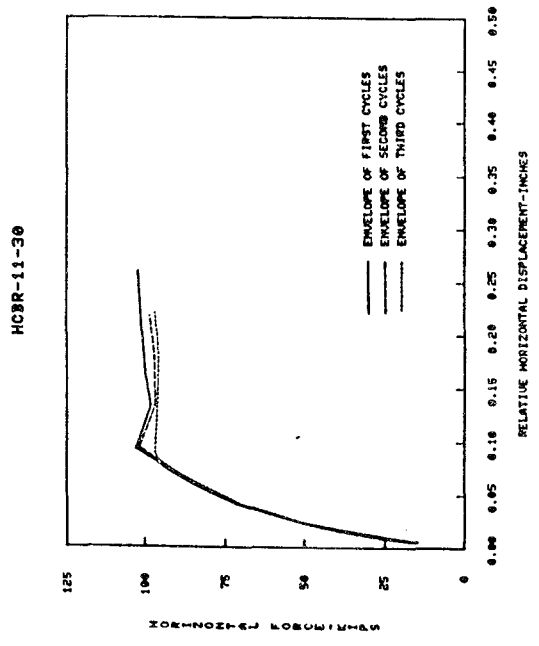


FIG. A.26a EXPERIMENTAL RESULTS (HCBR-11-30)

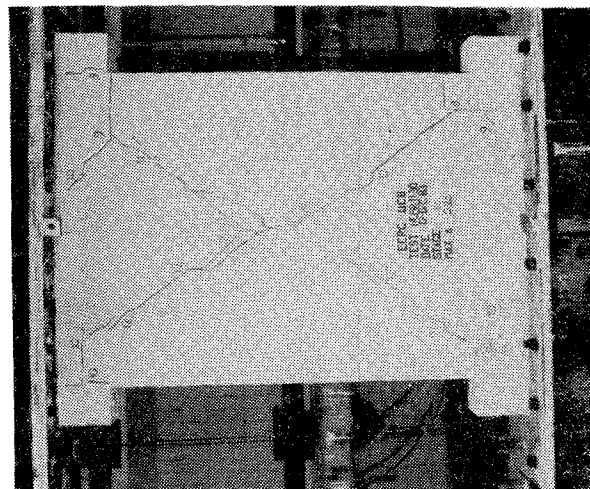
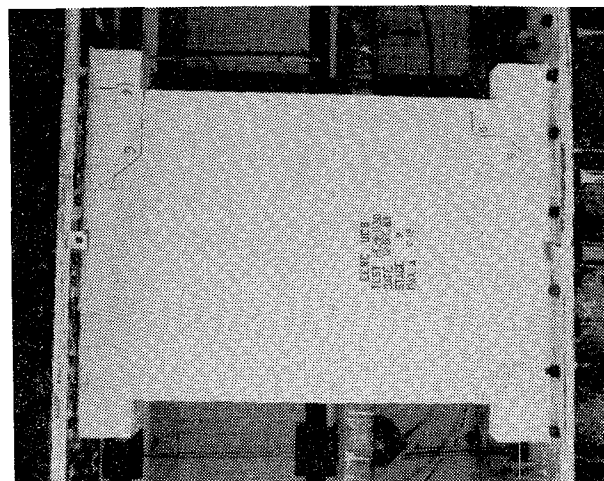
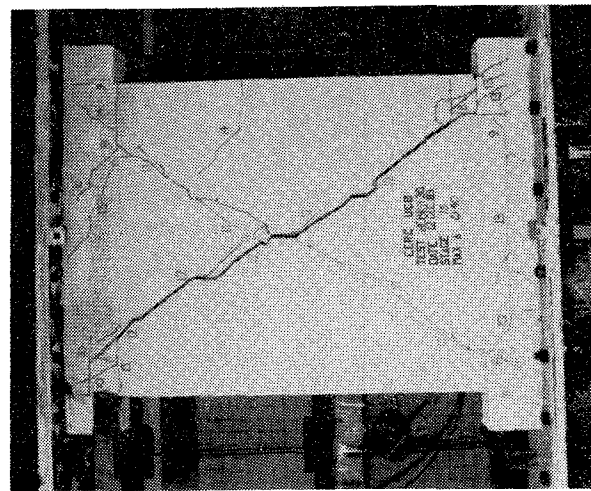
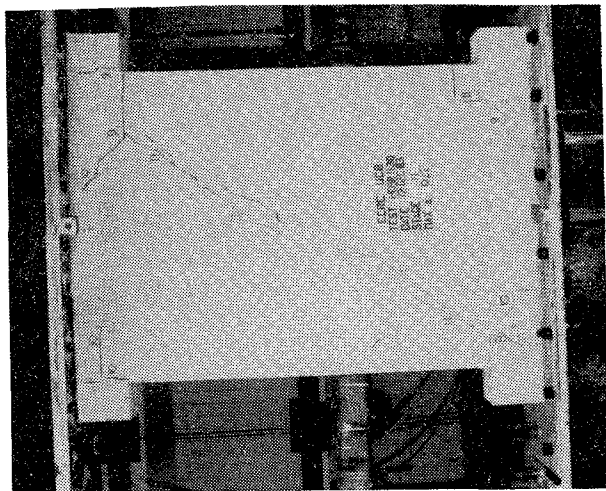


FIG. A.26b SUCCESSIVE CRACK FORMATION (HCBR-11-30)

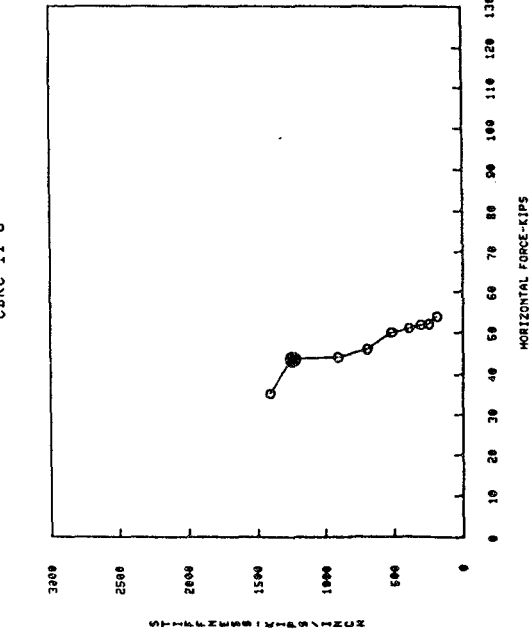
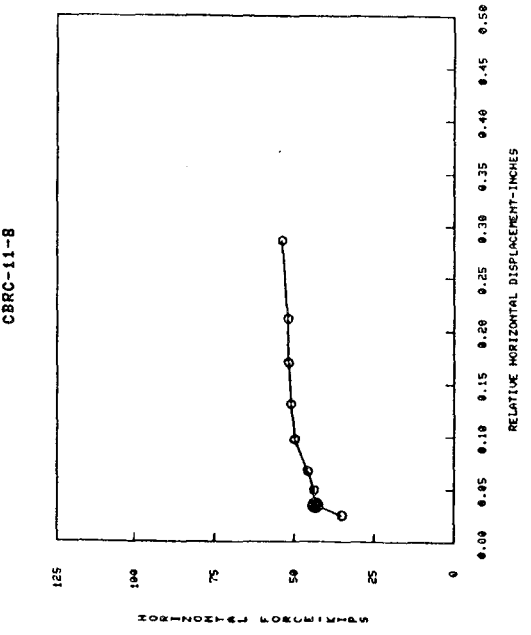
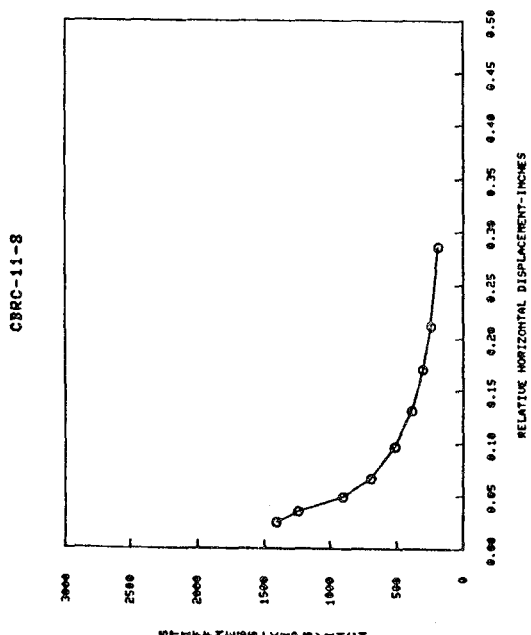
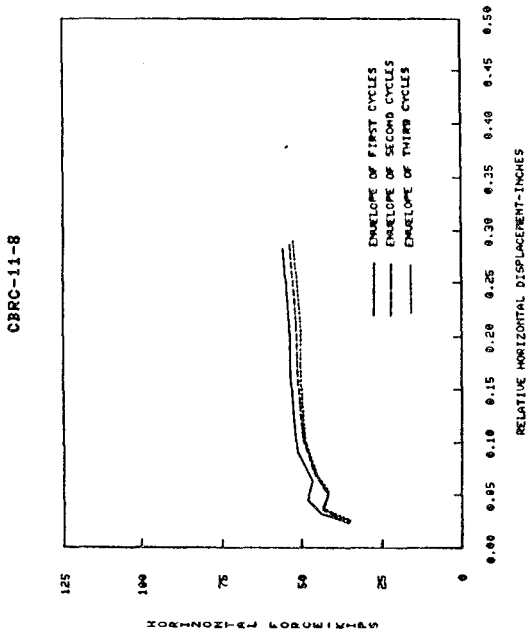


FIG. A.27 EXPERIMENTAL RESULTS (CBRC-11-8)

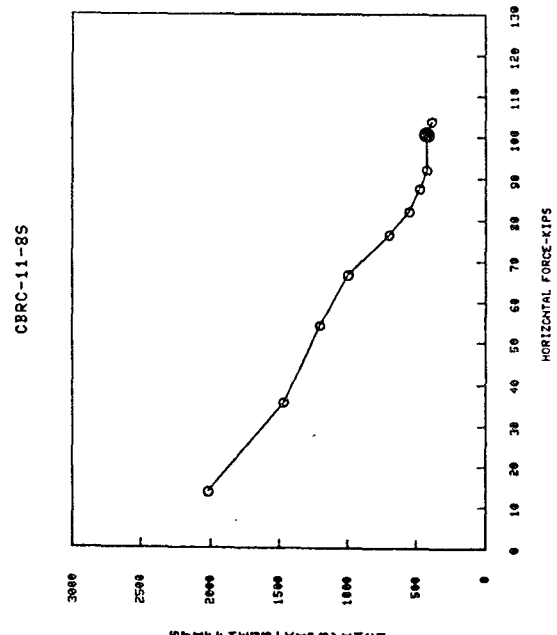
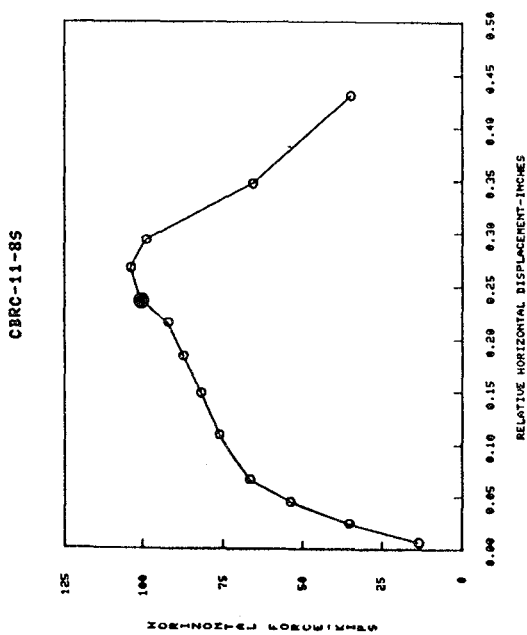
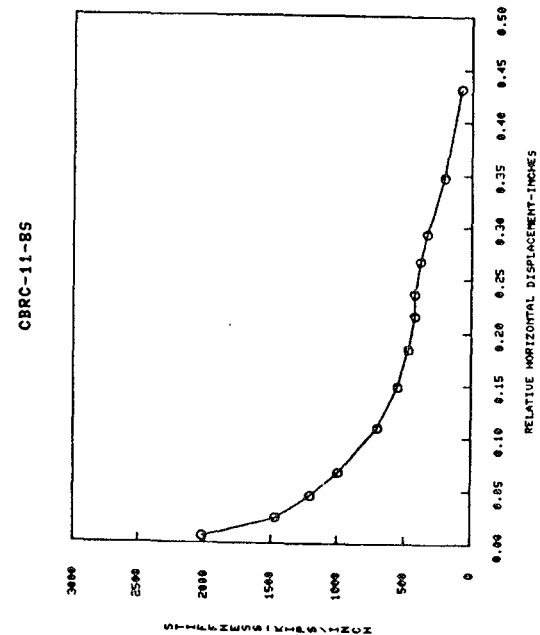
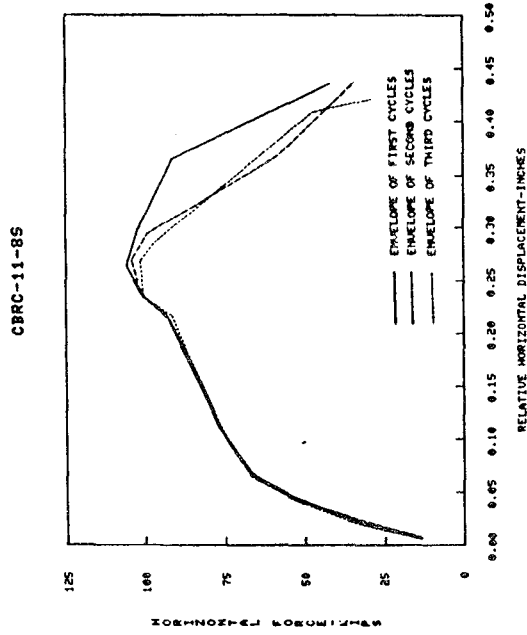


FIG. A.28 EXPERIMENTAL RESULTS (CBRC-11-8S)

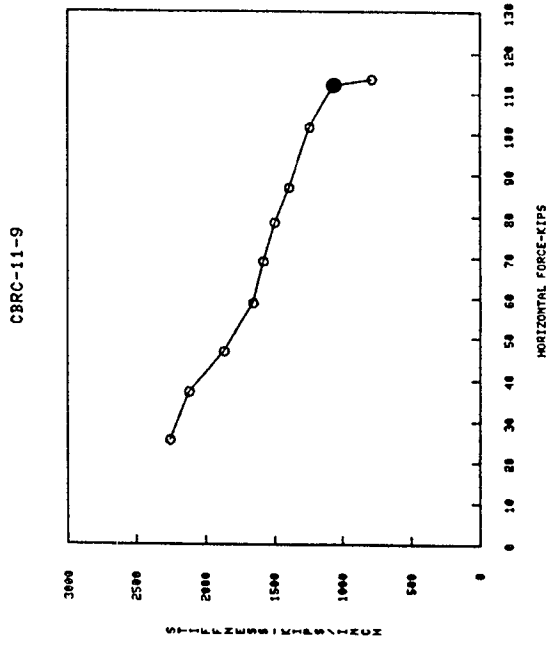
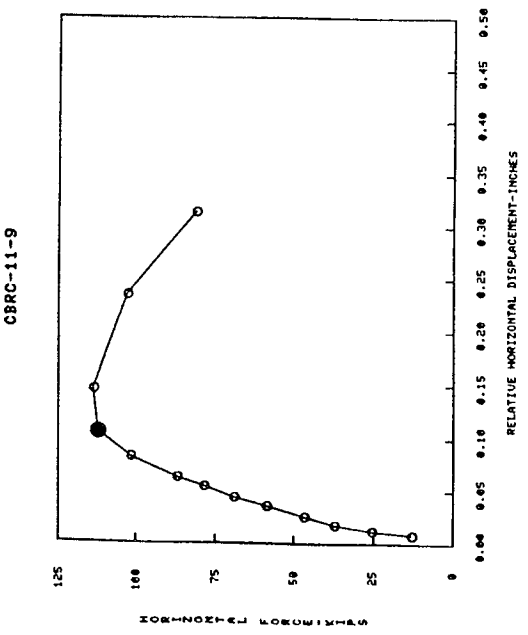
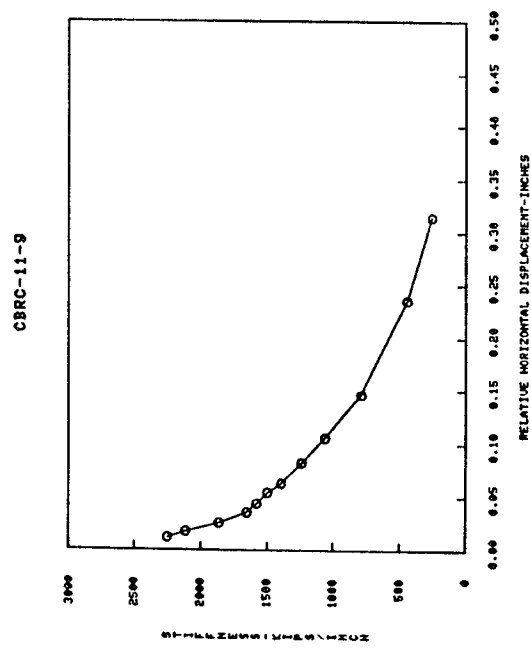
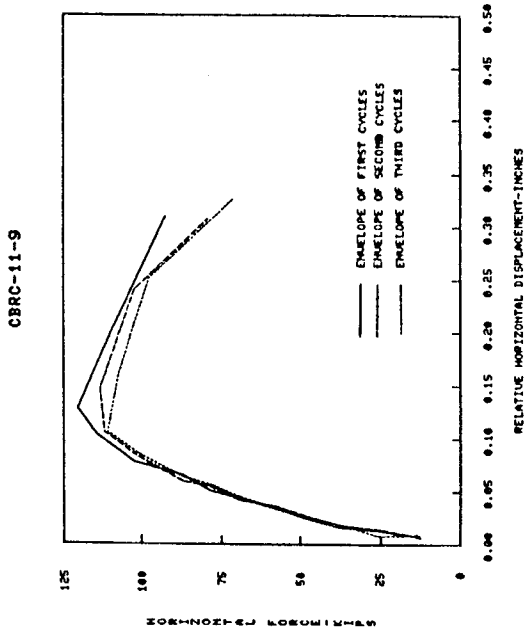


FIG. A.29a EXPERIMENTAL RESULTS (CBRC-11-9)

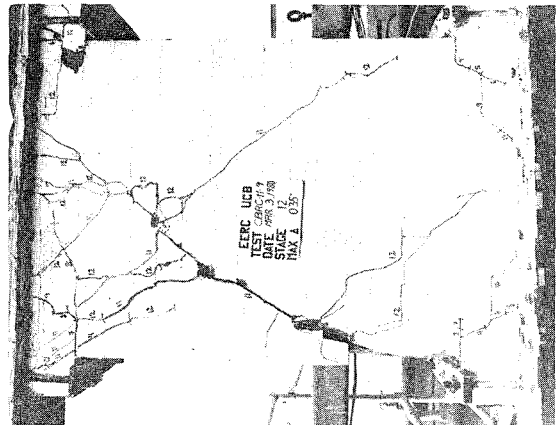
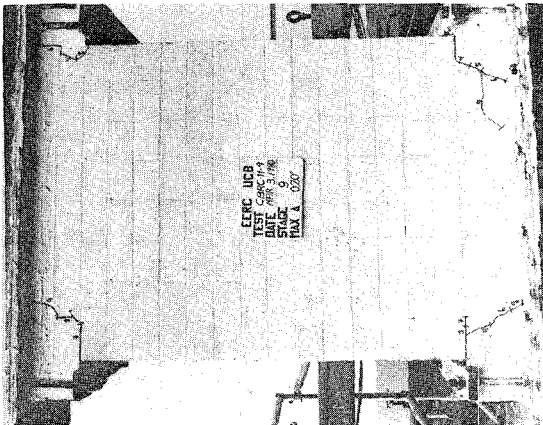
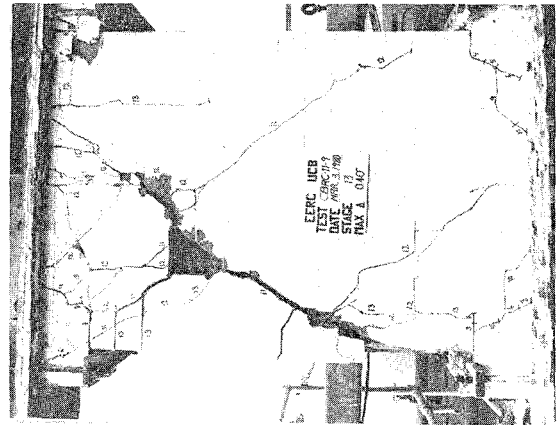
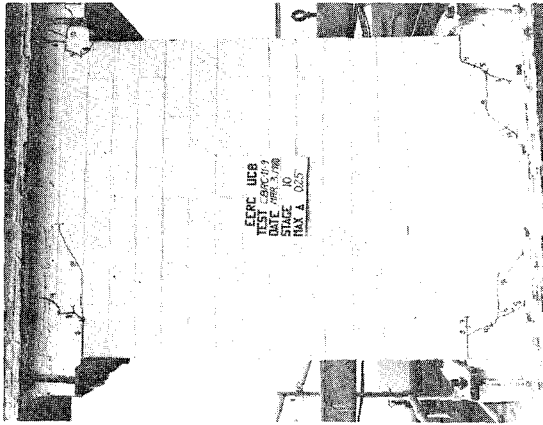
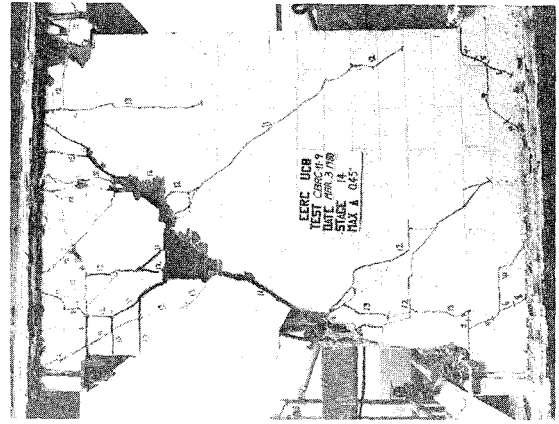
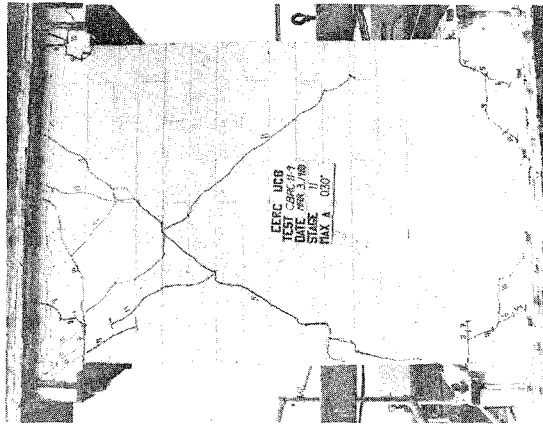


FIG. A. 29b SUCCESSIVE CRACK FORMATION (CBRC-11-9)

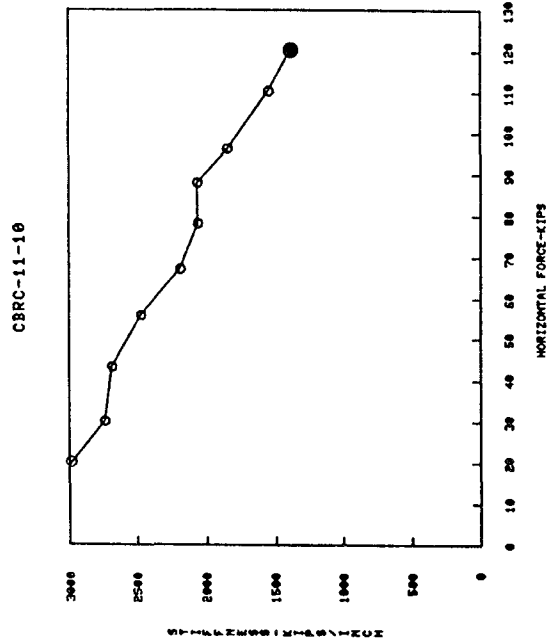
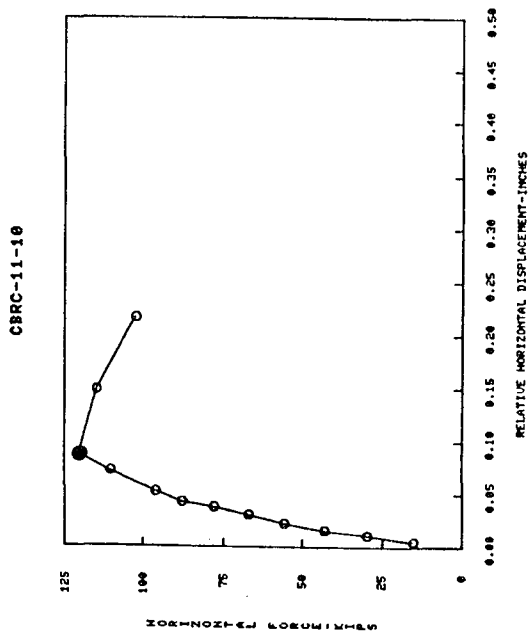
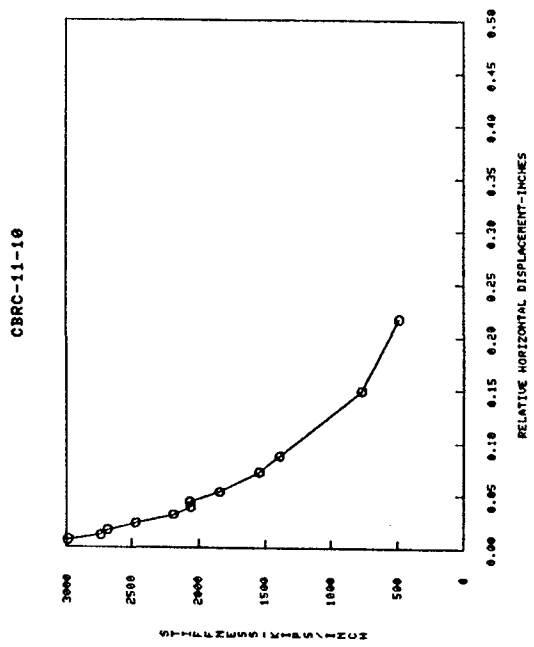
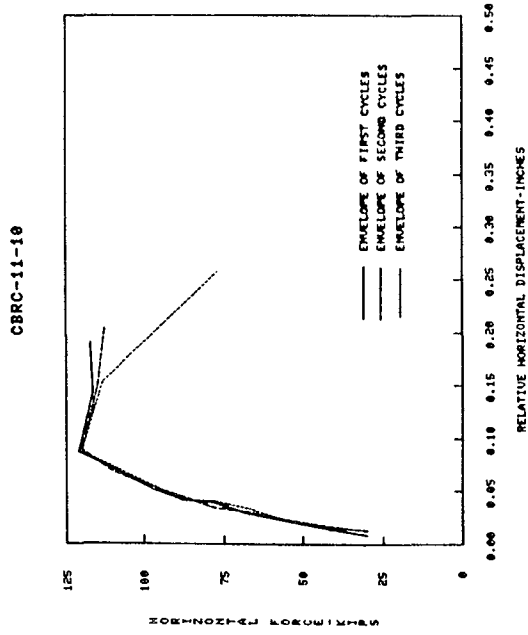


FIG. A.30a EXPERIMENTAL RESULTS (CBRC-11-10)

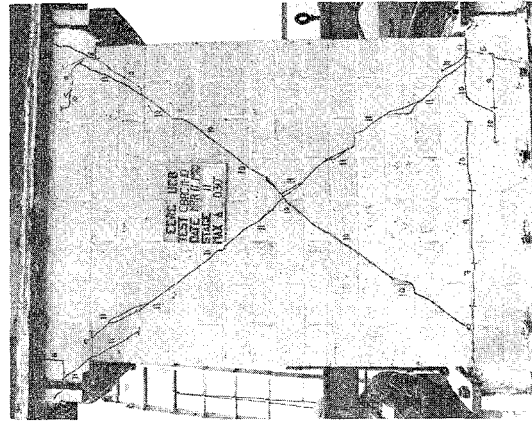
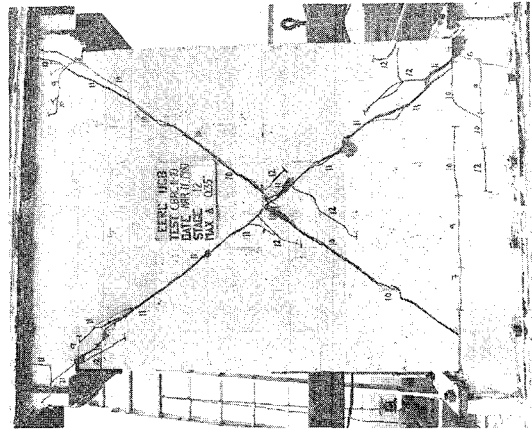
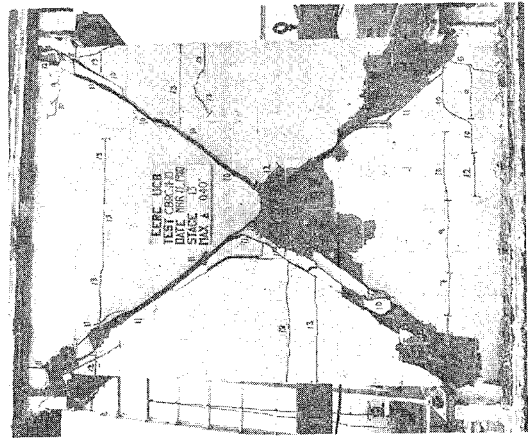
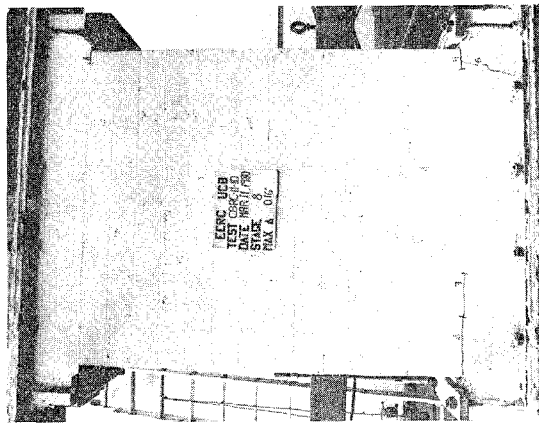
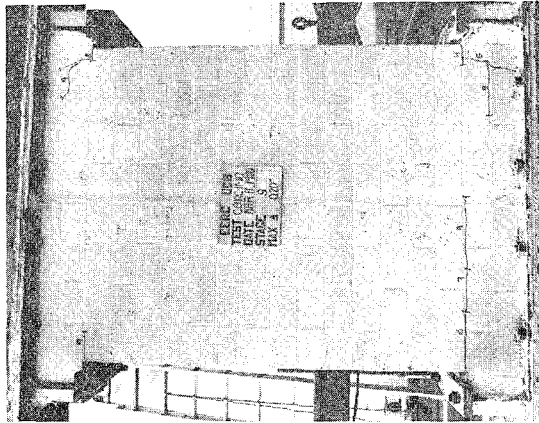
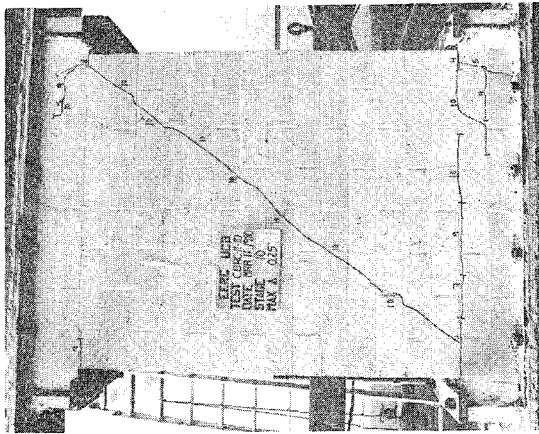


FIG. A. 30b SUCCESSIVE CRACK FORMATION (CBRC-11-10)

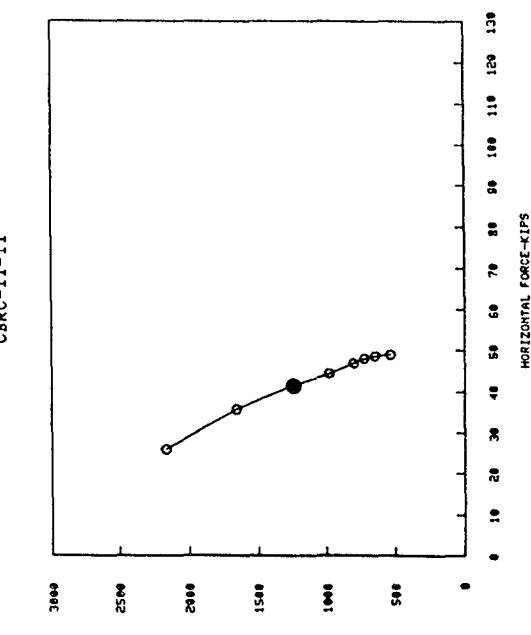
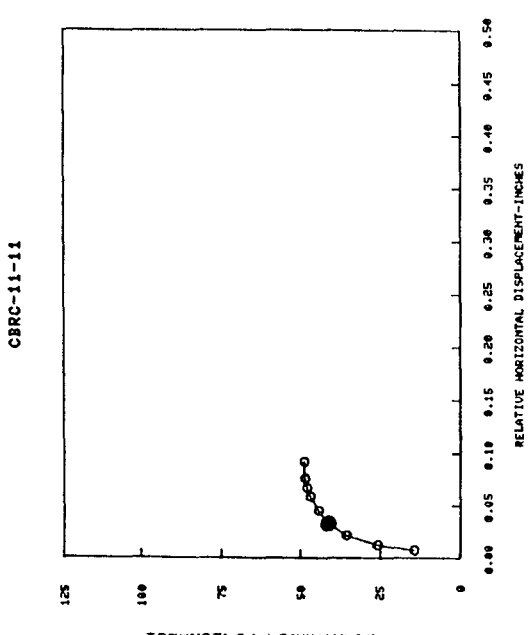
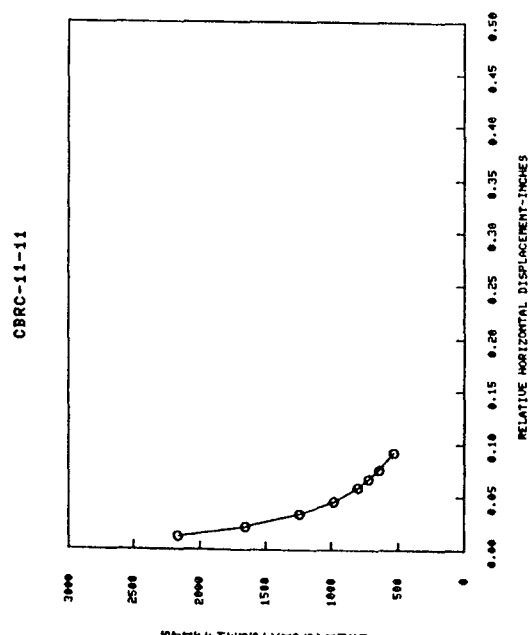
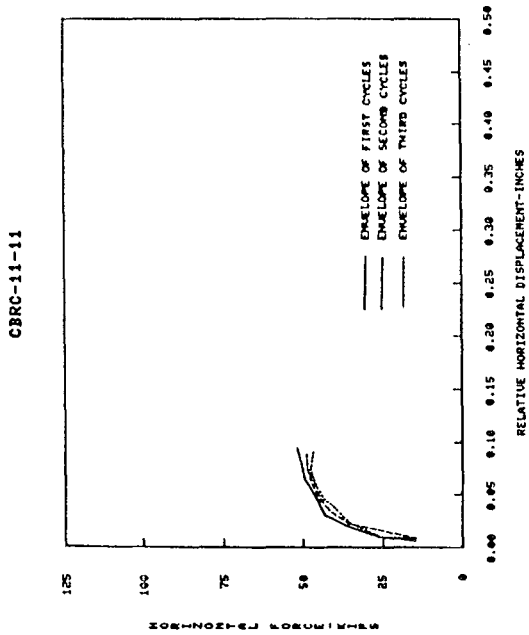


FIG. A.31a EXPERIMENTAL RESULTS (CBRC-11-11)

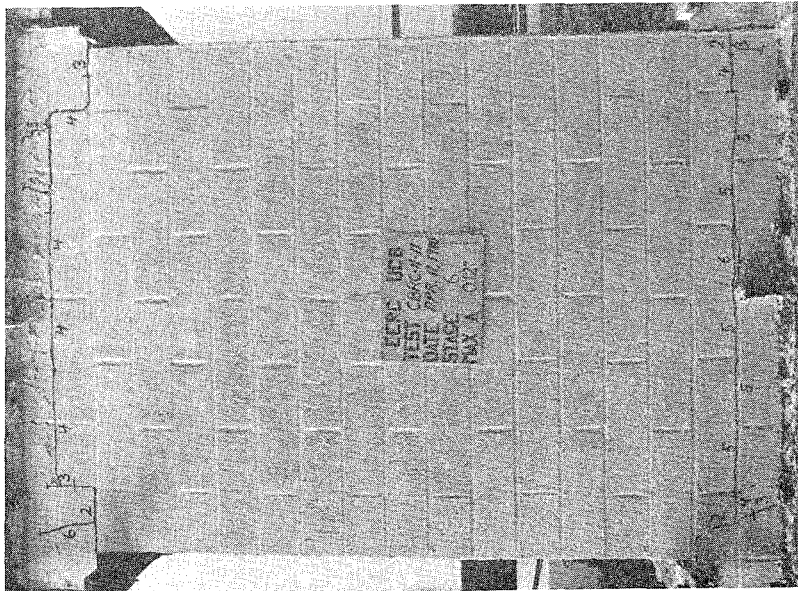
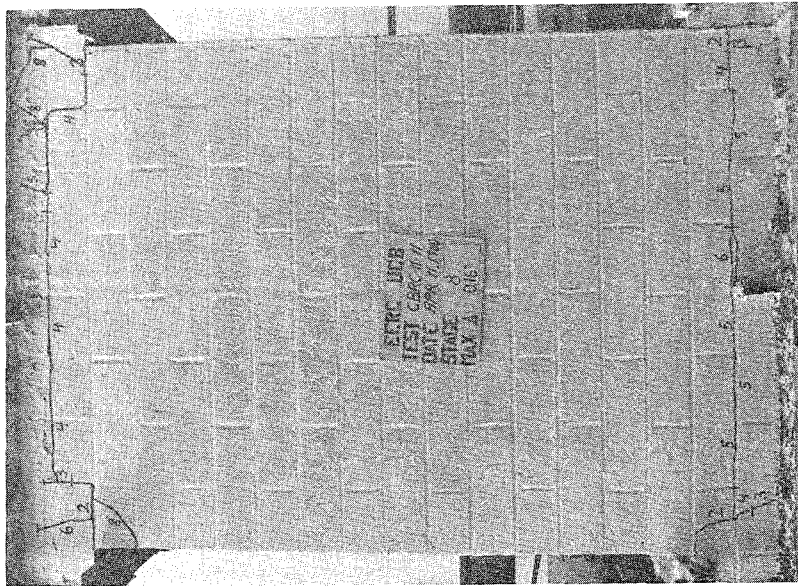
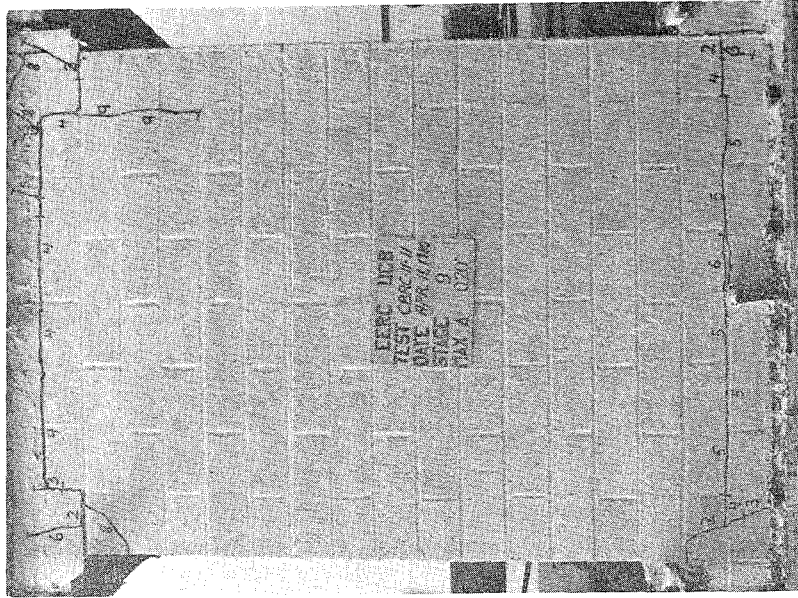


FIG. A.31b SUCCESSIVE CRACK FORMATION (CBRC-11-11)

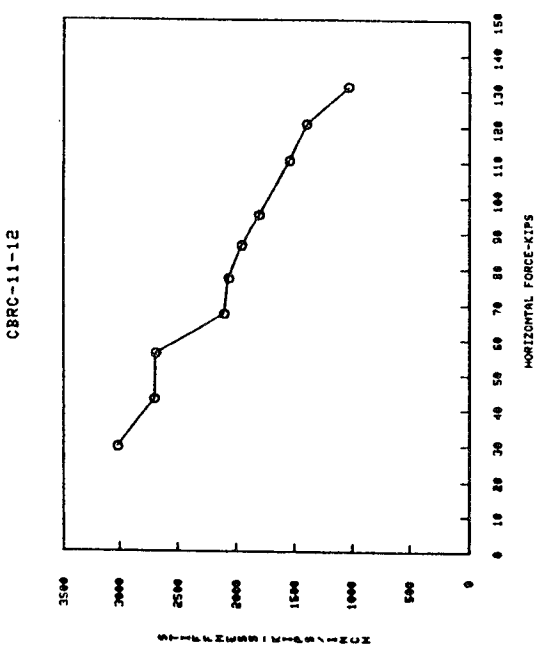
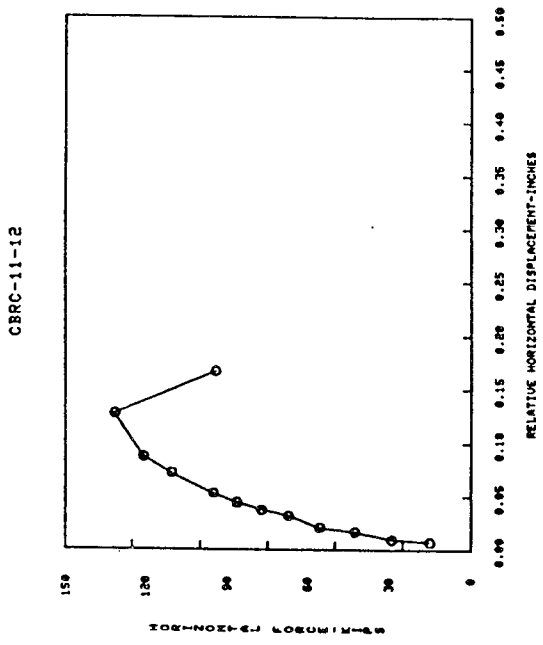
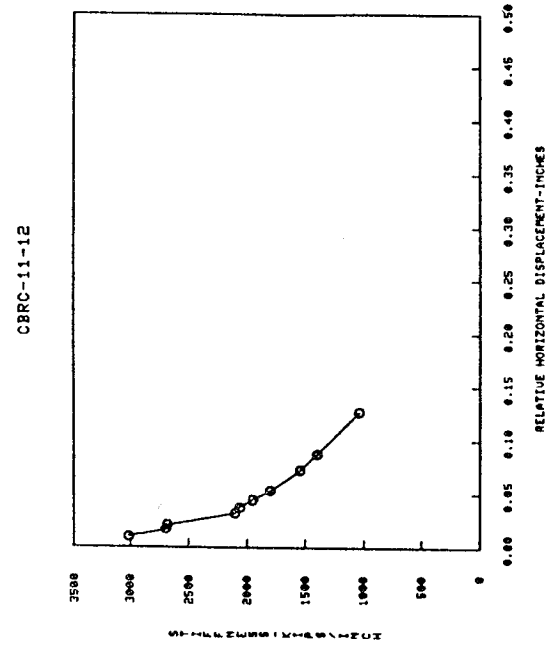
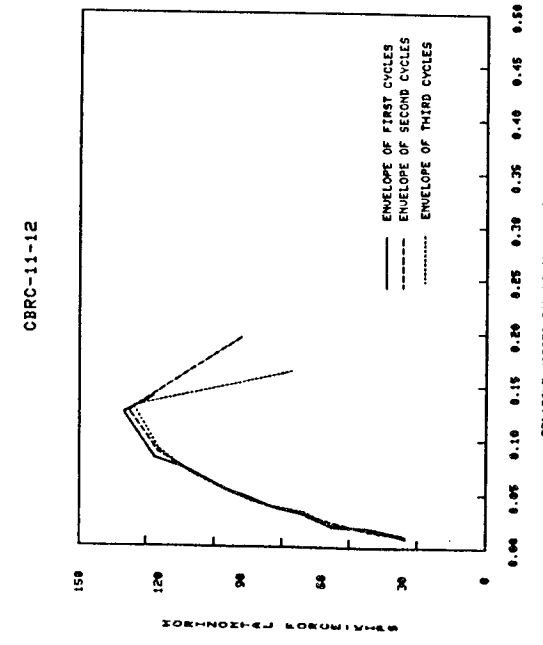


FIG. A.32a EXPERIMENTAL RESULTS (CBRC-11-12)

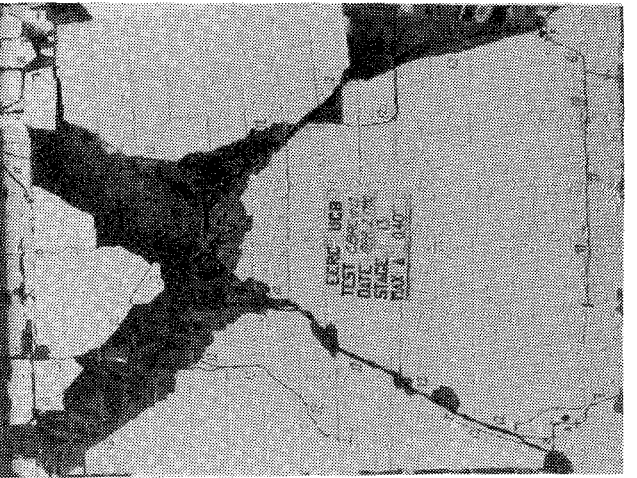
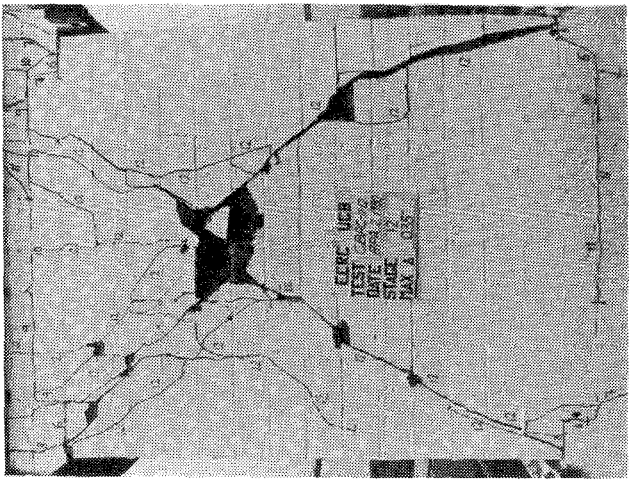
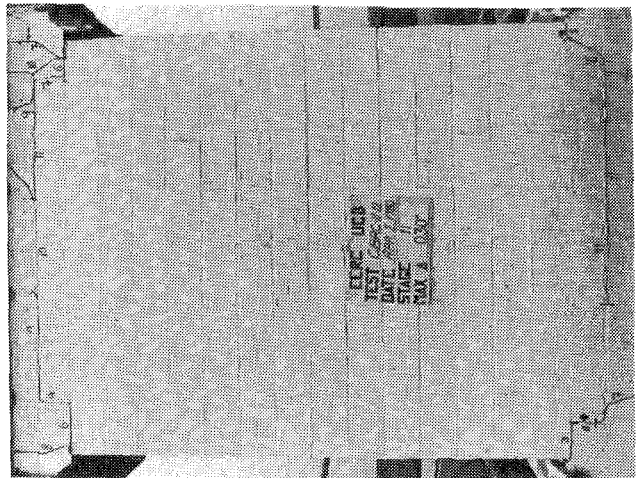
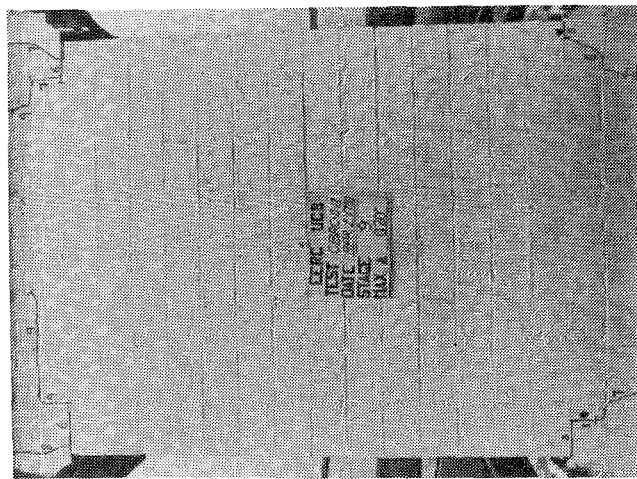
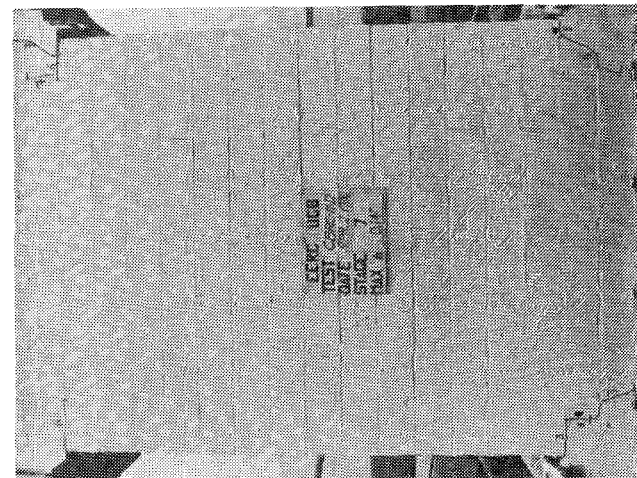


FIG. A. 32b SUCCESSIVE CRACK FORMATION (CBRC-11-12)

EARTHQUAKE ENGINEERING RESEARCH CENTER REPORTS

NOTE: Numbers in parentheses are Accession Numbers assigned by the National Technical Information Service; these are followed by a price code. Copies of the reports may be ordered from the National Technical Information Service, 5285 Port Royal Road, Springfield, Virginia, 22161. Accession Numbers should be quoted on orders for reports (PB --- ---) and remittance must accompany each order. Reports without this information were not available at time of printing. The complete list of EERC reports (from EERC 67-1) is available upon request from the Earthquake Engineering Research Center, University of California, Berkeley, 47th Street and Hoffman Boulevard, Richmond, California 94804.

- UCB/EERC-79/01 "Hysteretic Behavior of Lightweight Reinforced Concrete Beam-Column Subassemblages," by B. Forzani, E.P. Popov and V.V. Bertero - April 1979(PB 298 267)A06
- UCB/EERC-79/02 "The Development of a Mathematical Model to Predict the Flexural Response of Reinforced Concrete Beams to Cyclic Loads, Using System Identification," by J. Stanton & H. McNiven - Jan. 1979(PB 295 875)A10
- UCB/EERC-79/03 "Linear and Nonlinear Earthquake Response of Simple Torsionally Coupled Systems," by C.L. Kan and A.K. Chopra - Feb. 1979(PB 298 262)A06
- UCB/EERC-79/04 "A Mathematical Model of Masonry for Predicting its Linear Seismic Response Characteristics," by Y. Mengi and H.D. McNiven - Feb. 1979(PB 298 266)A06
- UCB/EERC-79/05 "Mechanical Behavior of Lightweight Concrete Confined by Different Types of Lateral Reinforcement," by M.A. Manrique, V.V. Bertero and E.P. Popov - May 1979(PB 301 114)A06
- UCB/EERC-79/06 "Static Tilt Tests of a Tall Cylindrical Liquid Storage Tank," by R.W. Clough and A. Niwa - Feb. 1979 (PB 301 167)A06
- UCB/EERC-79/07 "The Design of Steel Energy Absorbing Restrainers and Their Incorporation into Nuclear Power Plants for Enhanced Safety: Volume 1 - Summary Report," by P.N. Spencer, V.F. Zackay, and E.R. Parker - Feb. 1979(UCB/EERC-79/07)A09
- UCB/EERC-79/08 "The Design of Steel Energy Absorbing Restrainers and Their Incorporation into Nuclear Power Plants for Enhanced Safety: Volume 2 - The Development of Analyses for Reactor System Piping," "Simple Systems" by M.C. Lee, J. Penzien, A.K. Chopra and K. Suzuki "Complex Systems" by G.H. Powell, E.L. Wilson, R.W. Clough and D.G. Row - Feb. 1979(UCB/EERC-79/08)A10
- UCB/EERC-79/09 "The Design of Steel Energy Absorbing Restrainers and Their Incorporation into Nuclear Power Plants for Enhanced Safety: Volume 3 - Evaluation of Commercial Steels," by W.S. Owen, R.M.N. Pelloux, R.O. Ritchie, M. Faral, T. Ohhashi, J. Toplosky, S.J. Hartman, V.F. Zackay and E.R. Parker - Feb. 1979(UCB/EERC-79/09)A04
- UCB/EERC-79/10 "The Design of Steel Energy Absorbing Restrainers and Their Incorporation into Nuclear Power Plants for Enhanced Safety: Volume 4 - A Review of Energy-Absorbing Devices," by J.M. Kelly and M.S. Skinner - Feb. 1979(UCB/EERC-79/10)A04
- UCB/EERC-79/11 "Conservatism In Summation Rules for Closely Spaced Modes," by J.M. Kelly and J.L. Sackman - May 1979(PB 301 328)A03
- UCB/EERC-79/12 "Cyclic Loading Tests of Masonry Single Piers; Volume 3 - Height to Width Ratio of 0.5," by P.A. Hidalgo, R.L. Mayes, H.D. McNiven and R.W. Clough - May 1979(PB 301 321)A08
- UCB/EERC-79/13 "Cyclic Behavior of Dense Course-Grained Materials in Relation to the Seismic Stability of Dams," by N.G. Banerjee, H.B. Seed and C.K. Chan - June 1979(PB 301 373)A13
- UCB/EERC-79/14 "Seismic Behavior of Reinforced Concrete Interior Beam-Column Subassemblages," by S. Viathanatepa, E.P. Popov and V.V. Bertero - June 1979(PB 301 326)A10
- UCB/EERC-79/15 "Optimal Design of Localized Nonlinear Systems with Dual Performance Criteria Under Earthquake Excitations," by M.A. Bhatti - July 1979(PB 80 167 109)A06
- UCB/EERC-79/16 "OPTDYN - A General Purpose Optimization Program for Problems with or without Dynamic Constraints," by M.A. Bhatti, E. Polak and K.S. Pister - July 1979(PB 80 167 091)A05
- UCB/EERC-79/17 "ANSR-II, Analysis of Nonlinear Structural Response, Users Manual," by D.P. Mondkar and G.H. Powell July 1979(PB 80 113 301)A05
- UCB/EERC-79/18 "Soil Structure Interaction in Different Seismic Environments," A. Gomez-Masso, J. Lysmer, J.-C. Chen and H.B. Seed - August 1979(PB 80 101 520)A04
- UCB/EERC-79/19 "ARMA Models for Earthquake Ground Motions," by M.K. Chang, J.W. Kwiatkowski, R.F. Nau, R.M. Oliver and K.S. Pister - July 1979(PB 301 166)A05
- UCB/EERC-79/20 "Hysteretic Behavior of Reinforced Concrete Structural Walls," by J.M. Vallenias, V.V. Bertero and E.P. Popov - August 1979(PB 80 165 905)A12
- UCB/EERC-79/21 "Studies on High-Frequency Vibrations of Buildings - 1: The Column Effect," by J. Lubliner - August 1979 (PB 80 158 553)A03
- UCB/EERC-79/22 "Effects of Generalized Loadings on Bond Reinforcing Bars Embedded in Confined Concrete Blocks," by S. Viathanatepa, E.P. Popov and V.V. Bertero - August 1979(PB 81 124 018)A14
- UCB/EERC-79/23 "Shaking Table Study of Single-Story Masonry Houses, Volume 1: Test Structures 1 and 2," by P. Gülkan, R.L. Mayes and R.W. Clough - Sept. 1979 (HUD-000 1763)A12
- UCB/EERC-79/24 "Shaking Table Study of Single-Story Masonry Houses, Volume 2: Test Structures 3 and 4," by P. Gülkan, R.L. Mayes and R.W. Clough - Sept. 1979 (HUD-000 1836)A12
- UCB/EERC-79/25 "Shaking Table Study of Single-Story Masonry Houses, Volume 3: Summary, Conclusions and Recommendations," by R.W. Clough, R.L. Mayes and P. Gülkan - Sept. 1979 (HUD-000 1837)A06

UCB/EERC-79/26 "Recommendations for a U.S.-Japan Cooperative Research Program Utilizing Large-Scale Testing Facilities," by U.S.-Japan Planning Group - Sept. 1979(PB 301 407)A06

UCB/EERC-79/27 "Earthquake-Induced Liquefaction Near Lake Amatitlan, Guatemala," by H.B. Seed, I. Arango, C.K. Chan, A. Gomez-Masso and R. Grant de Ascoli - Sept. 1979(NUREG-CR1341)A03

UCB/EERC-79/28 "Infill Panels: Their Influence on Seismic Response of Buildings," by J.W. Axley and V.V. Bertero Sept. 1979(PB 80 163 371)A10

UCB/EERC-79/29 "3D Truss Bar Element (Type 1) for the ANSR-II Program," by D.P. Mondkar and G.H. Powell - Nov. 1979 (PB 80 169 709)A02

UCB/EERC-79/30 "2D Beam-Column Element (Type 5 - Parallel Element Theory) for the ANSR-II Program," by D.G. Row, G.H. Powell and D.P. Mondkar - Dec. 1979(PB 80 167 224)A03

UCB/EERC-79/31 "3D Beam-Column Element (Type 2 - Parallel Element Theory) for the ANSR-II Program," by A. Riahi, G.H. Powell and D.P. Mondkar - Dec. 1979(PB 80 167 216)A03

UCB/EERC-79/32 "On Response of Structures to Stationary Excitation," by A. Der Kiureghian - Dec. 1979(PB 80166 929)A03

UCB/EERC-79/33 "Undisturbed Sampling and Cyclic Load Testing of Sands," by S. Singh, H.B. Seed and C.K. Chan Dec. 1979(ADA 087 298)A07

UCB/EERC-79/34 "Interaction Effects of Simultaneous Torsional and Compressional Cyclic Loading of Sand," by P.M. Griffin and W.N. Houston - Dec. 1979(ADA 092 352)A15

UCB/EERC-80/01 "Earthquake Response of Concrete Gravity Dams Including Hydrodynamic and Foundation Interaction Effects," by A.K. Chopra, P. Chakrabarti and S. Gupta - Jan. 1980(AD-A087297)A10

UCB/EERC-80/02 "Rocking Response of Rigid Blocks to Earthquakes," by C.S. Yim, A.K. Chopra and J. Penzien - Jan. 1980 (PB80 166 002)A04

UCB/EERC-80/03 "Optimum Inelastic Design of Seismic-Resistant Reinforced Concrete Frame Structures," by S.W. Zagajeski and V.V. Bertero - Jan. 1980(PB80 164 635)A06

UCB/EERC-80/04 "Effects of Amount and Arrangement of Wall-Panel Reinforcement on Hysteretic Behavior of Reinforced Concrete Walls," by R. Iliya and V.V. Bertero - Feb. 1980(PB81 122 525)A09

UCB/EERC-80/05 "Shaking Table Research on Concrete Dam Models," by A. Niwa and R.W. Clough - Sept. 1980(PB81 122 368)A06

UCB/EERC-80/06 "The Design of Steel Energy-Absorbing Restrainers and their Incorporation into Nuclear Power Plants for Enhanced Safety (Vol 1A): Piping with Energy Absorbing Restrainers: Parameter Study on Small Systems," by G.H. Powell, C. Oughourlian and J. Simons - June 1980

UCB/EERC-80/07 "Inelastic Torsional Response of Structures Subjected to Earthquake Ground Motions," by Y. Yamazaki April 1980(PB81 122 327)A08

UCB/EERC-80/08 "Study of X-Braced Steel Frame Structures Under Earthquake Simulation," by Y. Ghanaat - April 1980 (PB81 122 335)A11

UCB/EERC-80/09 "Hybrid Modelling of Soil-Structure Interaction," by S. Gupta, T.W. Lin, J. Penzien and C.S. Yeh May 1980(PB81 122 319)A07

UCB/EERC-80/10 "General Applicability of a Nonlinear Model of a One Story Steel Frame," by B.I. Sveinsson and H.D. McNiven - May 1980(PB81 124 877)A06

UCB/EERC-80/11 "A Green-Function Method for Wave Interaction with a Submerged Body," by W. Kioka - April 1980 (PB81 122 269)A07

UCB/EERC-80/12 "Hydrodynamic Pressure and Added Mass for Axisymmetric Bodies," by F. Nilrat - May 1980(PB81 122 343)A08

UCB/EERC-80/13 "Treatment of Non-Linear Drag Forces Acting on Offshore Platforms," by B.V. Dao and J. Penzien May 1980(PB81 153 413)A07

UCB/EERC-80/14 "2D Plane/Axisymmetric Solid Element (Type 3 - Elastic or Elastic-Perfectly Plastic) for the ANSR-II Program," by D.P. Mondkar and G.H. Powell - July 1980(PB81 122 350)A03

UCB/EERC-80/15 "A Response Spectrum Method for Random Vibrations," by A. Der Kiureghian - June 1980(PB81 122 301)A03

UCB/EERC-80/16 "Cyclic Inelastic Buckling of Tubular Steel Braces," by V.A. Zayas, E.P. Popov and S.A. Mahin June 1980(PB81 124 885)A10

UCB/EERC-80/17 "Dynamic Response of Simple Arch Dams Including Hydrodynamic Interaction," by C.S. Porter and A.K. Chopra - July 1980(PB81 124 000)A13

UCB/EERC-80/18 "Experimental Testing of a Friction Damped Aseismic Base Isolation System with Fail-Safe Characteristics," by J.M. Kelly, K.E. Beucke and M.S. Skinner - July 1980(PB81 148 595)A04

UCB/EERC-80/19 "The Design of Steel Energy-Absorbing Restrainers and their Incorporation into Nuclear Power Plants for Enhanced Safety (Vol 1B): Stochastic Seismic Analyses of Nuclear Power Plant Structures and Piping Systems Subjected to Multiple Support Excitations," by M.C. Lee and J. Penzien - June 1980

UCB/EERC-80/20 "The Design of Steel Energy-Absorbing Restrainers and their Incorporation into Nuclear Power Plants for Enhanced Safety (Vol 1C): Numerical Method for Dynamic Substructure Analysis," by J.M. Dickens and E.L. Wilson - June 1980

UCB/EERC-80/21 "The Design of Steel Energy-Absorbing Restrainers and their Incorporation into Nuclear Power Plants for Enhanced Safety (Vol 2): Development and Testing of Restraints for Nuclear Piping Systems," by J.M. Kelly and M.S. Skinner - June 1980

UCB/EERC-80/22 "3D Solid Element (Type 4-Elastic or Elastic-Perfectly-Plastic) for the ANSR-II Program," by D.P. Mondkar and G.H. Powell - July 1980(PB81 123 242)A03

UCB/EERC-80/23 "Gap-Friction Element (Type 5) for the ANSR-II Program," by D.P. Mondkar and G.H. Powell - July 1980 (PB81 122 285)A03

UCB/EERC-80/24 "U-Bar Restraint Element (Type 11) for the ANSR-II Program," by C. Oughourlian and G.H. Powell July 1980(PB81 122 293)A03

UCB/EERC-80/25 "Testing of a Natural Rubber Base Isolation System by an Explosively Simulated Earthquake," by J.M. Kelly - August 1980(PB81 201 360)A04

UCB/EERC-80/26 "Input Identification from Structural Vibrational Response," by Y. Hu - August 1980(PB81 152 308)A05

UCB/EERC-80/27 "Cyclic Inelastic Behavior of Steel Offshore Structures," by V.A. Zayas, S.A. Mahin and E.P. Popov August 1980(PB81 196 180)A15

UCB/EERC-80/28 "Shaking Table Testing of a Reinforced Concrete Frame with Biaxial Response," by M.G. Oliva October 1980(PB81 154 304)A10

UCB/EERC-80/29 "Dynamic Properties of a Twelve-Story Prefabricated Panel Building," by J.G. Bouwkamp, J.P. Kollegger and R.M. Stephen - October 1980(PB82 117 128)A06

UCB/EERC-80/30 "Dynamic Properties of an Eight-Story Prefabricated Panel Building," by J.G. Bouwkamp, J.P. Kollegger and R.M. Stephen - October 1980(PB81 200 313)A05

UCB/EERC-80/31 "Predictive Dynamic Response of Panel Type Structures Under Earthquakes," by J.P. Kollegger and J.G. Bouwkamp - October 1980(PB81 152 316)A04

UCB/EERC-80/32 "The Design of Steel Energy-Absorbing Restrainers and their Incorporation into Nuclear Power Plants for Enhanced Safety (Vol 3): Testing of Commercial Steels in Low-Cycle Torsional Fatigue," by P. Spencer, E.R. Parker, E. Jongewaard and M. Drory

UCB/EERC-80/33 "The Design of Steel Energy-Absorbing Restrainers and their Incorporation into Nuclear Power Plants for Enhanced Safety (Vol 4): Shaking Table Tests of Piping Systems with Energy-Absorbing Restrainers," by S.F. Stiemer and W.G. Godden - Sept. 1980

UCB/EERC-80/34 "The Design of Steel Energy-Absorbing Restrainers and their Incorporation into Nuclear Power Plants for Enhanced Safety (Vol 5): Summary Report," by P. Spencer

UCB/EERC-80/35 "Experimental Testing of an Energy-Absorbing Base Isolation System," by J.M. Kelly, M.S. Skinner and K.E. Beucke - October 1980(PB81 154 072)A04

UCB/EERC-80/36 "Simulating and Analyzing Artificial Non-Stationary Earthquake Ground Motions," by R.F. Nau, R.M. Oliver and K.S. Pister - October 1980(PB81 153 397)A04

UCB/EERC-80/37 "Earthquake Engineering at Berkeley - 1980," - Sept. 1980(PB81 205 874)A09

UCB/EERC-80/38 "Inelastic Seismic Analysis of Large Panel Buildings," by V. Schricker and G.H. Powell - Sept. 1980 (PB81 154 338)A13

UCB/EERC-80/39 "Dynamic Response of Embankment, Concrete-Gravity and Arch Dams Including Hydrodynamic Interaction," by J.F. Hall and A.K. Chopra - October 1980(PB81 152 324)A11

UCB/EERC-80/40 "Inelastic Buckling of Steel Struts Under Cyclic Load Reversal," by R.G. Black, W.A. Wenger and E.P. Popov - October 1980(PB81 154 312)A08

UCB/EERC-80/41 "Influence of Site Characteristics on Building Damage During the October 3, 1974 Lima Earthquake," by P. Repetto, I. Arango and H.B. Seed - Sept. 1980(PB81 161 739)A05

UCB/EERC-80/42 "Evaluation of a Shaking Table Test Program on Response Behavior of a Two Story Reinforced Concrete Frame," by J.M. Blondet, R.W. Clough and S.A. Mahin

UCB/EERC-80/43 "Modelling of Soil-Structure Interaction by Finite and Infinite Elements," by F. Medina - December 1980(PB81 229 270)A04

UCB/EERC-81/01 "Control of Seismic Response of Piping Systems and Other Structures by Base Isolation," edited by J.M. Kelly - January 1981 (PB81 200 735)A05

UCB/EERC-81/02 "OPTNSR - An Interactive Software System for Optimal Design of Statically and Dynamically Loaded Structures with Nonlinear Response," by M.A. Bhatti, V. Ciampi and K.S. Pister - January 1981 (PB81 218 851)A09

UCB/EERC-81/03 "Analysis of Local Variations in Free Field Seismic Ground Motions," by J.-C. Chen, J. Lysmer and H.B. Seed - January 1981 (AD-A099508)A13

UCB/EERC-81/04 "Inelastic Structural Modeling of Braced Offshore Platforms for Seismic Loading," by V.A. Zayas, P.-S.B. Shing, S.A. Mahin and E.P. Popov - January 1981(PB82 138 777)A07

UCB/EERC-81/05 "Dynamic Response of Light Equipment in Structures," by A. Der Kiureghian, J.L. Sackman and B. Nour-Omid - April 1981 (PB81 218 497)A04

UCB/EERC-81/06 "Preliminary Experimental Investigation of a Broad Base Liquid Storage Tank," by J.G. Bouwkamp, J.P. Kollegger and R.M. Stephen - May 1981(PB82 140 385)A03

UCB/EERC-81/07 "The Seismic Resistant Design of Reinforced Concrete Coupled Structural Walls," by A.E. Aktan and V.V. Bertero - June 1981(PB82 113 358)A11

UCB/EERC-81/08 "The Undrained Shearing Resistance of Cohesive Soils at Large Deformations," by M.R. Pyles and H.B. Seed - August 1981

UCB/EERC-81/09 "Experimental Behavior of a Spatial Piping System with Steel Energy Absorbers Subjected to a Simulated Differential Seismic Input," by S.F. Stiemer, W.G. Godden and J.M. Kelly - July 1981

- UCB/EERC-81/10 "Evaluation of Seismic Design Provisions for Masonry in the United States," by B.I. Sveinsson, R.L. Mayes and H.D. McNiven - August 1981 (PB82 166 075)A08
- UCB/EERC-81/11 "Two-Dimensional Hybrid Modelling of Soil-Structure Interaction," by T.-J. Tzong, S. Gupta and J. Penzien - August 1981 (PB82 142 118)A04
- UCB/EERC-81/12 "Studies on Effects of Infills in Seismic Resistant R/C Construction," by S. Brokken and V.V. Bertero - September 1981 (PB82 166 190)A09
- UCB/EERC-81/13 "Linear Models to Predict the Nonlinear Seismic Behavior of a One-Story Steel Frame," by H. Valdimarsson, A.H. Shah and H.D. McNiven - September 1981 (PB82 138 793)A07
- UCB/EERC-81/14 "TLUSH: A Computer Program for the Three-Dimensional Dynamic Analysis of Earth Dams," by T. Kagawa, L.H. Mejia, H.B. Seed and J. Lysmer - September 1981 (PB82 139 940)A06
- UCB/EERC-81/15 "Three Dimensional Dynamic Response Analysis of Earth Dams," by L.H. Mejia and H.B. Seed - September 1981 (PB82 137 274)A12
- UCB/EERC-81/16 "Experimental Study of Lead and Elastomeric Dampers for Base Isolation Systems," by J.M. Kelly and S.B. Hodder - October 1981 (PB82 166 182)A05
- UCB/EERC-81/17 "The Influence of Base Isolation on the Seismic Response of Light Secondary Equipment," by J.M. Kelly - April 1981 (PB82 255 266)A04
- UCB/EERC-81/18 "Studies on Evaluation of Shaking Table Response Analysis Procedures," by J. Marcial Blondet - November 1981 (PB82 197 278)A10
- UCB/EERC-81/19 "DELIGHT.STRUCT: A Computer-Aided Design Environment for Structural Engineering," by R.J. Bailing, K.S. Pister and E. Polak - December 1981 (PB82 218 496)A07
- UCB/EERC-81/20 "Optimal Design of Seismic-Resistant Planar Steel Frames," by R.J. Bailing, V. Ciampi, K.S. Pister and E. Polak - December 1981 (PB82 220 179)A07
- UCB/EERC-82/01 "Dynamic Behavior of Ground for Seismic Analysis of Lifeline Systems," by T. Sato and A. Der Kiureghian - January 1982 (PB82 218 926)A05
- UCB/EERC-82/02 "Shaking Table Tests of a Tubular Steel Frame Model," by Y. Ghanaat and R. W. Clough - January 1982 (PB82 220 161)A07
- UCB/EERC-82/03 "Behavior of a Piping System under Seismic Excitation: Experimental Investigations of a Spatial Piping System supported by Mechanical Shock Arrestors and Steel Energy Absorbing Devices under Seismic Excitation," by S. Schneider, H.-M. Lee and W. G. Godden - May 1982 (PB83 172 544)A09
- UCB/EERC-82/04 "New Approaches for the Dynamic Analysis of Large Structural Systems," by E. L. Wilson - June 1982 (PB83 148 080)A05
- UCB/EERC-82/05 "Model Study of Effects of Damage on the Vibration Properties of Steel Offshore Platforms," by F. Shahrivar and J. G. Bouwkamp - June 1982 (PB83 148 742)A10
- UCB/EERC-82/06 "States of the Art and Practice in the Optimum Seismic Design and Analytical Response Prediction of R/C Frame-Wall Structures," by A. E. Aktan and V. V. Bertero - July 1982 (PB83 147 736)A05
- UCB/EERC-82/07 "Further Study of the Earthquake Response of a Broad Cylindrical Liquid-Storage Tank Model," by G. C. Manos and R. W. Clough - July 1982 (PB83 147 744)A11
- UCB/EERC-82/08 "An Evaluation of the Design and Analytical Seismic Response of a Seven Story Reinforced Concrete Frame - Wall Structure," by F. A. Charney and V. V. Bertero - July 1982 (PB83 157 628)A09
- UCB/EERC-82/09 "Fluid-Structure Interactions: Added Mass Computations for Incompressible Fluid," by J. S.-H. Kuo - August 1982 (PB83 156 281)A07
- UCB/EERC-82/10 "Joint-Opening Nonlinear Mechanism: Interface Smeared Crack Model," by J. S.-H. Kuo - August 1982 (PB83 149 195)A05
- UCB/EERC-82/11 "Dynamic Response Analysis of Tachi Dam," by R. W. Clough, R. M. Stephen and J. S.-H. Kuo - August 1982 (PB83 147 496)A06
- UCB/EERC-82/12 "Prediction of the Seismic Responses of R/C Frame-Coupled Wall Structures," by A. E. Aktan, V. V. Bertero and M. Piazza - August 1982 (PB83 149 203)A09
- UCB/EERC-82/13 "Preliminary Report on the SMART 1 Strong Motion Array in Taiwan," by B. A. Bolt, C. H. Loh, J. Penzien, Y. B. Tsai and Y. T. Yeh - August 1982 (PB83 159 400)A10
- UCB/EERC-82/14 "Shaking-Table Studies of an Eccentrically X-Braced Steel Structure," by M. S. Yang - September 1982 (PB83 260 778)A12
- UCB/EERC-82/15 "The Performance of Stairways in Earthquakes," by C. Roha, J. W. Axley and V. V. Bertero - September 1982 (PB83 157 693)A07
- UCB/EERC-82/16 "The Behavior of Submerged Multiple Bodies in Earthquakes," by W.-G. Liao - Sept. 1982 (PB83 158 709)AC7
- UCB/EERC-82/17 "Effects of Concrete Types and Loading Conditions on Local Bond-Slip Relationships," by A. D. Cowell, E. P. Popov and V. V. Bertero - September 1982 (PB83 153 577)A04

UCB/EERC-82/18 "Mechanical Behavior of Shear Wall Vertical Boundary Members: An Experimental Investigation," by M. T. Wagner and V. V. Bertero - October 1982 (PB83 159 764)A05

UCB/EERC-82/19 "Experimental Studies of Multi-support Seismic Loading on Piping Systems," by J. M. Kelly and A. D. Cowell - November 1982

UCB/EERC-82/20 "Generalized Plastic Hinge Concepts for 3D Beam-Column Elements," by P. F.-S. Chen and G. H. Powell - November 1982 (PB83 247 981)A13

UCB/EERC-82/21 "ANSR-III: General Purpose Computer Program for Nonlinear Structural Analysis," by C. V. Oughourlian and G. H. Powell - November 1982 (PB83 251 330)A12

UCB/EERC-82/22 "Solution Strategies for Statically Loaded Nonlinear Structures," by J. W. Simons and G. H. Powell - November 1982 (PB83 197 970)A06

UCB/EERC-82/23 "Analytical Model of Deformed Bar Anchorages under Generalized Excitations," by V. Ciampi, R. Eligehausen, V. V. Bertero and E. P. Popov - November 1982 (PB83 169 532)A06

UCB/EERC-82/24 "A Mathematical Model for the Response of Masonry Walls to Dynamic Excitations," by H. Sucuoğlu, Y. Mengi and H. D. McNiven - November 1982 (PB83 169 011)A07

UCB/EERC-82/25 "Earthquake Response Considerations of Broad Liquid Storage Tanks," by F. J. Cambra - November 1982 (PB83 251 215)A09

UCB/EERC-82/26 "Computational Models for Cyclic Plasticity, Rate Dependence and Creep," by B. Mosaddad and G. H. Powell - November 1982 (PB83 245 829)A08

UCB/EERC-82/27 "Inelastic Analysis of Piping and Tubular Structures," by M. Mahasuverachai and G. H. Powell - November 1982 (PB83 249 987)A07

UCB/EERC-83/01 "The Economic Feasibility of Seismic Rehabilitation of Buildings by Base Isolation," by J. M. Kelly - January 1983 (PB83 197 988)A05

UCB/EERC-83/02 "Seismic Moment Connections for Moment-Resisting Steel Frames," by E. P. Popov - January 1983 (PB83 195 412)A04

UCB/EERC-83/03 "Design of Links and Beam-to-Column Connections for Eccentrically Braced Steel Frames," by E. P. Popov and J. O. Malley - January 1983 (PB83 194 811)A04

UCB/EERC-83/04 "Numerical Techniques for the Evaluation of Soil-Structure Interaction Effects in the Time Domain," by E. Bayo and E. L. Wilson - February 1983 (PB83 245 605)A09

UCB/EERC-83/05 "A Transducer for Measuring the Internal Forces in the Columns of a Frame-Wall Reinforced Concrete Structure," by R. Sause and V. V. Bertero - May 1983 (PB84 119 494)A06

UCB/EERC-83/06 "Dynamic Interactions between Floating Ice and Offshore Structures," by P. Croteau - May 1983 (PB84 119 486)A16

UCB/EERC-83/07 "Dynamic Analysis of Multiply Tuned and Arbitrarily Supported Secondary Systems," by T. Igusa and A. Der Kiureghian - June 1983 (PB84 118 272)A11

UCB/EERC-83/08 "A Laboratory Study of Submerged Multi-body Systems in Earthquakes," by G. R. Ansari - June 1983 (PB83 261 842)A17

UCB/EERC-83/09 "Effects of Transient Foundation Uplift on Earthquake Response of Structures," by C.-S. Yim and A. K. Chopra - June 1983 (PB83 261 396)A07

UCB/EERC-83/10 "Optimal Design of Friction-Braced Frames under Seismic Loading," by M. A. Austin and K. S. Pister - June 1983 (PB84 119 288)A06

UCB/EERC-83/11 "Shaking Table Study of Single-Story Masonry Houses: Dynamic Performance under Three Component Seismic Input and Recommendations," by G. C. Manos, R. W. Clough and R. L. Mayes - June 1983

UCB/EERC-83/12 "Experimental Error Propagation in Pseudodynamic Testing," by P. B. Shing and S. A. Mahin - June 1983 (PB84 119 270)A09

UCB/EERC-83/13 "Experimental and Analytical Predictions of the Mechanical Characteristics of a 1/5-scale Model of a 7-story R/C Frame-Wall Building Structure," by A. E. Aktan, V. V. Bertero, A. A. Chowdhury and T. Nagashima - August 1983 (PB84 119 213)A07

UCB/EERC-83/14 "Shaking Table Tests of Large-Panel Precast Concrete Building System Assemblages," by M. G. Oliva and R. W. Clough - August 1983

UCB/EERC-83/15 "Seismic Behavior of Active Beam Links in Eccentrically Braced Frames," by K. D. Hjelmstad and E. P. Popov - July 1983 (PB84 119 676)A09

UCB/EERC-83/16 "System Identification of Structures with Joint Rotation," by J. S. Dimsdale and H. D. McNiven - July 1983

UCB/EERC-83/17 "Construction of Inelastic Response Spectra for Single-Degree-of-Freedom Systems," by S. Mahin and J. Lin - July 1983

- NA UCB/EERC-83/18 "Interactive Computer Analysis Methods for Predicting the Inelastic Cyclic Behaviour of Structural Sections," by S. Kaba and S. Mahin - July 1983 (PB84 192 012)A06
- UCB/EERC-83/19 "Effects of Bond Deterioration on Hysteretic Behavior of Reinforced Concrete Joints," by F.C. Filippou, E.P. Popov and V.V. Bertero - Aug. 1983 (PB84 192 020)A10
- UCB/EERC-83/20 "Analytical and Experimental Correlation of Large-Panel Precast Building System Performance," by M.G. Oliva, R.W. Clough, M. Velkov, P. Gavrilovic and J. Petrovski - Nov. 1983
- UCB/EERC-83/21 "Mechanical Characteristics of Materials Used in a 1/5 Scale Model of a 7-Story Reinforced Concrete Test Structure," by V.V. Bertero, A.E. Aktan, H.G. Harris and A.A. Chowdhury - Sept. 1983 (PB84 193 697)A05
- NA UCB/EERC-83/22 "Hybrid Modelling of Soil-Structure Interaction in Layered Media," by T.-J. Tzong and J. Penzien - Oct. 1983 (PB84 192 178)A08
- UCB/EERC-83/23 "Local Bond Stress-Slip Relationships of Deformed Bars under Generalized Excitations," by R. Eligehausen, E.P. Popov and V.V. Bertero - Oct. 1983 (PB84 192 848)A09
- UCB/EERC-83/24 "Design Considerations for Shear Links in Eccentrically Braced Frames," by J.O. Malley and E.P. Popov - Nov. 1983 (PB84 192 186)A07
- NA UCB/EERC-84/01 "Pseudodynamic Test Method for Seismic Performance Evaluation: Theory and Implementation," by P.-S. B. Shing and S.A. Mahin - Jan. 1984 (PB84 190 644)A08
- UCB/EERC-84/02 "Dynamic Response Behavior of Xiang Hong Dian Dam," by R.W. Clough, K.-T. Chang, H.-Q. Chen, R.M. Stephen, G.-L. Wang and Y. Ghanaat - April 1984 (PB84 209 402)A08
- UCB/EERC-84/03 "Refined Modelling of Reinforced Concrete Columns for Seismic Analysis," by S.A. Kaba and S.A. Mahin - April 1984 (PB84 234 384)A06
- NA UCB/EERC-84/04 "A New Floor Response Spectrum Method for Seismic Analysis of Multiply Supported Secondary Systems," by A. Asfura and A. Der Kiureghian - June 1984 (PB84 239 417)A06
- NA UCB/EERC-84/05 "Earthquake Simulation Tests and Associated Studies of a 1/5th-scale Model of a 7-Story R/C Frame-Wall Test Structure," by V.V. Bertero, A.E. Aktan, F.A. Charney and R. Sause - June 1984 (PB84 239 409)A09
- UCB/EERC-84/06 "R/C Structural Walls: Seismic Design for Shear," by A.E. Aktan and V.V. Bertero
- UCB/EERC-84/07 "Behavior of Interior and Exterior Flat-Plate Connections subjected to Inelastic Load Reversals," by H.L. Zee and J.P. Moehle - August 1984 (PB86 117 629/AS) A07
- UCB/EERC-84/08 "Experimental Study of the Seismic Response of a Two-story Flat-Plate Structure," by J. P. Moehle and J.W. Diebold - August 1984 (PB86 122 553/AS) A12
- UCB/EERC-84/09 "Phenomenological Modeling of Steel Braces under Cyclic Loading," by K. Ikeda, S.A. Mahin and S.N. Dermitzakis - May 1984 (PB86 132 198/AS) A08
- UCB/EERC-84/10 "Earthquake Analysis and Response of Concrete Gravity Dams," by G. Fenves and A.K. Chopra - Aug. 1984 (PB85 193 902/AS)A11
- UCB/EERC-84/11 "EAGD-84: A Computer Program for Earthquake Analysis of Concrete Gravity Dams," by G. Fenves and A.K. Chopra - Aug. 1984 (PB85 193 613/AS)A05
- UCB/EERC-84/12 "A Refined Physical Theory Model for Predicting the Seismic Behavior of Braced Steel Frames," by K. Ikeda and S.A. Mahin - July 1984 (PB85 191 450/AS)A09
- UCB/EERC-84/13 "Earthquake Engineering Research at Berkeley - 1984" - Aug. 1984 (PB85 197 341/AS)A10
- NA UCB/EERC-84/14 "Moduli and Damping Factors for Dynamic Analyses of Cohesionless Soils," by H.B. Seed, R.T. Wong, I.M. Idriss and K. Tokimatsu - Sept. 1984 (PB85 191 468/AS)A04
- NA UCB/EERC-84/15 "The Influence of SPT Procedures in Soil Liquefaction Resistance Evaluations," by H.B. Seed, K. Tokimatsu, L.F. Harder and R.M. Chung - Oct. 1984 (PB85 191 732/AS)A04
- NA UCB/EERC-84/16 "Simplified Procedures for the Evaluation of Settlements in Sands Due to Earthquake Shaking," by K. Tokimatsu and H.B. Seed - Oct. 1984 (PB85 197 887/AS)A03
- UCB/EERC-84/17 "Evaluation of Energy Absorption Characteristics of Bridge under Seismic Conditions," by R.A. Imbsen and J. Penzien - Nov. 1984
- UCB/EERC-84/18 "Structure-Foundation Interactions under Dynamic Loads," by W.D. Liu and J. Penzien - Nov. 1984
- UCB/EERC-84/19 "Seismic Modelling of Deep Foundations," by C.-H. Chen and J. Penzien - Nov. 1984
- UCB/EERC-84/20 "Dynamic Response Behavior of Quan Shui Dam," by R.W. Clough, K.-T. Chang, H.-Q. Chen, R.M. Stephen, Y. Ghanaat and J.-H. Qi - Nov. 1984 (PB86 11517/AS) A07

- NA UCB/EERC-85/01 "Simplified Methods of Analysis for Earthquake Resistant Design of Buildings," by E.F. Cruz and A.K. Chopra - Feb. 1985 (PB86 112299/AS) A12
- UCB/EERC-85/02 "Estimation of Seismic Wave Coherency and Rupture Velocity using the SMART 1 Strong-Motion Array Recordings," by N.A. Abrahamson - March 1985
- UCB/EERC-85/03 "Dynamic Properties of a Thirty Story Condominium Tower Building," by R.M. Stephen, E.L. Wilson and N. Stander - April 1985 (PB86 118965/AS) A06
- UCB/EERC-85/04 "Development of Substructuring Techniques for On-Line Computer Controlled Seismic Performance Testing," by S. Dermitzakis and S. Mahin - February 1985 (PB86 132941/AS) A08
- UCB/EERC-85/05 "A Simple Model for Reinforcing Bar Anchorages under Cyclic Excitations," by F.C. Filippou - March 1985 (PB86 112919/AS) A05
- UCB/EERC-85/06 "Racking Behavior of Wood-Framed Gypsum Panels under Dynamic Load," by M.G. Oliva - June 1985
- UCB/EERC-85/07 "Earthquake Analysis and Response of Concrete Arch Dams," by K.-L. Fok and A.K. Chopra - June 1985 (PB86 139672/AS) A10
- UCB/EERC-85/08 "Effect of Inelastic Behavior on the Analysis and Design of Earthquake Resistant Structures," by J.P. Lin and S.A. Mahin - June 1985 (PB86 135340/AS) A08
- UCB/EERC-85/09 "Earthquake Simulator Testing of a Base-Isolated Bridge Deck," by J.M. Kelly, I.G. Buckle and H.-C. Tsai - January 1986
- UCB/EERC-85/10 "Simplified Analysis for Earthquake Resistant Design of Concrete Gravity Dams," by G. Fenves and A.K. Chopra - September 1985
- UCB/EERC-85/11 "Dynamic Interaction Effects in Arch Dams," by R.W. Clough, K.-T. Chang, H.-Q. Chen and Y. Ghanaat - October 1985 (PB86 135027/AS) A05
- UCB/EERC-85/12 "Dynamic Response of Long Valley Dam in the Mammoth Lake Earthquake Series of May 25-27, 1980," by S. Lai and H.B. Seed - November 1985 (PB86 142304/AS) A05
- UCB/EERC-85/13 "A Methodology for Computer-Aided Design of Earthquake-Resistant Steel Structures," by M.A. Austin, K.S. Pister and S.A. Mahin - December 1985 (PB86 159480/AS) A10
- UCB/EERC-85/14 "Response of Tension-Leg Platforms to Vertical Seismic Excitations," by G.-S. Liou, J. Penzien and R.W. Yeung - December 1985
- UCB/EERC-85/15 "Cyclic Loading Tests of Masonry Single Piers: Volume 4 - Additional Tests with Height to Width Ratio of 1," by H. Sucuoglu, H.D. McNiven and B. Sveinsson - December 1985

